Universidade de Aveiro Departamento de Química
2010

FABIANE COSTA OLIVEIRA

PREPARAÇÃO E CARACTERIZAÇÃO DE NOVOS NANOCOMPÓSITOS DO TIPO INORGÂNICO/POLISSACARÍDEO

PREPARATION AND CHARACTERIZATION OF NOVEL NANOCOMPOSITES OF INORGANIC/POLYSACCHARIDE TYPE

Universidade de Aveiro Departamento de Química
2010

FABIANE COSTA OLIVEIRA

PREPARAÇÃO E CARACTERIZAÇÃO DE NOVOS NANOCOMPÓSITOS DO TIPO INORGÂNICO/POLISSACARÍDEO

PREPARATION AND CHARACTERIZATION OF NOVEL NANOCOMPOSITES OF INORGANIC/POLYSACCHARIDE TYPE

Dissertação apresentada à Universidade de Aveiro para cumprimento dos requisitos necessários à obtenção do grau de Doutor em Química, realizada sob a orientação científica da Professora Doutora Ana Margarida Viegas de Barros-Timmons, e do Professor Doutor José António Teixeira Lopes da Silva, Professores Auxiliares do Departamento de Química da Universidade de Aveiro.

Apoio financeiro do POCTI no âmbito do III Quadro Comunitário de Apoio.

Apoio financeiro da FCT e do FSE no âmbito do III Quadro Comunitário de Apoio.

Ciência.Inovação 2010 Programa Operacional Ciência e Inovação 2010

À minha família e ao James pelo incansável apoio
Aos meus imensuráveis amigos

… as quatro virtudes que uma **PESSOA** precisa para ter uma vida segura e feliz:
a **I**nteligência, a **A**mizade, a **F**orça e a **P**oesia

Elizabeth Gilbert

o júri

presidente

Doutor José Manuel Lopes da Silva Moreira
Professor Catedrático da Universidade de Aveiro

Doutora Maria Helena Mendes Gil
Professora Catedrática da Universidade de Coimbra

Doutor Osvaldo Novais de Oliveira Júnior
Professor Catedrático da Universidade de São Paulo

Doutor Alessandro Gandini
Investigador Coordenador da Universidade de Aveiro

Doutor José António Teixeira Lopes da Silva
Professor Auxiliar da Universidade de Aveiro

Doutora Ana Margarida Madeira Viegas de Barros Timmons
Professora Auxiliar da Universidade de Aveiro

agradecimentos

A Deus e ao meu anjo da guarda que sempre estiveram ao meu lado, guiando e iluminando a minha vida com tantas bênçãos.

Aos meus orientadores Prof. Ana Barros e Prof. JALS pela orientação, pela amizade, pelo companheirismo nos momentos difíceis e essencialmente por me ensinarem a ser o que eu hoje sou, uma pessoa mais forte e mais determinada sem perder a ingénua verdade de que todos podemos ser felizes.

À Universidade de Aveiro e ao CICECO por possibilitarem a realização experimental desta dissertação. Ao Alβan e à FCT (SFRH/BD/23396/2005) pelas bolsas de doutoramento.

À Doutora Léa Lopes pela doação da goma xantana inicialmente estudada e aos professores amigos da Universidade de Aveiro, Alessandro Gandini, Ana Xavier, Armando Silvestre, Augusto Lopes, Carlos Pascoal, Carmen Freire, Cruz Pinto, Dmitry Evtyugin, Inês Portugal, José Cavaleiro, Rosário Domingues e Tito Trindade que por muitas vezes me ajudaram com esclarecimentos de dúvidas, com palavras de apoio e com ensinamentos académicos.

Aos atenciosos técnicos superiores pela ajuda na preparação e caracterização das minhas amostras. Um muito obrigado à Celeste Azevedo, pelos ensinamentos de FTIR; Marta Assunção, pelas belíssimas imagens de SEM e TEM; Dulce Helena Teixeira pelo apoio no laboratório de Bioquímica, Conceição da Costa, pelas análises BET; Hilário Rodrigues pelas análises de RMN; António Moraes, pela vidraria mais bem executada que já vi; Rosário Soares, pelas análises de raio-X; Cândido Casqueira, pelo socorro nas emergências; à Margarete Martinho, pelos litros e litros de solvente destilado e finalmente à minha querida amiga Sandra Magina, pelas as análises térmicas.

Às simpáticas pessoas da secretaria do departamento de química, Idpor e CICECO que tanto me ajudaram em diversas situações quando a burocracia "falou mais alto". Um obrigada especial para minha amiga Vera Fernandes e à Paula Fernandes do armazém.

Ao meu querido amigo, pai e irmão, Cláudio Bogó, tudo foi mais fácil na presença deste ser de luz. Contigo aprendi que a vida deve ser vivida com sabedoria sem perder o encanto e a magia. Foi contigo também que aprendi e vivi o "belo"; o seu senso artístico, a sua alma de borboleta e o seu coração pueril fizeram de mim um ser mais leve.

À minha querida amiga "bruxinha" Joana que levarei para sempre em meu coração. Um dos seres mais doces que passaram no meu caminho. O seu coração é tão grande e tão bondoso que irradia luz a todos que estão a sua volta. Saber perdoar, saber amar em plenitude e o saber ouvir foram coisas que vivi contigo. Obrigada pelo sincero carinho fraternal.

Aos casais maravilhosos que cruzaram o meu caminho e que me mostraram o quanto é belo o Amor; Daniela e Rodrigo, Andreia e Jorge, Dora e Roberto, Regina e Nelson, Susana e Laurent. Olhar para vocês me obriga a ser cada vez mais leve com o "outro". Vocês me ensinaram que repartir e doar são coisas essenciais. Admiração e carinho são coisas que sinto por vocês. Obrigada por serem meus companheiros de vida e de jornada.

À minha querida amiga Bartira, uma mulher “arretada”, detectora de uma sabedoria natural que tanto me ajudou a superar alguns percalços do caminho.

Aos meus amigos angelicais: Lúcia Oliveira, Sérgio Loureiro, Gisela Cunha, Mariana Valente e Victor Martins. Os vossos corações são tão leves e puros como uma pluma branca; apaziguadora e delicada.

Aos meus tantos amigos que chegaram, marcaram e partiram para o encontro da felicidade. Entre eles: Filipa Xavier, com as suas palavras doces e acertadas; Sara Lisboa (Índia) com seu carinho de mãe e companheirismo de irmã; Vanessa e Filipe (um casal na medida certa), que me deram a mão e o coração quando cheguei em terras lusitanas; Soninha, pela a sua ternura, a Paula Pinto pela a sua alegria contagiante e inspiradora; Ana Sofia pela sabedoria de saber dosar as melhores coisas da vida; Susana Peixoto e Marisa Valente, pela a alegria de compartilhar bancada e a vida laboral; Paula Alexandrina, pela sapiência, paciência e amizade

Às duas amigas e ao gato mais lindo do mundo que me deram um “Lar Doce Lar”. Foi nesta casa que encontrei a paz necessária para escrever esta tese, onde fiz amigos e onde essencialmente encontrei estes três seres especiais. A Flávia com um coração maior do que o próprio corpo, pura, ingénua mas com uma determinação de um “cacique”; uma verdadeira amiga para todos os momentos. Uma amiga que trouxe de volta o nosso amigo Lee. À Ana “Motorzinho” com um sorriso estampado no rosto todo o dia e com um “Hari om” na mente e no coração. E, finalmente, o Galileu Galilei, um Gato preto gorducho, meu grande companheiro quando as palavras não saíam, sempre a pedir comida e a dar beijinhos e arranhadelas. Mesmo em condições financeiras desfavoráveis, vocês me acolheram, me deram CARINHO, comida e roupa lavada. Ainda fizeram com que a “Flor de Laranjeira” cruzasse o meu caminho sem contar com o feliz encontro com a Nô e o Pipo. Amo vocês!

A todas as crianças que vieram ao nosso mundo durante esta caminhada, aos quais me intitulo por tia; Maria Eduarda Oliveira, Ana Cecília Oliveira, Laura Santiago, Maria Afonso Santiago, Joana Magina, Maria João Freire, Henrique Freire, Afonso Neves, Diniz Neves, Inês Margarida, Beatriz Monteiro, Maria João Pinto, Rita Fernandes, Mariana Lisboa, Inês Cerqueira, Maria Rita Fernandes.

Aos meus queridos amigos, aos quais muito humildemente descrevo-os com adjectivos: Carla Vilela, a organizadora; Juan Villaverde, o amigo guapo; Rui Domingues, o sem ouvidos; Lili, a dançarina; Sónia Santos, a integradora; Mónica Gomes, a companheira; Marina Matos, a falante; Ana Marques, a ouvinte; Natércia, a nova aquisição; Márcia Neves, a mãe artista; Ricardo Pinto, mão para toda obra; Gil, o quieto; Ana Reis, a sorridente; Catarina Ferreira, a paneleira; Ryana, a Raiana; Eliane Trovatti, a silenciosa; Juliana Vinholes, a bem disposta; Josi, a semelhante; Beta, a enciclopédia do laboratório; Isabel, a paz de alma; Flávia, a calma em pessoa; Claudia Passos, a lutadora; Claudia Nunes, a humana; Belzinha e Xana, as amigas para qualquer hora; Beatriz Veleirinho, a minha BiaHitz; Belinda, a multifunctinal. Para também outros amigos não menos importantes, Nuno Loureiro, Ana Margarida, Ângela, Diogo, Gonçalo, João, Alyssa, Carlones, Sérgio, Sandra e Ana Caetano. Para algumas destas pessoas gostaria de dedicar não um adjectivo, mas um texto repleto de adjectivos. Vocês acompanharam toda a minha história aqui. Mesmo nos momentos difíceis estavam ao meu lado me apoiando e me dando força para não cair. Um obrigado repleto de carinho e um beijo no coração.

Aos meus amigos que estão distantes, mas muito próximos do meu coração; Euler e Joyce Araujo, Vitor Araújo, Carolina Roma, Aline de Jesus, Rogério & Cristiane Pagano, Daniel & Ruskaja Sandrin, Marcos & Margarida Santos.

Aos meus familiares, tios, tias, primos, avó, etc. e, em especial ao meus pais, Euclides & Alice, à minha irmã e cunhado, Maria Odete & César e ao meu irmão Neto pelo o apoio incondicional. Amo vocês!

Finally, I would like to thank the person who has helped me throughout these years to see life with more lightness and colour. James, to you all my affection and my LOVE.

palavras-chave

nanocompósitos, polissacarídeos, SiO_2, suspensões, propriedades reológicas filmes finos, fibras, propriedades superficiais, propriedades de barreira, propriedades mecânicas, propriedades térmicas.

resumo

O uso de polímeros naturais no âmbito da preparação de nanocompósitos não tem sido tão amplamente estudado quando comparado com os polímeros sintéticos. Assim, esta tese tem como objectivo estudar metodologias para a preparação de novos materiais nanocompósitos sob a forma de dispersões e filmes utilizando polissacarídeos como matriz. A tese está dividida em cinco capítulos sendo o último capítulo dedicado às conclusões gerais e a sugestões para trabalhos futuros.

Inicialmente é apresentada uma breve revisão bibliográfica sobre os principais temas colocando esta tese em contexto. Considerações sobre o uso de polímeros naturais e a sua combinação com a utilização de nanopartículas inorgânicas para a fabricação de novos bionanocomposites são descritas e os objectivos e *outline* da tese são também apresentados.

No segundo capítulo, a preparação de partículas de sílica puras ou modificadas bem como a sua caracterização por FTIR, SEM, TEM, TGA, DLS (tamanho e potencial zeta) e medições de ângulo de contacto são discutidas. De modo a melhorar a compatibilidade da sílica com os polissacarídeos, as partículas SiO_2 foram modificados com dois compostos do tipo organosilano: 3-metacril-oxipropil-trimetoxissilano (MPS) e 3-aminopropil-trimetoxissilano (APS). As partículas SiO_2@MPS foram posteriormente encapsuladas com de poli(metacrilato de glicidilo) utilizando a técnica de polimerização em emulsão. A utilização dos nanocompósitos resultantes na preparação de dispersões de bionanocompósitos não foi bem sucedida e por esse motivo não os estudos não foram prosseguidos. O uso de SiO_2@APS na preparação de dispersões bionanocomposite foi eficiente.

No terceiro capítulo é apresentada uma revisão sobre dispersões bionanocompósitas e respectiva caracterização destacando aspectos fundamentais sobre reologia e microestrutura. Em seguida, é discutido o estudo sistemático realizado sobre o comportamento reológico de dispersões de SiO_2 utilizando três polissacarídeos distintos no que concerne a carga e as características gelificantes: a goma de alfarroba (não iónica), o quitosano (catiónico) e a goma xantana (aniónica) cujas propriedades reológicas são amplamente conhecidas. Os estudos reológicos realizados sob diferentes condições demonstraram que a formação de géis frágeis e/ou bem estruturados depende do tamanho SiO_2, da concentração, do pH e da força iónica. Estes estudos foram confirmados por análises microestruturais usando a microscopia electrónica a baixas temperaturas (Cryo-SEM).

No quarto capítulo, são apresentados os estudos relativos à preparação e caracterização de filmes bionanocompósitos utilizando quitosano como matriz. Primeiramente é apresentada uma revisão sobre filmes de bionanocompósitos e os aspectos fundamentais das técnicas de caracterização utilizadas. A escolha do plasticizante e da sua concentração são discutidas com base nas propriedades de filmes de quitosano preparados. Em seguida, o efeito da concentração de sílica e dos métodos utilizados para a dispersar na matriz de polissacarídeo, bem como o efeito da modificação da superfície da sílica

é avaliado. As características da superfície e as propriedades de barreira, mecânicas e térmicas são discutidas para cada conjunto de filmes preparados antes e após a sua neutralização. Os resultados obtidos mostraram que a dispersão das cargas no plasticizante e posterior adição à matriz polissacarídica resultaram apenas em pequenas melhorias já que o problema da agregação de sílica não foi ultrapassado. Por esse motivo foram preparados filmes com SiO_2@APS os quais apresentaram propriedades melhores apesar da agregação das partículas não ter sido completamente impedida. Tal pode estar relacionado com o processo de secagem dos filmes.

Finalmente, no capítulo 5, são apresentadas as principais conclusões obtidas e algumas sugestões para trabalho futuro.

keywords

bionacomposites, polysaccharides, SiO_2; dispersions, rheological properties, thin films, surface properties, barrier properties, mechanical properties, thermal properties

abstract

As the use of natural polymers to prepare polymer based nanocomposites has not been so extensively studied as compared to the synthetic polymers, this thesis aims to study methodologies for the preparation of new nanocomposite materials in the form of dispersions and films using polysaccharides as matrices. The thesis is divided in five chapters, the last one dedicated to general conclusions and future work.

Initially a brief literature review of the main topics discussed in this thesis is presented putting it in context. Considerations about the use of natural polymers combined with inorganic particles for fabrication of new bionanocomposites are described and the aims and outline of the thesis are also presented.

In the second Chapter the preparation of bare and modified silica particles as well as their characterization by a variety of techniques such as FTIR, SEM,TEM, TGA, DLS (size and zeta potential) and contact angle are discussed. In order to improve the compatibility of silica with polysaccharides, SiO_2 particles were modified with two organosilane compounds: 3-methacryloxypropyltrimethoxysilane (MPS) and 3-aminopropyltrimethoxysilane (APS). SiO_2@MPS was further encapsulated with poly(glycidyl methacrylate) via emulsion polymerization. The use of the ensuing nanocomposites directly in the preparation of bionanocomposite dispersions proved unsuccessful and was not pursued. The use of SiO_2@APS in the preparation of bionanocomposite dispersions was efficient.

In the third Chapter a review on bionanocomposite dispersions and their characterization highlighting fundamental aspects on their rheology and microstructure are presented. Next, a systematic study of the rheological behaviour of SiO_2 dispersions in three distinct polysaccharides is carried out. Polysaccharides of different charge and gelling ability have been tested: a non-ionic one, locust bean gum, a cationic polysaccharide, chitosan, and an anionic one, xanthan gum which is well known for its peculiar rheological properties. Rheological studies under different conditions showed that weak-gels and/or structured systems can be obtained depending on SiO_2 size, concentration, pH and ionic strength. These studies were supported by microstructural analyses using cryo-SEM.

In the fourth Chapter, bionanocomposite films using chitosan as matrix were prepared and characterized. First, a review of bio-based films and fundamental aspects of the characterization techniques used is presented. The choice of plasticizer and concentration is then discussed considering pristine chitosan films. Next the effect of silica concentration and of the methods used to disperse it in the polysaccharide matrix as well as the effect of silica modification is assessed. The surface morphology, barrier, mechanical and thermal properties are discussed for each set of as prepared films and upon neutralization. The results showed that dispersion of the fillers in the plasticizer prior to addition to the polysaccharide matrix only yielded minor improvements due to silica aggregation and that surface modification of the filler was required.

Films prepared with SiO_2@APS had in fact better properties though aggregation was not fully prevented.

Finally, in the fifth Chapter, the principal conclusions are reported and some suggestions for future work are given.

SCI Papers

OLIVEIRA, F. C.; BARROS-TIMMONS, A. M.; LOPES-DA-SILVA, J. A.; *"Preparation and Characterization of Chitosan/SiO_2 Composite Films"*. Journal of Nanoscience and Nanotechnology, **2010**, 10, 2816–2825.

OLIVEIRA, F. C.; MONTEIRO, S. R.; BARROS-TIMMONS, A. M.; LOPES-DA-SILVA, J. A.; *"Weak-gel formation in dispersions of silica particles in a matrix of a nonionic polysaccharide: Structure and rheological characterization"*. Carbohydrate Polymers, **2010**, (*submitted*).

Proceedings

OLIVEIRA, F. C.; FERREIRA, P. O.; FERREIRA, C. O.; LOPES-DA-SILVA, J. A.; BARROS-TIMMONS, A. M.; *"PVA/SiO_2 and PVA/modified SiO_2 nanofiber mats obtained by electrospinning"*. V International Conference on Science and Technology of Composite Materials (COMATCOMP2009) and 8° Congresso Nacional de Materiales Compuestos, **2009**, 7-9 October, San Sebastian-Spain.

OLIVEIRA, F. C.; MONTEIRO, S. R.; LOPES-DA-SILVA, J. A.; BARROS-TIMMONS, A. M.; *"Soft-gel formation induced by silica particles in non-gelling polysaccharides dispersions"*. Iberian Meeting on Rheology, **2008**, 11-12 September, Madrid-Spain.

OLIVEIRA, F. C.; LOPES-DA-SILVA, J. A.; BARROS-TIMMONS, A. M.; *"Rheological Properties of SiO_2/Polysaccharides Nanocomposites"*. World Polymer Congress/41st International Symposium on Macromolecules, **2006**, 16-21 July, Rio de Janeiro-Brazil.

OLIVEIRA, F. C.; LOPES-DA-SILVA, J. A.; BARROS-TIMMONS, A. M.; *"SiO_2/Locust Bean Gum and SiO_2/Chitosan Nanocomposites: Rheological Behavior"*. III Brazilian Conference on Rheology, **2006**, 12-14 July, Rio de Janeiro-Brazil.

Abstracts (oral presentations)

OLIVEIRA, F. C.; LOPES-DA-SILVA, J. A.; BARROS-TIMMONS, A. M.; "Inorganic/polysaccharides nanocomposites". III SIEBRAP- Seminário dos Estudantes Brasileiros da Universidade de Aveiro, **2006**, 13-14 December, Aveiro-Portugal.

Abstracts (poster presentations)

BARROS-TIMMONS, A. M.; LOPES-DA-SILVA, J. A.; OLIVEIRA, F. C.; *"SiO_2 functionalisation towards improved chitosan based nanocomposite film"*. VII Brazilian Materials Research Society Meeting (SBPMat), **2008**, September 28-October 2, São Paulo-Brazil.

OLIVEIRA, F. C.; LOPES-DA-SILVA, J. A.; BARROS-TIMMONS, A. M.; *"Functionalised SiO_2/chitosan nanocomposite films"*. 2nd International Conference on

Advanced Nano Materials, **2008**, 22-25 June, Aveiro-Portugal.

OLIVEIRA, F. C.; LOPES-DA-SILVA, J. A.; BARROS-TIMMONS, A. M.; *"Preparation and characterization of chitosan/SiO_2 nanocomposite films"*. 21st Conference of the European Colloid and Interface Society (ECIS 2007). **2007**, 10-14 September, Geneva- Switzerland.

OLIVEIRA, F. C.; LOPES-DA-SILVA, J. A.; BARROS-TIMMONS, A. M.; *"SiO_2/Polysaccharides Nanocomposites: A Rheological Study"*. XX National Meeting of the Portuguese Chemistry Society, **2006**, 14-16 December, Lisbon-Portugal.

OLIVEIRA, F. C.; LOPES-DA-SILVA, J. A.; BARROS-TIMMONS, A. M.; *"SiO_2/Polysaccharides Nanocomposites: A Rheological Study"*. III CICECO Meeting, **2006,** 13-14 January, Aveiro-Portugal.

OLIVEIRA, F. C.; LOPES-DA-SILVA, J. A.; BARROS-TIMMONS, A. M.; *"Comparative Study of the Rheological Behaviour of SiO_2/Xanthan Gum Nanocomposites – Effect of SiO_2 size and pH"*. 6 GLUPOR - III Iberian Carbohydrate Meeting, **2005**, 11-15 September, Coimbra-Portugal.

ABREU, V. L. R. G.; LAPČÍKOVÁ, B.;BARROS-TIMMONS, A. M.; LEHOCKÝA, M.; ESTEVES, A. C; OLIVEIRA, F. C.; LAPČÍK, L. J.; *"Polymer nanocomposites preparation/ characterization: zeta potential and particle size measurements"*. International Conference on Surfaces, Coatings and Nanostructured Materials, **2005**, 7-9 September, Aveiro-Portugal.

Contents

List of Abbreviations

AD	Average diameter
AFM	Atomic force microscopy
AIBA	2,2'-Azobis(2-methylpropionamidine) dihydrochloride
APS	3-aminopropyltrimethoxysilane
ATR	FTIR equipped with attenuated total reflectance
C*	Dilute concentration regime
C**	Concentrate concentration regime
CHI	Chitosan
CMC	Critical micelle concentration
Cryo-SEM	Low temperature scanning electron microscopy
CTAB	Cetyltrimethylammonium bromide
DA	Degree of acetylation
DD	Degree of deacetylation
DLS	Dynamic light scattering
DMA	Dynamical Mechanical Analysis
E	Young's modulus (MPa)
EG	Ethylene glycol
FTIR	Fourier Transformed infrared
G*	Complex modulus (Pa)
G'	Storage modulus (Pa)
G''	Loss modulus (Pa)
GLY	Glycerol
GMA	Glycidyl methacrylate
KPS	Sodium persulfate
LBG	Locust bean gum
MPS	3-methacryloxypropyltrimethoxysilane
MW	Molecular weight
PEG	Poly(ethylene glycol)
PG	Propylene glycol
PGMA	Poly(glycidyl methacrylate)
PMMA	Poly(methyl methacrylate)
RH	Relative humidity
SDS	Sodium dodecyl sulfate
SEM	Scanning electronic microscopy
SPM	3-sulfopropyl methacrylate potassium salt
TEM	Transmission electronic microscopy
TEOS	Tetraethoxysilane

T_g	Glass transition temperature (^oC)
TGA	Thermogravimetric analysis
THEOS	Tetrakis (2-hydroxy ethyl) orthosilicate
TMOS	Tetramethoxysilane
WCA	Water contact angle (^{o})
WVP	Water vapour permeability
WVTR	Water vapour transmission rate
XG	Xanthan gum

tan δ	Loss tangent
Δ	Relaxation exponent
$\dot{\gamma}$	Shear rate (s^{-1})
ε_b	Elongation at break (%)
η	Viscosity (Pa.s)
η*	Complex viscosity (Pa.s)
η_∞	Viscosity at infinite shear rate (Pa.s)
η_{ap}	Apparent viscosity (Pa.s)
η_o	Viscosity at zero shear rate (Pa.s)
θ	Real contact angle (^{o})
θ_{ap}	Apparent contact angle (^{o})
ρ	Density (g/cm^3)
σ	Shear stress
σ_b	Tensile strength at break (MPa)
ω	Oscillation frequency (rad/s)

List of Tables

List of Figures

1 Introduction:

Aims and outline of the thesis

1.1. General considerations

The use of natural polymers to prepare polymer based nanocomposites has been intensively investigated as a possibility to replace petroleum-derived polymers. Synthetic polymers have been a growing concern hence there is an increasing urgency for the development of greener polymeric materials that would be more environmentally friendly both in terms of manufacture and degradability of the products. For these reasons the development of biodegradable composite materials with controlled properties has been a subject of great research challenge to the community of materials scientists and engineers [24].

On this scene, the preparation of nanostructured composite materials from natural, abundant, and low-cost biodegradable components obtained from renewable sources has been investigated. This new and promising class of materials named "bionanocomposite or green nanocomposites" has been defined as composites constituted by a biopolymer in combination with inorganic materials which have at least one dimension on the nanometer scale [1, 2, 25-27]. In fact, organic–inorganic composite materials due to combination of the organic and inorganic components properties possess very unusual properties, different from their microscale counterparts [28, 29]. The development of these materials represents an emerging and interdisciplinary topic at the border of Life Sciences, Material Sciences and Nanotechnology [27].

In addition, bionanocomposites show the remarkable advantage of exhibiting biocompatibility, biodegradability and, in some cases, additional functional properties provided by either the biological or inorganic moieties [1, 26, 30-35]. They are of great interest due to their versatile applications in relevant areas mainly in regenerative medicine as well as drug vectorization and delivery, where the use of biocompatible materials is usually required. Moreover, the use of these new materials in packaging in the food industry, agriculture or the building industry, among other areas, will help to reduce the amount of waste products and to diminish environmental pollution, contributing to a sustainable development [26].

Despite of the interesting characteristics of natural polymers to prepare polymer based nanocomposites they have not been so extensively studied when compared to their synthetic counterparts [26]. This fact is supported by the number of scientific publications in both areas according to the Institute for Scientific Information (ISI) database shown in Figure 1.1.

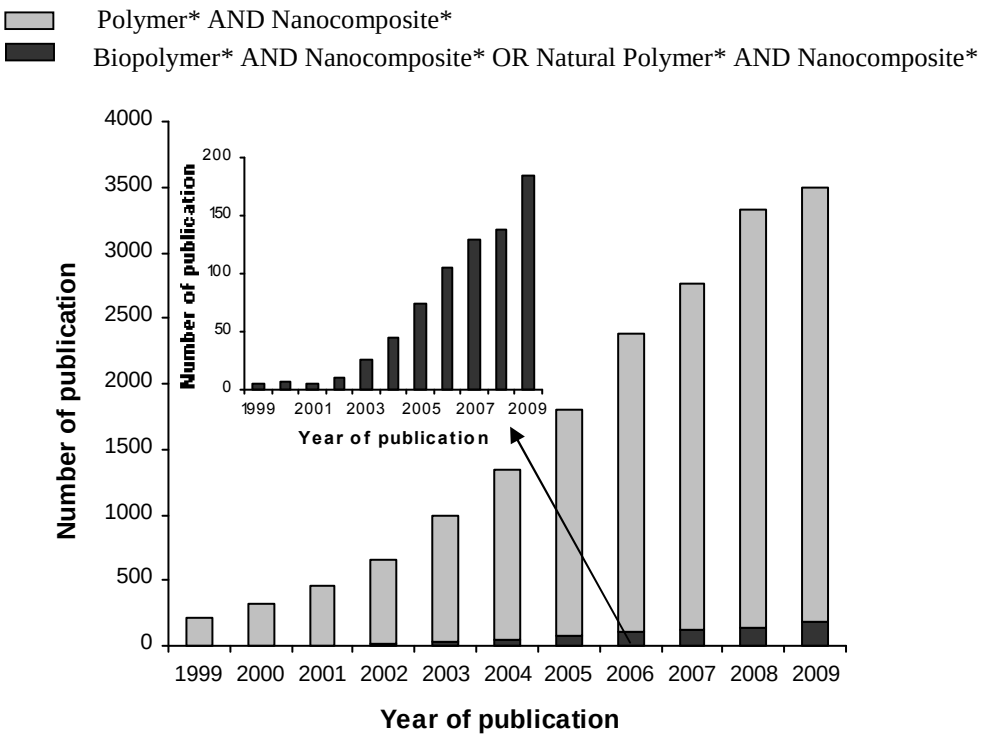

Figure 1.1: Number of publications per year related to polymer-based nanocomposites versus biopolymer-based nanocomposites. Data collected from the ISI Web of Knowledge in 24/01/2010.

The choice of the constituents of these bionanocomposites will depend on the application to be given to the material, the availability and the cost of the components involved. Nature is the source of a wide number of bio-macromolecules that can be used in the preparation of bionanocomposites. For this purpose, a variety of renewable biopolymers such as polysaccharides, proteins, lipids, and their composites derived from plant and animal resources have been explored [1]. In addition, inorganic particles incorporated into the bionanocomposites can have diverse nature with different chemical compositions, textures and geometries (fibers, flakes, spheres, particulates) [2, 25], which determine the properties of the resulting materials. Single elements such as transition metals and carbon particles, metal oxides, metal alkoxides, silica and hydroxides, silicates, carbonates and phosphates are typical inorganic components of bionanocomposites [2, 27].

According to Alexandre *et al*. [36], fillers can be distinguished depending on how many dimensions they have in the nanometric range. When the three filler dimensions are in the order of nanometers, we are dealing with isodimensional nanoparticles, such as spherical silica nanoparticles obtained by *in situ* sol-gel methods [37, 38] or modified silica particles obtained by polymerization promoted directly from their surface [29, 39], but they can also include semiconductor nanoclusters [40] and others. Nanotubes [41-44] and whiskers [45] are examples of

fillers with two dimensions in the nanometer scale and the third being larger, forming an elongated structure. The third type of inorganic solid is characterized by only one dimension in the nanometer range. In this case the filler is present in the form of sheets of one to a few nanometer thick to hundreds to thousands nanometers long as is the case of nanoclays [46] or graphene sheets [47]. In general, this last type of fillers with a high aspect ratio i.e., a high ratio of the largest to the smallest dimension are particularly interesting because of their high specific surface area [29, 39, 44, 48], providing better reinforcing effects [49, 50].

Regardless of the structure of the fillers, it is well established that the affinity between the inorganic and the bio-organic counterparts is a fundamental feature in the preparation of bionanocomposites [31]. The uniformity and stability of the particles involved in their manufacture is also very important. A uniform dispersion of nanoparticles leads to a very large matrix/filler interfacial area, which changes the molecular mobility, the relaxation behaviour and the subsequent thermal and mechanical properties of the material [25]. However, according to Jordan *et al.* [51] there is no universal trend that can be modelled and explained for different types of polymer nanocomposite systems. Yet, most observations show that the behaviour of nanocomposites differs from composites with larger fillers.

The effects of the interface on the behaviour of a composite depend upon the interparticle distance. For a constant filler content, the reduction of particle size increases the number of filler particles, bringing the particles closer to one another. Moreover, experimental data suggest that in well dispersed polymer based nanocomposites each nanoparticle is surrounded by an interface zone where polymer mobility is significantly different from that of the matrix. This can lead to a percolating interphase network inside the composite which makes it difficult to fully predict and model polymer based composites [52].

Despite of the complexity involved, nature being a source of inspiration for the development of synthetic approaches to bionanocomposites, has been driving a variety of studies on this field, some of which are briefly discussed next.

Mother of pearl and marine shell, coral, teeth and bones are examples of bioinorganic nanocomposites which have special arrangements at the nanometric level of biopolymers and inorganic counterparts. For instance, nacre also known as mother of pearl (Figure 1.2) is a good example of a natural bionanocomposite, formed by the stacking of highly oriented calcium carbonate (aragonite) platelets cemented by a fibrous protein. This supra-architecture shows exceptional mechanical properties compared to monolithic calcium carbonate [4, 53].

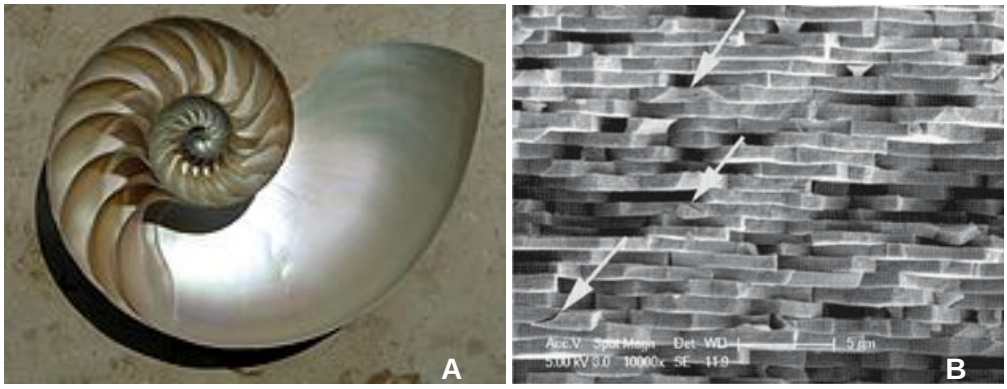

Figure 1.2: (A) The iridescent nacre inside a Nautilus shell and (B) microstructure of nacre platelet; the arrows identify the cracks at the platelet edges. Reproduced from Wikipedia website [3] and reference [4].

At the present time, bionanocomposites mimicking natural materials have been prepared following the concept of supramolecular chemistry, biomimetics and biominerilazation through advanced methodologies, which are also associated with the type and properties of the fillers. Among these methods it is possible to mention, intercalation, self-assembly, layer-by-layer adsorption, sol-gel process including template synthesis, besides simple mixture which has not been much exploited [27].

Similarly to the natural structure of nacre mentioned above, polymer/clay composites have been prepared via intercalation. Mineral clays are one of the most abundant groups of inorganic solids [54], amongst which the most widely studied is montmorillonite, a hydrated alumina-silicate layered clay consisting of an edge-shared octahedral sheet of aluminium hydroxide between two silica tetrahedral layers. The preparation of bionanocomposites materials based on organoclays has been recently reviewed by Chivrac *et al.* [46], who reported the use of different polysaccharides and methods of preparation of these new materials. Special attention has been given to the preparation of new composites using the chitosan [55-59]. The analysis of these materials has revealed improvements on mechanical properties of chitosan/montmorillonite nanocomposite [56, 59]. Since clay layers constitute a barrier to gases and water, forcing them to follow a tortuous path, the introduction of nanoclays into the polymer matrix has been shown to greatly improve barrier properties [60, 61].

The self-assembly process has been used for example to obtain collagen and hydroxyapatite/collagen/poly(lactic acid) composites by Liao *et al*. [62] in order to promote bone formation. The poly(lactic acid) gave to the hydroxyapatite/collagen composite better compatibility and mechanical strength resulting in composites that yielded new bone formation as they were implanted in adult male rabbits with segmental bone defects.

Pinto *et al.* [38] have prepared SiO_2/cellulose nanocomposites by deposition of morphological well-defined SiO_2 nanoparticles at the fibres surfaces via polyelectrolytes assembly (layer-by-layer approach, LbL). The LbL assembly method consists on the adsorption of alternating layers of oppositely charged polyelectrolytes on a solid surface. This technique is a straightforward method to fabricate multicomposite films mainly based on electrostatic interactions between anionic and cationic polymers. This nanocomposite was compared with the nanocomposite prepared by the synthesis of SiO_2 nanoparticles via tetraethoxysilane (TEOS) hydrolysis in the presence of cellulose fibres. The authors found that both methods were able to produce SiO_2/cellulose composites with final morphological properties strongly depend on the synthetic strategy employed. Whereas in the LbL approach cellulosic fibres covered with discrete spherical SiO_2 nanoparticles have been obtained, for the *in situ* synthesis of SiO_2, nanocomposites consisting predominantly on fibres homogeneously coated with a SiO_2 film have been obtained. For both composites a significant decrease in the water uptake capacity of cellulose fibres was observed.

Sol-gel processing is a well known technique for preparing silica particles, organic-inorganic nanocomposites and forms the basis for various routes employed in the fabrication of a wide diversity of functional materials [34, 63]. The idea of the sol–gel process is to use metal (namely silicon) alkoxides as molecular precursors and exploit their reactivity in solution towards hydrolysis and condensation in a very large range of pH and at room temperature [31, 34, 63, 64].

Despite the promising results obtained, the sol-gel technology offers some disadvantages: (1) the starting materials are expensive and moisture sensitive, (2) removal of solvent and organic by-products from gel is relatively difficult and (3) the volume shrinkage upon sol-gel transition is large [65]. Furthermore, sol–gel reactions are affected by many reaction parameters such as structure and concentration of reactants, solvents and catalysts [66]. Another aspect that should be taken into account is the impossibility of preparing hybrid inorganic materials by sol-gel method, such as SiO_2@Ag_2S [67], SiO_2@Bi_2S_3 [48], SiO_2@ZnO [68], SiO_2@CdSe [69], SiO_2@CdS [70] and others which could prevent composite leaching, as well as improve their properties and/or confer them multifunctional characteristics.

Graham [71] was the first researcher that investigated possible interactions between silicic acid and biopolymers more than a hundred years ago. Nowadays, biocompatible polymers associated to silica have been intensely studied not only focusing on obtaining materials with improved mechanical resistance, higher thermal and chemical stability and biocompatibility [26, 27, 63] as well as in some cases, other improved functional properties such as anti-fungal characteristic [67], optical properties [72] and reduced water uptake capacity of the biopolymer [38]. Moreover, biopolymer/silica nanocomposites with suitable porosity can be used for the design of membranes

and coatings, drug delivery systems and also for encapsulation of bioactive molecules such as enzymes, antibodies, yeast and plant cells or even bacteria, resulting in functional biomaterials for different biotechnological applications, including biosensors and bioreactors [73].

Coradin *et al*. [31, 64, 74-78] have investigated the preparation and application in biotechnology of biopolymer/silica nanocomposites produced using the sol-gel method. The imprisonment of enzymes in the pores of the silica matrix preserves its catalytic activity, since the silica matrix may exert a protective effect against enzyme denaturation even under harsh conditions. Gill and Ballesteros [79] have extensively reviewed the use of a wide number of alkoxysilanes for this purpose. The biomolecules entrapped often retain a sufficient level of activity and functionality presumably because of sufficient retention of their native-state conformations. Meanwhile, the matrix pores allow the diffusion of reactant molecules and their reaction with the entrapped biomolecules.

Nevertheless, natural biomolecules can not usually be involved in the common sol-gel processing to fabricate homogeneous hybrid materials. The main restriction is the poor biocompatibility of general silica precursors. Furthermore, in opposite to biopolymers that are present in most biological environments, silica does not constitute a natural medium for most biomolecules or cells. As a consequence, sol-gel mineral hosts exhibit several properties, including swelling behaviour, mechanical strength and, maybe even more crucial, surface physico-chemistry, that may not fit to the requirements of fully-maintained biological activity [31, 63].

Still on the subject matter of bionanocomposites based silica, Shchipunov's group has intensively investigated the use of polysaccharides as organic component in the preparation of this type of materials [63, 80-85]. This is the case for three-dimensional hybrid matrices resulting from the combination of tetrakis (2-hydroxy ethyl) orthosilicate (THEOS) with xanthan, locust bean gum or a cationic derivative of hydroxyethylcellulose, which have been reported as excellent networks for the long term immobilization of $1\rightarrow3$-β-D-glucanase and α-D-galactosidase.

Chitosan is one the most studied natural polysaccharide regarding the preparation of silica-based hybrid materials prepared by the sol–gel method. The resulting composites can be prepared with different physical forms such as films or colloidal suspensions as it will be discussed in next sessions. For example, silica generated by the sol–gel method from TEOS or TMOS in the presence of chitosan, yields biopolymer-silica nanocomposites whose morphology and applications can be determined by the experimental conditions adopted for the preparation [86-90]. Similarly to amorphous silica, microfibrous crystalline silicates such as sepiolite, (a complex magnesium silicate, $Mg_4Si_6O_{15}(OH)_2.6H_2O$), which contains silanol groups (Si-OH) covering the external mineral surface [91] have been effectively linked to the biopolymer.

Taking into account the film-forming property of chitosan and the great promise of silica xerogels for biomedical applications, Lee *et al*. [90] have recently reported on chitosan–silica xerogel hybrid membranes prepared by sol–gel hybridization with advantageous properties as bioactive guided bone regeneration (GBR) membranes. Moreover, the bone bioactive and drug-carrying potential of the xerogel [92] improved wound healing and bone-forming ability of the chitosan polymer. This fact was proven by the higher adhesion and active growth of osteoblastic cells on the hybrid membrane than those observed on the pristine chitosan membrane.

In addition to the nanocomposite studies mentioned above, a large number of bionanocomposites obtained by sol-gel or other methods have also been studied by our research group using vegetal cellulose and SiO_2 [38, 93, 94], bacterial or vegetable cellulose and $AgNO_3$ [95, 96], vegetable cellulose and TiO_2 [97, 98], vegetable cellulose and ZnO [99], vegetable cellulose and $CaCO_3$ [100], bacterial cellulose and Au@SiO_2 [72], kappa-, iota- and lambda- carrageenan and Fe_3O_4 [101, 102] and kappa-carrageenan and SiO_2 [101-103].

1.2. Aims and outline of the thesis

Despite the attractive properties of bionanocomposites, the available studies on this subject are still very scarce in comparison to synthetic polymer-based nanocomposites. The heterogeneity inherent to natural samples, their intrinsic characteristics as well as the not so wide knowledge about the appropriated routes for the preparation of bionanocomposites constitute some of the impediments to the development of these new materials. Hence, in this thesis we have tried to overcome at least some of these difficulties by preparing new biopolymer based nanocomposites under different experimental conditions in order to obtain materials with improved properties and to contribute to a better understanding of the structure-function relationships in the bionanocomposites prepared.

In view of the limitations of the sol-gel method discussed before, the direct addition of silica (SiO_2) particles suspension to the polysaccharidic matrix has been used as an alternative approach. This strategy was reported for charged polysaccharides such as xanthan gum [104] and *k*-carrageenan [103] and is studied in this thesis to prepare bionanocomposite suspensions and films.

As regards the inorganic fillers, in spite of the functional properties conferred to composites by fillers with a high aspect ratio discussed before, in this thesis spherical silica particles were chosen as the inorganic component to be incorporated into the bionanocomposites. Besides the fact that silica involves an easy preparation/production method it allows control over shape and size. Moreover, the particles have also a high surface area, which can promote changes in the polymer

matrix and it offers various possibilities of surface modification [29, 105, 106]. Furthermore, it provides a model for the study of a variety of hybrid nanoparticles consisting of different cores but having in common a silica shell, such as SiO_2@ZnO [68, 107], SiO_2@CdS [69], SiO_2@ZnS [108, 109] and others which have been prepared in our research laboratory and elsewhere [110].

An important aspect that must be taken into account whilst reading this thesis is that silica particles with average diameter of 100 nm or greater have been used in the preparation of the different biocomposites. Yet, nanoparticles and associated technologies refer strictly to the use of particles with at least one dimension of 100 nm or less.

Three different polysaccharides were used as the biopolymeric matrix and silica or modified silica particles as the fillers to obtain polysaccharide/silica nanocomposites. A simple mixture method of each component was used for this purpose.

The main objectives of this thesis were:

1. To prepare novel polysaccharide based nanocomposites by simply dispersing morphologically well-defined SiO_2 particles in the polysaccharidic matrix alternatively to the sol-gel method;
2. To understand the effect of nanosized silica fillers on the structure and rheological properties of locust bean gum, chitosan and xanthan gum dispersions, with particular interest in the effects of silica load, particle size, pH and ionic strength of the system;
3. To enhance the functional properties of chitosan films through incorporation of silica particles and to improve the dispersability of SiO_2 particles and their compatibility with the biopolymer matrix in order to obtain a better understanding of the interface behaviour between inorganic/organic compounds, which might help predict the main properties and applications of these bionanocomposites whether on suspension or film form.

This thesis comprises essentially 5 (five) chapters in which are described and discussed the principal characteristics of the bionanocomposites obtained.

In the first Chapter, a general introduction regarding bionanocomposites, their different natures and applications is presented. Considerations on the use of polysaccharides as matrices and distinct types of inorganic particles as fillers, including silica particles, used in this work, are also described.

The second Chapter is devoted to the synthesis and characterization of spherical SiO_2 particles. As referred above these particles were used as fillers in the polysaccharide matrix because of their morphological, surface and chemical characteristics were crucial. In order to enhance the

compatibility with the biopolymer the SiO_2 surfaces were modified and characterized. Initially, SiO_2 nanoparticles were modified with two different silane coupling agents, i.e. 3-methacryloxypropyltrimethoxysilane (MPS) and the 3-aminopropyltrimethoxysilane (APS). Silica modified with MPS was then encapsulated with poly(glycidyl methacrylate) (PGMA) via emulsion polymerization and used directly in the bionanocomposite suspensions. SiO_2 modified with APS was used in the preparation of bionanocomposites films. The characterization of these particles was carried out by infrared spectroscopy (FTIR), scanning electronic microscopy (SEM), transmission electronic microscopy (TEM), thermogravimetric analysis (TGA), dynamic light scattering (DLS) (size and zeta potential) and contact angle measurements.

In the third Chapter the preparation and characterization of polysaccharide/silica suspensions is described. The characterization of these bionanocomposite suspensions was based on their mechanical and morphological properties through the study of their rheological properties and microstructure by cryo-SEM analysis. Three types of polysaccharides were tested: a non-ionic (locust bean gum), a cationic (chitosan) and an anionic (xanthan gum) polysaccharide with different gelling properties. The characteristics of these composite suspensions were evaluated under different conditions. Weak and/or more structured systems could be obtained depending on the concentration and size of the silica nanoparticles, pH and ionic strength of the system.

In the fourth Chapter, the preparation and characterization of chitosan/silica bionanocomposite films is described. Chitosan/silica films were obtained via solvent casting method. In order to improve the dispersion of the SiO_2 nanoparticles into the polysaccharidic matrix, these particles were modified with APS as described in the Chapter 2. Moreover a polyol was added to the mixture aiming at reducing the chitosan stiffness and improving nanoparticle dispersability. The characterization of the surface, barrier, mechanical and thermal properties of the bionanocomposite films was carried using different techniques, such as, uniaxial tension tests, FTIR, TGA, contact angle and vapour water permeability measurements, SEM and atomic force microscopy (AFM).

In the fifth and last Chapter the principal conclusions from the thesis are reported as well as some suggestions for future work.

2 Silica nanoparticles: preparation and surface modification

2.1. Introduction

Numerous references about nanoparticles with different size and morphologies have been found for distinct applications [37, 38, 41, 43, 111-118]. In this Chapter, the synthesis and the characterization of silica nanoparticles is discussed as well as their surface modification for subsequent use as fillers in the preparation of polymer based nanocomposites.

Nanoparticles have a high surface area and when dispersed in polymeric matrices they can promote changes in the properties of the matrix which are related to the specific interactions between the fillers and the polymer. Such interactions can influence the molecular dynamics of the polymer, resulting in significant changes in its physical properties, particularly in its thermal and/or mechanical behaviour [29].

The possibility to combine properties of organic, bio and inorganic components in a unique material is an old challenge starting with the beginning of the industrial era [119]. Many chemical modification methods for inorganic particles have been developed in order to improve the compatibility between these materials. Amongst inorganic fillers, silica (SiO_2) particles have been the most studied. Alcohols, polystyrene, chlorides, Grignard reagents and silane coupling agents are some of the compounds that have been used to modify SiO_2 surfaces [120]. These modified SiO_2 particles are then able to be linked to polymer matrices yielding new nanostructured materials with novel or improved properties such as flammable retardancy, barrier properties, thermal and mechanical properties [121].

As discussed in the Chapter 1 apart from nanomaterials prepared using petroleum-derived polymers, the use of SiO_2 in biobased materials is currently growing [2, 26, 27, 31, 103]. However, the affinity between the inorganic and the bioorganic counterparts, which determines the stability of the resulting biocomposites, depends on the interaction mechanisms governing the assembly processes. In our case, SiO_2 surface modification has been the alternative studied to increase the compatibility with the polysaccharide and to improve the bionanocomposite properties. In this Chapter special attention will be given to the preparation of silica and modified silica particles as well as their stability and characterization.

2.1.1. SiO_2 nanoparticles

As mentioned above, among numerous inorganic fillers, silica nanoparticles are commonly reported in the literature. This particular interest may be due to the ease of synthesis and precise control of the size, shape, composition and size distribution of the particles [105, 106].

Colloidal SiO_2 particles with narrow size distribution have wide application not only in the field of physical-chemistry dealing with the dynamic behaviour and stability of particle systems [122] but also in industries including pigments, pharmacy, photographic emulsions, ceramics, chromatography, catalysts, and chemical mechanical polishing [117]. SiO_2 nanoparticles act differently in each of these applications. In fact, the quality of some of these products is highly dependent on the size and size distribution of the particles [115].

Sol-gel methodology has been extensively studied for several decades as a method to prepare ceramic precursors and inorganic glasses at relatively low temperatures. Since Ebelmam [123, 124] observed in the mid-1800s that the hydrolysis of tetraethoxysilane (TEOS, $Si(OC_2H_5)_4$) under acid conditions yielded SiO_2, several researchers have studied and optimized new methods for preparing SiO_2 nanoparticles with controlled dimensions and shapes.

Back in 1968, Stöber *et al.* [37] reported a simple synthetic method to prepare monodisperse spherical silica particles which is still the most popular method used up to now though with some modifications. The synthesis proceeds via the hydrolysis of a silicon alkoxide and polycondensation reaction(s). The most common silicon alkoxide used is TEOS because it is readily purified and has a relatively slow and controllable rate of reaction [125]. Thus, in this thesis the sol-gel reaction medium used to prepare silica consisted of TEOS in a mixture of alcohol, water and ammonia (catalyst).

The sol-gel reactions of alkoxysilane are described in Scheme 2.1. This reaction scheme is naturally a simplification of the more complex process that leads to the formation of silica particles [117]. In general, the hydrolysis reaction gives the singly hydrolyzed TEOS monomer (Equation 2.1). This hydrolyzed intermediate undergoes condensation to eventually form the silica three-dimensional network (Equations 2.2 and 2.3).

(1) Hydrolysis:

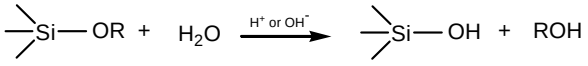

Equation 2.1

(2) Polycondensation:

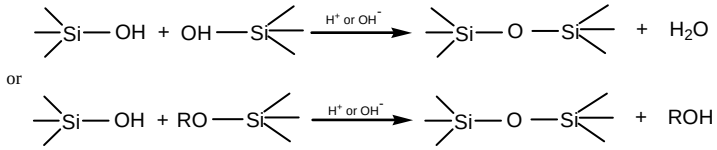

Equations 2.2 e 2.3

Scheme 2.1: Reactions from sol-gel method: (1) hydrolysis and (2) polycondensation of alkoxysilane. Adapted from [126].

If these sol-gel reactions are complete, full condensed silica is obtained in this process that can be summarized by the following equation:

$$Si(OR)_4 + 2H_2O \xrightarrow{H^+ \text{ or } OH^-} SiO_2 + 4ROH \qquad \text{Equation 2.4}$$

The resultant particles are stabilized by electrostatic repulsions due to the ammonia ions as shown in Scheme 2.2. A number of research groups have reported studies related to the mechanisms of particle nucleation and growth to explain the highly monodisperse nature of these particles [112, 116, 127].

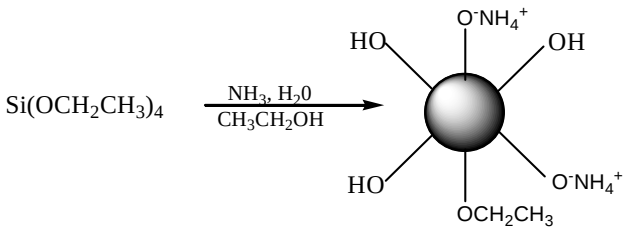

Scheme 2.2: Silica particles stabilization. Reproduced from [106].

According to Park *et al.* [115], the main factors affecting the preparation of SiO_2 nanoparticles are: reaction temperature, the ratio of reagents R=([H_2O]/[TEOS]), concentration of ammonia (NH_4OH), and the feed rate of reactant. SiO_2 nanoparticles with a narrow size distribution, generally called "monodisperse" and spherically uniform were obtained by Pinto *et al*. [38]. Based on the Stöber method [37] these authors have found that there was a linear dependence of the particle diameter with the logarithm of NH_3 concentration within the range investigated. As a consequence, the synthesis of well-defined SiO_2 nanoparticles for a selected interval of particle sizes between 100 and 500 nm could be performed just by varying the concentration of NH_3 and maintaining all the other experimental parameters constant. Following the work of these researchers, the strategy used in this thesis was to vary the NH_3 concentration to obtain monodisperse SiO_2 nanoparticles with different sizes (300 and 500 nm) as it will be discussed later.

Although small SiO_2 nanoparticles obtained by the sol-gel method are monodisperse [37, 38], their surface energy is very high and as a consequence they tend to agglomerate. A way to overcome this effect is the use of stabilizers. This is the case of the commercial colloidal silica particles used in this thesis. Apart from the tendency for agglomeration of the bare SiO_2, its dispersability in polymer matrix is difficult due to its hydrophilic nature in contact with the more hydrophobic polymer. Therefore, to reach a good dispersion of the inorganic particles and

to increase their compatibility with the polymer, several physical or chemical approaches have been used to modify the nanoparticles surface [106, 112, 120] as will be discussed in the next sessions.

2.1.2. Modification of SiO_2 nanoparticles

As mentioned above one important factor that should be taken into account in the choice of the filler is its stability. Colloidal particles in a dispersion medium always show Brownian motion and hence collide with each other frequently. The stability of colloids is thus determined by the interaction between the particles during such collisions. There are two basic interactions: one being attractive and the other repulsive. When attraction dominates flocculation will occur, and when repulsion dominates, the system will be stable [128].

The high surface energy of nanoparticles makes them reactive, and most systems undergo aggregation without protection of their surfaces. The protection of particle surface is simply to provide long range repulsions between the particles to impart stability. This repulsion should be at least as strong as the attractive forces [128]. Colloidal stability can be obtained by surrounding colloidal particles with:

- an electrical double layer (electrostatic or charge stabilization);
- adsorbed or chemically attached molecules (steric and/or electrostatic stabilization);
- free polymer in the dispersion medium (depletion stabilization);

The affinity between the inorganic fillers and polymers is also an important aspect to consider in the preparation of materials. The compatibility of the fillers with the matrix can be improved through surface chemical modification of components. In this thesis the surface modification was focused on the silica particles. The modification of the nanoparticle surfaces has been widely investigated for a large variety of applications in the areas of sorption, separation, wetting, adhesion, corrosion, dispersion, and to prepare advanced optical or electronic devices [129].

As it is well-known SiO_2 nanoparticles can improve for example the scratch and abrasion resistance, hardness, thermal stability, rheological and barrier properties of composites and they can be widely used in plastics, rubbers, coatings, and adhesives, among other materials and applications. Nevertheless, bare SiO_2 is not easy to use in common organic or polymer systems due to its hydrophilic surface [120] and thus often becomes necessary to modify its surface to increase its stability in the medium and its affinity with the other components.

One first approach used in this thesis to improve the silica features was to modify its surface with silane coupling agents which are commonly used in its surface functionalization. Silicon alkoxides promote the chemical compatibility between the components via hydrogen bridging, electrostatic interactions or covalent bonds at the inorganic/organic interface [29]. Moreover, SiO_2 surface functionalization not only facilitates the compatibility of the different components but it also allows the introduction of different functional groups in the inorganic material [110] which can provide different properties and applications depending on the "active group" (amine, epoxide, acrylate, vinyl, isocyanate group, etc.) on the SiO_2 surface [6, 105, 111, 112, 118, 130, 131].

Among the silane coupling agents commonly found in the literature to be attached on the silica surface, the 3-methacryloxypropyltrimethoxysilane (MPS) [132] and 3-aminopropyltrimethoxysilane (APS) [165] have been widely used and studied. Moreover, these coupling agents are dually functional, hence in this thesis they were chosen in accordance with the final application of the modified nanoparticles. Their chemical structures are shown in Figure 2.1.

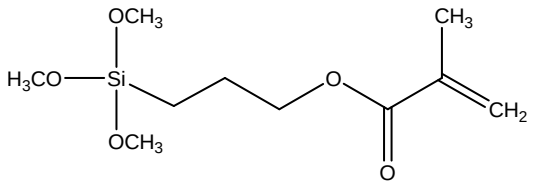

3-methacryloxypropyltrimethoxysilane

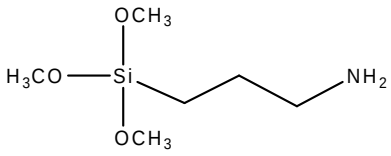

3-aminopropyltrimethoxysilane

Figure 2.1: Silane coupling agents used in the surface functionalization of SiO_2 particles.

As regards MPS the alkoxysilane moiety it is used for attachment onto the silica surface whilst the terminal C = C double bond can be of particular interest to promote covalent bonding in the case of *in situ* polymerization of a polymer matrix or shell [120, 132, 133]. The mechanisms involving each of these functional groups have been extensively discussed by Philipse and Vrij [134] and Bourgeat-Lami and Lang [39].

First, the methoxy groups of MPS hydrolyze under the influence of the base and water, both present in the alcosol. Silanols are formed which associate and form oligomers. These oligomers adsorb on the silica surface by hydrogen bonding and condense on drying to form siloxane linkages. SiO_2 nanoparticles modified with MPS (SiO_2@MPS) were used in the preparation of polymer nanocomposite using glycidyl methacrylate (GMA) by conventional radical polymerization as it will be discussed next.

In the case of APS, the chemical path involved in the functionalization of SiO_2 particles is more complex. According to Vrancken *et al*. [135] the mechanism involves adsorption of APS onto the silica surface via hydrogen bonds between some of its amine groups and the silanol on the SiO_2 particles adopting an amine-down position. At a later stage these APS molecules flip and adopt the amine-up position after acting as catalyst during the condensation reaction between the silane moiety of adjacent APS molecules and the silanol groups on the silica surface yielding siloxane bonds in the absence of the water [135, 136].

Since the amino groups of the APS molecule change the electrical double layer in the medium, it is expected a better silica colloidal stability and/or better compatibility with polymer matrices.

Therefore, silica nanoparticles modified with APS (SiO_2@APS) were used in the preparation of chitosan composite films as it will be discussed in Chapter 4.

Another approach used in this thesis to improve silica stability was to disperse the silica particles polyols to yield steric and/or electrostatic stabilization using poly(ethyleneglycol 4000) (PEG) and glycerol (GLY). It is known that, in aqueous dispersions, the electrostatic stabilization of the bare silica dispersion will be eliminated at high ionic strength as the electrostatic repulsion then only has a very short range and no longer protects the silica particles against coagulation. In both polar and apolar solvents, the colloidal particles can be stabilized sterically by the presence of polymers adsorbed on or chemically bound to the surface of the colloidal particles [137, 138]. The polymer layer on the particle surface can prevent the coagulation of the particles or, when the layer is not thick enough, it may reduce the coagulation rate [139]. An example of this approach is the work of Hao *et al.* [137], who prepared monodisperse spherical PEG–coated silica nanoparticles at room temperature. The PEG-coated silica nanoparticles showed enhanced colloidal stability when re-dispersed into aqueous solutions from the dried state as a result of the steric stabilization function of the PEG polymer grafted on the surface of particles. Moreover, a non-specific protein-binding test was also carried out to show that the PEG coating can help reduce protein adsorption onto the surface of the particles ensuring to the biocompatibility of these PEG-coated particles.

The stabilization of the silica particles using PEG and/or GLY will be discussed in the Chapter 4.

2.1.3. Preparation of polymer/SiO_2 nanocomposites

Surface functionalization of inorganic fillers with a polymer shell is attracting attention because polymer coatings alter the interfacial properties of these modified particles. Whilst nanoparticles physical properties are governed by both the size and shape of the inorganic core and the surrounding organic layer [106] it is known that mechanical and thermal properties of the matrix polymers in hybrid systems can be improved by the compatibility of the nanoparticles with the matrix [29].

On the other hand, the nanocomposites properties are greatly influenced by both the dispersing degree of nanoparticles in the matrix polymer and the interfacial adhesion between the inorganic and organic components [140]. This can be achieved by manipulating the components characteristics during the synthetic steps and controlling the synthesis parameters. Four general preparative methods of polymer/silica nanocomposites are depicted in Scheme 2.3.

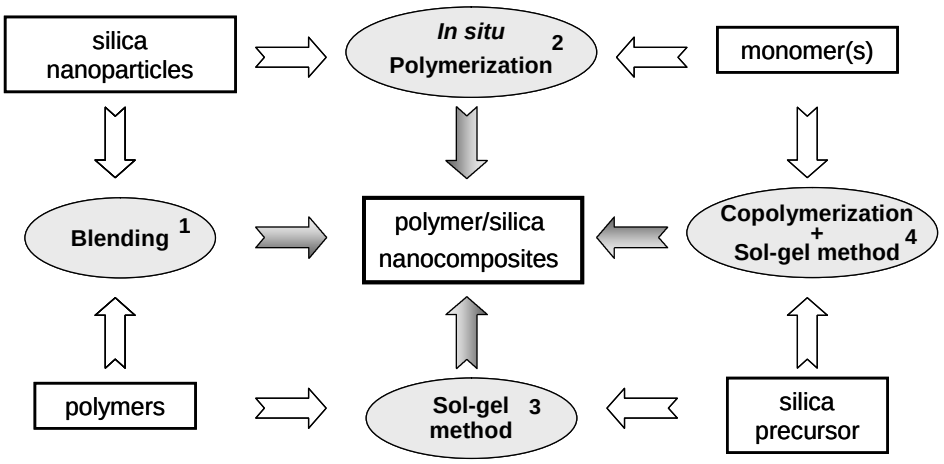

Scheme 2.3: Synthetic strategies to prepare polymer/silica nanocomposites. Adapted from [121].

Although good results have been obtained when nanocomposites are prepared by the expeditious and economical process of simple mixture of components (1, Scheme 2.3), the dispersing degree of nanoparticles and the interfacial adhesion are not always sufficient to obtain desirable material properties [141]. Therefore, other synthetic approaches to prepare nanocomposites with controlled composition and microstructure have been extensively reported in the literature [121, 142-148].

Recently Zou *et al.* [121] revised the main methods to prepare polymer/silica nanocomposites, the characterization techniques, properties, and applications. In general, synthetic strategies involving *in situ* synthesis allow the control at the molecular level of the final nanocomposite

and have gained an important role in this area [29], since new advanced technological applications require highly structured and homogeneous nanomaterials.

There are several advantages in using the *in situ* polymerization method (2, Scheme 2.3). These include ease of handling, the speed of the process, and better performance of the final products [149]. Generally, the process of *in situ* polymerization involves three continuous steps. First, the nanoscale additives are pretreated with appropriate surface modifiers and then the modified additives are dispersed into monomer. This is followed by polymerization and then the nanocomposites are formed *in situ* during the polymerization [121].

Regarding the types of *in situ* polymerization methods, polymer based nanocomposites can be prepared using different techniques such as polymerization suspension [150, 151], dispersion [39, 152, 153], emulsion [130, 146] and mini-emulsion processes [140, 143, 148]. By introducing coupling agents or reactive groups onto the surface of nanoparticles, a good interfacial adhesion between inorganic and organic components can be achieved. Bulk and solution polymerization can also be used but they are not so attractive. Among the polymerization techniques mentioned above, emulsion polymerization is very frequently referenced in the literature for the monomer used in this thesis (GMA) [146, 154, 155], consequently this technique was chosen and is discussed next.

Another synthetic strategy which was already discussed is the sol-gel process (3, Scheme 2.3). In this method silica precursors are added to the polymer which acts as template and sol-gel reactions take place. The silica is synthesized *in situ* in a polymer solution reinforces the structure of the final nanocomposites yielding polymer/silica hybrid materials. This method is widely used to prepare polysaccharide/silica nanocomposites and it has been often referred in the literature [31, 63, 64, 74, 75, 80-82, 84, 85, 156].

The last and perhaps the less investigated method in the literature consist in the initial copomolymerization of latex systems and subsequent addition of an alkoxysilane (4, Scheme 2.3). In general, these reactions involve the formation of self-cross linking films, however, in order to obtain stable latexes with good shelf stability it is essential that premature hydrolysis and cross linking reactions must be avoided. Marcu *et al*. [157] proposed an alternative to protect the silane moieties from hydrolysis and premature cross-linking through of the incorporation of alkoxysilanes into acrylate latex systems via *in situ* polymerization.

2.1.3.1. Preparation of polymer/SiO_2 nanocomposites using emulsion polymerization

Emulsion polymerization is a heterogeneous free radical polymerization process which involves the reaction of free radicals with relatively hydrophobic monomer molecules within submicron polymer particles dispersed in a continuous aqueous phase [158]. The reaction system is characterized by the emulsified monomer droplets (*ca.* 1–10 μm in diameter) that act as reservoirs dispersed in the continuous aqueous phase with the aid of a surfactant at the very beginning of polymerization. Monomer swollen micelles (*ca.* 5 – 10 nm in diameter) may also exist in the reaction system provided that the concentration of surfactant in the aqueous phase is above its critical micelle concentration (CMC). Only a small fraction of the relatively hydrophobic monomer is present in the micelles (if present) or dissolved in the aqueous phase. The polymerization is initiated by the addition of a water-soluble initiator [147].

Due to the poor compatibility between the polymer produced and water, a large oil-water interfacial area is generated as the particle nuclei form and grow in size during the polymerization. Thus, effective stabilizers such as ionic and nonionic surfactants, or protective colloids (e.g., hydroxyethyl cellulose, polyvinyl alcohol, polyvinyl pyrrolidone and dextrin), which can be physically adsorbed or chemically incorporated onto the particle surface, are generally required to prevent the interactive polymer particles from coagulation [158].

In real systems the monomer can be partitioned between the different phases. The amount of partitioning that occurs will depend on the thermodynamic characteristics of the system (temperature, pressure, pH, composition, type and concentration of surfactant, etc.) [159]. Among these parameters different types of surfactant were tested in this thesis in order to tune the surface charge of the resulting polymer particles. Appropriate initiator was chosen depending on the surfactant used.

The polymerization is one of the most important methods used in the surface modification of inorganic particles. Early in the 1990s, Espiard *et al*. [132, 160, 161] reported results on the encapsulation of silica particles via emulsion polymerization using MPS as coupling agent. The silane molecule allows the grafting of a significant amount of polymer from the early stages of polymerization because MPS provides reactive double bonds for covalent attachment of the growing polymer chains on the silica surface. Furthermore, emulsion polymerization offers strong potential advantages for modifying the surface of nanosized particles via polymer encapsulation of functionalized particles and/or using small amounts of surfactant [160].

Bourgeat-Lami [5] proposed three main steps for the mechanism of emulsion polymerization in the presence of inorganic nanoparticles as illustrated in Figure 2.2. 1) the surfactant adsorbs to the surface of inorganic solids forming micellar aggregates around them; 2) the monomer is solubilised in the micelles adsorbed on the inorganic solids surface and 3) the polymerization reaction occurs from monomers and oligo-radicals present inside the micelles resulting in inorganic materials encapsulated with polymer [29].

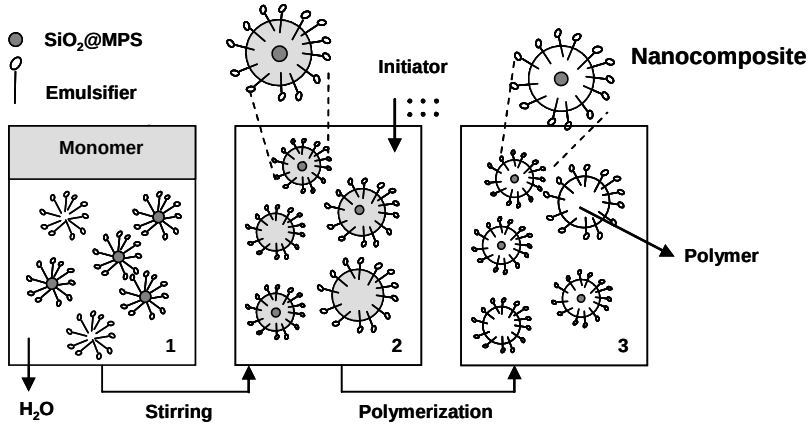

Figure 2.2: General illustration of the principle of encapsulation by emulsion. Adapted from [5].

Silica nanoparticles encapsulated with polymer were prepared in this thesis aiming at a better compatibility between inorganic particles and the polysaccharides. For this purpose poly(glycidyl methacrylate) (PGMA) was selected to coat silica particles in order to take advantage of the versatility of the epoxy group to promote strong interactions with polysaccharide matrices.

The use of this monomer has also been explored by Zeng *et al.* [146] to prepare epoxy-functionalized polystyrene/silica (PGMA@PS/SiO_2) core–shell composite nanoparticles via emulsion polymerization using a mixture of ionic sodium dodecyl sulfate (SDS) and non-ionic (mono-*p*-nonyl phenyl ether) surfactants. Li *et al.* [162] prepared via reversible addition-fragmentation chain ransfer polymerization (RAFT) well-defined tethered brushes PGMA polymer on a silicon wafer. Recently, surface-initiated atom transfer radical polymerization (ATRP) technique was used to prepare functional (or multifunctional) nanoparticles/silica microsphere assemblies. A thin shell of PGMA was grafted on the surface of silica and then, various types of nanoparticles, including water-soluble CdTe quantum dots, Au nanoparticles and oil-soluble Fe_3O_4 nanoparticles were assembled on silica microspheres, respectively, or simultaneously [163].

Despite the variety of mechanisms for the silica encapsulation mentioned in literature, in this work emulsion polymerization combined with conventional radical was chosen as the preparative method of PGMA@silica particles since it has a faster polymerization rate besides

the fact that the polymers obtained have high molecular weights, although this is not the major issue in this case. In addition, as discussed before, emulsion polymerization is a versatile method to prepare nanocomposites in aqueous media and is more practical than other ones.

2.2. Experimental part

2.2.1. Reagents

Tetraethoxysilane (TEOS, Sigma-Aldrich) 98%, 3-methacryloxypropyltrimethoxysilane (MPS, Sigma-Aldrich), 3-aminopropyltrimethoxysilane (APS, Fluka), ammonia aqueous solution 25% NH_3 (Merck), and ethanol (Fluka) were used as purchased without further purification. Water was purified using a Sation 8000/ Sation 9000 purification unit. The monomer glycidyl methacrylate (GMA, Sigma-Aldrich) was purified over a column of neutral aluminium oxide to remove the inhibitor and stored at 4^{o} C. The free radical initiators sodium persulfate (KPS, Acros 98%) and 2,2'-Azobis(2-methylpropionamidine) dihydrochloride (AIBA, Sigma-Aldrich), as well as the surfactants sodium dodecyl sulfate (SDS, Sigma-Aldrich), cetyltrimethylammonium bromide (CTAB, Sigma-Aldrich), and 3-sulfopropyl methacrylate potassium salt (SPM, Sigma-Aldrich) were used as purchased. Xanthan gum (XG) used as emulsifier was kindly provided by Kelco Oilfield Group. Colloidal silica particles SYTON HT-50 (Sigma-Aldrich) were used as purchased.

2.2.2. Characterization methods

Particle size and zeta potential were determined by dynamic light-scattering (DLS) using a Brookvaven Zeta PALS and zeta-potential analyzer.

The infrared spectra were recorded using a Mattson 7000 with Fourier Transformed (FTIR), with a resolution of 2 cm^{-1} and an acquisition speed of 128 scans/min for each spectrum in the wavenumber range of 4400 cm^{-1} to 200 cm^{-1}. Solid samples were mixed with KBr (Riedel de Häen, 99.5 %) (~1% wt. sample to KBr), ground and pressed in order to obtain optically transparent disks. In the case of liquid samples, they were dissolved in appropriate solvents, and films were casted on a NaCl window.

Thermal analyses were performed on a Shimadzu TGA-50 analyzer from 25 up to 700 ºC under N_2 flow and heating rate of 10 ºC/ minute.

The absorbance spectra were recorded in a double beam spectrophotometer Jasco V-560 UV/VIS.

Scanning electron microscopy (SEM) images were obtained using a FEG-SEM Hitachi S4100 microscope operating at 25 kV. For the as-prepared nanocomposite latex the samples were centrifuged for 5 minutes at 3500 rpm. The solid was kept and the supernatant discarded. A diluted aqueous suspension was prepared. One drop of that suspension was deposited on the metallic support and left to evaporate the solvent after which a carbon thin layer was deposited.

Transmission electron microscopy (TEM) was carried out on a Hitachi H-9000 microscope operating at 250 kV. The samples were prepared in a high dilution factor as described for SEM analysis.

Wettability measurements were recorded using a NIMA 9000 tensiometer equipped with a Washburn cup in accordance with the method described in the literature [164]. Three separated results were measured to obtain representative values of water contact angles (WCA).

2.2.3. Synthesis of nanoparticles

2.2.3.1. Preparation of SiO_2 nanoparticles

A stabilized suspension of SiO_2 particles with average diameter (AD) equal to 100 nm (Si-100) was purchased from Aldrich-Sigma and used after drying in an oven at 105 ºC for 16 h. SiO_2 particles with AD ~ 300 and 500 nm (named Si-300 and Si-500) were prepared using the Stöber method [37] with some minor modifications [38]. In a typical synthesis, TEOS was rapidly added to an Erlenmeyer flask containing ethanol, deionised water and ammonia aqueous solution (NH_3), under constant stirring. The reaction was allowed to proceed for 24 h, at room temperature, under moderate stirring covered with a plastic stopper to prevent evaporation and jamming. The SiO_2 particles were then collected by centrifugation, washed once with ethanol and twice with deionised water and, finally dried in an oven to dry at 50 ^{o}C for 24 h. Table 2.1 summarizes the volume of reagents used in the preparation of Si-300 and Si-500.

Table 2.1: Volume of reagents used in the preparation of spherical SiO_2 particles with different diameters.

Reagents	**Si-300 nm (mL)**	**Si-500 nm (mL)**
Ethanol	42.10	41.30
H_2O	4.5	4.5
NH_3	1.15	1.95
TEOS	2.25	2.25

Si-300 and Si-500 were used in the preparation of the nanocomposites after calcination at 700 ^{o}C for 4 h. Silica particles were characterized by FTIR spectroscopy, zeta potential, dynamic light scattering (DLS) and water contact angle (WCA) measurements. The morphology was analysed by scanning electron microscopy (SEM).

2.2.4. Surface modification of nanoparticles

2.2.4.1. Surface modification of SiO_2 particles with MPS

A silane coupling agent, the 3-methacryloxypropyltrimethoxysilane (MPS) was used in the surface modification of Si-100, Si-300 and Si-500 following Bourgeat-Lami and Lang procedure [39] (Scheme 2.4). In an Erlenmeyer, silica (0.5g) was dispersed in ultra-pure water (50 mL). This dispersion was submitted to an ultra-sound probe for 5 minutes in order to obtain well-dispersed silica particles. Then, the pH was verified and adjusted to 6 -7.5 with HCl or NaOH to avoid the homocondensation of MPS and at the same time avoid silica aggregation.

Next MPS was added to the dispersion. The amount of MPS necessary to cover the nanoparticles surface was estimated in accordance with the surface area of spherical silica (A_S) (Equation 2.5) as mentioned by Bourgeat-Lami and Lang [39]. A_S was calculated taking into account its AD obtained from SEM images or by DLS measurements. Moreover, based on the literature [111], the density (ρ) of the silanol groups on the silica surface was considered to be 1.8 g/cm^3. Based on this, an excess of MPS was added to SiO_2 previously prepared corresponding to an amount of MPS 2.5 times higher than the concentration of silanol groups on the surface of SiO_2 nanoparticles.

$$A_S = \frac{6000}{AD \times \rho}\left(m^2/g\right) \qquad \text{Equation 2.5}$$

where the number 6000 is a unit conversion factor

The silica dispersion with MPS was kept under stirring during four days. After this the free MPS was removed by dialysis using a cellulose membrane tube (Membra Cell from Polylabo size 2 Inf Dia 18/32'', 14.3 mm) previously boiled in distilled water (3 times). Membrane tubes were around 30 cm long containing *ca.* 15 mL of the dispersion. The extraction of non-reacted MPS was monitored by UV/Vis analysis. The absorption band of MPS at 206 nm was taken as

reference for the UV measurements until the absorbance measured was below 0.06 which takes around four days [110, 145, 148]. SiO_2@MPS samples were characterizated by FTIR spectroscopy, thermogravimetric analyses (TGA), zeta potential, DLS and WCA.

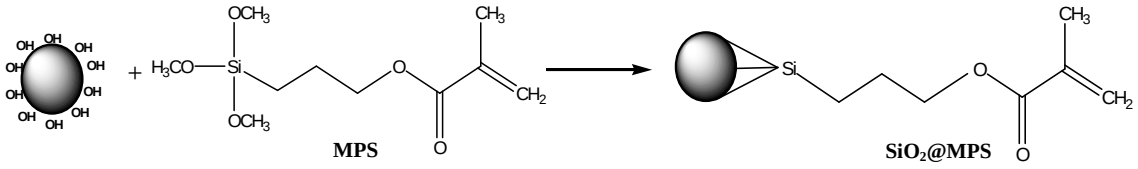

Scheme 2.4: Reaction scheme of surface modification of silica with MPS

2.2.4.2. Surface modification of SiO_2 particles with APS

Following Foschiera *et al.* method [165] (Scheme 2.5) Si-300 and Si-500 had their surface modified with 3-aminopropyltrimethoxysilane **(**APS). In a two-neck round-bottom flask, APS (140 μL, 802 μmol) was added to Si-300 (0.5g) dispersed in toluene (30 mL). The mixture was stirred for 22 h under reflux (110 ± 1 ^{o}C) under N_2 atmosphere. The resulting modified silica was filtered under vacuum using a polyamide membrane (NL16, 100 STUCK, 0.2 μm and ϕ 50 mm) and washed with toluene to eliminate unreacted 3-aminopropyltrimethoxysilane. The solid collected was dried in a desiccator at ambient temperature. The amounts used in this functionalization, also took into consideration the calculation of the surface area of silica particles mentioned above. SiO_2@APS samples were characterized by FTIR spectroscopy, TGA analyses, zeta potential, DLS and WCA.

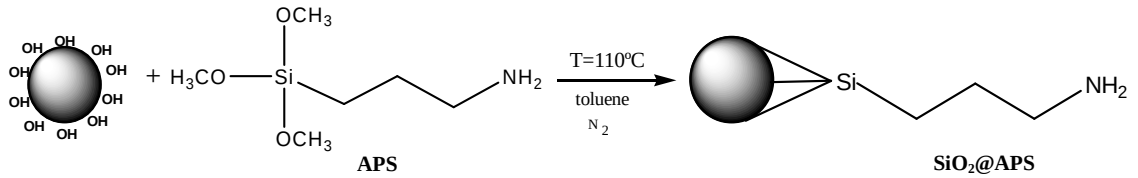

Scheme 2.5: Reaction scheme of surface modification of silica with APS.

2.2.4.3. Preparation of SiO_2@MPS@polymer nanocomposites

In a typical recipe for *in situ* emulsion polymerizations the surfactant SDS ($1.7x10^{-4}$ mol) was dissolved in Si-300@MPS aqueous dispersion (approx. 24g of Si-300@MPS aqueous dispersion containing 0.24g of Si-300). The mixture was introduced in a 25 mL jacket glass reactor equipped with a mechanical stirrer, N_2 inlet, thermostatic bath and a condenser. After

degassing the reaction medium with N_2 for ~10 minutes at room temperature, the monomer glycidyl methacrylate (GMA, 0.024 mol) and the initiator potassium persulfate solution (KPS, $4.62x10^{-5}$ mol) also previously degassed under a N_2 stream for ~ 10 min., were added to the reactor at 70ºC under stirring (4000 rpm). The polymerization reactions were carried out for 5 hours. At the end of the polymerization the conversion of the monomer was gravimetrically calculated by addition of methanol which led the PGMA to precipitate. The free GMA was removed from medium by filtration and washing with methanol.

Subsequent to polymerization, free PGMA particles were separated from the composite particles (Si-300@MPS@PGMA) by successive centrifugation and re-dispersion cycles using ultra pure water (15 min, 3000 rpm). This operation was repeated until the supernatant was clear. The Si-300@MPS@PGMA nanocomposite was dried in an oven at 40 ^{o}C for 24 h and then characterized by FTIR spectroscopy, TGA analyses and DLS. The morphology was analysed by TEM. This procedure was repeated using Si-100@MPS and different surfactant/emulsifiers and initiators, which are summarized in Table 2.2.

Table 2.2: Surfactant/Emulsifiers and initiators tested for the preparation of Si-100@MPS@PGMA nanocomposites.

Samples	Surfactant/Emulsifiers	Initiator*
Si-100@MPS@PGMA- 1	SDS (0.05g)	KPS
Si-100@MPS@PGMA-2	CTBA (0.062g)	AIBA
Si-100@MPS@PGMA-3	SPM (0.042g)	KPS
Si-100@MPS@PGMA-4	-	KPS
Si-100@MPS@PGMA-5	XG (0.05g)	KPS

PGMA - poly (glycidyl methacrylate); SDS - sodium dodecyl sulfate; KPS - potassium persulfate; CTAB - cetyltrimethylammonium bromide; AIBA - 2,2'-Azobis(2-methylpropionamidine) dihydrochloride; SPM - 3-sulfopropyl methacrylate potassium salt; XG - xanthan gum
***** 0.0125g of initiator.

2.2.5. Dispersion and analysis of modified silica particles in polysaccharide solutions

The improvement of the compatibility of modified silica particles (Si-100@MPS@PGMA) was preliminary tested by their addition to a polysaccharide (xanthan gum) solution. Initially the xanthan gum solution was prepared by dissolution of the gum powder in water, followed by its centrifugation at 12000 rpm for 20 minutes to remove residues. The aqueous xanthan gum solution (0.8 wt.%) was mixed (1:1) with Si-100@MPS@PGMA suspension as obtained after

emulsion polymerization. Upon adjusting the pH to 3 with HCl and/or NH_4OH, the colloidal stability of the system was assessed visually. The most stable suspensions were then stirred for 30 minutes and submitted to mild vacuum for 30 minutes in order to remove air bubbles and then transferred to a rheometer for testing its rheological behaviour.

2.3. Results and discussion

2.3.1. Characterization of SiO_2 particles

Calcinated SiO_2 nanoparticles (Si-300 and Si-500) were initially characterized by SEM in order to investigate their morphology and size as shown in Figure 2.3.

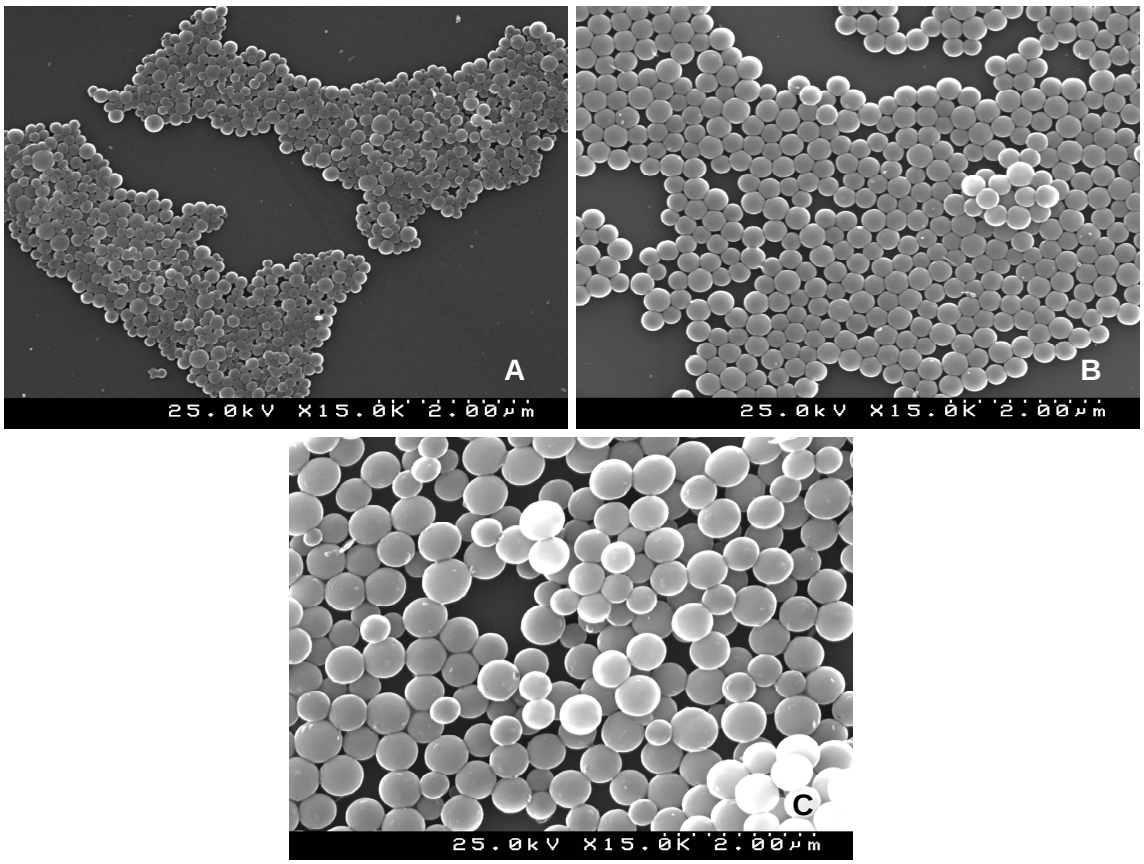

Figure 2.3: SEM images of SiO_2 particles: (A) Si-100, (B) Si-300 and (C) Si-500.

In general, SEM images revealed that both SiO_2 particles, commercial and prepared in laboratory (Figure 2.3A, B and C) were essentially spherical with uniform size and shape. Moreover, using ImageJ program at least 50 size measurements were obtained for each silica sample through their SEM images enabling to construct the size histograms of the SiO_2 particles shown in Figure 2.4.

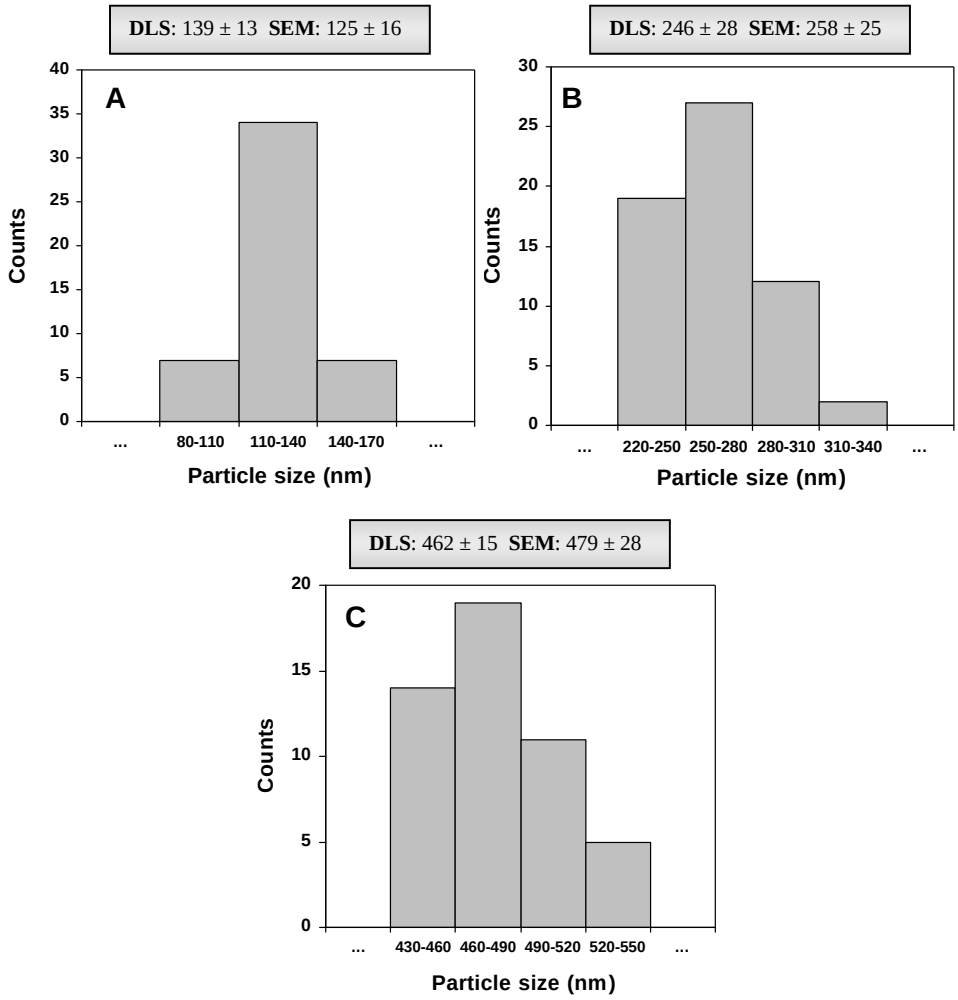

Figure 2.4: Particle size histograms obtained from SEM images of SiO_2 particles using ImageJ program: (A) Si-100, (B) Si-300 and (C) Si-500. For comparison the sample average diameters were also measured by DLS and SEM as is indicated in the inset.

A narrow size distribution of Si-100 spherical particles was obtained as observed in Figure 2.4A, however the Si-100 average size obtained from SEM images and DLS measurements was higher than that specified on its label. On the other hand, in Figure 2.4B and 2.4C, it is observed that in spite of the narrow particle size distributions for Si-300 and Si-500 prepared in our laboratory, these particles showed average sizes (DLS and SEM results) slightly smaller than those predicted by the procedure adopted [38].

Following the procedure established by Pinto *et al.* [38] in the preparation of both Si-300 and Si-500 the amount of water was kept constant but for si-500 a higher concentration of NH_3 was used. Taking into account the volatility of ammonia and consequently the effect of storage time, the quantity of ammonia used in the preparation of Si-300 and Si-500 was an approximation of that predicted in the experimental procedure [38], which may be responsible for the smaller

particle sizes observed in Figure 2.4B and C. These results are in agreement with the studies of Park e*t al*. [115] who observed that SiO_2 particles diameter increases with increasing NH_3 concentration. Indeed, these authors have shown that exact control of particle size requires full control of rection conditions in particular the concentration of NH_3. This is due to the fact that the NH_3 acts as a catalyst, promoting the hydrolysis and the polymerization (condensation) rate of TEOS, resulting in faster kinetics, and lager particle sizes as reported by Matsoukas and Gulari [166].

Silica particles were also characterized by FTIR spectroscopy and the typical vibrational bands of amorphous SiO_2 particles were easily identified for all samples and are summarised in Table 2.3. An illustrative FTIR spectrum for Si-300 after calcination is shown in Figure 2.5.

Table 2.3: FTIR characteristic bands of silica particles after thermal activation.

Attribution	**Group frequency (cm^{-1}) Experimental**			**Group frequency (cm^{-1}) Literature**
	Si-100	**Si-300**	**Si-500**	
ν O-H	3462	3445	3478	3700-3200 [167]
ν_A Si-O-Si	1119	1118	1120	1110-1000 [167]
ν_S Si-O-Si	808	824	816	800-820 [168]
δ Si-O-Si	478	476	478	450 -460 [168]

ν - Stretching δ - Bending A - asymmetric S – symmetric

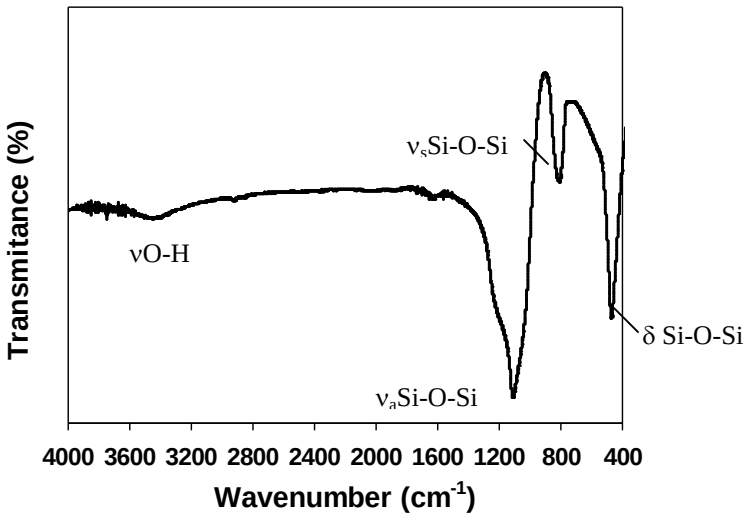

Figure 2.5: FTIR spectrum of Si-300 after calcination.

Although the characteristic band of the silanol groups on the silica surface has not been identified (910-830 cm^{-1}) it is not possible to conclude that the Si-OH groups are not present. The presence of the band between 3300 up to 3700 cm^{-1} can be associated to the free silanol groups on its surface [168]. In fact, this and other difficulties regarding silica characterization

have been reviewed by Iller [111], which gives a perspective of the complexity of silica surfaces.

Besides the effect of synthetic parameters it is known that the conditions (temperature, time and atmosphere chemistry) of the heat treatment are crucial for the final composition of the nanoparticle surface. Therefore, thermal activation of silica particles up to specific temperatures is an important step for subsequent functionalization, since the silica surface becomes richer in silanol groups, which promote the establishment of covalent bonds such as Si-OR (R = functional group) [111]. FTIR spectra of silica samples before and after thermal activation obtained from our group [110, 145, 148] have shown that for calcinated samples, a significant decrease in the absorption band of the hydroxyl groups and possibly of NH_2 occurs due to the elimination of organic impurities on silica surface. Moreover, the surface topology also seems to be affected after calcination of Si-300 as illustrated in Figure 2.6. Similar results have also been obtained for Si-500 particles in our group [169].

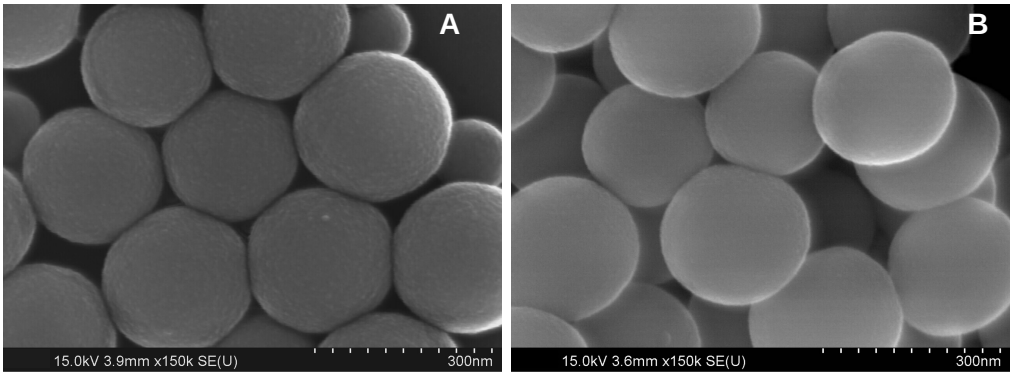

Figure 2.6: SEM images of Si-300 (A) before and (B) after calcination at 700 ^{o}C during 4 hours.

The BET area for Si-300 before and after thermal activation was also determined and the results are summarised in Table 2.4.

Table 2.4: BET surface area of Si-300.

Sample	**Surface area (m^2/g)**
Si-300	7
Si-300 calcinated	21

As noticed in Table 2.4 the surface area of Si-300 after calcination is around 3 times higher than that prior to thermal activation. This result may be justified by the removal of water and non washed residues from nanoparticles synthesis as referred above. Hence, Si-300 and Si-500, were calcinated before analyses and use.

SiO_2 surface properties were also evaluated for their wettability by H_2O through water contact angles (WCA) measurements, which were performed using the Washburn cup method [164]. WCA results for SiO_2 samples are shown in the Table 2.5.

Table 2.5: Water contact angle of SiO_2 samples.

Samples	**WCA**
Si-100	44^{o}
Si-300	32^{o} [a]
Si-500	14^{o} [a]

[a] calcinated samples

Among the different SiO_2 particles used in this work, commercial silica (Si-100) exhibited the highest water contact angle which is possibly due to the presence of residues from preparation and/or stabilizer as the thermal activation step was not performed on these samples to prevent aggregation. The WCA of Si-300 was higher than that obtained for Si-500 in spite of the fact that the experimental procedure followed was the same. This fact may be explained by the concentration of hydroxyl groups on the surface.

The surface chemistry and reactivity of silica gels are mainly determined by its surface hydroxyl groups. During the polymerization of silicic acid, the residual uncondensed hydroxyl groups remain, although the ultimate particles that make up the silica gels can be regarded as polymers of silicic acid, consisting of interlinked SiO_4 tetrahedra. At the surface, as depicted in Scheme 2.1, the structure terminates in either a siloxane group Si–O–Si with the oxygen on the surface, or one of several forms of silanol groups Si–OH [6]. At a sufficiently high concentration of OH groups at the surface, the silica surface will be more hydrophilic but, on the other hand, predominance of siloxane bridges at the silica surface makes the surface more hydrophobic [118]. In fact, the hydrophobic or hydrophilic character of the silica surface is closely related to the dehydration and dehydroxylation processes which silica particles are submitted. Dehydration is the loss of physisorbed water as a function of increasing temperature, whilst dehydroxylation stands for the condensation of hydroxyl groups to form siloxane bonds which depends on the curvature of the silica surface [6] as shown in Figure 2.7.

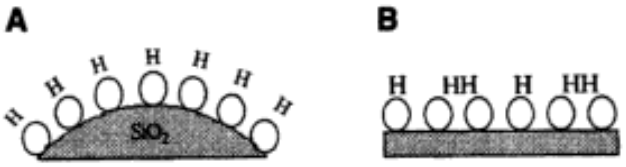

Figure 2.7: Effect of curvature of the silica surface on dehydroxylation. (A) small radius of curvature (small particles) with fewer hydrogen bonds is more easily dehydroxylated and (B) large radius of curvature (large particles) with more hydrogen bonds is less readily dehydroxylated. Reproduced from [6].

Considering that both Si-300 and Si-500 were calcinated, the effect of dehydration can be considered of minor relevance. The difference between the WCA results registered for Si-300 and Si-500 (Table 2.5) suggests that the dehydroxylation process is more extensive on the Si-300 surface yielding more siloxane bonds.

The zeta potential technique was also used to further characterize the surface of SiO_2 particles in order to measure particle charge density under the experimental conditions employed in the preparation of polysaccharide suspensions which will be discussed in the following Chapters. Figure 2.8 shows the zeta potential of spherical SiO_2 particles as a function of pH.

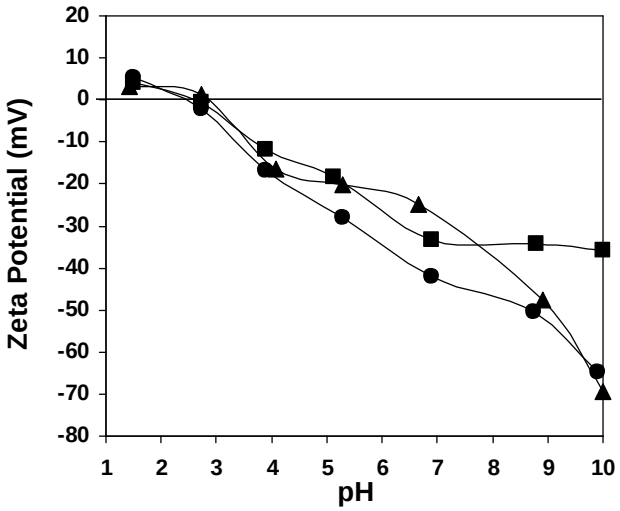

Figure 2.8: Zeta potential measurements of the aqueous solutions of: (■) SiO_2 100 nm, (▲) SiO_2 300 nm, (●) SiO_2 500 nm as a function of the pH.

With this study the isoelectric point of colloidal silica was identified at around pH 3 and at higher pH values, the surface potential of SiO_2 particles becomes negative. Moreover, it was observed that above the isoelectric point charge density increases more or less gradually. Si-100 being a commercial sample that is electrostatically stabilized, the average surface charge was constant from pH 7 onwards. As regards the silica samples prepared in our laboratory, it was

observed that in the whole pH interval, essentially from pH 4 up pH 9, Si-500 presented higher surface charge density in comparison to Si-300. This fact might be explained by the higher amount of OH surface groups on Si-500, as suggested by the WCA results (Table 2.5).

The effect of pH on nanoparticles aggregation was also assessed by DLS. Figure 2.9 shows the variation of the particle diameter as a function of pH. As expected, near the isoelectric point the particles show an apparent higher diameter resulting from particle aggregation, since the charge density of the silica nanoparticles is close to zero at these pH values. However, above pH 4 the surface silanol groups at the surface are readily ionized when in contact with the aqueous medium. Consequently, the particle surface gained more negative surface charges as determined by zeta potential measurements (Figure 2.8). The dissociation of silanol groups leads to a reduction in the number of OH groups available to interact with other silica particles and the resulting strong electrostatic repulsion between SiO_2 particles prevents aggregation. In fact, above pH 4 and up to 8.5 the particles are individualized and their size is near constant.

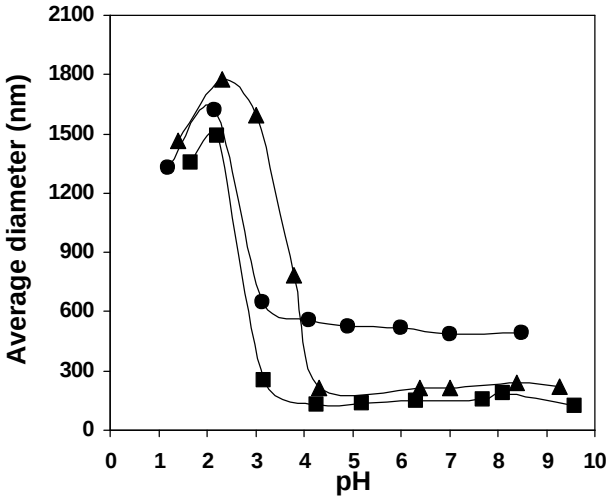

Figure 2.9: Hydrodynamic size measured by DLS in aqueous solutions as a function of the pH for: (■) SiO_2 100 nm, (▲) SiO_2 300 nm, (●) SiO_2 500 nm.

Although in this thesis Si-100 and Si-500 were used in the initial experiments, Si-300 particles were used in most of the experiments since they did not have any unknown stabilizer as in the case of commercial Si-100, their surface and structural properties were quite homogenous, and the size and size distribution were very reproducible from different batches. On the other hand, Si-300 is a compromise between Si-100 and Si-500 in terms of size and WCA, whilst it dependence of the charge density as a function of pH is not significantly distinct from that of Si-500.

In order to explore the use of these particles in distinct media the effect of ionic strength was also assessed. Figure 2.10 summarizes the effect of ionic strength on particle aggregation and as

a function of pH for two concentrations of NaCl, i.e. 0.1 and 0.2 mol/L. For comparison, the size variation of Si-300 in pure water is also plotted.

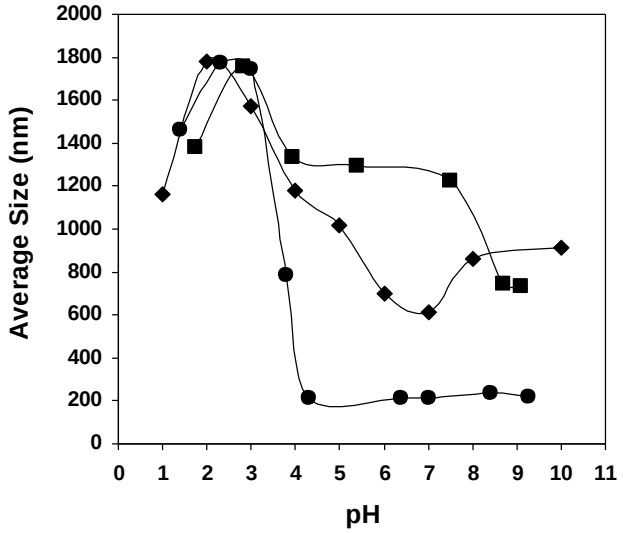

Figure 2.10: Hidrodynamic size measured by DLS for Si-300 suspensions prepared in different media as a function of the pH: (■) NaCl 0.1 mol/L, (♦) NaCl 0.2 mol/L, (●) water.

As it can be observed in Figure 2.10, in a saline medium Si-300 is aggregated in the whole pH interval studied as opposed to what was observed in aqueous medium where the aggregates were only formed at low pH values, i.e. close to the isoelectric point.

According to the Derjaguin, Landau, Verwey and Overbeek (DLVO) theory the presence of electrolytes tends to reduce the extension of the diffuse layer and thereby reduces the repulsive contribution, resulting eventually in reversible or irreversible aggregation [170, 171]. In fact, Johnson *et al* [172] have studied the aggregation behaviour of silica particles in the presence of electrolytes (LiCl, NaCl, KCl, RbCl, and CsCl) and demonstrated that the relative stability of the aggregates varied depending on the type of counterion.

2.3.2. Surface modification of SiO_2 particles with alkoxysilanes

In order to improve the interactions between the polymeric matrix and silica particles and to study their influence on the composites properties, SiO_2 surface modifications were performed using 3-methacryloxypropyltrimethoxysilane (MPS) and 3-aminopropyltrimethoxysilane **(**APS).

The Si-300 surfaces were modified with MPS (Si-300@MPS) for subsequent use in the polymerizations whilst Si-300 modified with APS (Si-300@APS) was added directly to the

biopolymer.

Following Bourgeat-Lami *et al*. [39], the chemical modification of Si-300 with MPS was carried out using an excess of this silane coupling agent in aqueous Si-300 solutions at pH slightly basic. At the end of the reaction the free MPS was eliminated from the MPS grafted to silica by dialysis as discussed in § 2.2.4.1.

Si-300 modification with APS was performed following the method described by Foschiera *et al*. [165] in which silica is dispersed in toluene medium and stirred under N_2 atmosphere for 22 h at 110 ^{o}C (§ 2.2.4.2). Both Si-300@MPS and Si-300@APS were characterized by FTIR spectroscopy, thermogravimetric analysis and contact angle measurements to monitor the grafting of the organoalkoxysilanes onto Si-300 nanoparticles. In Table 2.6 the principal FTIR absorption bands ascribed to MPS and APS on Si-300 surface are summarized.

Table 2.6: FTIR bands characteristics of Si-300@MPS and Si-300@APS.

Attribution	**Group frequency (cm^{-1}) Experimental**		**Group frequency (cm^{-1}) Literature**
	Si-300@MPS	**Si-300@APS**	
$\nu_A CH_3$	2975	2982	2950-2970[39, 165, 167, 173]
$\nu_S CH_2$	2870	-	2845-2865[39, 167, 173]
ν C=O	1728	-	1725-1750[39, 167, 173]
ν C=C	1648	-	1620-1680[39, 167, 173]
δ Si-O-Si	477	472	450-460 [168]
ν_A Si-O-Si	1118	1119	1000-1260 [168]
ν N-C	-	1648	1600[165]
$\nu_A NH_2$	-	-	3360[165]
δ NH_2	-	833	850-750 [167]
δ Si-CH_2	-	1399	1410 [165]

ν - Stretching δ - Bending A - asymmetric S - symmetric

The typical bands of MPS and APS [39, 165] were identified by FTIR spectra. For both samples the presence of absorption bands of colloidal silica was also identified around 1119 and 472 cm^{-1}, corresponding to the stretching and bending of the Si-O-Si bonds respectively. For Si-300@APS the characteristic stretching band of the NH_2 group at 3360 cm^{-1} was not observed possibly because it was overlapped by the large stretching band on the O-H group.

Thermogravimetric analyses (TGA) were carried out for both samples, Si-300@MPS and Si-300@APS. For comparison unmodified Si-300 also was evaluated. The thermograms are illustrated in Figure 2.11.

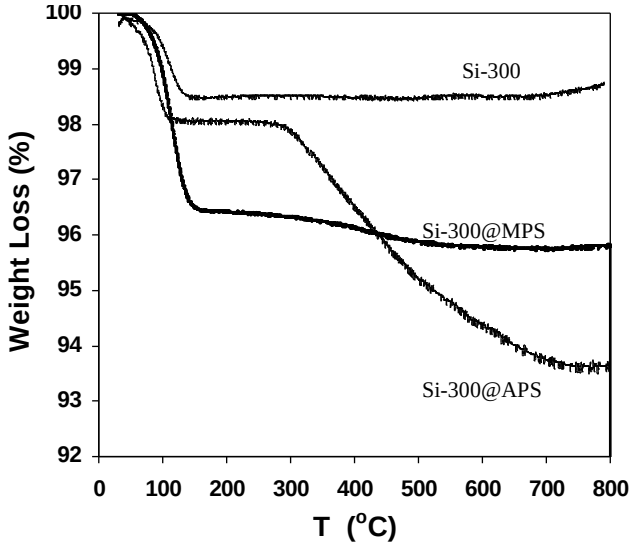

Figure 2.11: Thermograms of Si-300, Si-300@MPS and Si-300@APS.

As expected, the thermal degradation pattern of the modified Si-300@APS particles is divided into two stages. The primary degradation stage is ascribed to water loss around 100 °C, similarly to pure Si-300. The second degradation stage around 300 °C is related to the degradation of APS. As regards Si-300@MPS, only the first degradation step is clearly indentified which is attributed to water loss as in the previous samples. This indicates that either the amount of MPS is very low to be detected and/or that the decomposition of this silicon alkoxide takes place in the same temperature range as water. In fact, the more expressive mass loss registered at this temperature when compared with the previous samples, combined with previous results obtained in our laboratory, confirm that MPS actually decomposes in this region.

The SiO_2 surface properties of Si-300@MPS and Si-300@APS were also evaluated by water contact angle. As cited before in § 2.2.2, WCA was determined using the Washburn method [164] and the results for modified Si-300 as well as for pure Si-300 are summarised in Table 2.7.

Table 2.7: Water contact angle of Si-300, Si-300@MPS and Si-300@APS samples.

Samples	WCA
Si-300	32°
Si-300@MPS	73°
Si-300@APS	66°

From the water contact angle results it was verified that the presence of MPS on Si-300 surfaces makes it more hydrophobic comparatively to pure Si-300. This result confirms that MPS not only provides double bonds to promote covalent bonding between the silica particle and polymer chains, but also increases the silica hydrophobicity, which may promote successful reaction with monomer during polymerization, as will be discussed in the next section.

As regards Si-300@APS, the WCA was higher than pure Si-300 but lower than Si-300@MPS, indicating that Si-300@APS is less hydrophobic than Si-300@MPS due to presence of the hydrophilic NH_2 group at the surface.

Whilst Si-300@MPS was prepared to be further modified via radical polymerization with a synthetic polymer, Si-300@APS was prepared to be added directly to a polysaccharide to prepare composite films as will be discussed in Chapter 4. Therefore Si-300@APS particles surface characteristics namely the zeta potential (Figure 2.12) and the average size (Figure 2.13) were studied as a function of pH.

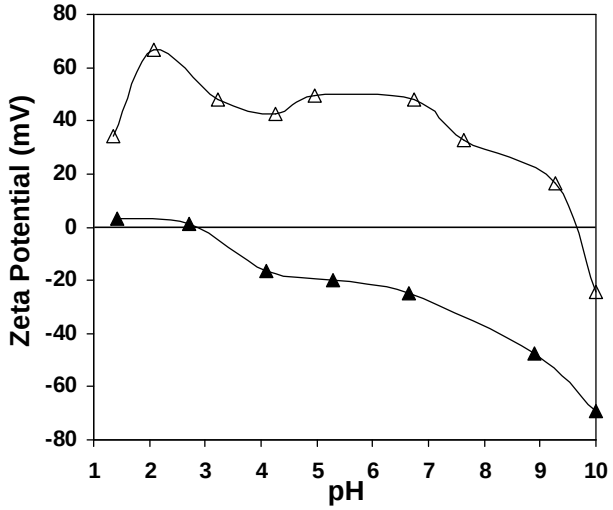

Figure 2.12: Zeta potential measurements of aqueous solutions of: (▲) Si-300 and (Δ) Si-300@APS as a function of the pH.

As forecasted for Si-300@APS, the surface charges were positive except at pH higher than 9. Over this pH value the isoeletric point is achieved around 9.5 and the surface charge of Si-300@APS becomes slightly negative. Moreover, a peak was observed at pH around 2, indicating a maximum protonation of the Si-300@APS sample.

As mentioned before Si-300 was modified with APS in order to prepare chitosan composite films which require dissolution of this polysaccharide in 0.1 mol/L CH_3COOH. For that reason,

size distribution of Si-300@APS at different pH values was studied by DLS as shown in Figure 2.13. For comparison Si-300 suspension prepared in 0.1 mol/L CH_3COOH is also shown.

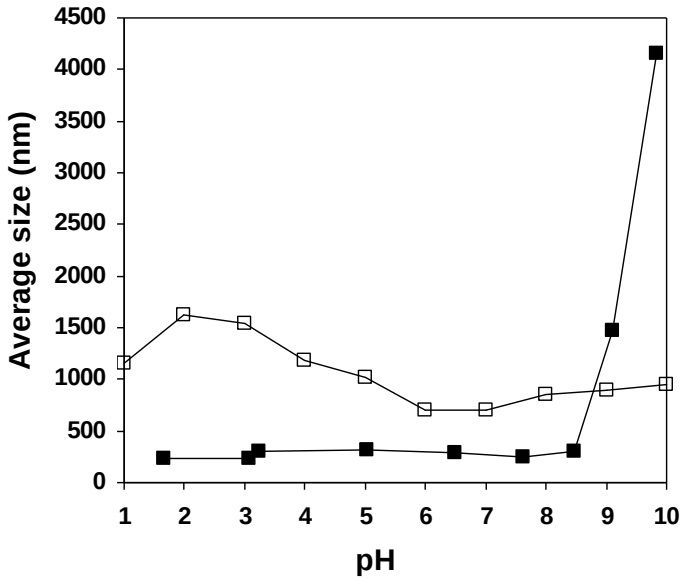

Figure 2.13: Size distribution measured by DLS technique as a function of the pH for Si-300 (□) and Si-300@APS (■) suspensions prepared in 0.1 mol/L CH_3COOH.

From Figure 2.13, it is clear that the Si-300@APS suspension is monodisperse in the whole pH interval up to the isoeletric point where the repulsion forces decrease. The stability of Si-300@APS is in contrast with that was observed for the Si-300 suspension, both prepared in 0.1 mol/L CH_3COOH.

2.3.3. Surface modification via radical polymerization

In order to promote a better compatibility between the polysaccharic matrix and the inorganic fillers and avoid phase segregation, SiO_2@MPS was encapsulated with PGMA to obtain SiO_2@MPS@PGMA. The presence of the epoxy group in PGMA was expected to favour the compatibility with the polysaccharide matrices and/or be explored in crosslinking reactions. Conventional radical polymerization via emulsion technique was used to coat the silica surface. As discussed in § 2.1.3.1, emulsion polymerization is a versatile and simple technique much used to prepare nanocomposites and it allows the use of different surfactant/emulsifiers and initiators allowing tuning of surface charges.

Grafting of PGMA onto silica nanoparticles modified with MPS via emulsion polymerization using SDS as surfactant and KPS as initiator was studied in order to use the versatility of the epoxy group to promote strong interactions with polysaccharide matrices (Figure 2.14).

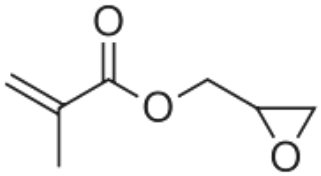

Figure 2.14: Chemical structure of GMA.

Initially, a blank PGMA sample was prepared, i.e. without silica particles and conversion was followed gravimetrically. During the reaction it became clear that the colloidal stability of the emulsion was jeopardized as aggregates could be clearly seen. According to Zeng *et al*. [146] studies on the polymerization of GMA in the presence of SiO_2 coated with PS, excess of GMA in the system destabilizes the electric double layer of micelles. This is due to the ability of GMA polar groups (carbonyl and epoxy) to interact with the electric charges of the surfactant. As a consequence of this instability polymer particles aggregate and conversion tends to drop.

Similarly to Zeng *et al*. [146] studies we have also obtained a rather low monomer conversion during the polymerization of GMA, i.e. 30% upon 5 hours of reaction. Luo *et al.* [130] also obtained low conversion values during the emulsion polymerization of this monomer in the presence of nanosized silicone carbide. According to their detailed studies on the polymerization mechanism involved, the reaction conditions play a major role. These include the concentration of surfactant, namely when working above or below the critical micelle concentration (CMC), or even in its absence, monomer concentration, and temperature.

In this thesis, SDS was used as surfactant in a concentration of 6.8 mmol/L which is slightly above the CMC of SDS (CMC_{water} = 6.0 mmol/L) [174]. This fact together with the nature of the surfactant and all the other reaction parameters discussed above may be responsible for the low conversion achieved. Furthermore, the gravimetrical method used in the conversion measures is not the most reliable one due to the hygroscopic characteristics of PGMA.

Despite of the low conversion, the characterization analysis (FTIR spectroscopy and TGA analyses) depicted in Figure 2.15 confirm the formation of PGMA. From the FTIR spectrum (Figure 2.15A) the characteristic band of the carbonyl (C=O) group can be clearly observed at 1748 cm^{-1}. Two vibrational bands at 990 and 910 cm^{-1} associated with the asymmetric and symmetric epoxy ring bending are also present.

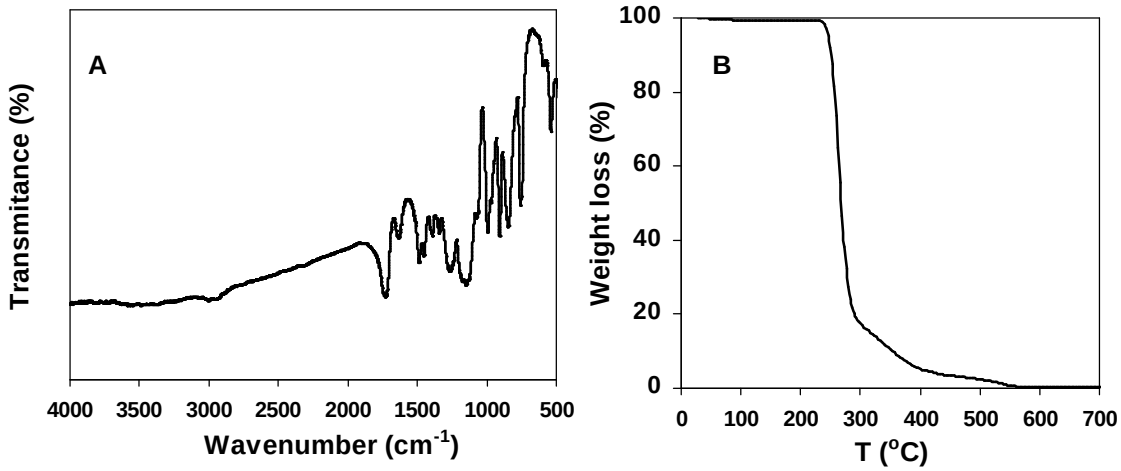

Figure 2.15: FTIR spectrum (A) and (B) thermogram of PGMA.

The TGA analysis (Figure 2.15B) shows that the onset of decomposition of PGMA is around 240 ^{o}C which is agreement with the literature [175, 176].

Having prepared the blank PGMA, the preparation of SiO_2/PGMA was studied. As mentioned in § 2.2.4.1, the silica modified with MPS was used to prepare silica particles coated with PGMA. Although some factors that affect the encapsulation of particles [130, 146] with GMA had been reported in the literature, including monomer concentration, initiator, reaction temperature, reaction time, etc, in this thesis special attention was given to the type of initiator and surfactant. Different types of initiators and surfactant/emulsifiers were tested in order to tune the surface properties of the silica/PGMA particles for subsequent interaction with polysaccharides. For these studies Si-100 being commercially available was firstly used.

Notice should be made that in the case of CTBA, being a cationic surfactant, a water soluble azo initiator (AIBA) was used to prevent aggregation. Table 2.2 in the experimental part summarizes the conditions studied.

Regardless of the different nature of the initiators and surfactant/emulsifiers tested in the preparation of Si-100@MPS@PGMA, large aggregates were always formed which did not disperse in any of the solvents tested (chloroform, toluene, acetonitrile, ethyl acetate and tetrahydrofuran). Attempts to remove free polymer by soxhlet extraction using toluene did not yield any separation suggesting that aggregates are thermodynamically very stable and /or some degree of cross-linking may have occurred.

In view of the results obtained and the fact that commercial silica is supplied with a colloidal stabilizer whose characteristics were not provided by the company, Si-300@MPS prepared in our laboratory was also tested using SDS as surfactant and KPS as initiator following the same procedure.

Upon 5 h of polymerization the monomer conversion was around 25% i.e. slightly lower than that obtained for PGMA without silica particles. In addition, aggregates were also formed and precipitated during the reaction. The precipitated material was purified by three successive decantation/precipitation cycles using water and then further characterized. Si-300@MPS@PGMA was characterized by FTIR spectroscopy and TGA analyses as illustrated in Figure 2.16.

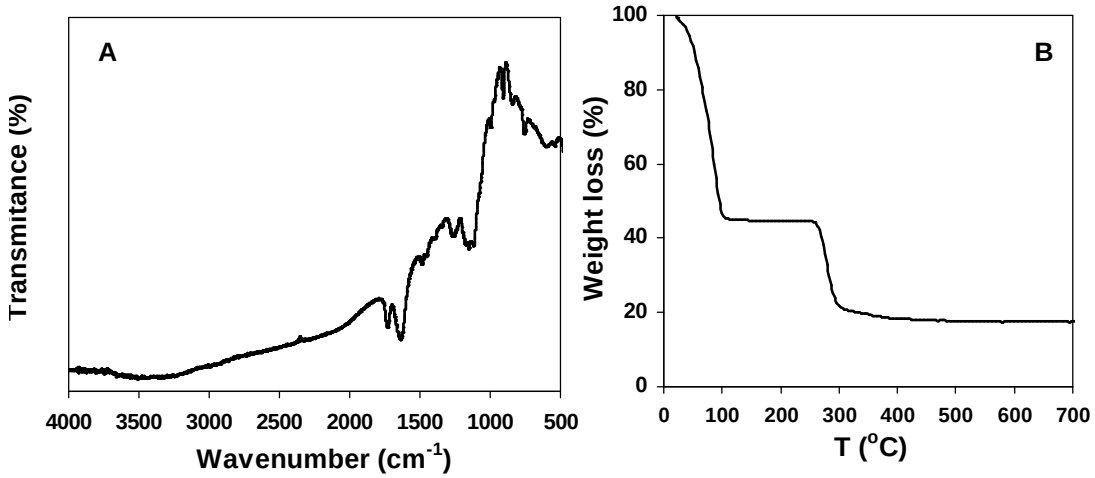

Figure 2.16: FTIR spectrum (A) and (B) thermogram of Si-300@MPS@PGMA.

From the FTIR spectrum of the material collected (Figure 2.16A) the presence of PGMA was confirmed by the strong absorption of carboxyl groups at 1743 cm^{-1}. Moreover, the appearance of the peaks at 913 and 1028 cm^{-1} attributed to the epoxide groups also confirms the presence of the polymer. On the other hand, similarly to pure PGMA a band at 1652 cm^{-1} is also clearly seen, which may be due to the presence of water. Alternatively this band might be attributed to unreacted GMA. However this hypothesis is not very plausible as unreacted monomer would have been removed during purification.

The TGA analysis of the Si-300@MPS@PGMA (Figure 2.16B) shows two stages of degradation. The first stage up to 105 ^{o}C is associated with the loss of water. The second, between 260 and 405 ^{o}C is associated with the degradation of PGMA and corresponds to a mass loss of 25% which is in agreement with the conversion determined gravimetrically and well below 92% as expected if the monomer conversion was complete. Moreover, the increase of the onset of decomposition temperature of PGMA from 240 ^{o}C to 260 ^{o}C is indicative of encapsulation of SiO_2 nanoparticles by PGMA.

The morphology of the Si-300@MPS@PGMA was examined by TEM (Figure 2.17). As it can be seen in Figure 2.17B the presence of a polymer shell is clearly visible. For comparison the TEM image of Si-300 is also shown (Figure 2.17A).

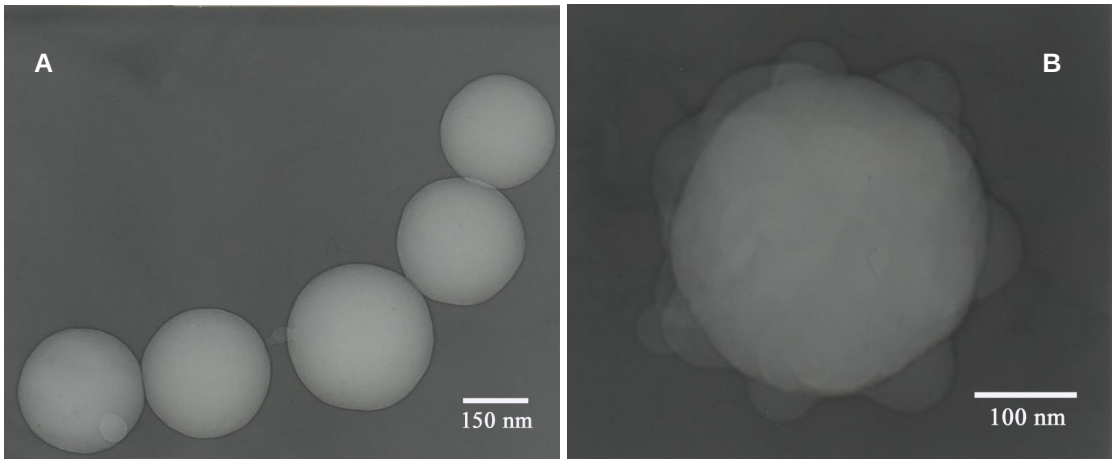

Figure 2.17: TEM images of Si-300 (A) and Si-300@MPS@PGMA (B).

2.3.4. Effect of Silica modification towards its dispersion in polysaccharides

As the main objective of the studies discussed in this Chapter was to promote the compatibility between the silica nanoparticles and polysaccharides, some preliminary tests were carried out.

Si-100@MPS@PGMA composite suspension prepared using various surfactant/emulsifiers was added to the xanthan gum (an anionic polysaccharide) aqueous solutions to assess the stability of the mixtures. Generally, all mixtures proved unstable and precipitation was observed. The most promising result was obtained for the composites prepared in the absence of surfactant/emulsifiers and those prepared using 3-sulfopropyl methacrylate potassium salt (SPM) as reactive surfactant in presence of potassium persulfate (KPS) as initiator.

Whilst the nanocomposite Si-100@MPS@PGMA - 2 prepared using CTBA as surfactant and AIBA as initiator was expected to precipitate immediately due to the presence of opposite charges, the instability of the mixtures involving the remaining composites containing negative charges was not, particularly for Si-100@MPS@PGMA – 5 as it was prepared using xanthan gum as emulsifier whose stabilizing properties are well known. In view of the results obtained a rather detailed study would be required. Yet, due to time constraints this strategy was not pursued.

In contrast to the results above, the much simpler surface modification of silica particles with APS proved to be a rather interesting route to improve dispersion and stability of silica particles at the low pH values required for chitosan dissolution. This was verified by diameter value of 365 nm determined by DLS analysis of the chitosan/Si-300@APS composite dispersion.

2.4. General conclusions

From this study the need for thorough control of silica surface proved to be of paramount importance to achieve good particle dispersion in distinct media and prevent agglomeration when mixed with polysaccharidic matrices in the preparation of bio-nanocomposites.

The principal considerations regarding the preparation of silica nanoparticles and their surface modifications were identified and are summarized as follows:

1. The size of the spherical silica particles seems to influence their surface properties. This fact was supported by progressive reduction of WCA for bigger spherical silica and distinct particles charge densities as function of pH.
2. As expected, at lower pH, silica aqueous dispersions tended to aggregate, since the particle-particle interactions are favoured, whereas at higher pH values the silica particles showed the expected average sizes for individual particles, due to the repulsive forces. In contrast, at higher ionic strength the silica particles have a tendency to aggregate in the whole pH interval. This results from the reduction of the extension of the diffuse layers and repulsive contribution.
3. Silica particles modified with APS dispersed in CH_3COOH medium did not aggregate in practically the whole pH interval studied contrarily to bear silica. This result could be explained by the presence of the amine group on the silica surface, which prevent interparticles interactions.
4. Coating silica particles with PGMA via emulsion polymerization was achieved. Yet, the materials obtained aggregated and the yield was rather low. Attempts to improve this using different surfactant/emulsifiers were not very successful neither. Therefore, a detailed study of this system would be required to optimise it. Furthermore, in view of the disappointing preliminary results obtained when aqueous dispersions of SiO_2@MPS@PGMA were mixed with xanthan gum this route was not pursued.

In future, special attention should be given to the modification of the silica surface particles via *in situ* polymerization which should include the use of controlled living radical polymerization mechanisms from the surface in order to improve coating of SiO_2 particles and of the properties of ensuing composites. As regards the inorganic particles, amongst other aspects, true nanometric particles (AD < 100 nm) should be considered.

3 Polysaccharide/silica dispersions

3.1. General considerations

As mentioned in Chapter 1, the preparation of inorganic/biopolymer nanocomposites is an attractive strategy for the development of novel materials with interesting and tailorable properties. These composites combine the advantages of both the inorganic material and the organic polymer, often providing improved properties to the composite. One important feature is the remarkable increase in the interfacial area, due to the small size of the fillers, creating a significant volume fraction of interfacial polymer with properties different from the bulk polymer even at low loadings.

From the rheological point of view, many interesting properties can be obtained and have been described for inorganic/polymer nanocomposites. The sol-to-gel transition and viscoelastic properties are particularly significant to characterize these systems in view of several potential applications in the areas of physical and biological sciences and engineering.

Many studies on the linear viscoelastic properties of polymer nanocomposites, mainly on polymer melts with a diversity of fillers (clays, carbon nanotubes, silica particles, etc.), have suggested that strong enhancements in the elasticity of these systems occur with increasing concentrations of the particulate phases, often manifesting by transitions from liquid-like to solid-like rheological behaviour at relatively low particle loadings, and solid-like behaviour with a plateau in the storage modulus G'(ω) persisting at even extremely low frequencies [177-182]

The properties and structures of these composite systems are complex and the mechanisms involved can be diverse depending on several characteristics of the polymer, inorganic particle and solvent. Indeed, the precise origin of the improvement of the nanocomposite rheological properties when compared with the pure matrix remains unclear in many cases. Colloidal dispersions often gel under a narrow range of volume fractions and under appropriate conditions of temperature, pH or ionic strength. Silica particles are not an exception and when dispersed in liquids are prone to form by their own aggregates of diverse dimensions by flocculation via silanol-silanol hydrogen bonding. These aggregates or flocs can interconnect and originate a network with solid-like rheological behaviour. Formation of fractal clusters and a model of colloidal gels as kinetically controlled aggregates which percolate and/or jam is generally accepted [183]. Scaling concepts may then be applied to obtain power law exponents for the dependence on the elastic modulus and the critical strain of the solids concentration, which are often dependent on the nature of the particle-particle interactions [183-185].

For silica particles or other kind of fillers dispersed in polymer solutions or melts, arguments considering only the geometric properties of the filler particles, based on fractal, jamming and percolation mechanisms, have also been used to explain the solid-like behaviour observed in filler polymer systems [177, 178, 182, 186], although also stressing the importance of favorable polymer-particle interactions.

It was also demonstrated that the rheology of the polymer matrix affects the structure of the composite dispersions and gels [187, 188].

Other observations (and simulations) reinforced the role of polymer-particle interactions and suggested that the polymer segments can be "immobilized" near the particles, leading to the formation of particle-mediated transient polymer networks [180, 189]. While percolation seems to be a necessary condition for the appearance of solid-like behaviour, it is not always a sufficient condition. The lifetimes of the percolating clusters have to be long enough for the percolating structure become effective at sustaining stress [190].

In fact, at high nanoparticle concentrations, physical gelation, elasticity and the formation of composite networks are strongly dependent on the polymer-filler interactions. For high concentrations of non-adsorbing polymers, depletion flocculation is likely to occur pushing the particles into a small volume of concentrated phase, as observed for polystyrene latex particles in the presence of nonadsorbing sodium carboxymethylcellulose [191] or poly(acrylic acid) polymer chains [192]. Another possible mechanism responsible for polymer/filler gelation occurs for adsorbing polymers, which can bridge particles together, when the adsorbed layers on the particle surface are unsaturated, forcing the particles to share the available polymer chains. This effect was observed for such diverse systems as talc particles in cross-linked poly(acrylylglycinamide) hydrogels [193], xanthan/silica dispersions [104], or dispersions of styrene-methyl acrylate copolymer particles in polyacrylic acid [194], and it was recently described using polymer mean field theory and Monte Carlo simulations [195].

Among the numerous inorganic/organic nanocomposites, polymer/silica composites are the most commonly reported in the literature [121]. However, most of the nanocomposites have been prepared using synthetic polymers. The use of biopolymers can bring additional advantages to the nanocomposites, related to their renewable sources, biocompatibility and biodegradability, although some of the traditional advantages of the organic polymer (e.g., mechanical resistance, ductility, and processability) may be compromised. In fact, in recent years, a wide variety of biopolymers has been employed to produce biopolymer/silica nanocomposites and their potential applications investigated [31].

As mentioned previously, a variety of biopolymers, including proteins (gelatin and collagen) and polysaccharides (xanthan, galactomannans, alginates, carrageenans, chitosan, and cellulose derivatives) have been employed to produce biopolymer/silica nanocomposites [31, 80, 82, 156]. In this thesis, the attention was focused on polysaccharides nanocomposites.

Polysaccharides are versatile biopolymers and the most abundant organic polymers obtained by biosynthesis and available everywhere from different vegetal and animal sources and with a variety of structures. In nature they hold a wide range of different functions. Sometimes they behave as energy storage materials and well known examples are starch, glycogen and some plant seed polysaccharides such as locust bean gum and guar gum. They can contribute to the structural integrity and mechanical strength of plant tissues by forming a hydrated crosslink three-dimensional network (pectins play this role in land plants while carrageenans, agar and alginate have an equivalent function in marine species). On the other hand, polysaccharides such as cellulose and chitin and, less frequently, xylans and mannans can generate hard, solid structures or tough fibers by a close packing of the chains [196].

The polysaccharides, also designed hydrocolloids [197] have attracted many researches since they present various advantages, namely: (i) their renewable character, (ii) their biodegradability, (iii) their relatively low cost and (iv) their easy conversion into different derivates due to their reactivity towards many organic molecules [198]. In addition, these biopolymers have found useful applications in different areas due to their rheological properties into aqueous media where they are incorporated. The main areas of application include the food, the inks, oil industry, the photography, the biomaterials and the pharmaceutical industry [199].

The reported properties observed for polysaccharide/silica composites are also diverse and strongly dependent on the polymer-particle affinity and interactions.

Pashkovski *et al*. [188] described the structure and formation of particulate silica networks in biopolymer solutions and showed that the elasticity of the polymer matrix plays an important role in particle aggregation as well as on the kinetics of structural recovery after preshear. The fractal dimension of the silica network was found to be lower in polymer solutions with high elasticity (xanthan) in comparison to those with low elasticity (carboxy methyl cellulose).

Shchipunov and co-workers [80, 82, 84, 156] have shown that polysaccharides can mediate the formation of hybrid silica nanocomposites by sol–gel processes and that non-gelling polysaccharides, such as chitosan and hyaluronate, can be gelled by generating silica *in situ* via a sol–gel process, using a water-soluble precursor compatible with the biopolymers. In this case gelation was explained by a process resembling biomineralization, causing the polysaccharide chains to strength and to cross-link. Coradin *et al*. [74] have studied aqueous solutions of gelatine

and sodium silicate under conditions also leading to the formation of silica nanoparticles *in situ*, and found that addition of silica decreases the stability of the gels by inducing gelatine depletion in solution. In this case, the strong interactions between silicates and gelatine lead to composite gels with stability lower than pure biopolymer gel. In fact, most of the studies on polysaccharide/silica composites have employed a sol-gel method to prepare the silica particles *in situ* from a percursor. Daniel da Silva and co-workers [32] have also recently shown that the addition of preformed silica nanoparticles also impairs the gelation of κ-carrageenan, an effect dependent on silica load and particle size and attributed to a steric barrier effect caused by the presence of the silica particles weakening polysaccharide aggregation and gelation, under ionic conditions where both components bear negative charges.

In this Chapter, aiming to investigate the possible development of new thickening and/or soft-gel systems through the formation of biopolymer/inorganic nanocomposites, we have studied the rheology and structure of polysaccharide/silica dispersions, using dynamic and steady shear rheological tests and scanning electron microscopy analysis. The biopolymers used were xanthan gum, chitosan and locust bean gum. The first was chosen as a representative of an anionic polysaccharide with wide industrial use, well-known for its high-viscosity and shear-thinning properties and formation of pseudo gels in aqueous dispersions under certain ionic conditions. The second was chosen as a representative of a cationic polysaccharide and the last, locust bean gum, as a representative of a non-ionic polysaccharide also well-known for its applications as a thickening agent. The polymer nanocomposites were prepared via a simple blending method of both components. We foresee that the rheological properties of these dispersions can be tailored by controlling the particle loading and charge, which can be dependent, among other factors, on the pH medium and the composition of the dispersion. Therefore, this study is expected to provide a better understanding on the influence of particle loading and ionic effects on the structure and gelation behaviour of these systems, with practical relevance as models for specific technological applications (e.g., colloidal stability in several industrial processes, adhesives, coatings, etc).

3.2. Bionanocomposite characterization

In this work mainly two different techniques have been used to characterize the polysaccharide/silica dispersions and they will be discussed in this section: rheological methods and microstructure analyses.

In terms of bionanocomposite dispersions it is expected that the presence of biopolymers in aqueous medium results in thickening and/or in the gelation. As observed above in the few

examples from literature, the presence of silica particles can facilitate or not the gelation effects. Rheology, as the science that studies the flow and deformation of materials, has been used as the principal approach to analyse these effects [199].

Another important characteristic to be studied is the microstruture that these systems assume under different conditions. For this purpose, we have used cryo-scanning electron microscopy (cryo-SEM) analysis, trying to establish relationships between the rheological behaviour and the structural organization of the polymer and filler.

3.2.1. Rheological Measurements

As mentioned above, rheology is a fundamental tool to understand the macromolecular organization of biopolymers under different conditions. It is known that certain polysaccharides such as starch, cellulose, locust bean gum and others show limited solubility in water or in electrolyte solutions forming dispersions in aqueous media and non real solutions. In addition, as we have studied mainly dispersions of silica particles in the biopolymer solutions, we will be dealing essentially with heterogeneous systems. Hence, we expect to observe complex rheological behaviours, probably dependent on a diversity of factors, including sample history. Therefore, we had additional care during sample preparation and analysis in order to obtain meaningful results.

The knowledge of flow properties of aqueous solutions and dispersions of polysaccharides is essential to the understanding of the molecular origin of thickness process and particularly important in the application fields of these materials [200]. Following this idea, in the next sections a succinct introduction about the principal rheology concepts used in this thesis will be discussed.

3.2.1.1. Rheology principles

The Rheology is defined as the science of the deformation and flow of matter, which studies how the materials respond to an applied stress or strain. This definition, originally given by Eugene Cook Bingham in 1929, is still universally accepted [201].

All materials present a response to an external force between the two extremes of the ideal behaviour: an elastic solid and a viscous liquid. The first is described by Hooke's law, while an ideal viscous liquid follows the Newton's law. However, the majority of materials show viscoelastic behaviours, i.e. an intermediate behaviour with solid- and liquid-like characteristics, depending on the stress applied and time. There are a diversity of rheological tests that can be used

to characterize a certain material, depending on its properties and purpose of the test. In this work, we have used dynamic oscillatory tests at low strain amplitude in order to evaluate our systems under unperturbed conditions, and steady-shear flow tests to evaluate their flow properties under conditions closer to their handling and processability.

3.2.1.1.1. Rheological properties at high deformation

In general, the materials tend to resist the flow. This physical property is called viscosity and is an important tool in understanding the structural phenomena that govern the macroscopic behaviour of materials when subjected to deformation [196].

Viscosity is a physical property used for measuring the internal friction of a fluid. This friction becomes apparent when a layer of fluid moves in relation to another layer. The amount of force required to cause this movement is called shear. Shear occurs when the fluid is physically moved or distributed. Highly viscous fluids require larger forces to move a layer to the other than those less viscous materials [7].

Rheological characterization is typically performed in steady flow state, since the viscosity is seen conventionally as the most important property of the material. Newton formulated a equation for the definition of viscosity [201]. When a fluid is subjected to a flow, the viscosity (η) is the constant of proportionality between the shear stress (σ) and the shear rate ($\dot{\gamma}$) as shown in Equation 3.1.

$$\sigma = \eta . \dot{\gamma} \qquad \text{Equation 3.1}$$

The relationship proposed by Newton has been extensively used in the rheology field but it is only valid for Newtonian fluids. Newtonian fluids are those that present a viscous ideal behaviour where the variation in the shear rate versus the shear stress is linear.

Diverse fluids do not obey Newton's law, so called non-Newtonian fluids. The constant of proportionality shown in Equation 3.1 then becomes known as apparent viscosity η_{ap}. In the case of non-Newtonian fluids the viscosity is dependent on the shear rate. The types of flow curves are presented in Figure 3.1.

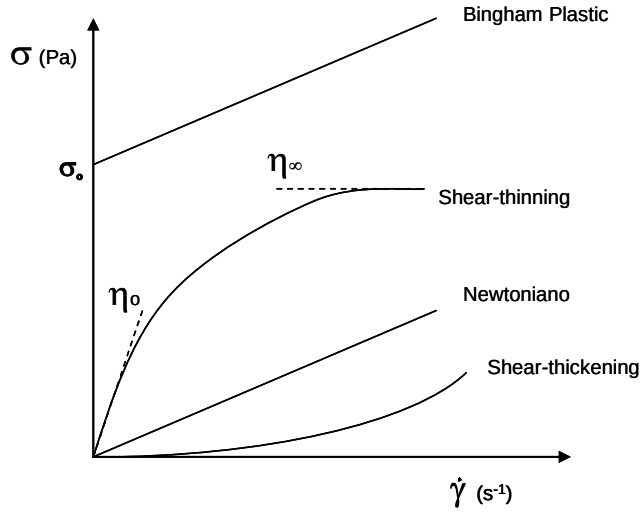

Figure 3.1: Flow curves of Newtonian and non-Newtonian fluids. Adapted from [7].

Dilute biopolymer solutions usually exhibit Newtonian behaviour whereas semi-dilute and concentrated solutions or dispersions exhibit a shear-thinning behaviour, i.e. the apparent viscosity decreases with increasing shear rate imposed on the system [199]. This behaviour can be explained based on the concept of macromolecular entanglement and its progressive disruption and alignment of macromolecules in the flow direction as the shear rate increases [202]. This fact can be visualised in Figure 3.2, where the particles that compose a liquid (dispersion) orientate or deform in the direction of flow.

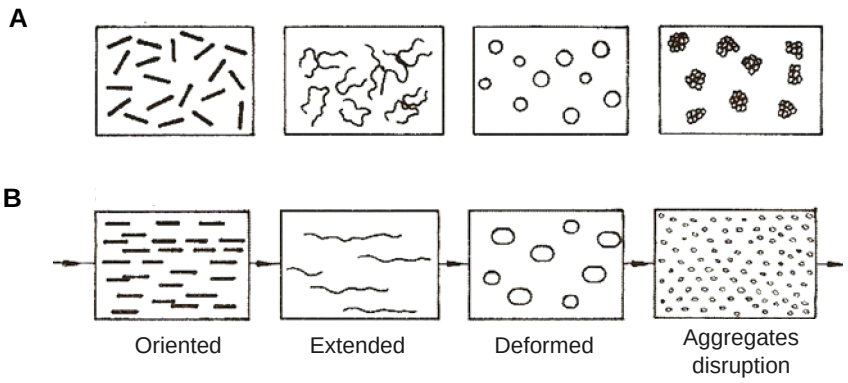

Figure 3.2: Characteristics of a liquid in a quiescent state (A) and in flow state (B). Adapted from [8].

Fluids more structured mainly due to network macromecular formation may show regions with viscosity nearly constant (η_o, viscosity at zero shear rate) at low rates of deformation (Figure 3.1) while at higher strain rate a decreasing of viscosity is verified, which can be related to changes in the material structure as a function of the applied strain.

In recent years, there was a large development of rheometer and rheological models in order to understand the shear-thinning behaviour of biopolymers at low and at high shear rates. This way, difficult parameters to determine such as η_o and η_∞ (viscosity at infinite shear rate) began to be studied more regularly.

Among the rheological models used commonly to describe the effect of shear rate on the viscosity of polysaccharide solutions can be cited the Cross and Carreau Models, expressed in the following equations:

$$\eta = \eta_\infty + (\eta_o - \eta_\infty)/(1 + \alpha\dot{\gamma}^m)$$
$$\eta = \eta_\infty + (\eta_o - \eta_\infty)/(1 + (\lambda\dot{\gamma})^2)^N$$

Equations 3.2 and 3.3

where η is the apparent viscosity, η_o is the viscosity at zero shear rate, η_∞ is the viscosity at infinite shear rate, $\dot{\gamma}$ is shear rate, α and λ are specific relaxation times and *m* and *N* are constants.

3.2.1.1.2. Rheological properties at low deformation

Small-amplitude oscillatory shear has become one of the most popular deformation modes, since it offers the opportunity of studying the viscoelastic behaviour of materials in a relatively large range of kinematic conditions. Working with deformations of small amplitude is a necessary condition to ensure the non-destructive nature of the test. This, in turn, allows us to express the results in terms of linear viscoelastic properties, typical of an equilibrium state of the system. At the same time, the possibility of extending indefinitely the time of each experiment make oscillatory tests prime candidates among all rheometrical techniques for kinetic studies of chemical and physical processes involving substantial structural changes [196]. In addition, these dynamic assays are particularly interesting to evaluate conformational aspects and intermolecular interactions of biopolymers [199]. A variety of experimental techniques are included in the class of dynamic tests. Among them are those that make use of free vibration, forced vibration and propagation of pulses or waves [203].

The tests most known are called harmonics or oscillatory. Oscillatory motion conditions can be achieved by conventional rheometers, rate- or stress-controlled, by imposing to one of the two boundary surfaces a displacement or a force, respectively, both sinusoidally varying with time (Figure 3.3).

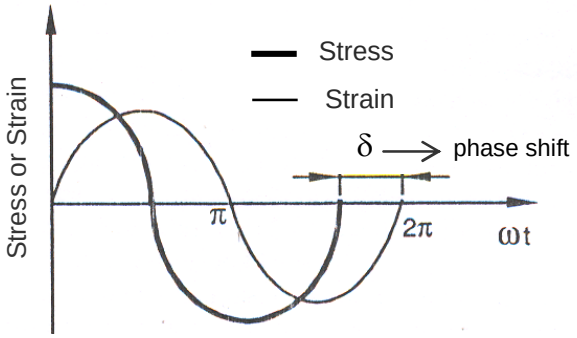

Figure 3.3: Schematic representation of the oscillatory rheological test.

In order to simplify, it was considered the unsteady motion of fluid contained between two parallel plates, when the upper one undergoes a sinusoidal motion of small amplitude in its own plane with frequency ω. At any given instant, the velocity profile can be taken to be linear in the direction normal to the plates on the condition that inertial effects can be neglected. The strain and shear rate distributions are uniformly described by the following relationships:

$$\gamma = \gamma_o \sin \omega t \qquad \text{Equation 3.4}$$

$$\gamma = \gamma_o \, \omega \cos \omega t \; = \dot{\gamma}^o \; \cos \omega t \qquad \text{Equation 3.5}$$

where γ_o is the maximum strain, corresponding to the ratio of the maximum displacement of the upper plate and the width of the gap between the plates, and $\dot{\gamma}^o$ is the maximum shear rate during oscillating motion. For Newtonian fluids, the response reduces to the shear stress, which is in phase with the shear rate.

The shear stress oscillations have the same frequency, but are shifted with respect to the strain, whereas the normal stresses are characterized by a frequency 2ω and a nonzero mean value [196]. The shear stress is given by equation 3.6:

$$\sigma = \sigma^o \sin(\omega t + \delta) \qquad \text{Equation 3.6}$$

where σ^o and δ are the maximum shear stress and the phase shift, respectively. Thus, we can break the shear stress response into two parts as follows:

$$\sigma = \sigma^o \cos \delta . \sin \omega t + \sigma^o \sin \delta . \cos \omega t \qquad \text{Equation 3.7}$$

The first term is in phase with the strain representing the contribution due to fluid elasticity, whereas the viscous contribution is given by the second term, which is in phase with the shear rate. In fact, in the two limiting cases $\delta = 0$ and $\delta = \pi/2$, we obtain the purely elastic and viscous behaviours respectively and for viscoelastic materials the δ value should be between these limits.
The relation between stress and strain maximum amplitude defines the complex modulus $|G^*|$. When we consider $|G^*|$ as a vector quantity, this vector can be decomposed into two components as shown in the following relations:

$$G' = |G^*| \cdot \cos \delta \qquad \text{Equation 3.8}$$

$$G'' = |G^*| \cdot \sin \delta \qquad \text{Equation 3.9}$$

G' and G'' are called the storage (elastic) and the loss (viscous) modulus, respectively, and, in general, are functions of the frequency ω. They represent the elastic and viscous contributions to the properties of the fluid, and are related to the corresponding viscosity functions η' and η'' through:

$$G' = \eta'' \cdot \omega \qquad \text{Equation 3.10}$$

$$G'' = \eta' \cdot \omega \qquad \text{Equation 3.11}$$

For a Newtonian fluid, the dynamic viscosity η' coincides with the shear viscosity η and G' is reduced to zero, whereas for a purely elastic solid $G'' = 0$ and the elastic modulus is equal to the shear modulus G. Both function pairs can be treated as real and imaginary parts of complex quantities, which measure the magnitude of the total response of the fluid. The complex viscosity η^* is then defined by equation 3.12.

$$\eta^* = |G^*| / \omega \qquad \text{Equation 3.12}$$

Similar behaviour under steady and oscillatory shear flow conditions is a feature common to all isotropic polymer solutions; for these systems, then, the Cox-Merz rule can be used for a reliable prediction of the functional dependence of $\eta(\dot{\gamma})$ when that of $\eta'(\omega)$ is known, and vice versa. In the presence of aggregated structures among polymer chains (polymer dispersions and gels), and among particles in a disperse phase (disperse systems), or of ordered molecular configurations like those encountered in polymer liquid crystal, the values of the relevant quantities (in oscillatory and steady shear) are considerably different, even if the functional dependences can still be similar.

Thus, the Cox-Merz rule constitutes a possible criterion for the distinction between structured and ordinary polymer systems [196].

The viscoelastic behaviour of a fluid is rheologically characterized when some properties are known such as the value of $|G^*|$, the dynamic moduli *G'* and *G''* or any other combination of two quantities, besides the ratio *G'' / G' = tan* δ (loss tangent) which indicates wheter a material is typically elastic or viscous, obeying the following conditions:

- tan δ > 1 indication of dilute polymeric solutions (material more viscous)
- tan δ < 1 indication of polymeric gels (material more elastic)

The viscoelastic behaviour for dilute solutions of biopolymers at low oscillatory frequencies is controlled by translational movement of the macromolecules and the loss modulus is higher than storage modulus. Complex viscosity is practically independent of the frequency, since the behaviour of the system approaches that of the Newtonian. For high frequencies *G'* increases approaching the *G''* magnitude due to macromolecular distortion. The macromolecules are now forced to assume conformations under tension, and more elastic energy is stored [199].

For semi-dilute and concentrated solutions or dispersions, the observed behaviour can be divided in two different types: 1) For biopolymers that interact only by physical interpenetration, topological, as is the case of polysaccharides with disordered conformation in solution (ex. galactomannans) and 2) For biopolymers with conformations more rigid and structures more ordered in solution (ex. xanthan gum).

The viscoelastic behaviour at low frequencies for the first group of biopolymers is similar to that observed for dilute solutions, with *G'' > G'*. For higher frequencies, when the time interval corresponding to an oscillation period is low to allow the breaking of macromolecular entanglements, *G'* increases. For even higher frequencies *G'* becomes even higher than *G''* and less dependent on the oscillation frequency. The frequency corresponding to the intersection point between the two viscoelastic modules is reduced when the degree of macromolecular entanglement increases, i.e. for solutions more concentrated.

For biopolymers from the second group, the presence of more specific molecular interactions between the ordered zones of the macromolecules leads to important changes in the viscoelastic behaviour. The storage modulus (*G'*) is higher and its dependence on the frequency decreases. Moreover, the complex viscosity (*G**) does not reach the *Newtonian plateau*. The magnitude of these differences depends on the concentration and on the biopolymer in question [199].

3.2.1.2. Concentration dependence of the rheological behaviour

When the concentration of the biopolymer exceeds the *critical overlap concentration*, C^*, we enter in the region called semi-dilute and concentrated solutions. In these regions of concentration a gel may be formed. The degree of "non-ideality" increases and mainly phenomenological descriptions are used for the characterization of the physical properties [9].

The *critical overlap concentration* C^* characterizes the situation where a continuous contact between the polymer coils in the solution exists. Further increasing of the biopolymer concentration, one new concentration called *double critical overlap concentration*, C^{**}, is reached. In this state, the polymer coils are interlaced with a uniform distribution of the segments. A typical illustration of these different concentrations is depicted in Figure 3.4.

The effect of the biopolymer concentration on zero-shear viscosity (η_o) can be expressed in terms of dimensionless parameters: the *coil overlap parameter* $c[\eta]$, and the specific viscosity $\eta_{sp} = [(\eta_o - \eta_s)/\eta_s]$, where c is the biopolymer concentration and η_s is the viscosity of solvent. The former takes into account both the concentration and the hydrodynamic volume of the macromolecule, which is directly related to the total volume occupied by the polymer. Based on graphical treatments of log η_{sp} versus log $c[\eta]$, it is possible to obtain master curves that generalize and describe the behaviour of certain groups of biopolymers [204, 205].

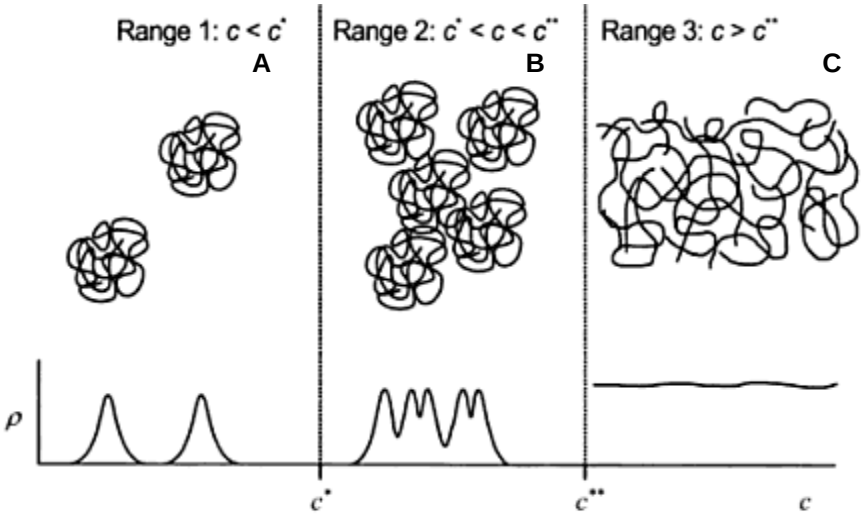

Figure 3.4: Crossover between dilute and concentrated solutions: (A) dilute, (B) semi-dilute and (C) concentrated. C^* - critical overlap concentration equivalent to transition between dilute and semi-dilute regimes, C^{**} - double critical overlap concentration equivalent to transition between semi-dilute and concentrated regimes. The distribution of the density of polymer segments (ρ) is shown schematically. Reproduced from [9].

Clarifying some definitions:

Dilute solution: $C<C^*$, the concentration of polymer is lower than the critical overlap concentration C^*. There is not a continuous contact between the polymer molecules.

Semi-dilute solution: $C^*<C< C^{**}$, the transition between the dilute and concentrated regimes does not occur in a well-defined concentration, corresponding to an interval of concentrations. The polymer concentration is larger than C^* and the polymer molecules are in continuous contact with each other. A gel may be formed if there is a strong physical or chemical interaction between the molecules.

Concentrated solution: $C>C^{**}$, the concentration of polymer is so high that we have an uniform distribution of polymer *segments* among the solvent molecules.

3.2.1.3. Rheology of gels

Rheological studies can provide useful information on sol-gel and gel-sol transitions, as well as on the characteristics of a gel [206]. Hermans [207] defined a gel as a two-component system (i.e., gelling polymer and the solvent) formed by a solid finely dispersed or dissolved in a liquid phase, exhibiting solid-like behaviour under deformation; in addition, both components extend continuously throughout the entire system, each phase being interconnected. According to Burchard and Ross-Murphy [208], gel systems are those that possess at least one property which can stand as the operational definition of a gel; they possess a plateau in the real part of the complex modulus extending over an appreciate window of frequencies. Another requirement is that G'(ω) is considerably larger and preferably more than one order of magnitude higher than G"(ω) in the plateau region to ensure that the system is solid-like. At molecular level, gelation is the formation of a continuous network of polymer molecules, in which the stress-resisting bulk properties (solid-liquid behaviour) are imparted by a framework of polymer chains that extends throughout the gel phase [206].

Despite the existence of several definitions, the term gel indeed classically defines a range of systems which exhibit solid-like properties while a vast excess of solvent is present [209]. Most biopolymers form physical gels, structured by weak interactions (hydrogen, electrostatic, hydrophobic). Their polymer chains form extended junction zones by means of side-by-side associations of a physical nature, in contrast to the typical single covalent bonds found in chemically cross-linked networks. Consequently, in physical gelation the formation and breakdown of the junction zones are usually reversible and these junction zones have a finite lifetime [206].

Based on the macroscopic behaviour of gel systems, a practical and useful distinction between the classes of networks can be made. Those systems that are free-standing and arise from a three-dimensional network are called true gels whilst those systems characterized by a tenuous gel-like network which is easily broken when submitted to a high enough stress or time are called weak gels. Moreover, in true gels, the molecular rearrangements within the network are much reduced over the time scales analyzed, G' is higher than G'' throughout the frequency range, and is almost independent of frequency. In weak gels there is a higher dependence on frequency for the dynamic moduli, suggesting the existence of relaxation processes occurring even at short time scales, and a smaller difference between moduli values, indicating that a lower percentage of the stored energy is recovered. Xanthan gum is very often taken as an example of a weak gel [210]. The others polysaccharides studied in this thesis, chitosan and locust bean gum are considered non-gelling polysaccharides.

During gelation, a polymer undergoes a phase transition from a liquid to a gel. The sol-gel transition is a critical point where one characteristic length scale (i.e., the size of the largest molecule) diverges. It is a transition in connectivity between a sol, where the "monomers" are not connected, to a gel, where they are connected. This transition moment defines the gel point of a system. Based in the classical Flory theory [211], the gel point is attributed to the moment where the steady-shear viscosity tends to an infinite and exists a zero equilibrium modulus at zero frequency limit.

Small amplitude oscillatory shear techniques have been used to obtain useful properties of gels, and of gelation and melting through three principal types of dynamic measurements: (1) Frequency sweep studies in which G' and G'' are determined as a function of frequency (ω) at fixed temperatures. (2) Temperature sweep in which G' and G'' are determined as a function of temperature at fixed (ω). (3) Time sweep in which G' and G'' are determined as a function of time at fixed (ω) and temperature. As a reminder, all the above tests should be conducted in the linear viscoelastic interval, obtained in the strain sweep tests.

Specifically, the experimental detection of the gel point is not always easy. Some rheological criteria have been widely employed to detect the gel point of a system. Tung and Dynes [212] suggested one of the most applied criteria to identify the gel point. This method indicates that the gel point might occur at the time at which G' and G'' cross each other, i.e., when $G' = G''$ at a given frequency. Nevertheless the time of the G'-G'' crossover was found to be dependent on the oscillatory frequency in the case of both synthetic polymers and biopolymers [199, 206]. Since the gel time is an intrinsic property of the material, it can not be dependent of experimental conditions.

Hence, the *G' = G''* time can not be considered a general criterion for the determination of the gel point

Winter and Chambon [213] proposed a fundamental gel point criterion currently accepted as the most objective and reasoned for the moment corresponding to the sol-gel transition. This criterion is based on the power law relationship (equation 3.13). At gel point, the dynamic moduli are parallel and proportional to frequency over the entire frequency range.

$$G'(\omega) \sim G''(\omega) \sim \omega^{\Delta}$$
$$\tan(\delta) = G''/G' = \text{constant} = \tan(\Delta\pi/2) \qquad \text{Equation 3.13}$$

where Δ is the relaxation exponent and the phase shift is independent of frequency, i.e, $\delta = \Delta\pi/2$

Experimental evidence has suggested that, for stoichiometrically balanced gels $\Delta = 0.5$. In this case, *G''* is equal to *G'* and we found the simple criterion suggested by Tung and Dynes [212] previously discussed. For imbalanced systems with crosslinker deficiency, larger Δ values have been found and, correspondingly, *G''* is greater than *G'*.

As it will be explained later, one of the main purposes of this work is to investigate the capability of the silica particles, when dispersed in solutions of non-gelling polysaccharides, to induce the gelation of the biopolymer.

3.2.1.4. Rheology of dispersions

The preparation and rheological characterization of different bionanocomposites dispersions requires the understanding of the rheology of dispersions.

The rheology of dispersions has been the subject of important research for many years, mainly because of its obvious importance in a wide range of industrial applications. Dispersions include cement, paint, printing inks, coal slurries, drilling muds and many products like medicines, biological fluids, liquid abrasive cleaners and foodstuffs [214, 215].

Three kinds of forces coexist to various degrees in flowing dispersions. First, there are those of colloidal origin that arise from interactions between the particles. These forces can result in an overall repulsion or attraction between the particles. The second type of forces refers to the ever-present Brownian (thermal) randomising forces. For particles of all shapes, this constant randomisation influences the form of radial distribution function (i.e. the spatial arrangement of

particles as seen from the centre of any one particle). Thirdly, the viscous forces acting on the particles must be taken into account. The viscous forces are proportional to the local velocity difference between the particle and the surrounding fluid [214, 216].

Dispersions basically show strong divergences from single Newtonian laws of fluid flow and hence form complex rheological systems. When the dispersing medium is a Newtonian fluid or behaves like one under a given range of shear rates, then the dispersion exhibits Newtonian behaviour at low concentration of solids and non-Newtonian behaviour with increasing concentration. When the suspending medium is a polymer solution which itself is non-Newtonian in character, the presence of solid particles amplifies the complexities of its rheological behaviour [216].

The viscosity of Newtonian as well as non-Newtonian dispersions is affected by the characteristics of the solid phase such as shape, concentration and dimensions of the particles, its size distribution, the nature of the surface, etc. [216].

Among the different shape of particles used in the dispersions, spherical filler particles have received more attention than non-spherical and asymmetric particles [216]. In this thesis, spherical silica particles were the fillers used within the polysaccharide matrices, hence, in this section, the focus will be on spherical fillers.

Einstein [217] pioneered the study of the viscosity of dilute dispersions of neutrally buoyant rigid spheres without Brownian motion in a Newtonian liquid. He proposed the following relationship (Equation 3.14) between the relative viscosity of the dispersion η_r and the volume fraction of the suspended particles ϕ,

$$\eta_r = 1 + \alpha_E \phi \qquad \text{Equation 3.14}$$

where η_r is the ratio of the viscosity of the dispersion η_{sr} to the viscosity of the suspending medium η_o and α_E is the Einstein's constant.

Generally, when $0.1 < \phi < \phi_m$ the dispersion is considered to be concentrated and the above discussed equation does not apply. Here ϕ_m is defined as the maximum attainable concentration and has the following form: $\phi_m = 1 - \varepsilon$, where ε is the void fraction or porosity, and is defined as the ratio of the void volume to that total volume.

When the filler concentration is increased, various phenomena take place, for example (i) the number of particles per unit volume which come in contact during the flow increases, (ii) the interparticle attraction and repulsion effects become stronger due to electrostatic charges, which depend upon the polarity of the medium, (iii) the rotation of the particles during flow, as well as the

formation of doublets and their rotation during flow, produces additional dissipative effects which lead to an increase in the viscosity.

Unlike dilute dispersions, the size of the filler drastically changes the viscosity behaviour of concentrated dispersions [216]. When the fillers contained in a dispersion have small dimensions (in the μm range), a concentrated dispersion exhibits non-Newtonian behaviour and the viscosity increases with the decrease in the filler diameter.

The viscosity of a dispersion is also strongly influenced by the presence of different-sized particles. Dispersions containing mainly aggregated particles and relatively few monodisperse particles showed a marked decrease in the viscosity compared to an all aggregated dispersion. Contrarily, dispersions with monodisperse particles and a few aggregated particles showed slight differences in comparison with a totally monodisperse dispersion. It could thus be concluded that small particles are introduced between larger particles, causing a reduction in the interparticle impact resulting in a decrease in viscosity. In other words, the addition of a little amount of small particles acts a lubricant to facilitate the rotation of larger particles [218].

The presence of isolated particles means deviation of the fluid flow lines and hence an increased viscosity. At higher concentrations, more resistance arises because particles have to move out of each other's way. When particles form flocculated structures, even more resistance is encountered due to the relative immobilisation of a fraction of the suspended particles trapped in the agglomerates. Hence, the degree of flocculation of dispersed particles strongly influences the rheology of dispersions [201, 219].

When polymers are present, the stability of the dispersions can be enhanced due to the polymer influence on the surface properties of the fillers. Under certain conditions, polymers adsorb on particles and alter the interparticle forces which control the state of dispersion and rheological properties of the dispersion. An important criterion for achieving good particulate dispersion through steric stabilization is to ensure good coverage of the particle surfaces with the adsorbed polymer.

At low polymer adsorption density, the steric repulsive forces are likely to be too weak to prevent the approach of particles. As a consequence two phenomena can occur: (1) flocculation due to van der Waals atractive forces and (2) bridging flocculation due to polymer segments from one particle surface attaching themselves to the available surface site of another particle [220].

In the flow of dispersions, velocity gradient is known to cause two major effects: (1) migration of the particles towards the centre of the axis in a tube flow situation and (2) rotation of the particles. In pipe flow of a dispersion, the presence of a wall and a velocity gradient causes the particles to

migrate towards the tube axis and correspondingly decrease the concentration of the solid phase near the wall. In addition, a characteristic slippage at the wall surface can occur. A direct consequence of the slip is the increased flow rate through the tube compared to that which would occur if slip was absent.

At high concentration of the solid phase, the existence of a velocity gradient results in rotation of the particles, followed by an increase in the viscosity of the dispersion. Concentrated dispersions are known to exhibit non-Newtonian behaviour and hence viscosity would change as the shear rate changes.

When the dispersion particles are charged, the electroviscous effects that arise strongly influence the viscosity of the dispersion as was shown by the experiments of Fryling [221]. Electroviscous effects are essentially of three types. These combined effects on the viscosity of a dispersion, can be written in Equation 3.15:

$$\eta_r = 1 + (e_{v1} + e_{v2} + e_{v3})\phi \qquad \text{Equation 3.15}$$

where e_{v1}, e_{v2} and e_{v3} correspond to each of the three electroviscous effects.

The first electroviscous effect, e_{v1} is due to the electrostatic contribution of charged colloidal particles. The electrical double layer created around a charged particle in an electrolyte favours the increase of the viscosity. The second electroviscous effect e_{v2} is due to the electrostatic repulsion between particles approaching each other and is directly proportional to the square of the particle concentration. The essential feature about this effect is that it occurs at high concentrations of the dispersions and when there is an overlap of the double layer. The additional dissipative effects that appear as a result of the repulsion bring about an increase in the viscosity. The third electroviscous effect e_{v3} is due to the change of shape of suspending particles when their electrical free energy is modified by ionization and the presence of neutral salts. If a polymer molecule can undergo ionization, i.e. by reaction with a base or by reaction with some other ion-producing substance, electrostatic repulsion between the like charges introduced on the polymer chain modifies the molecular free energy of the polymer in the solution.

3.2.1.5. Reometry

The Rheometry is the area of rheology which focuses on the experimental measurement of the rheological characteristics of materials. For a Newtonian fluid, the rheological properties are practically characterized by a single measurement (viscosity) using a viscosimeter [203]. The equipment used to measure the viscoelastic properties of solid, semi-solid and non-Newtonian fluids is called rheometer [8]. The rotational rheometer is the most commonly used in determining the rheological properties of fluids.

The choice of an appropriate geometry of measurement (coaxial cylinders, cone-plate or parallel plates) used in a rotational rheometer is fundamental for the rheological analysis of a given material. In this thesis the measuring geometry chosen was the cone-plate type (Figure 3.5). The cone-plate geometry began to be used thirty years ago and is often adopted because it induces a constant shear rate across the sample and allows a simple measurement of first difference of normal stress and the implementation of assays of relaxation of tension. On the other hand, the cone-plate geometry was chosen because the amount of sample required is less than for other geometries [8] and this factor was crucial when silica particles were added into polysaccharides dispersions in the preparation of nanocomposites.

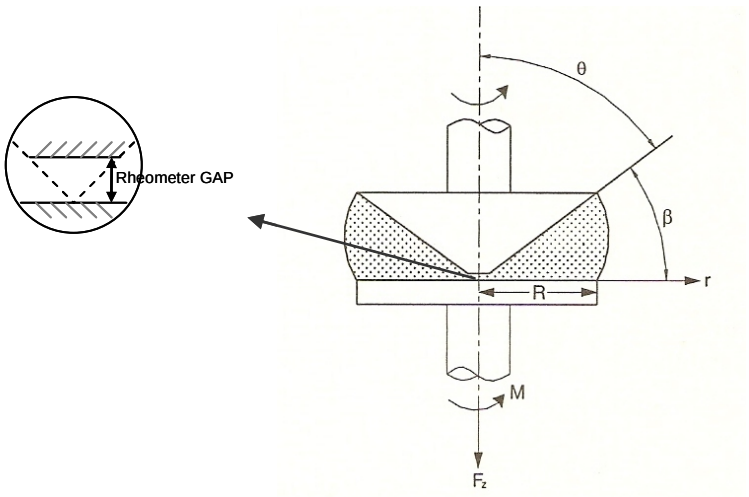

Figure 3.5: Cone-plate geometry.

This type of rheometer requires a robust and accurate building, since the effect of eccentricities, oscillations and misalignments is particularly relevant to low conicity. Additionally, some important factors should be noted about using rheometers and choosing the appropriated geometry. Among these factors, may be cited: calibration, artefacts, wall effects, evaporation, sedimentation/separation, chemical attack, mechanical damage, sampling, high-speed testing and suspended particles [215].

An apparent slip or lubrication occurs at the wall in the flow of any multiphase systems if the disperse phase moves away from smooth walls. This arises from steric, hydrodynamic, viscoelastic and chemical forces present in dispersions flowing near smooth walls and constraints acting on the disperse phase particles immediately adjacent to the wall [222].

The enrichment of the boundary near the wall with the continuous (and usually low-viscosity) phase means that any flow of the dispersion near such a boundary is easier because of the lubrication effect. Because this effect is usually confined to a very narrow layer-with typical thickness of 0.1-10 μm- it so resembles the slip of solids over surfaces that has historically been described by the same terminology. The restoring effect for all the forces that cause an increase in concentration as particles move away from walls is usually osmotic, and this always limit the movement of particles away from the walls, thus also limiting the effective slip [215].

Evaporation is often critical in cone-and-plate geometry, as drying at the edge of the samples leads to large errors in the measured torque, given that the effect is at the greatest distance from the centre. Two ways around this problem are: 1- create a saturated atmosphere in the air next to the sample or 2- flood the same area with solvent [215].

Another problem that can arise with long-term shearing is enhanced sedimentation. Even if the continuous phase dispersion has been thickened to slow down sedimentation at rest (as for instance in storage), when the sample is sheared, the continuous phase viscosity is greatly reduced and its ability to keep particles in dispersion can be severely impaired.

Finally, suspended particles can lead to two additional kinds of problem. First, large solid particles can become jammed in narrow parts. However, the cone truncation often used to prevent wear of the tip may help. Second, if the rheometer gap is not around five to ten times larger than the largest particles, then the correct viscosity of the material is not being measured, since the particles spatial distribution is being altered by the wall.

3.2.2. Microstructure analyses

Morphological and structural modifications at the nano or molecular level are responsible for changes in the properties of materials, hence a detailed and accurate characterization is required to establish structure-properties correlations. For this reason, electron microscopy has lately gained increasing importance [223].

Electron microscopy is an important technique to analyse the microstructure of the soft matter and therefore, very appropriate for bionanocomposites dispersions. The low temperature scanning

electron microscopy (Cryo-SEM) allows assessing the microstructures of the dispersions under their original aqueous form. Using this technique it is possible to control and to predict the resulting microstructures and morphology under quiescent conditions or during flow processing which is valuable for the design of new microstructures and hence textural characteristics [224].

Cryo-SEM was first performed in the 1960's but it wasn't until the 1980's that commercially available systems made it a routine facility in many laboratories. Cryo-SEM involves the examination of materials at below ambient temperature (typically between -100°C and -175°C), allowing the appearance of the sample to be preserved and recorded in the fully hydrated and chemically unmodified state.

First, the sample is cryo-fixed, generally by plunging it into sub-cooled nitrogen (nitrogen slush) close to the freezing point of nitrogen at -210 °C, then the sample is transferred *in vacuo* to the cold-stage of the SEM cryo-preparation chamber, where fracturing can be performed if necessary. The fully frozen sample is heated up to -95 °C to sublimate the near surface water to etch and contrast the structure. After sputter coating with metal (usually gold or platinum), the sample is transferred into the SEM chamber, where it remains frozen during imaging on another cold-stage, cooled by nitrogen [10]. The principal preparation steps are depicted in Figure 3.6.

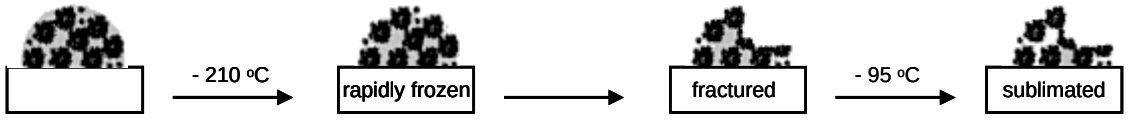

Figure 3.6: Preparation process of aqueous of composite dispersion for cryo-SEM investigations. Reproduced from [10].

Although still an expensive technique, this method is quick, relatively easy, and provides superior images to those dried samples (without previous treatment) visualised by SEM. It is also the only method that can be used successfully if one requires visualization of delicate or labile structures that would be lost during specimen drying processing. That is why cryo-SEM has become the method of choice for some polysaccharide/silica dispersions [80, 82, 156]. Another advantage is that large areas of an intact specimen can be studied, both at low and high magnification.

3.3. Rheology and microstructure of locust bean gum/silica dispersions

3.3.1. General considerations

3.3.1.1. Chemistry, structure and conformation of locust bean gum

The seeds of the carob tree have been known to be a pioneer source of seed galactomannans. Galactomannans represent an important group of plant mucilages, or plant gums which occur as storage polysaccharides in the seeds of numerous plants, particularly the Leguminoseae [225], composed of a mannan backbone partially substituted with single galactosyl groups. The two most important galactomannans are locust bean gum and guar gum, which are largely manufactured on industrial scale. In this thesis only locust bean gum features will be focused. Locust bean gum (LBG) is obtained from seeds of the carob tree *Ceratonia siliquia* [226]. This leguminous tree is native to the Mediterranean countries and extensively cultivated there. Current annual production in the world is estimated to be 415,000 tons and current prices are 12 to 22 Euros/kg or more depending on grade and supplier [227].

LBG is a natural non-ionic polysaccharide with a principal backbone (1-4) linked to a β-D-mannopyranosyl unit having side stubs of (1-6)-linked α-D-galactopyranosyl groups (Figure 3.7). This structure is commonly described as having an average of one D-galactosyl unit (G) for every four D-mannosyl unit[226, 228].

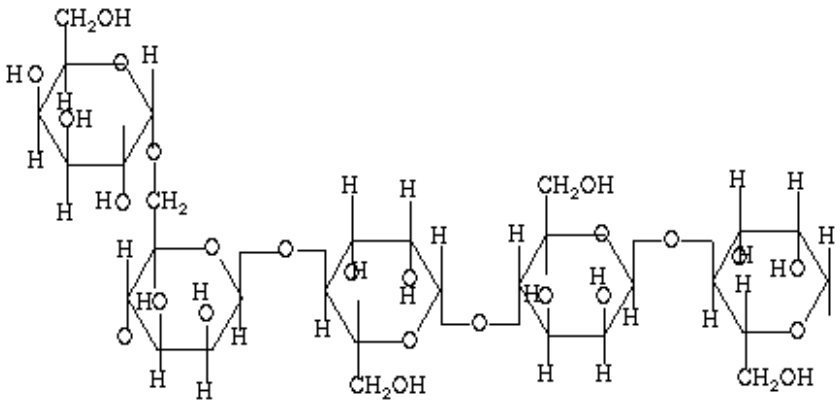

Figure 3.7: LBG structure.

In terms of chemical structure/property relationships, the average galactose content has been shown to strongly influence the physical properties of this galactomannan[229]. The degree of M/G may

vary depending on the origin, the variety and age of the plant (tree) and the growth conditions (climate, soil) of the seed [43, 46, 47]. Besides, the method used for extraction of the polysaccharide in terms of purification of crude gum may also influence the M/G of LBG [230]. The solubility of the galactomannan depends on the M/G ratio and on the distribution of galactose units along the mannan backbone chain: the larger the galactose content, the higher the solubility in water [13].

Among the major commercially available galactomannans (LBG, guar and tara gums), LBG galactomannan has the lowest galactose content [229-231] and as a consequence exhibits low solubility at ambient temperature and heat treatment is required for maximum solubilisation. Usually, LBG is completely dispersed in water after heating at ~ 80^{o} C for 20-30 minutes. The difficulty in dispersing LBG is presumably due to strong interactions between adjacent chains [230] i.e. when the mannose units of the backbone chain come in contact with mannose units of an adjacent chain, they bind strongly to one another and sufficient heat energy must be applied before these secondary bonds are broken [226]. Moreover, commercial LBG may show some turbidity caused largely by the presence of residues of germ and endosperm which depend on the degree of purification during the manufacturing process [225].

In aqueous solution, galactommanans exist in the random-coil conformation [232], and will only revert to a more ordered form if favourable conditions for aggregation or interaction with other species exist [230]. Following a computer simulated molecular space filling structure of LBG [11], it has been shown that the polysaccharide chains tend to be in a more stretched form in water than in vacuum (Figure 3.8), the helical structure being less complicated for LBG than for other galactomannans due to the lowest galactose units along the mannose chain.

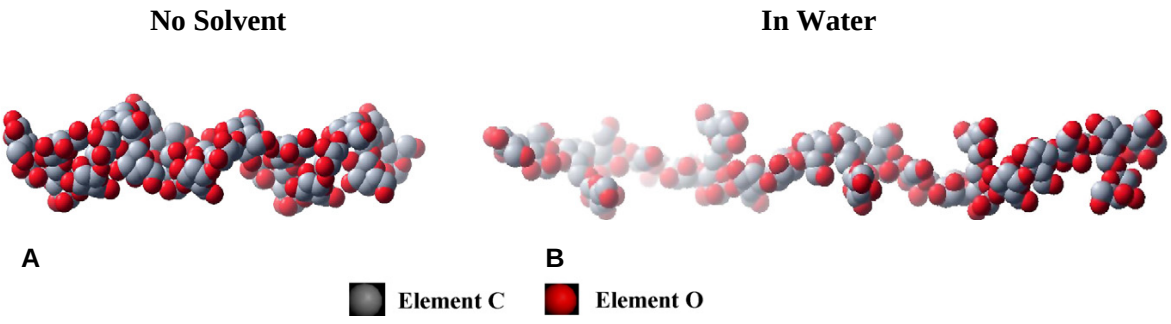

Figure 3.8: Computer simulated molecular of LBG structure: (A) LBG in vacuum (no solvent) and (B) LBG in aqueous media (each structure contains five repeat units) from [11].

3.3.1.2. Rheological properties of LBG solutions

LBG is one of the more efficient water-thickening agents among water-soluble gums. The rheological behaviour of its solutions is typically non-Newtonian classed as shear thinning. At relatively low concentrations (for example < 0.3%) the rheological behaviour in shear flow approximates to Newtonian. The maximum viscosity and the stability of the viscous solution during storage depend greatly on the gum dispersion conditions, including time and temperature [226, 230, 233]. However, in general, galactomannans solutions are rather stable and show practically no change in viscosity upon standing at room temperature, slight pH changes or addition of salts [225, 234]. They thin out reversibly when heat is applied and degrade irreversibly with the time when elevated temperature is maintained. The solutions resist shear degradation but it occurs progressively under high shear [226].

The two critical concentrations, C* and C**, defining the dilute, semi-dilute and concentrated regimes (§3.2.1.2), have been studied for LBG solutions and found to be around 0.1 wt.% [5] and 0.7 wt.% [14], respectively. In accordance with these results we can assume that LBG concentrations used in this thesis (0.4 up 0.5 wt.%) are in a semi-dilute region with $C^* < C < C^{**}$.

The molecular size and fine structure (galactose distribution in the mannose linear chain) influence the rheological properties of LBG; in particular, a higher mannose to galactose ratio (M/G) indicates a major linearity of the polymer (low number of galactose side chains) and a greater "effective volume" of the macromolecules [235], leading to higher thickening ability and higher propensity for aggregation processes [233, 234].

For LBG, Morris *et al*. [204] have used the term hyperentanglement to describe the lower concentration deviation of the coil overlap parameter at $c[\eta] \approx 2.5$ from that for random coil polymer solutions, $c[\eta] \approx 4$. This deviation to higher viscosity at lower concentrations along with the greater concentration dependence has been attributed to specific chain/chain interaction between galactose free mannan segments. Possibly in support of this interaction, the intrinsic viscosity increased as the average galactose content was reduced (11.7 dL/g for 19% galactose and 9.9 dL/g for 25% galactose) [236] and the level of hyperentanglement was more prevalent for galactomannans with a low galactose content, such as for LBG.

LBG can also undergo aggregation and gelation processes under certain conditions, namely self-association processes throughout interchain association of unsubstituted regions of the mannan backbone, induced by lowering temperature (freeze–thaw cycles or long aging at low temperatures) ou lowering water activity (in high concentration sugar solutions) [229, 231, 233]

3.3.1.3. Applications of LBG

LBG has long been used for moisture control and viscosity in food products. Since it is acid stable over a wide pH range and, therefore, used in both neutral and acidic systems.
Synergistic interactions with both xanthan gum and carrageenan have also created a demand for this polysaccharide [209, 237-239]. With xanthan, their interaction results in a gelled system suitable for structure and syneresis control in systems such as pet foods, processed and cream cheeses and dessert gels. When blended with carrageenan, the resulting gel is less brittle and more elastic than kappa carrageenan alone. In this blended system, locust bean gum also inhibits syneresis. This synergy is used extensively in ready-to-consume (RTC) shelf-stable dessert gels [240].

3.3.1.4. Inorganic–LBG composites

In view of the non-gelling nature of LBG some attempts have been made to increase its thickening and gelling properties including mixing with other biopolymers, cross-linking strategies, chemical modification, and preparation of inorganic-polysaccharide composites. Nevertheless, it is known that the use of cross-linking procedures and the chemical modification of LBG macromolecules may deteriorate the hydrogel biocompatibility of the biopolymer [156].

As previously mentioned (§ 3.1), Shchipunov *et al.* [81, 83, 85] have demonstrated that nongelable polysaccharide can be gelled by mineralizing their macromolecules with silica, including LBG. The potential use of LBG/SiO_2 composites for enzyme immobilization has also been demonstrated. For example, endo-1,3-β-D-glucanase was immobilized by sol-gel technology using LBG and other polysaccharides as templates for silica generated *in situ* [85]. The enzyme was entrapped into LBG-silica nanocomposites and it maintained its functioning. As a neutral polysaccharide LBG may have some advantages over charged polysaccharides such as cationic derivative of hydroxyethylcellulose or xanthan gum, which can act as cross-linking agents interacting with active centers of enzymes, decreasing or inhibiting their activity.

In this sub-Chapter, oscillatory and steady shear rheological methods as well as scanning electron microscopy were used to fully characterize the rheology and microstructure of locust bean gum/SiO_2 dispersions prepared by just mixing of the preformed silica nanoparticles into the biopolymer solution.

3.3.2. Experimental Part

3.3.2.1. Polysaccharide sample

Industrial grade locust bean gum (LBG) from *Ceretonia siliquia* was purchased from Sigma-Aldrich.

3.3.2.2. Preparation of LBG solutions and SiO_2 dispersions

LBG solutions (1.0 wt.%) were prepared in distilled water or in 0.1 mol/L NaCl by stirring moderately during 1 h at room temperature followed by 30 minutes at 90 ^oC. Finally the dispersions were centrifuged at 12000 rpm for 20 minutes.

Silica dispersions (10 up to 40 wt.%) were prepared by adding the activated silica powder to water or 0.1 mol/L NaCl at room temperature, stirring overnight, and then treated by ultra-sounds during 1 hour.

3.3.2.3. Preparation of LBG/silica dispersions

LBG/SiO_2 dispersions were prepared by simple mixture of components. Typically LBG solutions and dispersions of SiO_2 particles previously prepared were mixed (1:1), resulting in a final aqueous dispersion of 0.5 wt.% LBG and 5, 10 or 20 wt.% of SiO_2 particles. The pH was adjusted with HCl and/or NH_4OH. Finally the dispersion was stirred for 60 minutes under vacuum, in order to remove air bubbles, before being analysed.

3.3.2.4. Rheological measurements

Small-amplitude oscillatory and steady-state flow tests were performed using a rheometer operating in controlled stress mode (Bohlin CVO 120 HR) equipped with a cone-and-plate geometry (angle 4^o, diameter 4 cm).

Oscillatory linear viscoelastic experiments can provide useful information about the relaxation of the microstructure occuring in our samples. We have used different oscillatory shear tests in order to assess the rheological behaviour of the polysaccharide/SiO_2 dispersions. Time sweep tests, maintaining a small peak strain amplitude, at a fixed frequency ($2\pi\nu = \omega$) of 1 rad/s, were used to

ensure that slow relaxation processes were allowed to occur after loading the sample, avoiding any effects of shear during sample loading, and to assess any structure development processes depending on time.

Then, stress sweep tests were performed to identify the region of linear viscoelastic behaviour. All dynamic measurements were further performed at 20 ºC and at a low-strain amplitude inside the linear viscoelastic region as defined by the results obtained from the stress sweep tests.

The viscoelastic behaviour of the dispersions, namely the frequency dependence of the viscoelastic moduli G' and G'', after certain curing times onto the rheometer, was assessed from frequency sweep experiments (0.01-10 rad/s), at low strain amplitude within the linear viscoelastic regime.

Steady-shear flow tests were performed by an up–down step program applying a different shear stress range to each sample. The sample was held at each programmed stress for typically 60 s. Flow data were obtained typically between aprox. 0.01 and 1000 s^{-1}, depending on the sample.

3.3.2.5. Cryo-scanning electron microscopy (cryo-SEM)

The microstructure of the LBG/SiO_2 composites has been analysed by Cryo-scanning electron microscopy (cryo-SEM). Samples were maintained under quiescent conditions during 2 - 4 hours and frozen under liquid nitrogen. The frozen samples were sublimated at -95 ºC during 2 minutes and the fractured surfaces were coated with Au/Pd during 15 seconds. Analysis was performed at -140 ºC using a FE-SEM JEOL JSM6301F microscope operating at 15 kV and coupled with a Cryo-SEM unit Gatan model ALTO 2500.

3.3.3. Results and Discussion

The LBG/SiO_2 composite dispersions analysed in this Chapter were prepared from aqueous LBG solutions with concentration inside the semi-diluted regime [229, 241], in the range 0.4 - 0.5%, for two different pH (3 and 5) and especially for silica particles with AD ~ 300 nm (Si-300), at different amounts (0-20 wt. %). Some tests have been done also using 0.1 mol/L NaCl as solvent in order to investigate the effect of the ionic strength, especially on the ionic behaviour of the silica particles.

The characterization of the rheological behavior of the LBG/SiO_2 composites comprised the study of the (a) structure development under low strain amplitude (curing tests); (b) the linear viscoelastic behaviour (stress sweep tests); (c) the effect of oscillatory frequency (mechanical spectra), (d) the

flow behaviour, and (e) the applicability of the Cox-Merz rule. The microstructure of the prepared composite systems was analysed by cryo-SEM.

3.3.3.1. Rheological changes with time at constant frequency

After loading onto the rheometer measuring system, the composite dispersions were allowed to reach a mechanical equilibrium state as determined by measurements of the time-dependent moduli under low-strain harmonic shearing and constant oscillatory frequency (1 rad/s) and temperature (20 ºC) These ageing effect are illustrated in Figure 3.9.

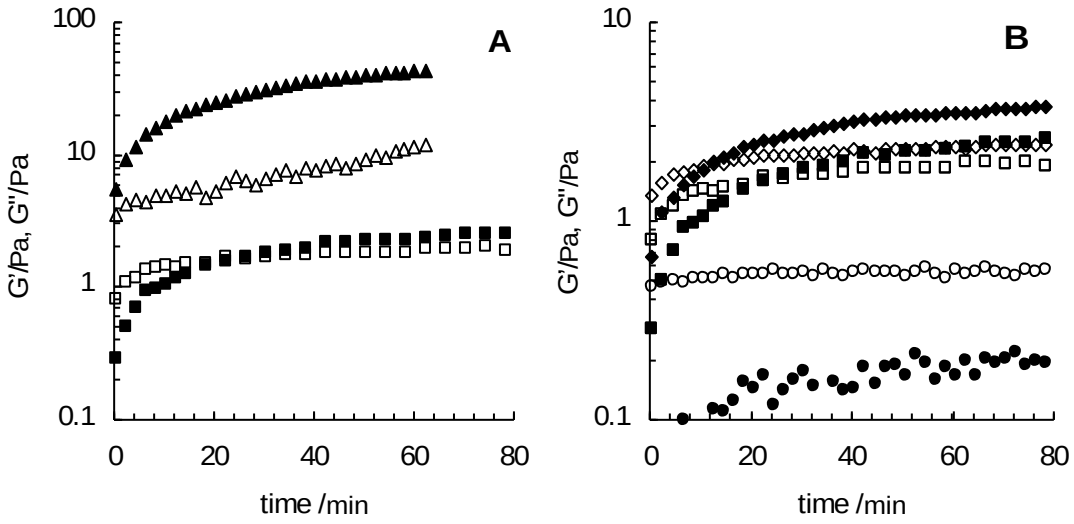

Figure 3.9: Evolution of the storage (*G'*) and loss (*G''*) shear modulus at ω = 1 rad/s for silica dispersions in 0.5 wt.% LBG: (**A**) in water at pH 3 for 10 (■,□) and 20 (▲,△) wt.% silica; (**B**) 10 wt.% silica under different ionic conditions – in water at pH 3 (■,□) and pH 5 (●,○), and in 0.1 mol/L NaCl at pH 3 (◆,◇).

The measured viscoelastic moduli for the LBG solutions alone did not change with time. However, kinetic effects were clearly evident for the LBG/SiO_2 dispersions, especially for particle loadings above 10 wt. %. The recovery time or the aging processes were different for each sample, with a clear dependence on particle concentration and ionic conditions. Typical behaviour involved an early stage, a relatively short period, in which the modulus rose more rapidly then followed by a second, longer period in which the modulus continued to increase at a lower rate. For 5 wt.% silica loadings, little ageing effects were observed with small changes on both viscoelastic moduli even after long time periods (24 hr maximum analysed – results not shown).

Both the storage (*G'*) and loss (*G''*) moduli increased with the ageing time. Certain samples showed already at the beginning a high structure with *G'* > *G''* as is the case of the 20 wt.% silica/LBG dispersions (Figure 3.9A). Especially for the 10 wt.% silica dispersions, initially *G''* > *G'* up to the crossover point, i.e., the point at which *G'* becomes larger than *G''*, indicative of a liquid-like to a solid-like transition.

Figure 3.9B also illustrates the evolution of the viscoelastic moduli for 10 wt.% silica dispersions in 0.5 wt.% LBG solutions, under different ionic conditions. NaCl addition is expected to significantly decrease the repulsive electrostatic forces between charged silica particles at pH 5. At an ionic strength of 0.1 mol/L NaCl the onset of this critical transition occurs faster (Figure 3.9B), and an opposite effect was observed by increasing the pH, which implies that the gelation was improved by lowering the charge density on the silica particles. Therefore, the viscoelastic moduli reach higher values, which correspond to more rigid structures at rest, and the rate of gelation increases as the particle loading or the ionic strength increase, or the pH decreases, at least within the ranges analysed for these variables.

3.3.3.2. Strain dependence of the viscoelastic response

After ageing until the moduli had become stationary, stress sweep tests were performed in order to analyse the strain sensitivity of the LBG solutions and LBG/SiO_2 dispersions. These tests will be important to obtain well resolved displacement readings (above the lower limit of the displacement measuring system), and to work in a region of linearity of the measured dynamic properties; in addition they can provide some information about the structural organization of the composite systems.

For better comparison the apparent complex modulus (G^*_{ap}) was plotted as its reduced form – $G^*_{ap}/G_0{}^*_{ap}$ as a function of strain for polysaccharide solutions and composite dispersions at different pH and for different particle loadings. Results obtained are shown in Figure 3.10 whilst those at higher ionic strength are illustrated in Figure 3.10B.

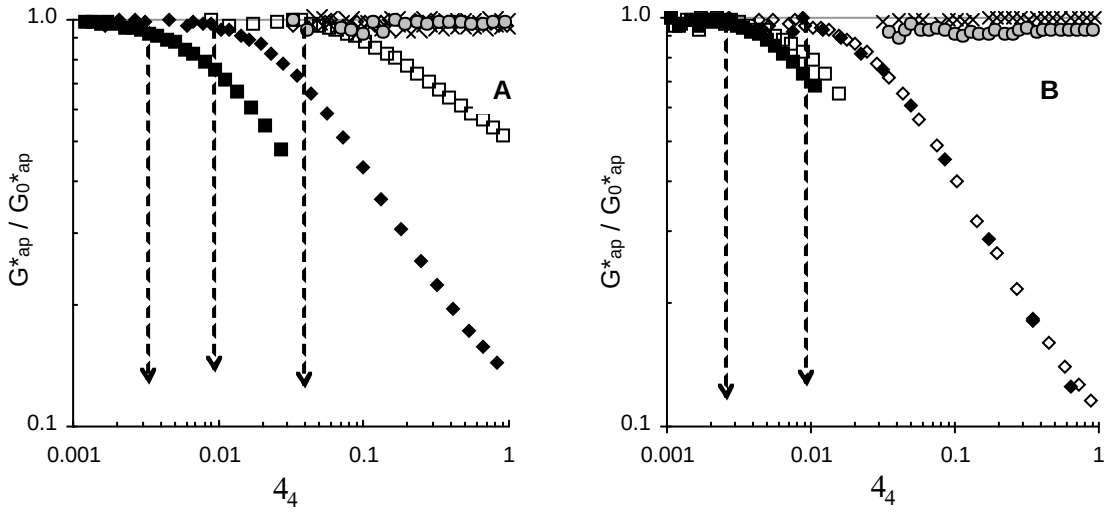

Figure 3.10: The reduced complex modulus ($G^*_{ap}/G_0{}^*_{ap}$) as a function of strain (γ_o) (frequency 1 rad/s at 20 ºC) for: (**A**) LBG in water, at pH 3 (⊙) and pH 5 (x) and LBG/10 wt.% SiO_2 in water, at pH 3 (◆) and 5 (◇), and LBG/20 wt.% SiO_2 in water, at pH 3 (■) and 5 (□); and (**B**) same composite dispersions in 0.1 mol/L aqueous NaCl. G^*_o denotes the G^* at the beginning of the stress sweep experiment, after meaningful results were obtained; the dashed lines are shown as guides to the eyes for the approximate strain limits of linearity (γ_{oc}).

The stress sweep experiments showed that the linear viscoelastic region for the LBG solutions, for concentrations in the range 0.4 to 0.5 wt. %, is quite extended, with linear viscoelastic limits extending to strain values around 100% or even higher. However, due to the lower limit of the instrument regarding the displacement measurements, well resolved displacement readings could be obtained only for strain values above 10% or higher.

The strain dependence of the viscoelastic response was noticeably different for the LBG/silica composite dispersions in comparison with LBG solutions.

In Figure 3.10, it is observed an elastic response until a certain critical strain amplitude value, after which the normalized (nonlinear) modulus, i.e. the reduced complex modulus decreases, slightly at first and then markedly. In certain cases and extensive disruption of the dispersions occurs, as it is evident by the marked decrease in the modulus.

The limit of the linearity decreases with the concentration of particles. The addition of salt (especially at pH 5) or lowering the pH resulted in a decrease in the value of the critical strain. Under higher ionic strength the pH effect is clearly masked (Figure 3.10B).

In general, the deviation from linear behaviour for the composite materials occurs at very low strains, in certain cases very close to the resolution limit of the rheometer, especially for the systems with 20 wt.% silica particles and under conditions of low ionization of the silica particles

or at high ionic strength where the counter-ions can shield the charges on the silica particles. The low value of the limit of the linear viscoelastic domain clearly suggests the presence of a relatively fragile ordered structure.

Many complex fluids exhibit indeed a nonlinear response even at very small applied strains. This behaviour is observed for diverse systems including waxy-oil gels [200], protein particulate gels [242], dough wheat flour (essentially a dispersion of starch granules in a protein matrix) [243], emulsions [244], a variety of colloidal dispersions [245-247]; inorganic-polymer dispersions [178, 182, 189], and several others colloidal systems, and is usually attributable to the strain-induced disruption of the fragile structural interactions among the network forming units (low energy interactions between structural units building up the colloidal system). Similar causes should apply for our systems, as it will be discussed in the next sections.

Additional details on the strain dependence of viscoelastic moduli, of the LBG/SiO_2 dispersions are shown in Figure 3.11.

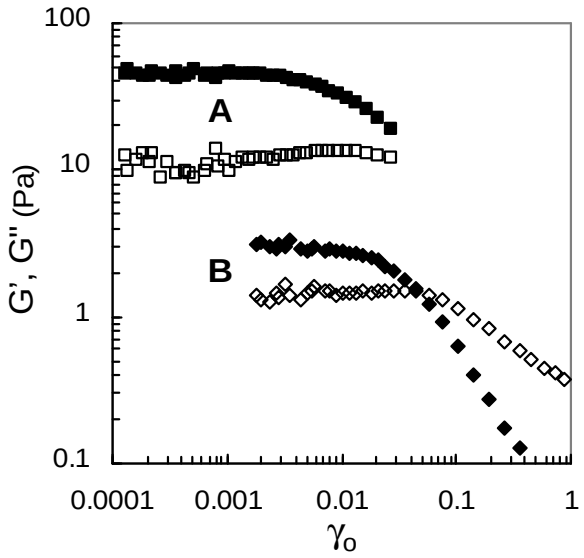

Figure 3.11: Variation of the storage (G', solid symbols) and loss (G'' open symbols) moduli with strain amplitude, γ_o (frequency 1 rad/s, 20 ºC), for: (**A**) a LBG/SiO_2 dispersion in water, at pH 3, at 20 wt.% SiO_2; and (**B**) a LBG/SiO_2 dispersion in 0.1 mol/L NaCl, at pH 5, at 10 wt.% SiO_2.

After an initial region of not-well resolved displacement readings, followed by a very short linear region, *G´* is shown to decrease rapidly above a strain exceeding a certain value, in this case 0.005 and 0.02 for 20 wt.% silica particles in water at pH 3 and for 10 wt.% silica particles in 0.1 mol/L NaCl at pH 5, respectively. The loss modulus, *G''* slightly increases initially after a short linear region, and then also decreases monotonically as the strain amplitude increases. At larger strains,

the power law exponent *a* of $G''_{ap} \propto |\gamma|^{-a}$ is about one half of the exponent associated with G'_{ap} (Figure 3.11B).

The initial increase of G''_{ap} with strain, until a certain strain limit value is reached, has been observed for dispersions of fumed silica [182, 245, 248] and attributed to the destruction of the structure or breakdown of the filler network, resulting in loosen polymer chains or a larger number of smaller size units which are more dissipative. Miyazaki *et al.* [249] have shown that this kind of dependence of the viscoelastic moduli on strain amplitude is a quite general process observed in metastable complex fluids and argued that it is associated to a strong decrease of the structural relaxation time at large strains. They argumented that this general behaviour should be observed for systems which exhibit slow dynamics and possess a broad band of solid-like behaviour above a crossover frequency where the storage modulus is larger than the loss modulus, i.e. behaving like an elastic solid at small strain but yielding and flowing at larger strains.

3.3.3.3. Viscoelastic behaviour: changes with oscillatory frequency

After the time sweep tests described before, frequency sweep tests were performed to characterize the viscoelastic behaviour of the polysaccharide/SiO_2 systems. We have focused mainly on the effect of the ionic conditions, silica amount and size of the silica particles.

3.3.3.3.1. Effect of particle size

As is well-known, the properties of the nanocomposites strongly depend on different properties of the polymer, filler and interface. The size of the particles is one of the composite characteristics that is expected to play an important role on their properties. The size of the particle is directly related to the area-to-volume ratio. Thus, assuming spherical shape and good particle dispersion in the polymer matrix, smaller particles will have higher surface area-to-volume ratio than bigger particles. This high surface area-to-volume ratio means that for the same particle loading, nanocomposites prepared with smaller particles will have a much greater interfacial area.

Having this in mind we have performed some tests in order to evaluate particle size effects on the rheological behaviour of the LBG/silica dispersions. Figure 3.12 shows the mechanical spectra (storage modulus *G'* and the loss modulus *G''*, the real and imaginary components of the complex dynamic modulus, respectively, as a function of the angular frequency, ω) for LBG composite

dispersions containing SiO_2 particles with different diameters (100, 300 and 500 nm) and concentrations (5, 10 and 20 wt.%), at pH 3.

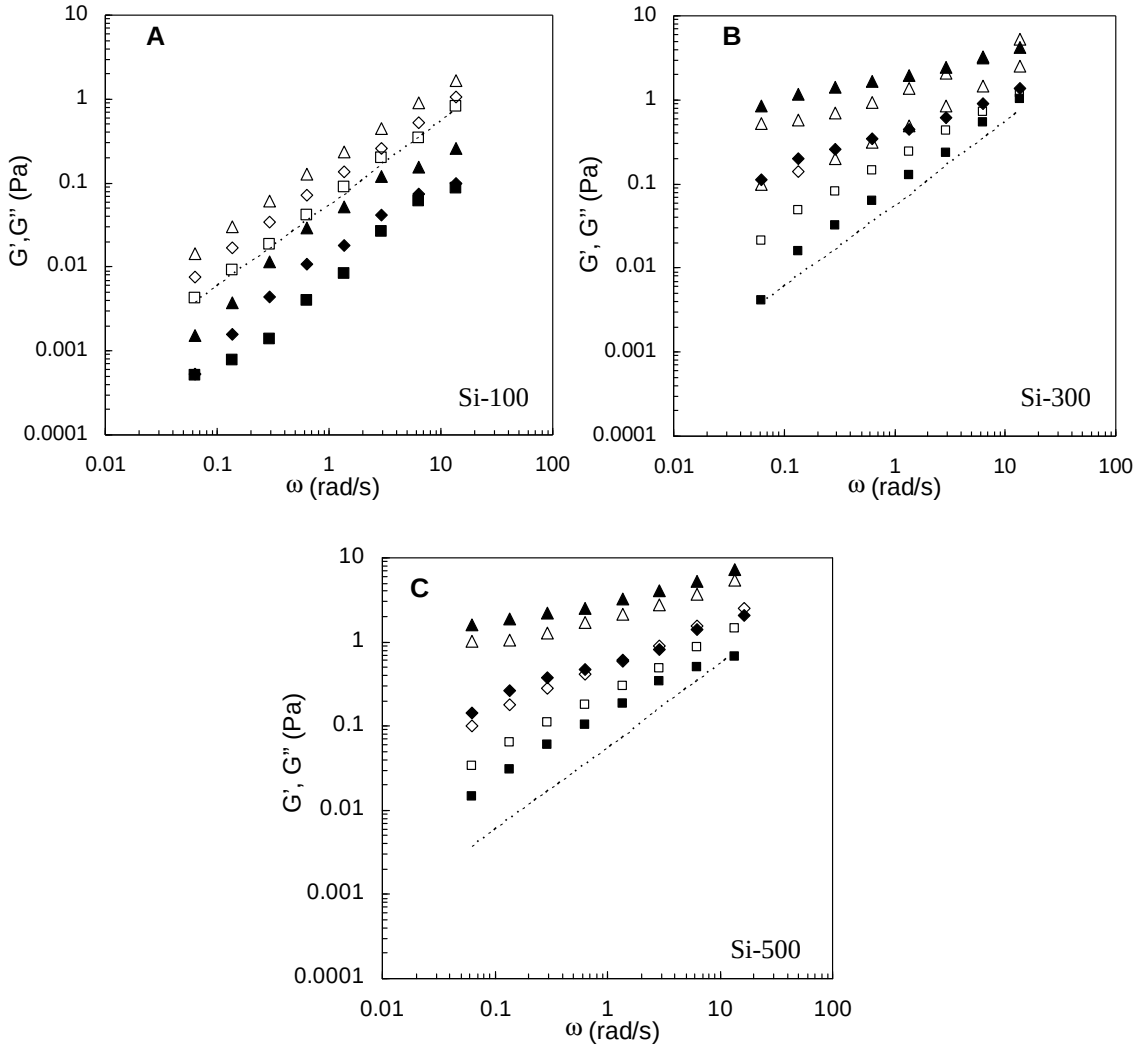

Figure 3.12: Dependency of the shear viscoelastic moduli (G', solid symbols, and G'', open symbols) against the oscillation frequency (ω) at pH3 for 0.4 wt.% LBG solutions, with different amounts and diameter of added silica particles, at (**A**) Si-100, (**B**) Si-300 and (**C**). Si-500. Lines denote G'' for the 0.4 wt.% LBG solution, and symbols denote the composite systems: (■,□) 5 wt.%, (◆,◇) 10 wt.% and (▲,△) 20 wt.% silica. G' values for the LBG solutions were below rheometer resolution and they are not shown.

In general, the presence of silica particles with different sizes influenced the gelling properties of the LBG 0.4 wt.% solutions, particularly at high particles loadings. Nevertheless for composite dispersions prepared with Si-100 at different silica concentrations (Figure 3.12A), the viscous component was higher than elastic component (G'' > G') in the whole experimental frequency interval.

For LBG/Si-300 and LBG/Si-500 dispersions (Figure 3.12B and 3.12C) it was observed that the increase of silica concentration yielded typical weak gel-like systems essentially at low frequencies. The viscoelastic moduli observed were practically equal for both dispersions in a specific SiO_2 concentration. However, for lower silica concentration (5 wt.%) the dependence of *G'* and *G"* on ω clearly increased resembling that of the biopolymer solution behaviour.

Despite the different surface properties obtained for Si-300 and Si-500 (§ 2.3.1) it seems that the size effect was masked by the presence of large aggregates at this pH as probed in Figure 2.9.

3.3.3.3.2. Effect of silica concentration at different ionic conditions

Figure 3.13 shows the mechanical spectra obtained for LBG/SiO_2 composite dispersions in water at pH 3 and pH 5, for different silica amounts. LBG/SiO_2 composite dispersion prepared in 0.1 mol/L NaCl was also plotted.

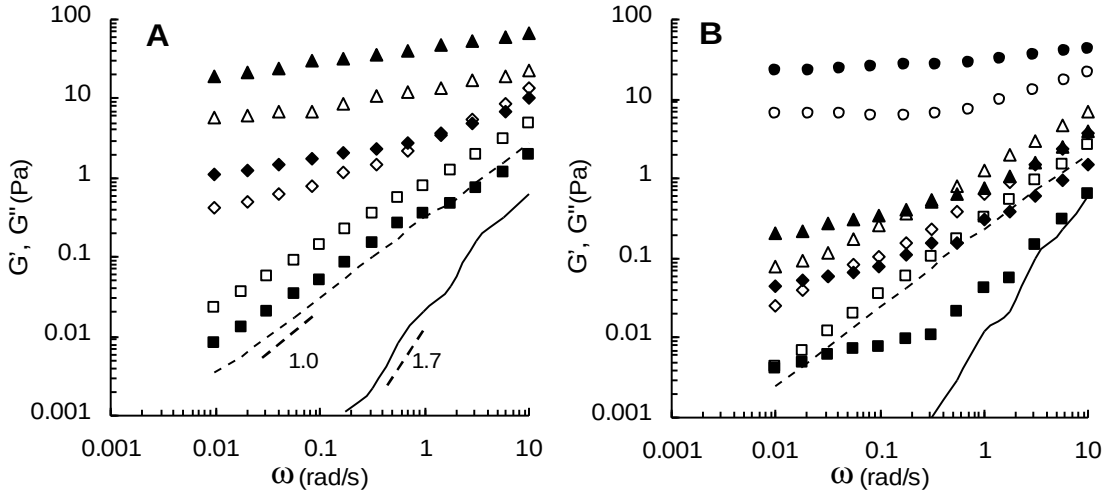

Figure 3.13: Dependency of the shear viscoelastic moduli (G', solid symbols, and G", open symbols) against the oscillation frequency (ω) for 0.5 wt.% LBG solutions with different amounts of added silica particles, at (**A**) pH 3 and (**B**) pH 5. Symbols for composite dispersions: (■,□) 5 wt.%, (◆,◇) 10 wt.% and (▲,△) 20 wt.% silica. The mechanical spectrum for LBG/20 wt.% SiO_2 in 0.1 mol/L NaCl at pH 5 (●,○) is also shown in (**B**). Lines denote G' and G'' for the 0.5 wt.% LBG solution.

At low frequencies the LBG chains exhibit typical terminal behaviour with the scaling properties of approximately $G'(\omega) \sim \omega^2$ and $G''(\omega) \sim \omega$, as is expected for a liquid system [250]. It is the characteristic behaviour observed for a disordered random-coil polysaccharide in aqueous solution, where the interactions between the polymer chains are physical and temporary, mainly van der

Waals and hydrogen bonds, and the influence of topological constraints (or entanglements) can be observed at higher frequencies or when the polymer concentration increases.

However, as the silica loading increases, this terminal behaviour disappears, and the dependence of G' and G" on ω clearly decreases, especially at low frequencies. Both moduli increase but the corresponding increase in the loss modulus G" is lower (i.e., reinforces the matrix). At low frequencies, G'(ω) becomes almost independent of the frequency as particle loading increases, suggesting an onset of solid-like behaviour in these composite systems, reaching the viscoelastic behaviour typical of a solid-like (soft) material. The effect of the filler is much higher at low frequencies than at high frequencies. Nevertheless, even at high frequencies, particularly at pH 3 or at high ionic strength, one can still observe the general increase of both moduli as the silica concentration increases, i.e. the short-range dynamics of the LBG chains is also influenced by the presence of the filler particles. In water at pH 5 the slopes at high frequencies do not change much (0.92-0.73), indicating that the viscous losses at high frequency are essentially the same as for the neat polysaccharide.

For low filler amount the moduli are still strongly dependent on the frequency and *G'* remains lower than G" whatever the frequency is within the analysed range and no plateau is noticed at low frequency, as expected for a typical viscoelastic liquid. However, even in this case, as one can observe in Figure 3.13A for the LBG/5 wt.% SiO_2 dispersion, the viscoelastic profile corresponds closely to the critical gel behaviour at the sol-gel threshold, characterized by a similar power-law relationship between each modulus and frequency, $G' = G''/\tan(n\pi/2) \propto \omega^n$, with $n = 0.78$.

Subsequently, at some critical loading level, a crossover of the *G'* and *G"* curves may be observed with the appearance of a plateau at low frequency and G' becomes higher than G", what is characteristic of a liquid–gel transition as mentioned before.

A transition to a solid-like viscoelastic response, especially at low oscillation frequencies, has been reported for several polymer nanocomposites, as the filler concentration was increased. These observations were reported mainly for filled polymer melts [178-181, 251].

Another indicator supporting that the LBG/silica dispersions exhibit more solid-like behaviour as the amount of the filler increases and essentially at low frequencies is revealed when the complex viscosity ($|\eta^*|$) of the composite dispersions is plotted against the frequency (ω) (Figure 3.14).

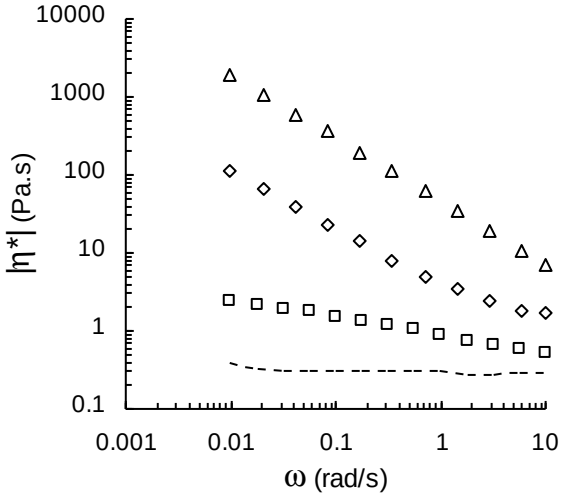

Figure 3.14: Dependency of the complex viscosity (|η*|) on frequency (ω) for 0.5 wt.% LBG solutions, with different amounts of added silica particles, in water at pH 3. Line denote the 0.5 wt.% LBG solution, and symbols denote the composite dispersions: (□) 5 wt.%, (◇) 10 wt.% and (△) 20 wt.% silica.

Consistent with the behaviour observed for the viscoelastic moduli at low frequencies, (Figure 3.13), the complex viscosity for the LBG/silica composites (Figure 3.14) also diverges at low frequencies, in contrast to the Newtonian plateau exhibited by the neat polysaccharide solution. At pH 3 in water dispersions, the frequency dependence of $|\eta^*|$ at low frequencies is ~ $\omega^{(-0.21)}$ for LBG/5 wt.%SiO_2 and increases to ~ $\omega^{(-0.81)}$ for the LBG/20 wt.%SiO_2 dispersion, indicative of a more solid behaviour as the silica loading increases.

The quantitative differences about this changing behaviour with pH can be observed by comparing Figure 3.13 A and B. The sol-to-gel transition occurs for a higher amount of silica at pH 5. The low-frequency power-law dependence of G' decreases monotonically with increasing particle loading, at pH 3 from $\omega^{1.7}$ to $\omega^{0.18}$ and at pH 5 from $\omega^{1.8}$ to $\omega^{0.25}$, for 0 and 20 wt.% SiO_2, respectively.

As expected for a neutral polysaccharide in this concentration range, changing the pH or ionic strength had not any significant effect on the viscoelastic behaviour. However, the influence of the silica particles on the viscoelastic behaviour of the composite materials is noticeably dependent on the ionic conditions. In water, at low ionic strength, clearly the higher effect of the silica particles on the rheological behaviour of the LBG solutions is observed at low pH (Figure 3.13A), under conditions of low ionization of the silica particles. At low ionization of the silica particles (pH 3) increasing the ionic strength (0.1 mol/L NaCl) only increases slightly the moduli and decreases their dependence on frequency as illustrated in Figure 3.15. However, at higher particle ionization

(pH 5), increasing the ionic strength has a drastic effect on the viscoelastic behaviour, similar to that observed at pH 3, as exemplified in Figure 3.13B for the LBG/20 wt.% SiO_2 composite dispersion.

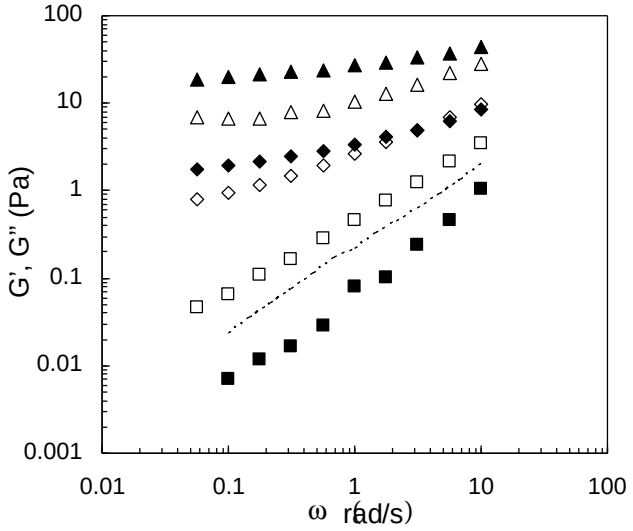

Figure 3.15: Mechanical spectrum (G', solid symbols, and G", open symbols) against the oscillation frequency (ω) for 0.5 wt.% LBG solutions with different amounts of added silica particles at pH 3. Lines denote the 0.5 wt.% LBG solution, and symbols denote the composite dispersions all prepared in 0.1 mol/L NaCl.: (■,□) 5 wt.%, (◆,◇) 10 wt.% and (▲,△) 20 wt.% silica.

3.3.3.4. Shear flow tests

The response of the biopolymer/silica systems to the steady shear tests, besides given some information about the microstructure of the material and how it responses to the applied high deformations, it will also provides useful information on the material processability.

The apparent viscosity as a function of shear rate for the LBG solution (0.5 wt.%) and for the composite systems prepared at the same polysaccharide concentration and different silica loadings, are shown in Figure 3.16. Figure 3.16 A and B reproduces these behaviours at pH 3 and pH 5, respectively. Moreover, flow curves obtained for LBG/20 wt.% silica at pH 3 and 5 with 0.1 mol/L NaCl are also shown in Figure 3.16 A and B to illustrate the significant effect of the salt upon the flow behaviour of the composite system at these pH.

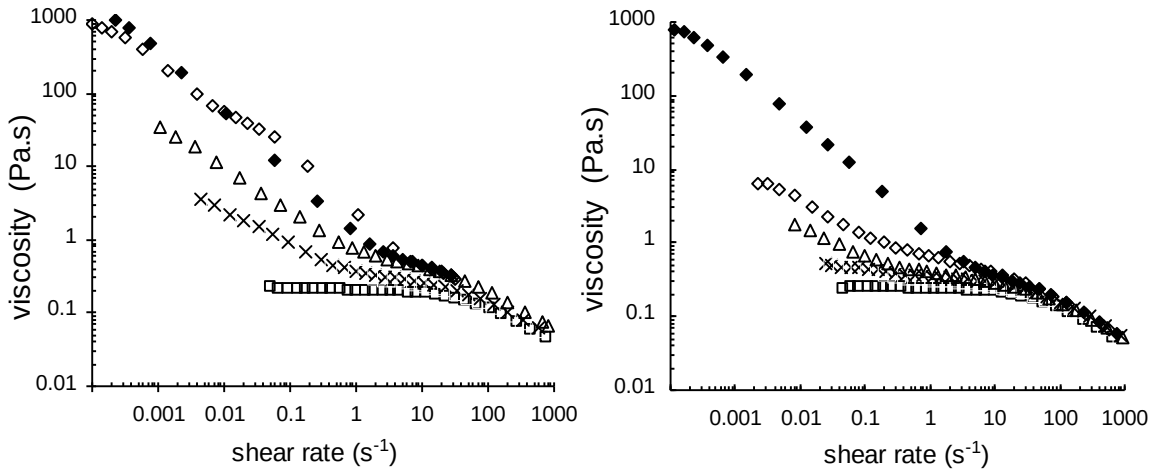

Figure 3.16: Apparent viscosity as a function of shear rate at 20 ºC for 0.5 wt.% LBG and LBG/SiO_2 dispersions, at (**A**) pH 3 and (**B**) pH 5: (□) neat LBG; (x) LBG/5 wt.% SiO_2; (△) LBG/10 wt.%SiO_2; (◇) LBG/20 wt.% SiO_2. Flow curves for LBG/20 wt.% SiO_2 prepared in 0.1 mol/L NaCl at pH 3 and pH 5 (◆). are also shown in Figure 16A and 16B respectively.

At pH 3 the LBG/SiO_2 dispersions showed similar flow behaviour with or without salt addition. The shear rate dependence of the steady shear viscosity clearly suggests that flow modifies the composite structure, as could be expected from the high strain sensitivity already observed.

LBG exhibited the characteristic behaviour of a random coil polysaccharide with the presence of a Newtonian viscosity plateau (η_0) at low shear rates and then a smooth transition to a power-law behaviour (shear-thinning).

The effect of the filler is observed mainly at low shear rates, namely in the shear rate range corresponding to the Newtonian plateau observed for the polymer solution (< 10 s^{-1}). In this shear rate range, the apparent viscosity increases and diverges as the silica loading increases, the Newtonian plateau vanishes, and the dispersions show an apparent "yield" behaviour. Qualitatively similar behaviour has been described for diverse colloidal dispersions [246] and many other filler/polymer nanocomposites [177, 179, 182, 252]. At higher shear rates the flow behaviour of the filled systems is quite similar to that showed by the biopolymer alone, irrespective of filler amount, pH or ionic strength, with viscosity values comparable to the unfilled biopolymer. These observations are consistent with the formation of a particle-mediated transient network, which is disrupted under shear, revealing essentially the polymer dynamics at high shear rate.

Even taking into account all the various limitations and stipulations inherent to the yield stress concept [253], the yield stress is still an useful engineering parameter and has an inherent important

physical meaning. In fact, the existence of yield stress has been recognized for long as a typical feature of rheological properties of filled polymers [254].

For the LBG/SiO_2 composite systems with high filler loading the apparent yielding after a critical stress to be reached is evident in the plots of viscosity as a function of shear stress illustrated in Figure 3.17.

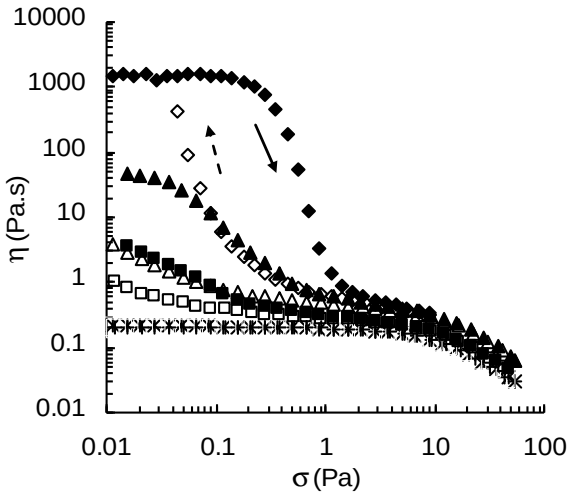

Figure 3.17: Apparent viscosity (η_{ap}) as a function of shear stress (σ) at 20 ºC for 0.5 % LBG and LBG/SiO_2 dispersions, at pH 3, showing the upward and downward curves, resulting from first increasing the applied stress, followed by the unload of the sample at a decreasing shear stress: (x up, + down) neat LBG; (■up, □down) LBG/5 wt.% SiO_2; (▲up, △down) LBG/10 wt.% SiO_2; (◆up, ◇down) LBG/20 wt.% SiO_2.

The polysaccharide solution showed no yield behaviour, with a Newtonian zone at low stresses followed by a smooth shear-thinning region at high stresses. This behaviour starts to change as the SiO_2 concentration increases, and for the system LBG/20 wt.% SiO_2 it can be clearly observed the typical yielding behaviour [253], with a high Newtonian viscosity at low stresses, followed by a sharp drop in viscosity, about 3 orders of magnitude, over a narrow range of higher stresses, i.e., an apparent yielding at about 1 Pa.

Also shown in Figure 3.17 are the upward and downward curves obtained by increasing and then decreasing the applied stresses. In the case of the LBG solutions, the up and down curves overlapped. However, for the LBG/silica dispersions, the up and down curves overlapped only at high stresses, but at low shear stresses, the down curve did not match the up curve anymore, the divergence being more pronounced as the silica concentration increases, suggesting a thixotropic behaviour, probably due to a partial breakdown of the weak network formed upon application of

shear. The pronounced hysteresis observed for the LBG/20 wt.% SiO_2 is typical of a gel-structured material.

Figure 3.18 displays the dependence of the complex viscosity (|η*|) on the complex modulus (G*) for the three composite samples at pH 3 and 5. Clearly, as the silica loading increases the viscosity diverges at a finite and large value of G*. The value of G* corresponding to the diverging viscosity can be taken as a crude measure of the yield stress [5]. Hence we can assume that the yield stress increases as the silica loading increases and/or as the silica charge decreases, in close accordance with the other indicators supporting that the composite composites exhibit a more pronounced solid-like behaviour as the amount of the filler increases and/or under low charge density of the silica particles.

We did not follow a semi-analytical procedure to quantify the yield stress, based on one of the possible equations predicting flow with a yield stress term, e.g. Casson or Herschel–Bulkley models. Suffice to mention that based on the stationary methods (Figure 3.17) or based on a dynamic approach (Figure 3.18) the LBG/silica composite dispersions show increasing apparent yield stresses as the silica loading increases, especially at pH 3 or in the presence of 0.1 mol/L NaCl, i.e., under conditions of low charge density on the filler surface.

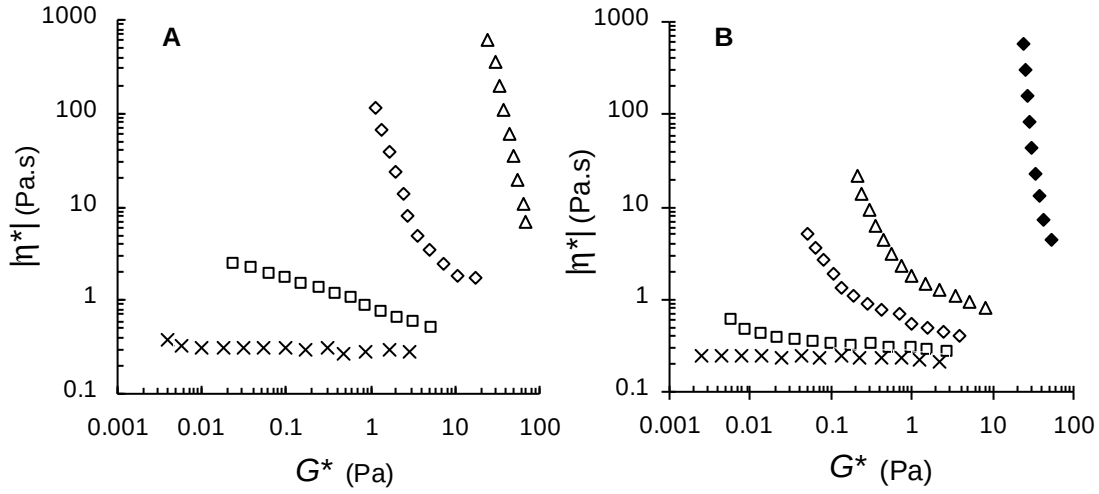

Figure 3.18: Complex viscosity (|η*|) against complex modulus (*G**) for 0.5 wt.% LBG solutions, with different amounts of added silica particles, in water at (**A**) pH 3 and (**B**) pH 5. Line denote the 0.5 wt.% LBG solution, and symbols denote the composite systems: (□) 5 wt.%, (◇) 10 wt.% and (△) 20 wt.% silica Curve for LBG/20 wt.% SiO_2 prepared in 0.1 mol/L NaCl at pH 5 (◆) is also shown in Figure 3.18B.

A thixotropic behaviour means that the viscosity of the dispersion will decrease under shear, but will return to its initial value after a rest time. However, in certain cases, if thixotropic by nature, full reversibility was not observed within the time range analysed. Also, in some cases, especially

at the lower shear rates, the time to attain the stationary flow was higher than 60 s at the applied shear stress. Therefore, all time-dependent phenomena should be analysed with caution. The flow curves and the measured yield stresses can actually be transient measurements dependent on the observation time.

3.3.3.5. Cox-Merz rule

We have also compared the steady-state apparent viscosity (η_{ap}) with the complex viscosity ($|\eta^*|$) obtained from the oscillatory experiments at low strain amplitude, in order to check the applicability of the Cox-Merz rule to our systems. The Cox-Merz rule is an empirical observation which states that the steady shear rate viscosity and the complex viscosity are closely superimposable for numerically equivalent values of shear rate ($\dot{\gamma}$) and frequency (ω) [35].

$$\eta(\dot{\gamma}) = \eta^*(\omega) \qquad \text{For } \dot{\gamma} = \omega$$

$$\text{With } \eta^*(\omega) = G^*(\omega)/\omega = \left[G'^2 + G''^2\right]^{1/2}/\omega \qquad \text{Equation 3.16}$$

Illustrative plots of steady shear rate viscosity and the complex viscosity against shear rate and angular frequency, respectively are shown in Figure 3.19 for the LBG/10 wt.% SiO_2 dispersions as examples of the observed behaviours.

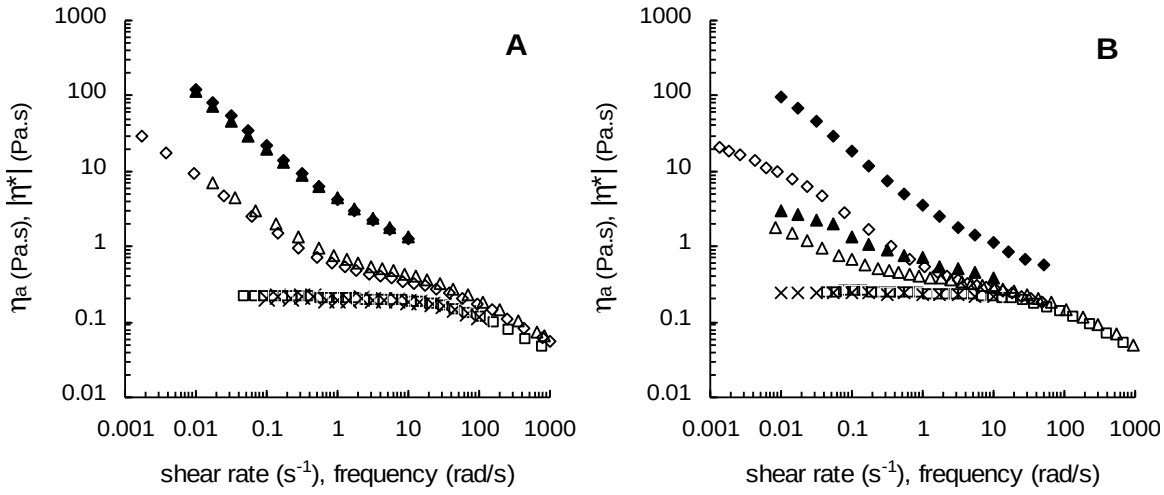

Figure 3.19: Comparison of the steady-shear apparent viscosity (η_{ap}) and the complex viscosity ($|\eta^*|$) for 0.5wt.%LBG/10 wt.% SiO_2 samples, at 20 ºC, at (**A**) pH 3 and (**B**) pH 5: (□-η, x-$|\eta^*|$) neat LBG; (△-η, ▲-$|\eta^*|$) LBG/10 wt.% SiO_2 in water; (◇-η, ◆-$|\eta^*|$) LBG/10 wt.% SiO_2 in 0.1 mol/L NaCl.

As opposed to what was observed for neat LBG solution, all the LBG/silica composite dispersions studied here fail to obey the Cox-Merz rule with $\eta(\dot{\gamma})$ always less than $\eta^*(\omega)$, being the discrepancies higher as the amount of silica increases. The structure of the materials is not affected under the linear oscillatory rheological tests where the strain was kept as low as possible to avoid any changes in the mesoscale structure, but the steady-shear viscosity is considerably lower than the oscillatory complex viscosity presumably because of an alteration in the mesoscale structure caused by the large displacements imposed during the steady shear experiments.

In Figure 3.19A one can observe that similar results and discrepancies to the Cox-Merz rule are observed for the LBG/silica dispersions in water or in 0.1 mol/L NaCl at pH 3. However, confirming what has been discussed above, at pH 5, for higher silica ionization (Figure 3.19B) the effect of salt is clearly significant, increasing the viscosities, and more important, increasing the departure to the Cox-Merz rule.

Failures of the Cox-Merz rule have been observed for other filled polymer systems and mesostructured materials [36], biopolymer dispersions with either hyperentanglements or aggregates [37] and complex food systems [38], and are generally associated to preferential orientation of the fillers, structure breakdown and/or disaggregation processes under the higher strains during the shear flow tests, what supports the existence of fragile networks in the biopolymer/silica dispersions under analysis.

3.3.3.6. SiO_2/LBG microstructure

Cryo-scanning electron microscopy was used to characterize the structure and morphology of the composite systems. Figure 3.20 shows cryo-SEM images (fracture surfaces broken in liquid nitrogen) reporting the microstructure of the SiO_2/LBG systems after curing for 2 h, under different conditions.

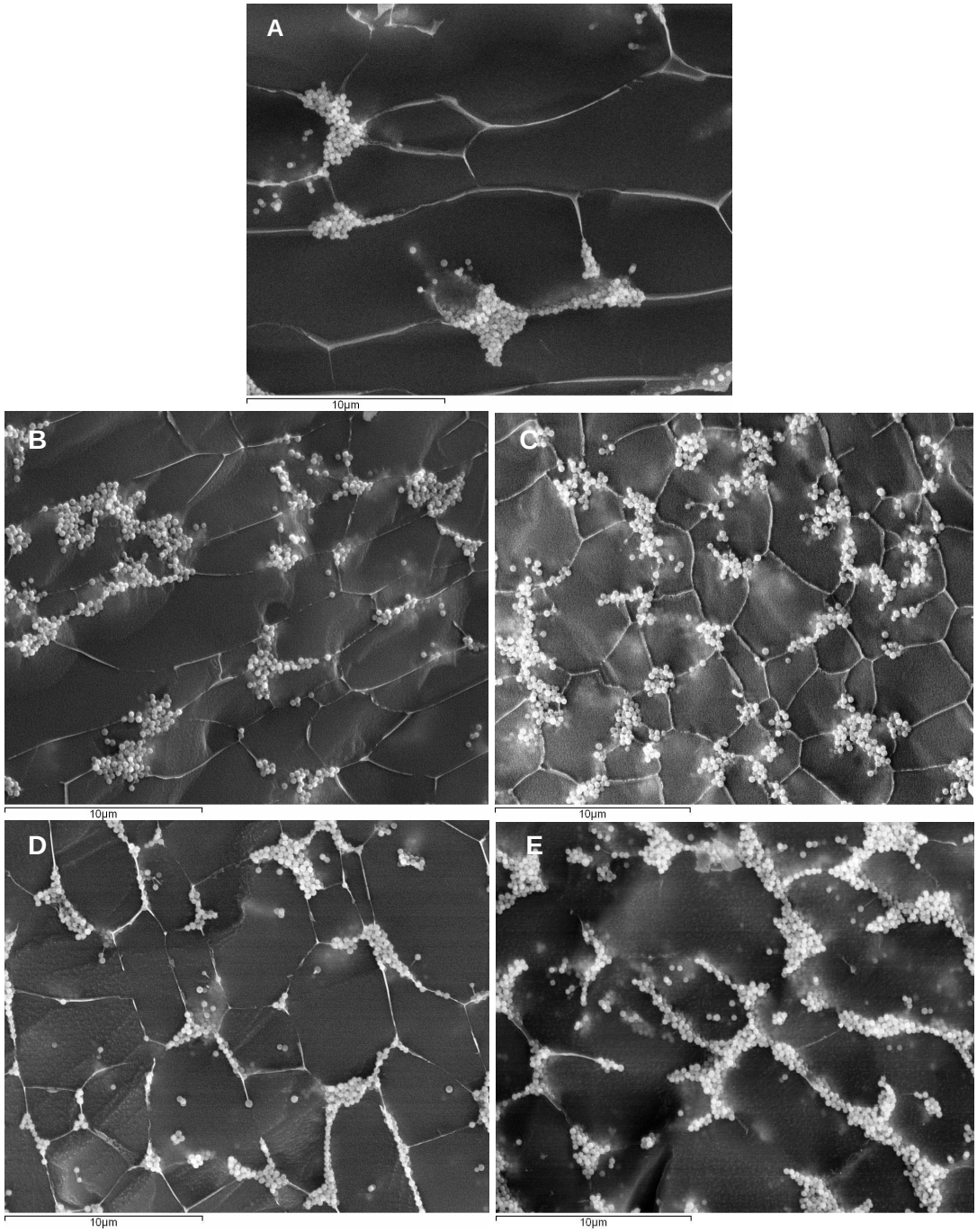

Figure 3.20: Cryo-SEM images of the LBG/SiO_2 composites: (**A**) 5 wt.% SiO_2 in water at pH 3; (**B**) 10 wt.% SiO_2 in water at pH 3; (**C**) 20 wt.% SiO_2 in water at pH 3; (**D**) 10 wt.% SiO_2 in water at pH 5; (**E**) 10 wt.% SiO_2 in 0.1 mol/L NaCl at pH 5.

The biopolymer chains seem to adopt stretched configurations and form a physical three-dimensional arrangement as seen by the thin fibrils or lamellar structures forming a regular meshed network. The particle distribution is not homogeneous in space. The silica particles are highly

organized forming aggregates around the polymer fibrils, contrarily to what was observed for some melt polymer nanocomposites [181].

The particle clusters seem to build a case around the polymer fibrils and the polymer appears to connect the filler clusters. Similar microstructural organization was also observed for hydrogels formed by sodium hyaluronate or cationic hydroxyethylcellulose and silica generated *in situ* by sol-gel processing [83]. Increasing the amount of silica added to the polymer matrix increases the number of silica clusters, and then also the number of polymer segments that are affected by the particles, but not their average size.

Changing the ionic charge of the particles, by increasing the pH (Figure 3.20D) or the ionic strength (Figure 3.20E) has a clearly effect on the size and morphology of the particle clusters surrounding the polymer chains. Whilst at pH 5 and in water medium the aggregates are more dispersed, at high ionic strength the aggregation is generalized. The polymer network reinforced by the particle clustering and some specific biopolymer-particle and particle-particle interactions would be the main responsible for the rheological behaviour previous described.

3.4. Rheology and microstructure of chitosan/silica dispersions

3.4.1. General considerations

3.4.1.1. Chitin occurrence and production of chitosan

The name chitin (χιτων from the Greek) means tunic or cover and it was given by Odier [255], who in 1923 isolated it from the elytrum of the cock-chafer beetle by treatment with hot alkaline solutions [255]. Because of its insolubility in the vast majority of common solvents, chitin was considered an intractable polymer and for many years it remained mainly a laboratory curiosity. Chitin is the second most abundant polysaccharide in nature after cellulose and the most abundant organic component of the skeletal structure of many classes comprising the group of invertebrates, such as arthropods, mollusks and annelids, constituting an important renewable resource. In animals, chitin occurs associated with other constituents, such as lipids, calcium carbonate, proteins and pigments. It has been estimated that the crustacean chitin present in the sea amounts to 1 560 million tons [256]. Chitin is also found as a major polymeric constituent of the cell wall of fungi and algae. However, these chitin sources are not large as compared with others, such as shrimps and crabs.

The knowledge about chitin polysaccharide led to the discovery of one most interesting functional biopolymer: chitosan. Chitosan is a linear heteropolysaccharide obtained by deacetylation of chitin consisting of 2-amino-2-deoxy-D-glucopyranose (glucosamine) and 2-acetamino-2-deoxy-D-glucopyranose (acetylglucosamine) units (Figure 3.21). However, since it is virtually impossible to completely deacetylate chitin, what is usually known as chitosan is a family of different chitins but always with low degrees of acetylation. The capacity of chitosan to dissolve in dilute aqueous solutions is the commonly accepted criterion to differentiate it from chitin [257].

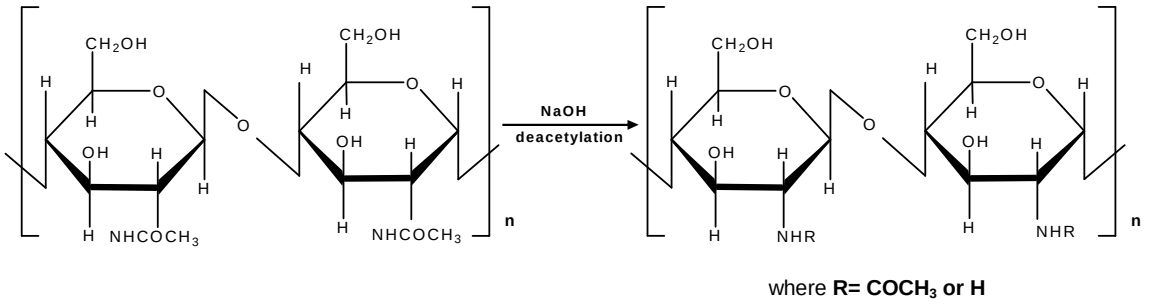

Figure 3.21: Chitin deacetylation to chitosan structure. Modified from [12].

The production of chitosan from crustacean shells obtained as a food industry waste is economically feasible, since the crescent amount of these sub-products constitute an environmental problem. Their biodegradation is slow, putrefying the proteins from shells and disabling their enzymatic compounds. The global production of shells of shrimp, prawns, lobsters, crabs, oysters, etc.., calculated on dry weight is estimated at 1.44 million tonnes [258]. This way, the discovery of many applications of the products extracted from these surpluses has had a remarkable impact particularly in obtaining chitin. Furthermore, the fact that chitin and chitosan are natural polymers, biodegradable, biocompatible and non-toxic, the reuse of these surpluses has become very important.

To obtain chitosan, the chitin deacetylation is performed by the hydrolysis of the acetamide groups at high temperature in a strongly alkaline medium. Generally the reaction is carried out heterogeneously using concentrated (40 - 50%) NaOH or KOH solutions at temperatures above 100°C, preferably in an inert atmosphere or in the presence of reducing agents, such as $NaBH_4$ or thiophenol, in order to avoid depolymerization. The specific reaction conditions depend on several factors, such as the starting material, the previous treatment and the desired degree of acetylation. Several treatments have been developed to prepare fully deacetylated chitosan. Their common characteristic is that they involve the repetition of consecutive deacetylation–washing–drying treatments as many times as required [257].

3.4.1.2. Chemistry, structure and conformation of chitosan

The degree of acetylation (DA) (ratio of acetylglucosamine to glucosamine structural units) is one of the more important chemical characteristics of chitin. This determines the content of free amino groups in the polysaccharide and has a striking effect on chitosan solubility and solution properties [12]. Varun *et al*. [259], and Aiba [260] besides other researches considered that when the DA of chitin is lower than about 50% (depending on the origin of the polymer and on the distribution of acetyl groups along the chains), it becomes soluble in aqueous acidic medium, and in these conditions, it is named chitosan.

Chitosan is distinguished from chitin by its solubility in dilute aqueous acid solutions. In it original conformation without modification, chitosan is insoluble in water, alkali and organic solvents, but is soluble in most solutions of organic acids when the pH of the solution is less than 6. Acetic and formic acids are two of the most widely used acids for dissolving chitosan. Some dilute inorganic acids, such as nitric acid, hydrochloric acid, percholoric acid and H_3PO_4, can also be used to prepare a chitosan solution but only after prolonged stirring and warming [261].

Chitosan becomes a polyelectrolyte in acidic conditions, which favours its solubility due to electrostatic repulsions; it is the only pseudo-natural cationic polymer and its solubility allows many applications [13, 262]. The solubilisation occurs by protonation of the $–NH_2$ function on the C2 position of the glucosamine repeat unit. The dependence of solubility upon DA may be explained by a decrease in the apparent pK_0-value (extrapolation of dissociation constant for a null charge) with DA or by a decreased possibility of aligning polymer chains when increasing the amount of randomly distributed acetylglucosamine units [259, 263].

The solubility of chitosan is a very difficult parameter to control: it is related to the DA, the ionic concentration, the pH, the nature of the acid used for protonation, and the distribuition of acetyl groups along the chain, as well as the conditions of isolation and drying of the polysaccharide showed below. It is important also to consider the intra-chain H bonds involving the hydroxyl groups [257, 264].

Another important characteristic to consider for these polymers is the molecular weight and its distribution. The difficulty encountered in this respect concerns the solubility of the samples and dissociation of aggregates often present in polysaccharide solutions [265].

Brugnerotto *et al*.[266] proposed the use 0.3 mol/L acetic acid/0.2 mol/L sodium acetate (pH = 4.5) as solvent to avoid aggregate formation in dilute solution. In this solvent, molecular weights are obtained by direct determination from steric exclusion chromatography using online differential

refractometry, viscometry and light scattering detectors, allowing then the determination of the parameters (K and α) from Mark–Houwink equation ($[\eta] = K \cdot M^{\alpha}$), and also the relation between the radius of gyration and the molecular weight.

The conformational analysis of chitin and chitosan with different degrees of acetylation (DA) has been developed by Mazeau *et al*. [267, 268]. They concluded that chitin and chitosan are semi-rigid polymers characterized by a persistence length (asymptotic value obtained at a high degree of polymerization) that depends on the DA of the molecule. From this analysis performed at 25 °C, chitosan, free of acetyl group, has an intrinsic persistence length L_p = 9nm when the electrostatic repulsions are screened; L_p increases when DA increases up to L_p = 12.5nm for DA = 60% and remains constant up to pure chitin. The local stiffness is related to the conformation of the molecule and especially to the intra-chain hydrogen bond network formed as shown in Figure 3.22 (one hydrogen bond involves OH-3 and O-5 and the second one OH-6 and N).

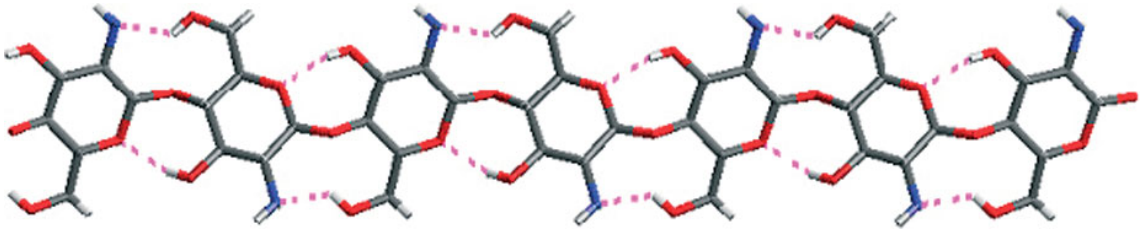

Figure 3.22: Molecular modelling of chitosan chain (two hydrogen bonds per sugar unit). Reproduced from reference [13].

Brugnerotto *et al*. [269] have also showed by ^{1}H NMR the decrease of the stiffness of chitosan when the temperature increases and this behaviour followed the prediction obtained from molecular modelling. A critical temperature around 40 °C was found where *L*p begins to decrease more significantly. This behaviour is very likely related to the destabilization of hydrogen bonds when temperature increases, indicating an increase of the chain mobility.

3.4.1.3. Rheological properties of chitosan

As mentioned for LBG solutions (§ 3.3) the chitosan solutions also behave generally as a typical non-Newtonian shear-thinning fluid [270]. The flow behaviour decreases with decreasing deacetylation degree (DD) and increasing solution concentration but it increases with increasing

temperature. Because of strong intermolecular hydrogen bonding even at low concentration, the chitosan molecules have a tendency to entangle forming a network [271].

The orientation of the dispersed asymmetric polymer macromolecules starts to occur in the shear stress experiment. With an increasing shear rate this effect will become more pronounced and will cause a progressive decrease of the internal friction of the molecules in solution because of a smaller effective interaction between the molecules.

The rheological properties of chitosan in solution are influenced by many factors, such as degree of deacetylation (DD), molecular weight, concentration, ionic strength, pH, storage stability and temperature [261, 271-273]. Hwang and Shin [262] observed that the shear rate dependence of viscosity increased with increasing chitosan concentration. As the polymer concentration is increased, the freedom of movement of the individual chains becomes restricted due to the increased number of entanglements. This gives rise to an increase of the time required to form new entanglements to replace those disrupted by the externally imposed deformation. Thus, the shear rate at which Newtonian behaviour is lost progressively moves toward lower values with the increasing polymer concentration. This explanation is consistent with the report of Morris *et al*.[204].

The effect of the deacetylation degree of chitosan on its rheological properties has also been studied by some authors [271, 274, 275]. In general, the viscosity of the chitosan solution at moderate concentrations decreases with increasing of DD. This behaviour can be attributed to the higher number of positively charged amino groups of chitosan. Moreover a higher molecular weight of chitosan sample causes its viscosity to increase.

No *et al* [273] studied the effect of storage temperature and time on the stability of chitosan solutions. They observed that the viscosity decreased with increased storage time. At 25 ^{o}C, the viscosity decreased rapidly by 46% (acetic acid as a solvent) and 43% (lactic acid) of the initial value (563 and 581 cP, respectively) after 1 week of storage. The viscosity then decreased by 81% (acetic acid) and 82% (lactic acid) of the initial value after 15 weeks of storage. On the other hand, the viscosity at 4 ^{o}C decreased gradually by 46% (acetic acid) and 47% (lactic acid) of the initial value after 15 weeks of storage. The trend of the decreasing rate of viscosity was similar between acetic and lactic acids in spite of the fact that acetic acid promotes acidic hydrolysis more effectively than lactic acid does [276]. The viscosity decrease observed over time is probably due to partial degradation of chitosan by organic acid solution.

The pH controls the ionization of the chitosan molecule, i.e. when the pH value is less than approx. 6.5, chitosan in solution carries a positive charge along its backbone. At pH-values greater than 6.5, since this value is approximately the pKa of the amino groups, chitosan solutions exhibit phase

separation. At pH values below 4, most of the amino groups of chitosan are supposed to be protonated, and since this effect promotes electrostatic repelling between charged groups of the same sign, it leads to enhanced swelling of the polymer network [277, 278]. Nystrom e*t al.* [279] observed that using a sample of chitosan with DD of 84% dissolved in 1% acetic acid (yielding a pH of approx. 3.) practically no pH dependence on its rheological properties was detected.

As reported for polyelectrolyte chains, the viscosity (η) of chitosan samples in aqueous solutions depends upon the ionic strength (I) of the medium: plots of η *versus* $1/\sqrt{I}$ are linear and the viscosity decrease with increasing salt concentration of the system is due to the shielding effect of the counterions [263]. This behaviour was also observed by Cho *et al* [272] for dilute and concentrated solutions of chitosan. They noted the presence of white-like precipitates formed above a specific I = 0.46 mol/L. This precipitation results from polymer-polymer interactions over those of polymer-solvent, and the decrease of the electrostatic repulsion by the salt screening effect.

3.4.1.4. Applications of chitosan

Due to the particular properties of chitosan already cited and depicted in Figure 3.23 it is easy to understand the great interest of many researches as well as industries for applications of chitosan and specific derivates [13, 257, 263].

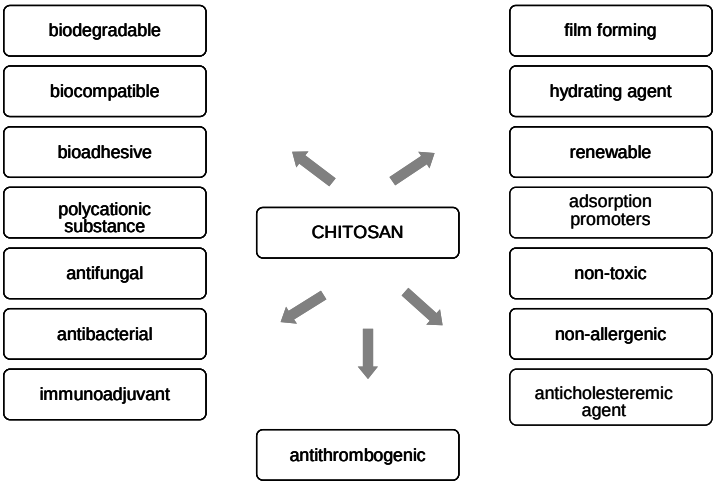

Figure 3.23: Main properties of chitosan. Modified from reference [13].

Chitosan is used to prepare hydrogels, films, fibres or sponges. The industrial production and use of chitosan has been steadily increasing since 1970s [261]. For a long time, the major applications of chitosan were focused on sludge dewatering, food processing and metal ion chelation. Nevertheless, the present trend, in industrial application is toward producing high value products,

such as cosmetics, drugs carriers, additives, semi permeable membranes and pharmaceutics including its potential use as biomaterial [261, 264, 280].

3.4.1.5. Chitosan/Inorganic composites

Chitosan at moderate concentration has not demonstrated gelling properties. However, there are numerous attempts to transfer it into the gelling group using different approaches. The general practice is to use a cross-linking procedure or modify their macromolecules chemically [83].

Inorganic particles have also be used as crosslinking agents, improving the physical and chemical properties of chitosan [156, 281, 282]. Silica is one the most widely investigated inorganic component in chitosan composites due to its compatibility and unique properties within natural composites leading to promising properties for the chitosan/silica composites, such as increase of mechanical and rheological properties, wettability, temperature degradation and others.

Chitosan/silica composite suspensions are more sparsely found in literature in spite of the importance to investigate their rheological properties before preparing composite membranes and for possible applications of these suspensions. Shchipunov *et al.* [156] have shown that nongelable polysaccharide could be gelled by their mineralizing with silica particles. Wang and Zhang [283] prepared a sol-gel chitosan-silica hybrid material to be used in the fabrication of an amperometric hydrogen peroxide biosensor. When the silica precursor THEOS was mixed with aqueous chitosan solution, no phase separation or precipitation was observed, showing a good compatibility. Moreover, the authors found that such mixing was sufficient to promote the synthesis of silica hybrid material. In the absence of chitosan, however, the sol-gel transition did not occur even at reduced temperature. It suggests that chitosan has a catalytic effect on the sol-gel process of THEOS. In fact, the gelation time and the dynamic rheological properties of the resultant gel matrix could be modulated by the amount of added THEOS.

In general, chitosan/silica composites have been studied in the form of films, which will be discussed in the Chapter 4. As referred above, in this sub-Chapter our interest is to study chitosan/silica composites under dispersions form.

As already mentioned the sol-gel processes show some disadvantages. An alternative route to prepare prepare chitosan/silica composites was proposed by Aubry *et al* [281], which consist of a direct addition of a silica particle dispersion to the polysaccharidic matrix. They studied dispersions of fumed silica particles (AD = 100 nm) in chitosan/acetic acid solutions at pH 4 under high ionic strength conditions. Chitosan chains were adsorbed on silica aggregates and the rheological properties of the chitosan/silica systems have been proved to depend mainly on chitosan

concentration regime, at least for silica volume fractions greater than 2%. Nevertheless, many questions remained opened, such as the size, shape and topology of the silica aggregates, as a function of silica content and chitosan concentration, in relation to adsorption.

Based on these questions we tried in this sub-Chapter to analyse through rheological measurements and microstructural analysis (cryo-SEM) the influence of silica aggregates on the gelling properties of chitosan at moderate concentrations. For this purpose, different concentrations of silica particles with distinct sizes were added to chitosan solutions in 0.1 mol/L CH_3COOH.

3.4.2. Experimental Part

3.4.2.1. Polysaccharide sample

Chitosan (CHI) from crab shells (with a degree of deacetylation of about 85% and medium molecular weight) was purchased from Sigma-Aldrich.

3.4.2.2. Preparation of CHI solutions and SiO_2 dispersions

CHI solutions were prepared in 0.1 mol/L CH_3COOH in a concentration range of 0.8 up to 1.8 wt.% by dispersion of the chitosan powder overnight under moderate stirring at room temperature followed by filtration under vacuum through a porous glass filter (G2).

Silica powder (10 up to 40 wt.%) with different sizes (100, 300 or 500 nm), prepared as described in § 2.2.3.1, was suspended in the same solvent used for chitosan solutions and maintained overnight under stirring and then treated by ultra sounds during 1 hour before the preparation of CHI/SiO_2 dispersions. To test the effect of ionic strength, the dispersion of silica particles was prepared in 0.1 mol/L CH_3COOH/0.1 mol/L NaCl aqueous solution.

3.4.2.3. Preparation of CHI/SiO_2 dispersions

CHI/SiO_2 dispersions were prepared by simple mixture of components. Typically CHI solutions and dispersions of SiO_2 particles previous prepared were mixed (1:1), resulting in a final aqueous dispersion of aprox. 0.4 - 0.9 wt.% of CHI and (5, 10 or 20 wt.%) of SiO_2 particles. The pH was adjusted with HCl and/or NaOH. The dispersion was then stirred for 30 minutes and submitted to mild vacuum for 30 minutes in order to remove air bubbles and then transferred to the rheometer measuring system for testing.

3.4.2.4. Rheological measurements

Small-amplitude oscillatory and steady-state flow tests were carried out using the same procedure described for LBG composite dispersions in § 3.3.2.4.

3.4.2.5. Cryo-scanning electron microscopy (cryo-SEM)

The microstructure of the XG/SiO_2 dispersions was analysed by Cryo-scanning electron microscopy (cryo-SEM) using the same procedure used for LBG composite dispersions mentioned in § 3.3.2.5.

3.4.3. Results and Discussion

Chitosan solutions (CHI) at semi-dilute concentrations were prepared in 0.1 mol/L CH_3COOH in a concentration range of 0.4 - 0.9% and mixed with silica particles at different contents (0 - 20 wt.%) forming composite dispersions. Due to the low solubility of chitosan at high pH values, the rheological measurements and the microstructure analysis of the chitosan composite dispersions were carried out at pH 3. In addition, some tests were performed in the presence of 0.1 mol/L CH_3COOH/0.1 mol/L NaCl aiming the investigation of the effect of the ionic strength on the behaviour of the nanocomposite dispersions.

Similarly to LBG/SiO_2 composite dispersions (§ 3.3) the characterization of the rheological behaviour of the CHI/SiO_2 composites comprised the study of the (a) evaluation of the linear viscoelastic range (strain effects), (b) structure development under low strain amplitude (curing tests); (c) the effect of oscillatory frequency (mechanical spectra), (d) the flow behaviour, and (e) the applicability of the Cox-Merz rule. The microstructure of the prepared composite systems was analysed by cryo-SEM.

Although we started by preparing CHI solutions in the same concentration range used for LBG solutions, it was noted that under these condition the viscosity of the chitosan solution was considerably lower than that 0.5 wt.% LBG. Hence, we tried to find a chitosan concentration that provided similar steady-state flow and viscoelastic moduli to those found for pristine LBG. A comparative illustration of the viscosity and the viscoeslatic moduli between CHI solutions with different concentrations and 0.5 wt.% LBG is shown in Figure 3.24.

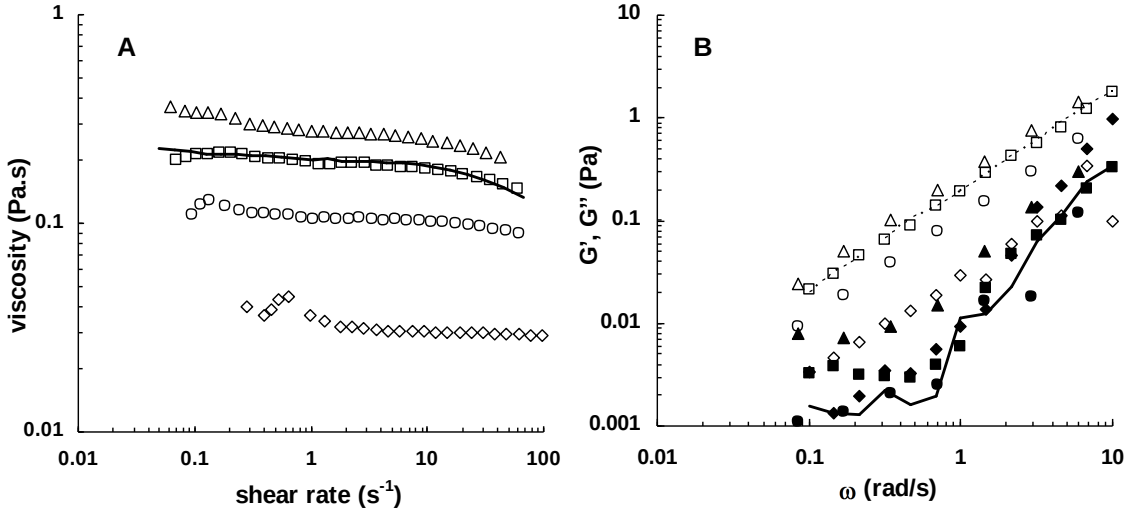

Figure 3.24: (**A**) Apparent viscosity (η_{ap}) as a function of shear rate and (**B**) storage modulus (G'; filled symbols) and loss modulus (G''; open symbols) as a function of the oscillation frequency (ω) for LBG 0.5% (—,¨) and for CHI solution with different concentrations: 1.0 wt.% (▲,Δ), 0.9 wt.% (■,□), 0.7 wt.% (●,○) and 0.4 wt.% (▲,Δ) at pH3. Also consider the open symbols for η.

Similar to the flow behaviour of LBG, CHI solutions exhibit a typical non-Newtonian shear-thinning fluid. In Figure 3.24A we can observe the presence of the Newtonian viscosity plateau (η_o) followed by the smooth transition to power-law behaviour. Increasing the concentration of CHI increases the apparent viscosity of the solution; the 0.9% chitosan solution showed a similar behaviour to the 0.5 wt.% LBG.

The viscoelastic profiles of CHI solutions were also similar to the LBG solution behaviour (Figure 3.24B). At low polysaccharide concentration, the G' and G'' follow the characteristic power relationship with frequency in the terminal zone, i.e. G' ~ ω^2 and G'' ~ ω, a typical behaviour of a disordered random-coil polysaccharide. Both viscoelastic moduli, in particular G'' increased with increasing of CHI concentration. As expected, the 0.9 wt.% CHI solution practically showed the same G'' values as those observed for 0.5 wt.% LBG solution.

3.4.3.1. Rheological changes with time at constant frequency

Oscillatory time sweep tests enabled to follow the viscoelastic moduli evolution over time of the chitosan composite dispersions under low-strain harmonic shearing and constant oscillatory frequency (1 rad/s). These time dependent curves were performed at 20 ^oC and they are shown in Figure 3.25.

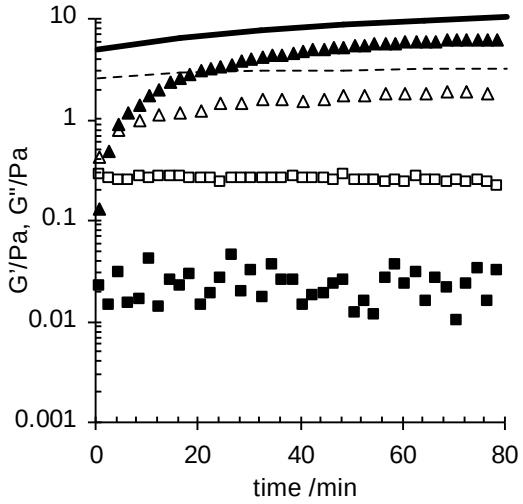

Figure 3.25: Evolution of the storage (G'; filled symbols) and loss (G''; open symbols) shear modulus at ω=1 rad/s for 0.9 wt.% CHI composite dispersions prepared in 0.1 mol/L CH_3COOH with different SiO_2 contents at pH 3: 10 (■, □) and 20 (─, ···) wt.% SiO_2. Curves for 0.5 wt.% CHI/20 wt.% SiO_2 (▲,△) prepared in 0.1 mol/L CH_3COOH are also shown.

Although not been shown for pristine CHI solutions the viscoelastic moduli did not change with time. However, a clear change on the ageing curve profile for CHI/SiO_2 dispersions was observed for the higher CHI concentration and for particles loadings above 10 wt.%, such as also observed for the time sweep tests performed for LBG composite dispersions (§ 3.3.3.1).

For 20 wt.% silica loadings, the dispersions with lower CHI concentration showed a increase of storage and loss moduli (G' and G'') in a relatively short period up to the crossover point, where G' becomes larger than G'', indicative of a liquid-like to a solid-like transition. After this point, G'' was almost constant and G' rose even to reach a plateau. For higher CHI concentration, both viscoelastic modulus were practically constant at the beginning with G' > G'', indicative of a more structured material. In agreement with Desbrieres [284], the chitosan overlap concentration to dilute regime (C*) was found to be equal to 0.1 wt.% whilst to concentrate regime (C**) was around 1.34 wt.%. Based on these results we can assume that the concentrations used in this section were in a semi-dilute region with C* < C < C**. However, it is evident that the 0.9 wt.% CHI solution is closer to the entanglement region, improving the gelling properties and the stability of the system.

The existence and nature of adsorption phenomena of polymers on solid particles are known to influence strongly the microstructure of polymer/polymer systems and very different rheological behaviours may be obtained due to the attractive or repulsive interparticle forces mediated by adsorbed and/or non-adsorbed polymer chains [285]. In fact, as regards chitosan, it is known from

literature [281, 282] that the presence of amino and hydroxyl groups allows these molecules to link to inorganic moieties. Chitosan chains are expected to adsorb on silica particles via two types of interactions: (1) electrostatic attraction between negative charges on silica particles and positive charge on chitosan molecules and (2) attraction mediated by hydrogen bonds between hydroxyl and/or amino groups of chitosan and silanol groups of silica [281].

3.4.3.2. Strain dependence of the viscoelastic response

The dynamic strain sweep tests of the CHI solutions and CHI/SiO_2 dispersions were carried out after the viscoelastic moduli had become stationary during the ageing test. The detection of the linear region of the measured dynamic properties as well as additional knowledge about the structural organization of the composite systems are some informations that this type of testing can provide. Figure 3.26 illustrates the dependence of the apparent complex modulus in its reduced form ($G^*_{ap}/G_o{}^*_{ap}$) on strain for the CHI solution and for some of the composite dispersions as examples.

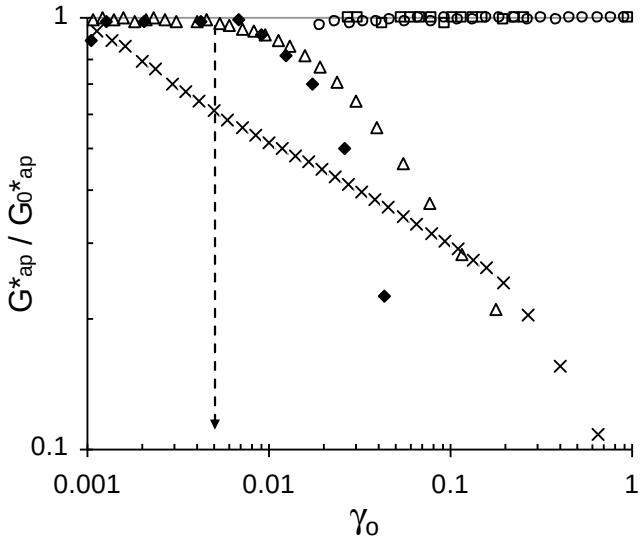

Figure 3.26**:** The reduced complex modulus ($G^*_{ap}/G_0{}^*_{ap}$) as a function of strain (γ_o) (frequency 1 rad/s at 20 ºC) for 0.9 wt.% CHI prepared in 0.1 mol/L CH_3COOH at pH 3 (○) and for its composite dispersions: CHI/10 wt.% SiO_2 (□) and CHI/20 wt.% SiO_2 (△) and CHI/20 wt.% SiO_2 prepared in 0.1 mol/L CH_3COOH/0.1 mol/L NaCl (X). Curve for 0.5 wt.% CHI /20 wt.% SiO_2 dispersion prepared in CH_3COOH at pH 3 (◆) was also shown. G^*_o denotes the G^* at the beginning of the stress sweep experiment, after meaningful results were obtained; the dashed line points to the approximate strain limits of linearity for the CHI/20 wt.% SiO_2 dispersions in CH_3COOH at pH 3.

The stress sweep tests showed that the linear viscoelastic region for the CHI solutions in the concentration range of 0.4 - 0.9 wt.% is quite large with strain limit values extending to around 100

% or even higher, such as was observed for LBG solutions (§ 3.3.3.2). This strain dependence profile was also observed for 0.9 wt.% CHI/10 wt.% SiO_2 dispersion since the presence of silica in this concentration does not seem to influence the polysaccharide structure as proved by the time sweep results (Figure 3.25).

Contrary to these results, the strain dependence on the viscoelastic response of CHI/silica composite dispersions was visibly more significant as a higher amount of silica particles (20 wt.%) was used as well as upon addition of electrolyte. The increase of silica contents into dispersion led to the lowering of the limit of linearity, an effect practically independent on chitosan concentration.

The most pronounced effect on strain linearity limit was observed when the dispersion was at higher ionic strength. The chitosan composite dispersion undergoes an abrupt disruption that is evident by the marked decrease in the modulus suggesting the presence of a fragile ordered structure. In this case the deviation from linear behaviour occurs at very low strains, below the displacement readings of the instrument. Taking into account this fact it is important to mention that the rheological quantitative response may be wrong and consequently great care should be taken when analyzing these results.

In general, well resolved displacement readings for chitosan solutions were obtained only for strain values above 10% or higher. A similar strain value was used for chitosan composite dispersion with 10 wt.% SiO_2. For other chitosan composite dispersions with 20 wt.% SiO_2 the linear region is shorter and the strain value used was 0.5 % while for the dispersion under higher ionic strength the strain used was 0.1 %. However, as mentioned above, even this low value is probably outside the linear viscoelastic range, and all the dynamic results obtained at higher ionic strength will be affected by errors and should be interpreted with caution.

The strain dependence behaviour observed for LBG composite dispersions (§ 3.3.3.2) was similar to the strain profile presented to the dispersions of chitosan with exception for the chitosan dispersion under higher ionic strength. As previously reported the addition of electrolyte to LBG dispersions in particular at pH 3 did not alter significantly their strain dependent modulus. Since pH effect on silica particles is the same the distinct behaviour observed for LBG/SiO_2 and CHI/SiO_2composite dispersions seems to be due to the nature of the polysaccharides. More details about this effect will be discussed in the next sections.

3.4.3.3. Viscoelastic behaviour: changes with oscillatory frequency

Frequency sweep tests were performed within the linear viscoelastic regime and after ageing tests in order to evaluate the frequency dependence of the viscoelastic moduli on the CHI/silica

dispersions. In this section we have focused mainly on the effect of the ionic conditions, silica amount and size of the silica particles.

3.4.3.3.1. Effect of silica particle size

In order to study the effect of particle size on the rheological behaviour of the CHI composite dispersions some frequency sweep tests were carried out. Figure 3.27 shows the mechanical spectra (storage (G') and loss (G'') moduli) as a function of the angular frequency (ω) for CHI composite dispersions containing SiO_2 particles with different average diameters (100, 300 and 500 nm) and concentrations (0, 5, 10 and 20 wt.%) at pH 3.

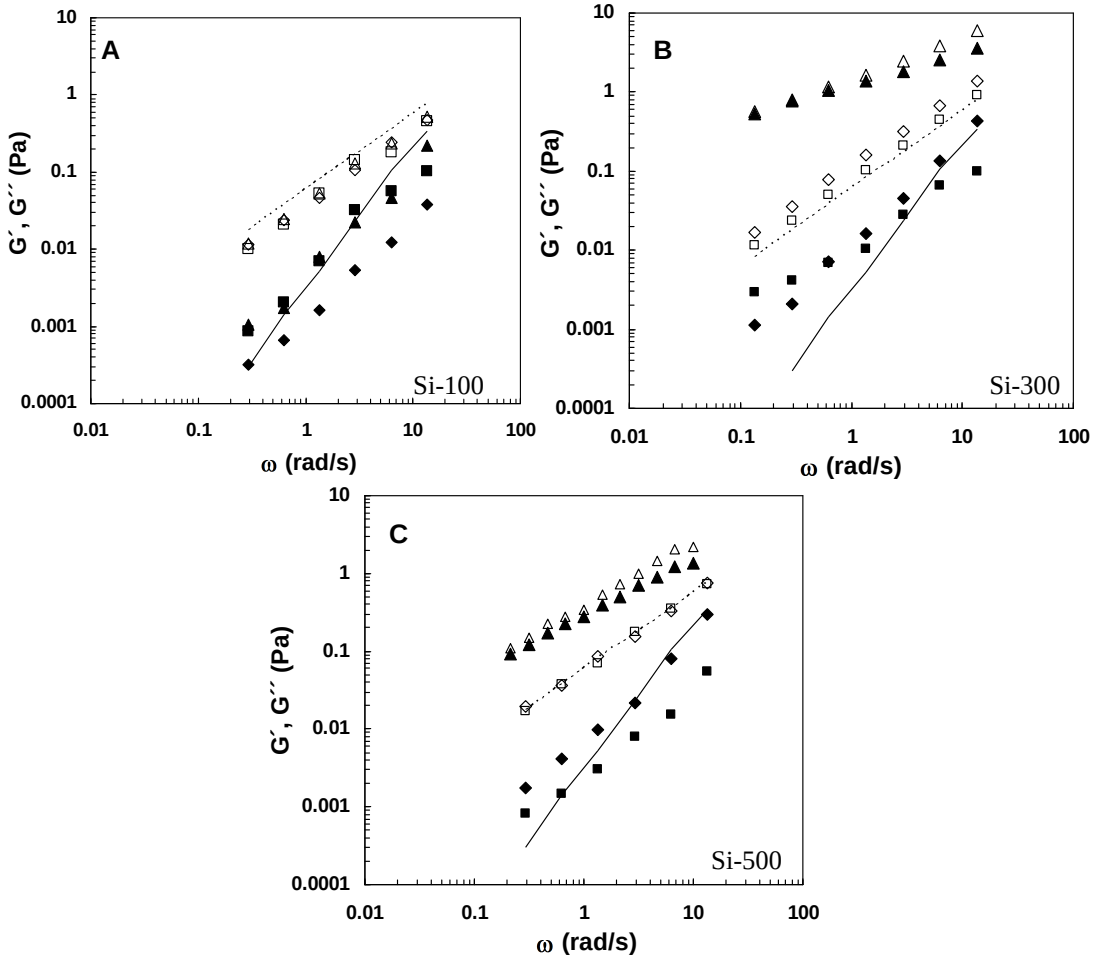

Figure 3.27: Dependency of the shear viscoelastic moduli (G', filled symbols, and G'' open symbols) against the oscillation frequency (ω) at pH3 for 0.4 wt.% CHI composite dispersions with silica particles at diameters of (**A**) Si-100, (**B**) Si-300 and (**C**) Si-500 and at different amounts: (■,□) 5 wt.%, (◆,◇) 10 wt.% and (▲,△) 20 wt.% of SiO_2. Lines (─, ⋯) denote the G' and G'' for 0.4 wt.% CHI solutions at pH3.

At low CHI concentration, the G' and G'' follow the typical power relationships with frequency in the terminal zone, i.e. $G'(\omega) \sim \omega^2$ and $G''(\omega) \sim \omega$, as is expected for a characteristic viscoelastic solution behaviour [250].

Oscillatory shear measurements for CHI composite dispersions with Si-100 (Figure 3.27A) showed a similar profile to that one obtained for the corresponding LBG dispersions (§ 3.3.3.3.1). For these dispersions containing different amounts of Si-100 the viscoelastic moduli were similar to those of the 0.4 wt.% chitosan solution with G'' > G' over the frequency interval studied. In view of the lack of information about the surface of Si-100 it is difficult to speculate what types of interactions are likely to occur between the polysaccharide and the silica particles.

Combined with the previous results from ageing tests it was expected that the presence of silica particles influenced G' and G'' viscoelastic moduli of the 0.4 wt.% CHI dispersions especially for high particle sizes and loadings. The frequency dependence of the viscoelastic moduli for CHI composite dispersions decreased slightly for the dispersions containing 20 wt.% of Si-300 and Si-500 (Figure 3.27B and C). Moreover, these dispersions presented higher G' and G'' values than those shown for pristine CHI solutions and at low frequencies G' tends to be higher than G'', which is characteristic of the formation of a typical weak gel-like system. In view of the similar results obtained for CHI composite dispersions with Si-300 and Si-500, in the next sections only composite dispersions containing Si-300 will be discussed.

3.4.3.3.2. Effect of silica concentration at different ionic conditions

Since chitosan in an acid medium is a polyelectrolyte and silica particles are negatively charged it is expected that the rheological properties of the polysaccharide dispersions are affected by the ionic strength. Hence, small amplitude oscillatory shear measurements were performed for CHI/Si-300 composite dispersions prepared in 0.1 mol/L CH_3COOH/0.1 mol/L NaCl. For comparison purpose CHI/Si-300 composite dispersions prepared in 0.1 mol/L CH_3COOH were also plotted. These curves are illustrated in figure 3.28.

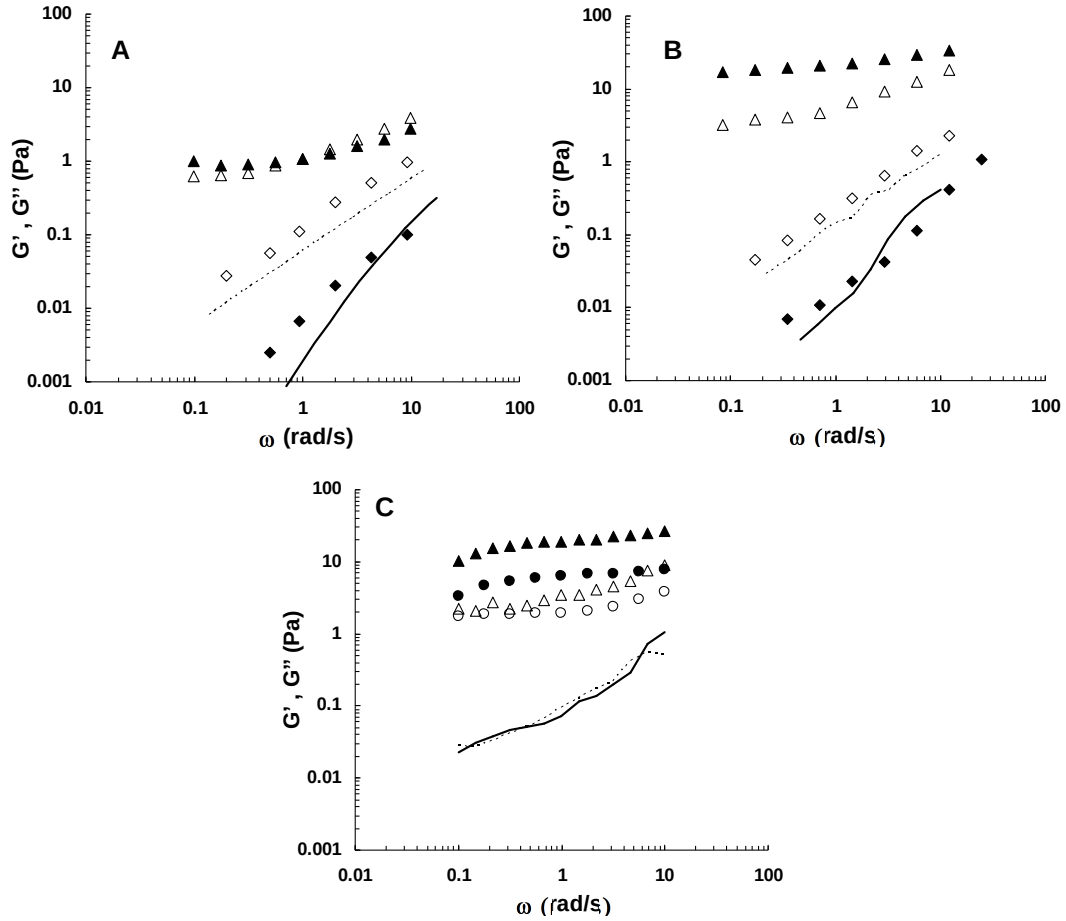

Figure 3.28: Dependency of the shear viscoelastic moduli (G', filled symbols and G", open symbols) against the oscillation frequency (ω) for (**A**) 0.5 wt.% and (**B**) 0.9 wt.% CHI solutions with different amounts of added silica particles: (◆,◇) 10 wt.% and (▲,△) 20 wt.% silica. Lines (─, ⋯) denote the G' and G'' CHI solutions. (**C**) Mechanical spectra for CHI/20 wt.% SiO_2 prepared in 0.1 mol/L CH3COOH/0.1 mol/L NaCl with (●,○) 0.5 wt.% and (▲,△) 0.9 wt.% CHI solutions are shown. Lines (─, ⋯) denote the G' and G'' for 0.9 wt.% CHI solutions also prepared in 0.1 mol/L CH3COOH/0.1 mol/L NaCl.

As previously mentioned the CHI chains in the concentration interval studied (0.4 – 0.9%) show a liquid classic behaviour [250]. Similar behaviour it is observed for CHI dispersions with lower filler amount (10 wt % SiO_2) with different CHI concentrations (Figure 3.28A and B). The viscoelastic moduli are visibly dependent on the frequency with G' < G'' in the whole studied frequency interval. Apart from this, the viscoelastic profile for these CHI/10 wt.% SiO_2 dispersions is characterized by the scaling law $G' = G''/\tan(n\pi/2) \propto \omega^n$, where *n* is called the critical relaxation exponent that ranges between 0 and 1. The lower the *n* value, the faster the gel point is achieved. The *n* value for G' curves of 0.5 wt.% CHI/10 wt.% SiO_2 and for 0.9 wt.% CHI/10 wt.% SiO_2 dispersions were 0.95 and 0.94 respectively. This result indicates that in spite of the difference in

CHI concentrations of the dispersions, the relaxation exponents are practically the same for the same silica loading.

However, in Figure 3.28A and B it is observed that increasing silica amount into dispersions, decreases the dependence of G' and G" on ω. For the dispersions with high CHI concentration (Figure 3.28B), both moduli increase but the corresponding increase in the loss modulus G" is lower. At low frequencies, for 20 wt.% silica, G'(ω) becomes almost independent of the frequency, suggesting an onset of solid-like behaviour in these composite systems, reaching the viscoelastic behaviour typical of a solid-like (soft) material.

The effect of the filler amount is less evident for dispersions with lower CHI concentration (Figure 3.28A). At low frequency G' is higher than G" and it is observed the appearance of a plateau characteristic of a liquid–gel transition. However, at a critical frequency around 1 rad/s a crossover of the G' and G" curves is pointed, indicating that the elasticity of the chitosan composite system was reduced.

In order to complement the studies of the viscoelastic behaviour observed in Figure 3.28A and B for CHI/SiO_2 composites we have also plotted the dependence of the complex viscosity ($|\eta^*|$) of the composite dispersions on the frequency (ω) (Figure 3.29).

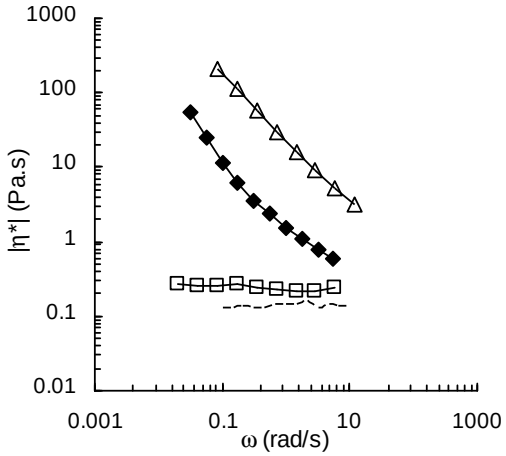

Figure 3.29: Dependency of the complex viscosity ($|\eta^*|$) on frequency (ω) for 0.9 wt.% CHI dispersions prepared in 0.1 mol/L CH_3COOH at pH 3with different amounts of SiO_2. Line denote for the 0.9 wt.% CHI solution, and symbols denote for its composite dispersions: (□) 10 wt.% and (△) 20 wt.% SiO_2. The symbol (◆) denotes the dispersion 0.5 wt.%CHI/20 wt.% SiO_2 prepared 0.1 mol/L CH_3COOH.

Analysing the curves from Figure 3.29 we have found that these results in comparison with those observed in Figure 28A and B are consistent. It is observed a more solid-like behaviour as the amount of the filler and CHI increases, especially at low frequencies. The frequency dependence of $|\eta^*|$ at low frequencies is ~ $\omega^{(-0.03)}$ for CHI/10 wt.%SiO_2 and increases to ~ $\omega^{(-0.88)}$ for the CHI/20 wt.%SiO_2 dispersion.

As regards the effect of increasing the ionic strength (Figure 3.28C), it was noted a significant effect on the chitosan solutions (0.4 - 0.9%) and on the composite dispersions For the 0.9 wt.% CHI solution prepared in 0.1 mol/L CH_3COOH/0.1 mol/L NaCl at pH 3, the moduli show a well-structured system, with G' approximately equal to G'' over the entire frequency range. In addition, the power-law dependence of G' decreased from $\omega^{1.7}$ (in 0.1mol/L CH_3COOH) to $\omega^{0.7}$ (in 0.1 mol/L CH_3COOH/0.1 mol/L NaCl). It is known that charges on a polyelectrolyte chain are increasingly screened when the ionic strength of the solution increases. The screening effect alters the conformation and the stiffness of polyelectrolytes in solution [286]. However, this effect is significantly dependent of the polyelectrolyte concentration. In agreement with Cho *et al.* [272] the now-Newtonian nature (elastic properties and shear-thinning behaviour) of the chitosan solutions increased with increasing chitosan concentration and decreasing ionic strength.

Although the oscillatory tests in particular for 0.9 wt.% CHI dispersion prepared in 0.1 mol/L CH_3COOH/0.1mol/L NaCl were not performed in the linear viscoelastic regime, the qualitative effect of the ionic strength on the viscoelastic moduli of CHI dispersions prepared with different chitosan concentrations is shown in the Figure 3.28C. For 0.9 wt.% CHI dispersion this effect was practically not significant as compared with the same dispersion prepared in 0.1mol/L CH_3COOH (Figure 3.28A). However, comparing the 0.5 wt.% CHI dispersion prepared in 0.1 mol/L CH_3COOH (Figure 3.28B) with that same dispersion prepared in 0.1 mol/L CH_3COOH/0.1mol/L NaCl (Figure 3.28C) it was clearly evident the positive effect of the ionic strength on the viscoelastic moduli. This ionic strength effect can be observed by the decrease of the power-law dependence of G' and G'' of 0.5 wt.% CHI dispersion at low frequencies, i.e. increasing ionic strength, the power-law dependence decreases from $\omega^{0.22}$ to $\omega^{0.15}$ for G' and $\omega^{0.41}$ to $\omega^{0.14}$ for G''.

3.4.3.4. Shear flow tests

Evaluation of the steady shear behaviour of the CHI/SiO_2 composite dispersions is important in the investigation of the microstructure of particulate dispersions as well as in the control of their rheological properties under flow field. The flow characteristics of particulate dispersions can be controlled by the particle shape, size distribution, interparticle forces, and the volume fraction of the dispersed phase [287].

Figure 3.30 represents the steady shear viscosity as a function of shear rate for 0.9 wt.% CHI solution and for its composite dispersions with 20 wt.% SiO_2 loading in salt and acid media at pH 3. Moreover, the flow curve obtained for CHI/20 wt.% SiO_2 dispersion prepared with 0.5 wt.% CHI is also shown.

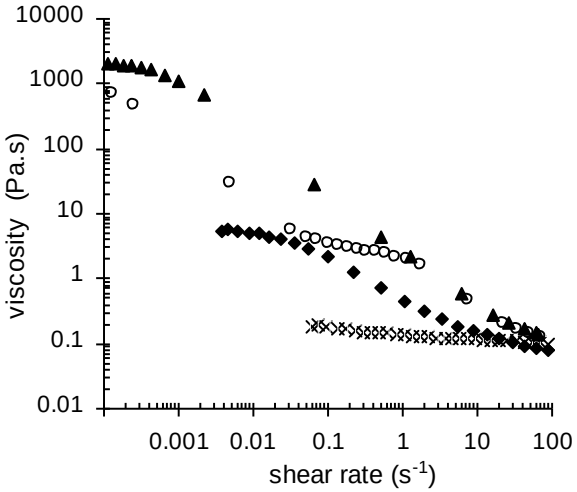

Figure 3.30: Apparent viscosity as a function of shear rate at 20 ºC for composite dispersions prepared in 0.1 mol/L CH_3COOH at pH 3: neat 0.9 wt.% CHI (×), 0.9 wt.% CHI/20 wt.% SiO_2 (▲) and 0.5 wt.% CHI/20 wt.% (◆). Flow curve for 0.9 wt.% CHI/20 wt.% SiO_2 (○) prepared in 0.1 mol/L CH3COOH/0.1 mol/L NaCl is also shown.

The chitosan solution behaves generally as a typical non-Newtonian shear-thinning fluid. The orientation of the dispersed asymmetric polymer macromolecules stars to occur in the shear stress experiment, i.e. with an appearance of a Newtonian viscosity plateau (η_o). With an increasing shear rate this effect will become more pronounced and will cause a progressive decrease of the internal friction of the solution because of smaller effective interactions between the molecules, giving rise to a shear-thinning effect [271]. This effect is more pronounced with increasing chitosan concentration. For 0.9 wt.% CHI solution shown in Figure 3.30 the smooth transition to a power-law behaviour (shear-thinning) occurred at a higher shear rate (> 100 s^{-1}) than that observed for LBG solution (§ 3.3.3.4). For chitosan solution the variation of the slope of the viscosity power-law (even if it is not the final one) with the polymer concentration is smaller that other polysaccharides and hence confirms the presence of intermolecular interactions even for concentrations below 2 wt.% [284].

At low shear rate an abrupt transition from Newtonian flow to non-Newtonian flow behaviour is observed for CHI dispersions with high silica loading. In this shear rate range, the apparent viscosity increases and diverges as the silica loading is 20 wt.%, the Newtonian plateau disappears, and the dispersions show an apparent “yield” behaviour. This effect is more evident for CHI dispersions prepared with higher CHI concentration (0.9 wt.%).

At higher CHI concentration, the CHI/20 wt.% SiO_2 dispersion prepared in NaCl showed a distinct flow behaviour than that presented for same dispersion prepared in CH_3COOH. The shear rate dependence of the steady shear viscosity clearly suggests that the salt addition modifies the

composite structure, as could be expected from the high strain sensitivity already observed for this dispersion (Figure 3.26). As referred for LBG systems (§ 3.3.3.4) these observations are consistent with the formation of a particle-mediated transient network, which is disrupted under shear, revealing essentially the polymer dynamics at high shear rate.

Taking into account the apparent yield stress observed for CHI composite dispersions, we have plotted their viscosity as a function of shear stress in order to highlight the apparent yielding showed by these dispersions. Due to the unreliable flow behaviour shown for the dispersion prepared in NaCl, the yield stress effect was represented only for the CHI solution and dispersions prepared in aqueous 0.1 mol/L CH_3COOH (Figure 3.31).

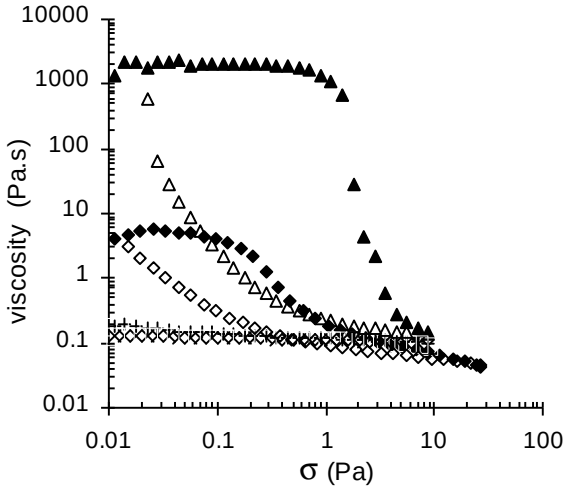

Figure 3.31: Apparent viscosity as a function of shear stress (σ) at 20 ºC for 0.9 wt.% CHI and 0.9 wt.% CHI/SiO_2 dispersions, at pH 3, showing the upward and downward curves, resulting from first increasing the applied stress, followed by the unload of the sample at a decreasing shear stress: (x up, + down) neat CHI and (▲up, △down) CHI/20 wt.% SiO_2 dispersion. Curves for CHI/20 wt.% SiO_2 prepared with 0.5 wt.% CHI solution (◆up, ◇down) are also shown.

Yield behaviour was not observed for the chitosan solution as it was not observed for LBG solution, both systems at semi-dilute concentration range. Nevertheless, for the system CHI/20 wt.% SiO_2 the typical yielding behaviour can be clearly observed, with a high Newtonian viscosity at low stresses, followed by a sharp drop in viscosity [253], about 4 orders of magnitude, over higher stresses, i.e., an apparent yielding at about 10 Pa.

The upward and downward curves obtained by increasing and then decreasing the applied stresses are also shown in Figure 3.31. In the case of the CHI solution the up and down curves are overlapped. However, for the CHI/silica dispersions, the up and down curves overlapped only at high stresses but at low shear stresses, the down curve did not match the up curve anymore, the divergence being more pronounced as the CHI concentration increases, suggesting a thixotropic

behaviour, probably due to a partial breakdown of the weak network formed upon application of shear. The pronounced hysteresis observed for the CHI/20 wt.% SiO_2 is typical of a gel-structured material.

3.4.3.5. Cox-Merz rule

The ability of CHI composite dispersions to alter their structure and orient their particles under shear flow was further analyzed by employing the empirical Cox-Merz rule. We have compared the steady-state apparent viscosity (η_{ap}) with the complex viscosity ($|\eta^*|$) obtained from the oscillatory experiments at low strain amplitude in order to check the applicability of the Cox-Merz rule to our CHI systems. The results obtained for 0.9 wt.% CHI/20 wt.% SiO_2 dispersions prepared in CH_3COOH and NaCl are showed in Figure 3.32.

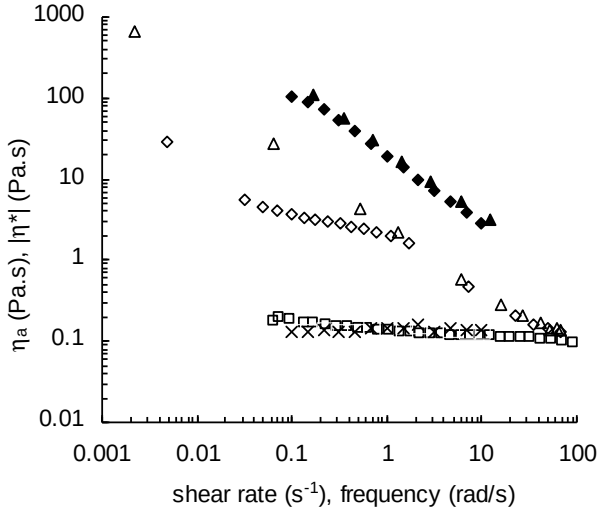

Figure 3.32: Comparison of the steady-shear apparent viscosity (η_{ap}) and the complex viscosity ($|\eta^*|$) for 0.9wt.%CHI and 0.9wt.% CHI/20 wt.% SiO_2 samples, at 20 ºC:(□-η, x-$|\eta^*|$) neat CHI; (△-η, ▲-$|\eta^*|$) CHI/20 wt.% SiO_2 in 0.1 mol/L CH_3COOH; (◇-η, ◆-$|\eta^*|$) CHI/20 wt.% SiO_2 in 0.1 mol/L CH_3COOH/ 0.1 mol/L NaCl.

The Cox-Merz relationship is generally acceptable for homopolymers and also some unfilled disordered liquid-like block copolymers [288]. However, for the highly filled polymer matrix $\eta^*(\omega)$ is always higher than η ($\dot{\gamma}$) with the magnitude of the difference increasing with the increase of filler loading [252, 289, 290].

In the Figure 3.32 we can observe that the CHI solution obeys the Cox-Merz rule whilst that for all chitosan dispersions $\eta^*(\omega)$ always exceeds η ($\dot{\gamma}$) over the entire range of shear flow, indicating a failure to the Cox-Merz rule. Although the strain was kept as low as possible to avoid any changes

in the mesoscale structure, it is difficult to affirm as done for LBG systems (§ 3.3.3.5) that the structure of the materials is not affected under the linear oscillatory rheological tests particularly for CHI composite dispersions prepared in 0.1 mol/L CH3COOH/0.1 mol/L NaCl.

As mentioned for LBG systems the steady-shear viscosity was considerably lower than the oscillatory complex viscosity presumably because of an alteration in the mesoscale structure caused by the large displacements imposed during the steady shear experiments. Beside this and in agreement with Liang *et al.* [290] work, for some filled polymer systems such a failure could arise due to some preferential orientation of the initial quiescent random arrangement of the particles under a steady shear.

3.4.3.6. CHI/SiO_2 microstructure

Further information about the microstructure of the CHI/SiO_2 dispersions prepared at different conditions was gained from SEM. Cryogenic preparation of these composite samples followed by sublimation of water from the network provided images are shown in the Figure 3.33.

The microstructural analysis revealed that the chitosan chains also adopt analogous physical three-dimensional arrangement observed for LBG chains previously illustrated in § 3.3.3.6. It is observed a lamellar structure forming a regular meshed network, “beehive type ”.

As expected the chitosan chains adsorbs on the silica particles. The cationic nature of chitosan as well as it OH surface groups alter the way as the filler silica particles are organized and distributed in the polymer matrix. The particles clusters are distributed more homogenously within biopolymers fibrils forming a semi-continuous three-dimensional network in the entire volume of the system suggesting a higher interaction than that observed for LBG/SiO_2 dispersions. The increase of silica amount into chitosan matrix decreased the size of the beehives and favoured the fill of empty spaces in the biopolymer fibrils. As a consequence, CHI/20 wt. % SiO_2 dispersion (Figure 3.33E) was the most affected by particles clusters, yielding a better polymer network reinforcement as probed through its rheological measurements.

From a microstructural point of view and in agreement with Aubry *et al.* [281], the yield stress observed for CHI/20 wt. % SiO_2 dispersion may be the mark of a percolating network of silica aggregates interacting through hydrogen bonds mediated most likely by silanol-silanol interactions and also probably by adsorbed chitosan chains, known to bear numerous potential H bonds. Despite the interaction observed between chitosan chains and silica particles (Figure 3.33) the resulting structure is rather elastic but fragile, as revealed by the small linear viscoelastic response region (Figure 3.26B).

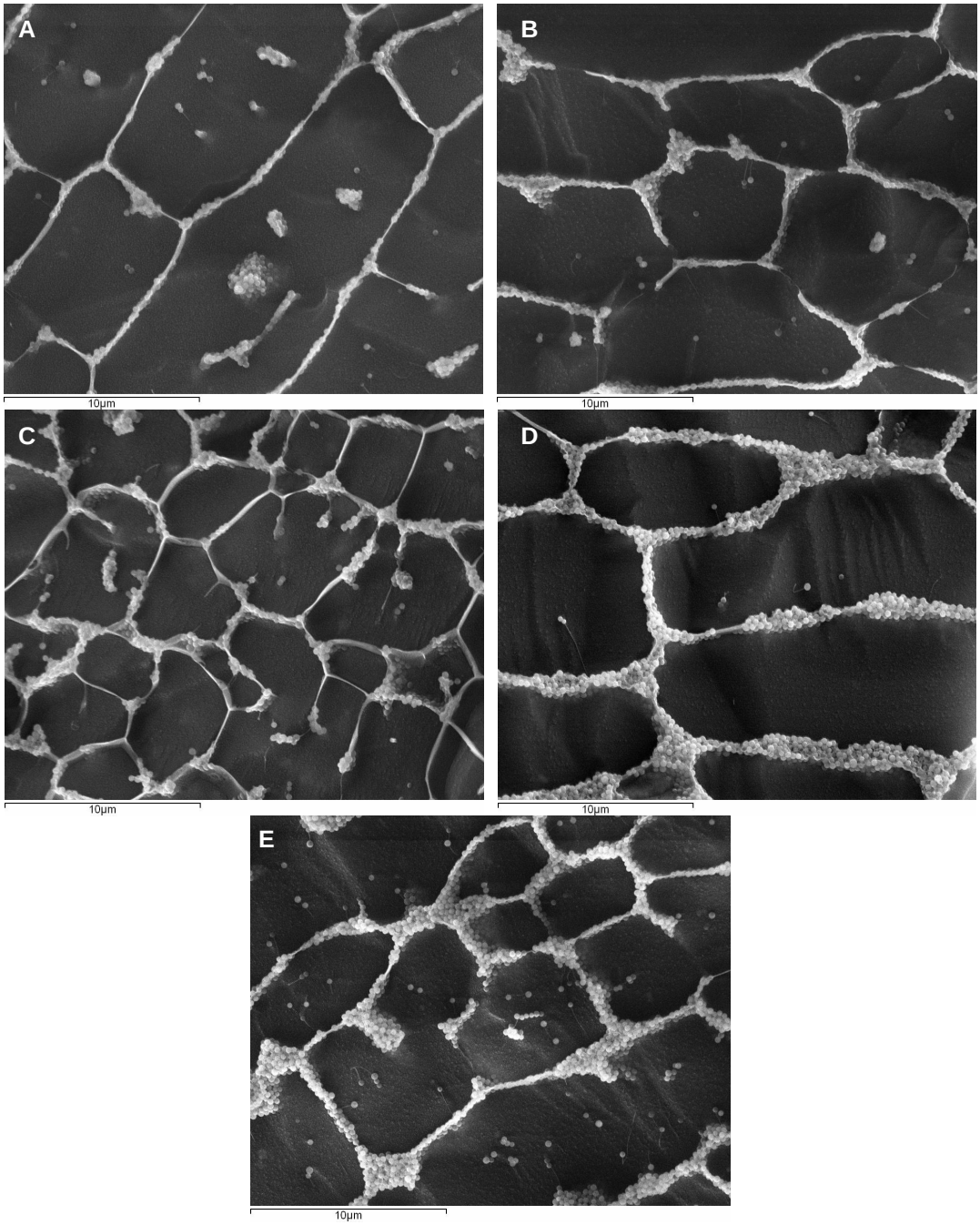

Figure 3.33: Cryo-SEM images of the 0.9 wt.% CHI/SiO_2 composites at pH 3: (**A**) 5 wt.% SiO_2 in CH_3COOH; (**B**) 10 wt.% SiO_2 in CH_3COOH; (**C**) 10 wt.% SiO_2 in 0.1 mol/L CH_3COOH/0.1 mol/L NaCl (2 h after preparation); (**D**) 10 wt.% SiO_2 in 0.1 mol/L CH3COOH/0.1 mol/L NaCl (6 h after preparation); (**E**) 20 wt.% SiO_2 in CH_3COOH at pH 3.

Increasing the ionic strength causes the distribution of the particle clusters within the chitosan matrix to be different to the other samples prepared in CH_3COOH, especially the dispersion prepared in 0.1 mol/L CH3COOH/0.1 mol/L NaCl and visualised under microscope in a short time after its preparation (Figure 3.33C). In this case, the system seems to have no time to organize the

clusters and the chitosan fibrils are not completely filled. Contrarily, the same sample viewed under microscope 6 hours after its preparation (Figure 3.33D) has the silica particles both completely aligned and/or aggregated into chitosan fibrils as shown for sample prepared in CH_3COOH (Figure 3.33E).

Regretfully we can not do a better comparison of results obtained by Cryo-SEM with those obtained from the rheological tests for samples prepared in NaCl, as these samples have a region of linearity below the displacement readings of the rheometer. Nevertheless, qualitatively the CHI dispersion prepared in CH_3COOH at high ionic strength show similar G' and G'' frequence dependence as illustrated in Figure 3.28. This similarity is in agreement with the images obtained by Cryo-SEM.

3.5. Rheology and microstructure of xanthan/silica dispersions

3.5.1. General considerations

3.5.1.1. Chemistry, structure and conformation of xanthan gum

Xanthan gum (XG) is a high-molecular-weight anionic polysaccharide produced from the fermentation broths of the bacterium *Xanthomonas campestris*. Its main chain is based on a linear backbone of 1,4-linked β-D-glucose and is similar to cellulose; at the C(3) position of every alternate glucose residue there is a charged trisaccharide side chain containing a glucuronic acid residue between two mannose units (Figure 3.34). The terminal β-D-mannose is linked β-1,4 to the glucuronic acid which, in turn, is linked α-(1,2) to the α-D-mannose. On approximately one half of the terminal mannose residues a pyruvic acid moiety is joined by a ketal linkage to the O(4) and O(6) positions. Acetate groups are present as substituents at the O(6) position of the non-terminal mannose [291].

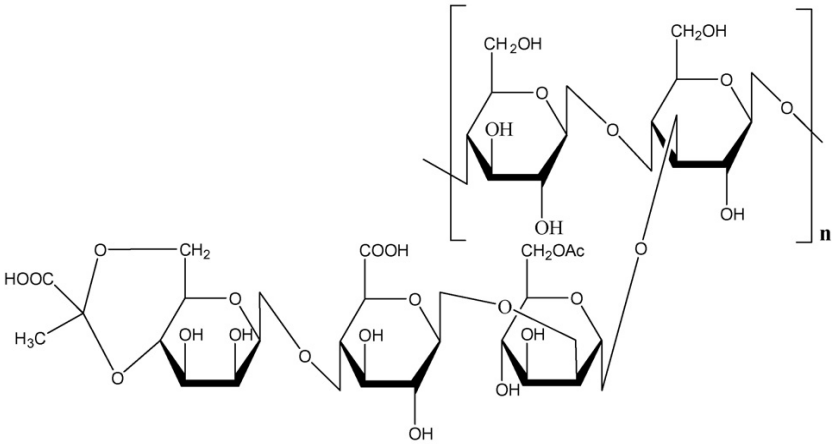

Figure 3.34: Schematic representation of a repetitive section of a xanthan molecule. Reproduced from [14].

The average molecular weight of natural xanthan lies in the range of 10^6 to 10^7 Da. This value depends on the association between chains which can form aggregates of many individual chains. The fermentation conditions can also influence the structure and the average molecular weight of the xanthan produced [292].

The conformational structure of xanthan in the solid state as well as in aqueous solution is only partially known at this time [14]. In a recent review, Rinaudo [13] referred that in the solid state the xanthan gum conformation is a 5_1 helix (fivefold). In addition, the xanthan molecule in solution undergoes a conformational transition from an ordered helix to a random coil (Figure 3.35) as the temperature is raised, which is also a function of ionic strength of the solution, the nature of the electrolyte, acetyl and pyruvate constituent contents and the pH [293-295].

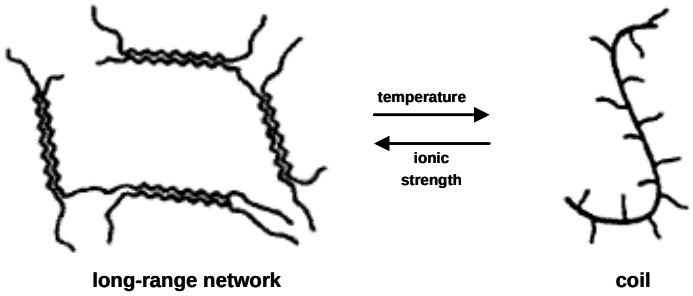

Figure 3.35: Xanthan order-disorder transition. Reproduced from [15].

The conformation of xanthan in solution has been much discussed in the literature. The debate is between a single or a double helix in aqueous solution and about the understanding of the molecular basis for the conformational transition. Morris *et al*. [296] predicted an intramolecular transition in which the ordered single-helical structure was destabilised by disruption of the intramolecular bonds, leading to the adoption of a "random coil" state. Milas and Rinaudo [297] agreed with this view. Liu and co-workers [298], on the other hand, proposed a model in which the double helix, upon heating, melts from both ends to form an expanded dimer comprising two molecules mainly in the random coil state but linked by a short region of double helix. Recently, Matsuda *et al.* [299] also studied the thermal denaturation and renaturation of the double-helical xanthan in aqueous solution. The authors found from circular dichroism measurements that xanthan looses the double helical conformation in pure water at 80 ^oC and almost recovers locally the native conformation in the renaturation.

Rochefort and Middleman [300] reported that in distilled water at 25 ^oC, the backbone is disordered but highly extended due to the electrostatic repulsions from the charged groups on the sidechains. This highly extended structure allows the molecules to align and associate (*via* hydrogen bonding) to form a weakly structured material. At a given ionic concentration, this conformation is stabilized

at low temperature. Therefore, when temperature increases, a transition to coil-like configuration occurs at a characteristic temperature T_m (determined for 50% of the transition), which causes the dissociation of the molecules and a subsequent change in the rheological properties [13, 300]. When salt is added to the xanthan solution at 25 ^oC, a disorder-order transition occurs in which the backbone takes on a helical conformation and the charged trisaccharide sidechains collapse down onto the backbone (due to charge screening effects) and stabilize the ordered conformation [301].

3.5.1.2. Rheological properties of xanthan solutions

Xanthan gum is soluble in both cold and hot water and possesses polyelectrolyte nature [292, 302]. The later feature comes obviously from the presence of charges along the chain and leads to intra- and intermacromolecular interactions. These interactions have strong consequences on both static and dynamic properties of the system [303].

Xanthan solutions are highly viscous even at low concentrations and exhibit a pronounced pseudoplastic or shear thinning behaviour. This polysaccharide shows distinctive weak gel properties [210, 304] (resulting in the thickening and/or in the gelation of media) which form the basis of its technological utility [305] which is readily reversible under shear.

The rheological properties of xanthan solutions change with polymer nature, that is to say, they depend on average molecular weight and acetate [306] and pyruvate [307] contents besides the biopolymer concentration used [304] as well as on the properties of the medium such as: ionic strength, temperature and pH [291, 292].

The influence of salt, temperature, and strain effects on the structure of semi-dilute xanthan solution has been studied by Rochefort and Middleman [300] using oscillatory and steady shear experiments. At the studied concentrations, the solutions exhibit gel-like behaviour and their rheological properties are governed by intermolecular associations. When the solution structure is disrupted by high shear or temperature, the recovery of dynamic properties is slow and incomplete in low salt, and fast and complete in high salt contents. A master curve of dynamic properties covering 6 decades of frequency has been obtained in highly saline solution.

Xanthan gum with a high level of acetylation and, especially, pyruvilation degree, increases the viscosity of its aqueous solutions because intermolecular associations are favoured. However, pyruvate free xanthan is more suitable for the preparation of mobility control solution used in enhanced oil recovery processes.

It has been reported that concentration has a considerable effect on the rheological characteristics of xanthan gum solutions whereas pH does not [292, 308]. Nevertheless, the pH has a some effect on viscosity of xanthan solutions as mentioned by Cotrell *et al.* [309].

Steady and dynamic shear properties of dilute solutions of xanthan gum in aqueous media at different concentrations and temperatures were investigated by Tiu et al. [310, 311]. They have reported that these solutions exhibit both shear-thinning and elastic characteristics even at extremely low concentrations and the temperature-concentration superposition principle using reduced variables are applicable to both steady and dynamic shear data. Moreover, the Cox-Merz relation is valid only in low shear rate and frequency regions. The existence of a yield stress in biopolymer/water systems was thoroughly discussed by Giboreau *et al*. [312]. In the same article, these authors comparing the steady and dynamic shear data also proved that the complex viscosity is larger than the steady shear viscosity, i.e. the systems do not obey the Cox-Merz relation.

Temperature has an important influence on the flow behaviour of xanthan gum solutions. The viscosity decreases as the measurement temperature increases. This behaviour is fully reversible between 10 and 80 ^{o}C [292]. Under conditions of elevated temperatures and/or under conditions of comparatively low ionic strength the chain flexibility is modified, and the local flexibility is very similar to that of other coil-like cellulose derivates. On cooling or an addition of salt, the molecule undergoes a conformational transition to an ordered and locally more rigid structure [313]. The temperature dependence of the xanthan viscosity is often related with the shear rate. Morris *et al.* [296] reported that the viscosity decreases with increasing temperature at a shear rate of 14 s^{-1} whilst the viscosity is independent of temperature at 127 s^{-1} and even increases when it is measured at 571 s^{-1}.

The effect of ionic strength on the viscosity of xanthan gum solutions depends upon the polymer solution concentration [309]. Changes in ionic strength at constant temperature also affect the viscoelastic behaviour. An increase in ionic strength reduces the viscosity of dilute xanthan gum, as expected for a polyelectrolyte due to the charge screening effects which allow a more compact structure [300]. Nevertheless, the addition of salt to xanthan solutions in the concentration range $0.2 \leq C \leq 3.0\%$ causes the viscosity to increase [300, 314]. As referred above, the concentration influences the rheological properties of xanthan gum. For salt free xanthan gum, the viscosity increases significantly as the concentration of xanthan is increased. This behaviour is attributed to the intermolecular interaction or entanglement, increasing the effective macromolecule dimensions and molecular weight [292].

3.5.1.3. Applications of xanthan

Xanthan gum is one the most important commercial microbial hydrocolloid. Due to the chemical reproducibility, relatively easy supply and superior properties of xanthan gum, it has become the preferred product to be used in different application areas and enables it to compete with most natural gums [315]. It is largely used as thickening, stabilizer and/or structuring agent in a broad range of industries, such as in food industry, agro-chemistry, crude oil recovery, medical and pharmaceutical, and chemical and cosmetic industries [13, 292, 300, 309].

The application in numerous industrial segments is due mainly to their rheological properties that allow the formation of viscous solutions at low concentration (0.05 - 1%), and a wide range of pH and temperature stability, such characteristics result from their branched structure and high molecular weight [292, 316, 317]. Besides, it is a biodegradable material hence an environmental friendly product [13].

3.5.1.4. Inorganic–xanthan composites

In view of its widespread use, XG has also attracted the attention of researches to use it in the preparation of composites. Shchipunov *et al.* [83] prepared xanthan gum/silica nanocomposite using the sol-gel processes. It was concluded that the xanthan exert a catalytic effect on the processes favouring the gelation of the system. Nevertheless it was observed that the increase of amounts of polysaccharide and silicate, when the content of the counterpart component remained unchanged, had opposite effects on the mechanical properties of the hydrogels. The former leads to a decrease in the mechanical strength, making them softer.

Another report regarding the preparation of xanthan gum/silica nanocomposites used the simple mixture of the components approach[104]. Silica with very small diameter (23.5 nm) was mixed with xanthan-gum solutions and the rheological properties of the nanocomposites were studied under different conditions. The authors observed that essentially at pH 2, i.e. near the isoelectric point of silica where electrostatic repulsion is very weak, the intermolecular hydrogen bonding or the strong interparticle bridging was favoured by adsorption of partially flexible xanthan molecules leading the dispersion to form a gel structure.

Taking into account the latest results obtained by simple mixture of the preformed silica nanoparticles into the biopolymer solution, in this sub-Chapter, XG/SiO_2 composite dispersions have been prepared in order to understand the silica stability in xanthan solution and the effect of silica particles on the rheological properties of XG. For these reasons, different conditions to that

previous work [104] such as different silica sizes and pH values were used. Besides this, the microstructure of the XG composite dispersions was analysed. Oscillatory and steady shear rheological methods and cryo scanning electron microscopy were used to fully characterize the rheology and microstructure of these nanocomposite dispersions.

3.5.2. Experimental Part

3.5.2.1. Polysaccharide sample

Industrial grade xanthan gum (XG) from *Xanthomonas campestris* was kindly provided by Kelco Oilfield Group.

3.5.2.2. Preparation of XG solutions and SiO_2 dispersions

XG solutions (0.8 - 1.0 wt.%) were prepared in distilled water or in 0.1 mol/L NaCl by dispersion of the xanthan gum powder for 44 h under moderate stirring at room temperature followed by centrifugation at 12000 rpm for 20 minutes.

Silica powder (10 up to 40 wt.%) with AD= 300 nm prepared as described in § 2.2.3.1, was suspended in the same solvents used for XG solutions and maintained overnight under stirring and then treated by sonication for 1 hour before the preparation of XG/SiO_2 dispersions. To test the effect of ionic strength, the dispersion of silica particles was also prepared in 0.1 mol/L NaCl aqueous solution.

3.5.2.3. Preparation of XG/SiO_2 dispersions

XG/SiO_2 dispersions were prepared by simple mixture of components. Typically, XG solutions and dispersions of SiO_2 particles previously prepared were mixed (1:1), resulting in a final aqueous dispersion of aprox. 0.5 wt.% of XG and (5, 10 or 20 wt.%) of SiO_2 particles. The pH was adjusted with HCl and/or NaOH. The dispersion was then stirred for 30 minutes and submitted to mild vacuum for 30 minutes in order to remove air bubbles and then transferred to the rheometer measuring system for testing.

3.5.2.4. Rheological measurements

Small-amplitude oscillatory and steady-state flow tests were carried out using the same procedure described for XG composite dispersions in § 3.3.2.4.

3.5.2.5. Cryo-scanning electron microscopy (cryo-SEM)

The microstructure of the XG/SiO_2 dispersions was analysed by Cryo-scanning electron microscopy (cryo-SEM) using the same procedure used for CHI composite dispersions described in § 3.3.2.5.

3.5.3. Results and Discussion

Considering that the size of silica did not have any significant effect on the polysaccharide dispersions studied before, for XG only Si-300 particles at different loadings (5 - 20 wt.%) have been discussed. As regards the concentration of the polysaccharide, the majority of the results presented refer to dispersions with 0.5 wt.% xanthan gum to allow comparisons with the previously discussed systems (i.e. LBG and CHI). However, some results previously obtained for dispersions prepared with 0.4% XG are presented as they are also within the semi-dilute concentration range.

Rheological measurements and microstructure analysis of the XG composite dispersions were carried out for dispersions prepared at pH 3 and/or pH 5. In addition, only some tests were performed in presence of 0.1 mol/L NaCl to investigate the effect of the ionic strength on the behaviour of the nanocomposite dispersions.

The characterization of the rheological behaviour of the XG/SiO_2 composites, similarly to LBG and CHI composite dispersions (§ 3.3 and § 3.4) included the study of the (a) structure development under low strain amplitude, curing tests; (b) effect of strain, the linear viscoelastic behaviour; (c) the effect of oscillatory frequency, mechanical spectra, and (d) the flow behaviour. The microstructure of the prepared composite systems was analysed by cryo-SEM.

3.5.3.1. Rheological changes with time at constant frequency

As mentioned before a simple test to determine if a system has time dependent rheological properties is the oscillatory time sweep. This test monitors if and how the material properties change after it has been loaded, by monitoring certain viscoelastic parameters as time advances.
Viscoelastic moduli (storage modulus, G’ and loss modulus, G’’) of the XG composite dispersions were measured as a function of the time under low-strain harmonic shearing and constant oscillatory frequency (1 rad/s) at 20 ^{o}C. The ageing effect is shown in Figure 3.36.

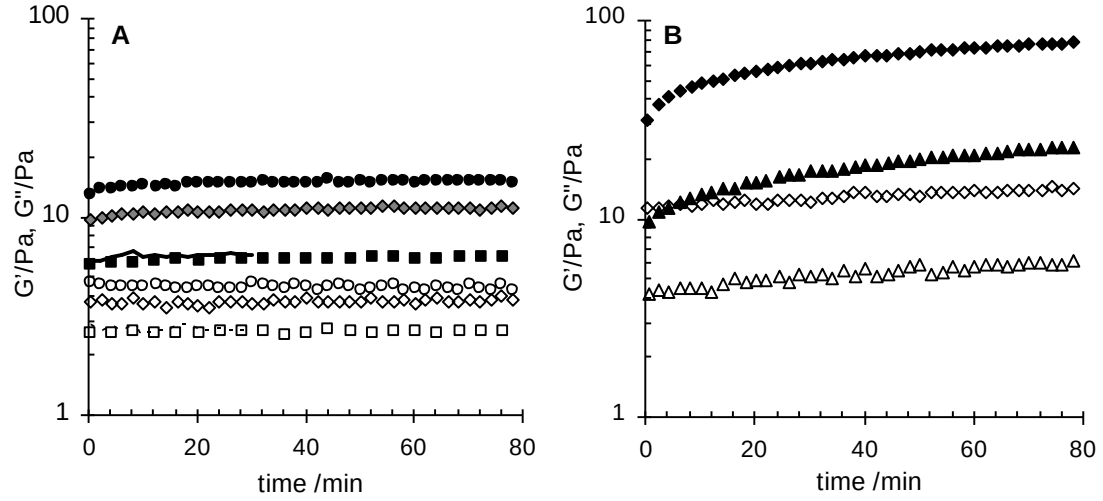

Figure 3.36: Evolution of the storage (*G'*, filled symbols) and loss (*G''*, open symbols) shear moduli at ω = 1 rad/s for XG solution and XG composite dispersions with: **(A)** 5 wt.% SiO_2 (■,□), 10 wt.% SiO_2 (◆,◇) at pH 3 and at 10 wt.% SiO_2 pH 5 (●,○). Curve for neat 0.5 wt% XG (—,···) at pH 3 is also shown. **(B)** XG/SiO_2 dispersions prepared with 20 wt.% SiO_2 at pH 3 in water (▲,△) and in 0.1 mol/L NaCl (◆,◇).

As mentioned in the literature the xanthan gum is an extracellular polysaccharide of great practical interest because of its widespread use in different application fields [318], since food [300, 309] to drilling industry [319, 320]. The exceptional rheological properties of the XG are related to both its high molecular weight and high structural chain rigidity, which provide the molecular basis for the enhanced long-term stability of this polysaccharide in a wide range of pH, ionic concentration, temperature [292, 309] and time.

At a semi-dilute concentration regime, weak association through hydrogen bonding of XG leads to a gel-like behaviour with G' > G'' as shown in Figure 3.36A. These results are in agreement with Rochefort and Middleman [300]. Moreover, the viscoelastic moduli for pristine XG did not change with time indicating its non ageing dependence. A similar result was obtained for the XG composite dispersion loaded with 5 wt.% of SiO_2. The presence of silica particles in this concentration doesn't seem to be sufficient to influence the viscoelastiv behaviour of the XG solution. However, a clear improvement on the viscoelastic moduli is achieved for 10 and 20 wt.% SiO_2 particles (Figure 3.36A and B), as it was also observed for LBG composite dispersions (§ 3.3.3.1). However, the ageing effects for XG/10 wt.% SiO_2 (Figure 3.36A) are still less significant in comparison with those observed for LBG/SiO_2 dispersions.

At pH 3, i.e. near to isoelectric point of the SiO_2 particles (Figure 2.8), XG molecule tends to be a partially flexible worm-like chain while the silica particles are not completely ionized. Under these conditions the electrostatic repulsions between both compounds become weaker allowing the XG

molecules to adsorb on the silica surface and a gel structure is formed. This behaviour is in agreement with that reported by Oh *et al*. work [104] when they studied the stability of 20 wt.% silica particles (AD= 23.5 nm) in the presence of XG at semi-dilute concentration.

Moreover in Figure 3.36A it is observed that the XG/10 wt.% SiO_2 composite dispersion prepared at pH 5 shows viscoelastic moduli slightly higher than those obtained at pH 3. This fact can be explained by the enhancement of the XG chain rigidity as the pH increases. Since xanthan gum is an anionic polysaccharide, at pH 5 charge repulsions are favoured and the molecule exhibits an extended conformation, leading to the increase of the viscoelastic moduli. As a consequence the moduli of the XG dispersion at higher pH are also improved.

Since at pH5 the XG composite dispersions seem to be influenced by the stiffness of polysaccharide chain and not by the presence of the silica, and the improvements were not significant, the following studies are focussed on rheological studies carried out at pH 3.

Changes in ionic strength at constant temperature also affect the viscoelastic behaviour of the XG dispersions. Whereas an increase in ionic strength reduces the viscosity of dilute xanthan solutions, as expected for a polyelectrolyte, additions of salt to xanthan solutions in the concentration range $0.2 \leq C \leq 3.0$ wt.% increase the viscosity [321]. Although the viscosity curves are not shown in this section, this polyelectrolyte effect is also observed in the viscoelastic moduli time dependence curves illustrated in Figure 3.36B.

In general, for XG/20 wt.% silica dispersions, the ageing effects are more pronounced and both moduli are higher than those obtained for dispersions with lower silica loadings. This effect is much more pronounced for XG dispersion prepared in 0.1 mol/L NaCl. According to Rochefort and Middleman study [4] when salt is added to the XG solution the viscoelastic moduli are highly enhanced as well as the system structure due to the fact that the salt screens the electrostatic repulsions between chains which in turn improve the XG chain rigidity. In fact, from Figure 3.36B it becomes clear that the silica particles are probably do not play the most important role in the enhancement of the rheological properties of the XG composite dispersions. Since at pH 3 both silica dispersions prepared in water or in high ionic conditions presented larger aggregates (Figure 2.10) the main reason for the improvement of the rheological properties of the XG dispersions can be related to the polysaccharide chain rigidity.

3.5.3.2. Strain dependence of the viscoelastic response

A convenient method to examine the structural organization in a solution/dispersion is to measure G', G'' in a strain sweep test at a constant frequency (sufficiently low to prevent nonlinear effects).

Figure 3.37 illustrates the strain dependence of the viscoelastic moduli (G' and G'') of XG solution and XG composite dispersions after time sweep test.

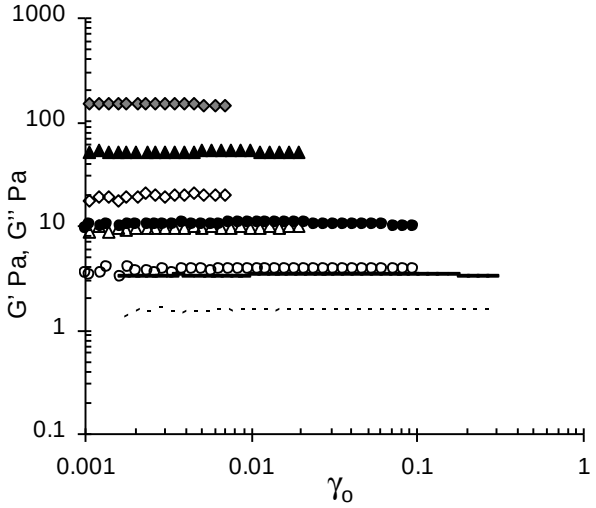

Figure 3.37: Dependence of the shear viscoelastic moduli (G', solid symbols, and G'' open symbols) against the strain (γ_o) at frequency 1 rad/s and at 20 ºC for XG solution and XG composite dispersions at pH 3 with different amounts of added silica particles: 10 wt.% SiO_2 (●,○), 20 wt.% SiO_2(▲,△) and 20 wt.% SiO_2 prepared in 0.1mol/L NaCl (◆ ,◇). Curve for neat 0.5 wt.% XG (─,¨) is also shown.

In general, the linear viscoelastic region for these samples extends to higher strain values than previously observed for some samples of LBG/SiO_2 and CHI/SiO_2 dispersions. However, in order to maintain the shear stability and structure of the XG solution and XG composite dispersions as well as ensuring well resolved displacement readings, rheological analyses were carried out for strain values around 0.3%.

The strain dependence of the viscoelastic response for all the XG and XG/silica dispersions presented in Figure 3.37 shows a similar profile. An elastic response is observed for all samples in the whole strain interval studied, including for XG solution. This behaviour confirms the existence of gel-like structures, as observed in the time sweep tests (Figure 3.36).

3.5.3.3. Viscoelastic behaviour: changes with oscillatory frequency

After time sweep tests the monitoring of the dynamic moduli as a function of frequency for xanthan composite dispersions was performed in order to study the viscoelastic behaviour of these dispersions. Taking into account that the effect of the silica size registered for both LBG and CHI composite dispersions was only felt at high silica loadings, in this section we have focused mainly on the effect of the silica amount using Si-300. Furthermore, it should be noted that previous tests

carried out using XG 0.4 wt.% and SiO_2 with different AD have also shown very little effect of particle size [322].

Frequency sweep tests were performed within the linear viscoelastic regime for XG solution and XG/SiO_2 composite dispersions. Figure 3.38 shows the mechanical spectra (storage and loss moduli) as a function of frequency for these composite dispersions at pH 3.

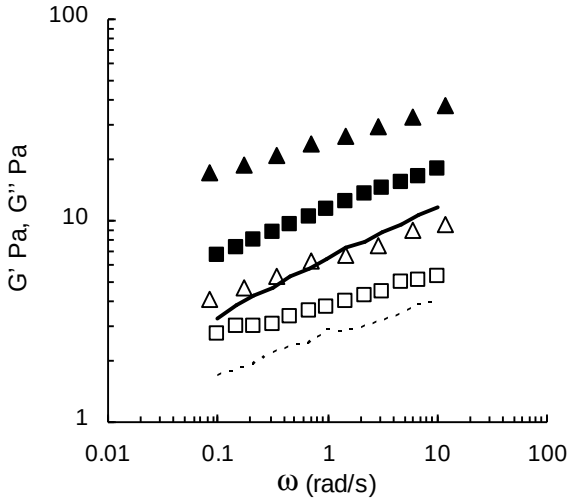

Figure 3.38: Dependency of the shear viscoelastic moduli (G', solid symbols, and G", open symbols) against the oscillation frequency (ω) at pH3 for 0.5 wt.% XG solution (─,¨), with different amounts of silica particles: (■,□) 10 wt.% and (▲,△) 20 wt.% SiO_2.

The viscoelastic behaviour shown for XG chains illustrates the typical behaviour of a weak gel with intermolecular interactions occurring on very long time scales. It is clear that $G' > G''$ in the whole frequency interval studied, so this sample displays dominating elasticity at small strains. However, the moduli are visibly dependent on the frequency obeying the scaling law $G' \sim \omega^p$ and $G'' \sim \omega^q$.

As the silica loading increases both moduli increase but the corresponding increase in the loss modulus *G"* is lower (i.e., reinforces the matrix). The dependence of *G'* and *G"* on *ω* continues to exist but the curve slopes are slightly lower than those registered for XG solution. The improvement of the solid-like character as the silica concentration increases is highlighted by the decreasing power-law dependence of G'. The *p* values were 0.21 and 0.15 respectively for XG/10 wt.% SiO_2 and XG/20 wt.% SiO_2 respectively, whilst for pristine polysaccharide p was 0.27.

It is known that at pH 3 the interparticle repulsion is reduced considerably and the silica particles tend to aggregate. Hence, in agreement with Oh *et al*. [104] the xanthan molecule adsorbed onto a silica particle could interact with the neighbouring particles through hydrogen bonding. The intermolecular hydrogen bonding or the strong interparticle bridging by the adsorbed

polysaccharide would cause the dispersion to form a gel structure. Thus, as the silica concentration increases the formation of gel structures is favoured.

The enhanced solid-like behaviour exhibited by XG/SiO_2 dispersions as the amount of the filler increases is also confirmed by the plot of complex viscosity ($|\eta^*|$) of the composite dispersions against frequency (ω) (Figure 3.39).

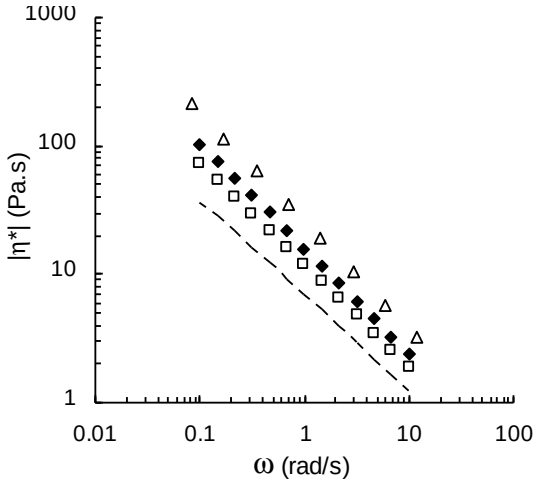

Figure 3.39: Dependence of the complex viscosity ($|\eta^*|$) on frequency (ω) for XG solutions with different amounts of added silica particles, in water. Line denotes the 0.5 wt.% XG solution, and symbols denote the composite dispersions: (□) 10 wt.% and (△) 20 wt.% SiO_2 at pH 3. The symbol (◆) denotes the dispersion XG/10 wt.% SiO_2 at pH 5.

As observed for the viscoelastic moduli frequency dependence of XG/SiO_2 composites, (Figure 3.39), the complex viscosity of these dispersions as well as that of the XG solution has also a high dependence upon frequency, decreasing according to a negative power law. At pH 3, the frequency dependence of $|\eta^*|$ increases slightly from $\omega^{(-0.74)}$ for XG solution to $\omega^{(-0.84)}$ for theXG/20 wt.% SiO_2 dispersion. This result indicates that despite of the small increase in the power law exponent of the XG dispersions a more solid behaviour was achieved as the silica loading increased.

The power law exponents for XG/10 wt.% SiO_2 composite dispersions prepared at pH 3 and 5, were $\omega^{(-0.79)}$ and $\omega^{(-0.81)}$ respectively. Practically no quantitative or qualitative differences were observed comparing these results. This fact could be indicative of the high rheological dependence of these dispersions on the XG chains structure and small dependence on the characteristics of the silica particles, since at pH 5 the silica particles have an higher charge density and they are much more monodisperse than at pH 3.

3.5.3.4. Shear flow tests

The microstructure of particulate dispersions as well as the control of their rheological properties under flow field was evaluated from steady shear tests. Initially, we studied the flow characteristics of neat XG solution. Although many studies in the literature affirm that XG molecules are unaffected by pH [291, 292, 300, 309, 314] our experimental results evidence the pH dependence on the viscosity of XG. Figure 3.40 represents the steady shear viscosity as a function of shear rate for 0.4 wt.% XG solution at different pH.

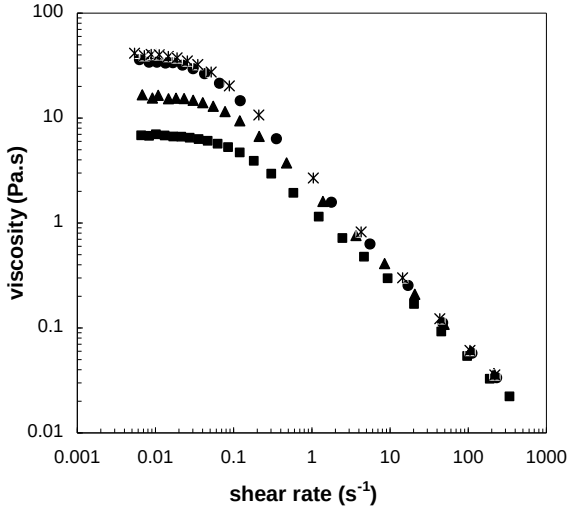

Figure 3.40: Shear viscosity as a function of the shear rate for 0.4 wt.% XG solutions at different pH values: (■) pH 1, (▲) pH 3, (●) pH 5 and (ж) pH 7.

From Figure 3.40, it is observed that the apparent viscosity markedly decreases with increasing shear rate, demonstrating the expected strong non-Newtonian shear thinning behavior of the xanthan in aqueous solutions. Moreover, as mentioned above, at low shear rates the viscosity of XG increases progressively up to pH 5, from which it is kept constant. In agreement with Oh *et al.* [104] the chain rigidity of the xanthan molecule increases with pH leading the shear viscosity to increase.

The effect of the addition of silica particles on shear viscosity of 0.5 wt.% XG solution was also studied. Figure 3.41 illustrates the dependence of shear viscosity of XG/10 wt% SiO_2 dispersion as well as that of the pristine XG solution as a function of shear rate.

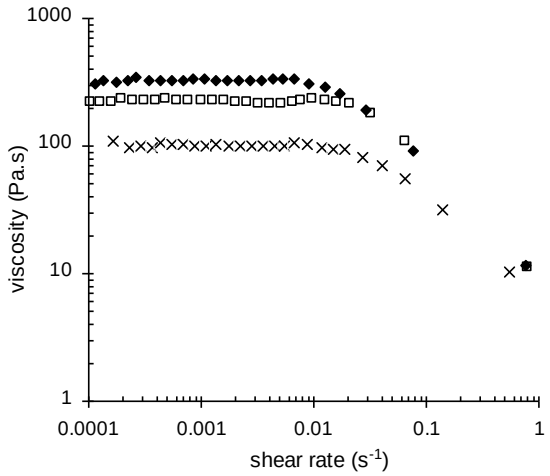

Figure 3.41: Apparent viscosity as a function of shear rate at 20 ºC for 0.5 wt.% XG (×) and XG/10 wt.% SiO_2 (□) dispersion at pH 3. Flow curve for (◆) XG/10 wt.% SiO_2 at pH 5 is also shown.

The XG solution exhibited a typical non-Newtonian shear-thinning fluid, qualitatively similar to that shown for 0.5 wt.% LBG solution (Figure 3.16) but quantitatively much more superior in viscosity value. In Figure 3.41 it is also noted an appearance of a Newtonian viscosity plateau (η_o) at lower shear rate and then a transition to a power-law behaviour occurred at a similar shear rate (> 0.01 s^{-1}) as compared to the 0.4 wt.% XG solution shown in Figure 3.40.

For the XG composite dispersions the presence of the fillers does not seem to alter the flow behaviour profile presented by pristine XG solution. However, the apparent viscosity increases due to the presence of the silica particles but the transition from Newtonian to non-Newtonian flow behaviour is observed practically at the same shear rate range. This flow behaviour is completely different to those observed for LBG and CHI composite dispersions (§ 3.3.3.4 and § 3.4.3.4) in which at lower shear rates the Newtonian plateau disappeared, and the dispersions showed an apparent "yield" behaviour. Moreover, at higher shear rates the flow behaviour for all the filled XG dispersions showed a similar profile to that illustrated for the biopolymer alone.

3.5.3.5. Xanthan/SiO_2 microstructure

Cryo-scanning electron microscopy (cryo-SEM) for the *in situ* study of hydrated XG/SiO_2 composite dispersions has been carried out. From this analysis, useful informations about the microstructure and morphology of these dispersions were obtained as depicted in Figure 3.42.

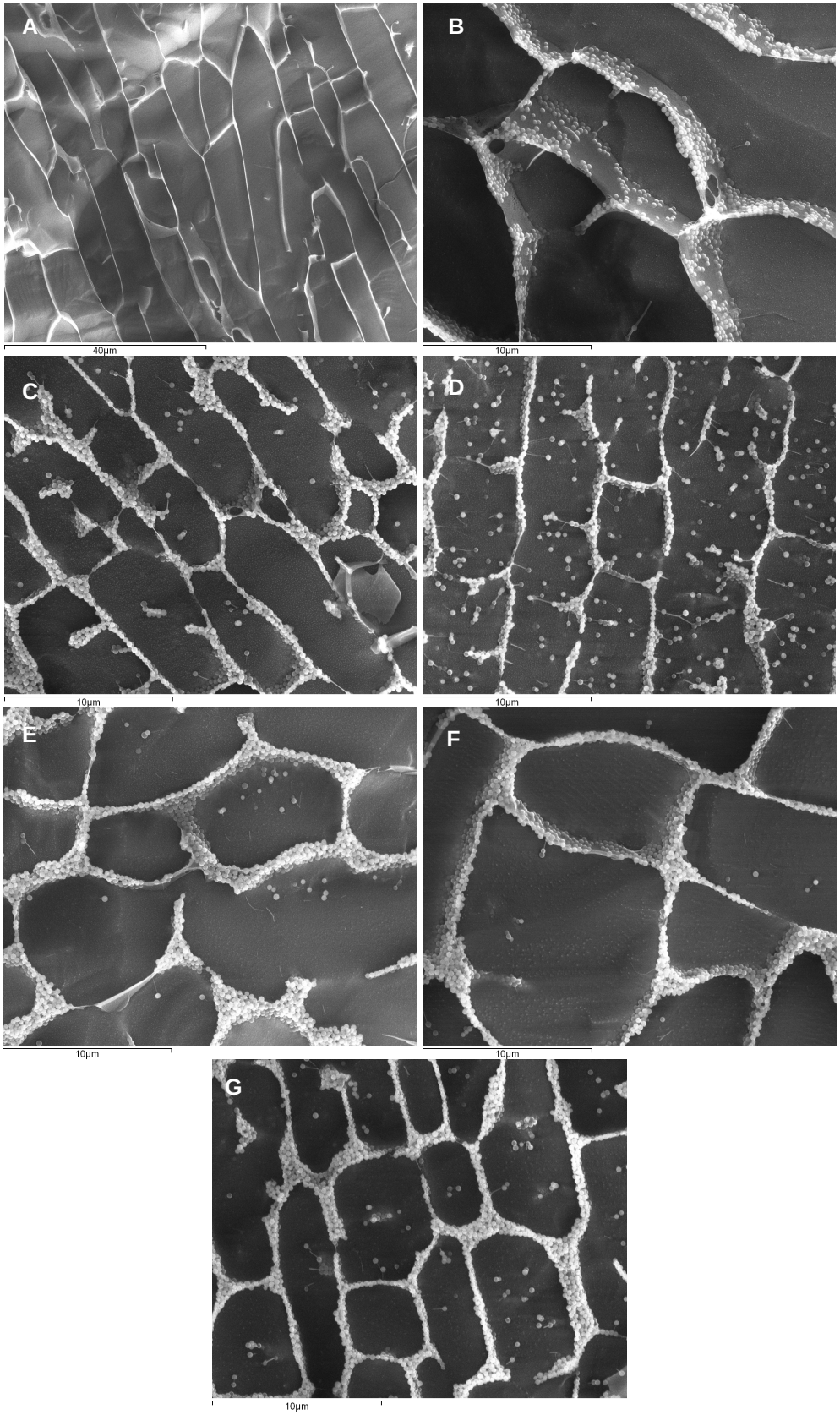

Figure 3.42: Cryo-SEM images of the (**A**) XG solution at pH 3 and XG/SiO_2 composites with different amounts of added silica: (**B**) 5 wt.% SiO_2 at pH 3; (**C**) 10 wt.% SiO_2 at pH 3; (**D**) 10 wt.% SiO_2 at pH 5; (**E**) 10 wt.% SiO_2 in 0.1M NaCl at pH 3; (**F**) 10 wt.% SiO_2 in 0.1M NaCl at pH 5 and (**G**) 20 wt.% SiO_2 at pH 3.

As previously illustrated in § 3.3.3.6 and § 3.4.3.6 for the microstructure of LBG and CHI dispersions, the cryo-SEM image for pristine XG (Figure 3.42 A) also revealed that the chains of this polysaccharide adopt an analogous physical three-dimensional arrangement.

The interaction between XG chains and silica particles is clearly noticed in Figure 3.42. The anionic nature of XG molecule due to its carboxylic groups when in contact with the aqueous medium together with their OH groups favours their adsorption onto silica particles. As observed for CHI composite dispersions (Figure 3.33), the increase of silica amount in the xanthan matrix also seems to reduce the dimensions of the three-dimensional arrangement of polysaccharide and favours the filling of empty spaces in the biopolymer fibrils (Figure 3.42B, C and G). This fact is in agreement with the progressive polymer network reinforcement probed through their rheological properties as silica loading increases.

It is known that at pH 3, electrostatic repulsions become noticeably weak which promotes the adsorption of the xanthan molecule to the surface of silica (Figure 3.42 A, B, C, E and G). Hence, as mentioned above, one possible justification given by Oh *et al*. [104] for the enhancement of the XG gel structure mediated by silica particles is that at low pH, the semi-flexible xanthan molecules adsorbed on the silica surface interpenetrate into the adsorbed layers of the near particles. Under these circumstances, the silica particles serve as junction points and the interpenetrating xanthan molecules provide the interparticle bridging bonds.

Although at pH 5 the repulsive forces in system are increased, it has been observed that the XG composite dispersions under this condition show rheological properties similar to those presented by those dispersions at pH 3. In fact, from Figure 3.42 D it is possible to note that the XG fibrils are filled of silica particles in a similar way as observed for the dispersions prepared at pH 3 (Figure 3.42C). Although for the XG/10 wt.% dispersion at pH 5 can be observed more isolated particles and dispersed out from XG chains. This behaviour is expected since at pH 5 the degree of particle aggregation is lower. Nevertheless, Figure 3.42D shows small XG fibrils linked to isolated silica; this fact associated to the increase of the rigidity of the XG chain at high pH, which contributes to the improved rheological properties observed for this dispersion.

Increasing the ionic strength (Figure 3.42E and F), the silica particles seem to be completely aligned and/or aggregated along the XG fibrils leading to composite dispersions with an higher level of structure, which is probed by their rheological properties.

3.6. General conclusions

For LBG composite dispersions, the microstructural analysis revealed that clusters of silica particles are not randomly dispersed within the polymer matrices. Instead, the silica particles form clusters that self-organize on the polymer fibrils or lamellar structures. Contrarily, for CHI and XG composite dispersions at least for the quantities of silica analysed, there is a continuous three-dimensional network formed by the silica particles in practically the entire volume of the system, suggesting a higher interaction between silica and these charged polysaccharides than that observed for non-ionic LBG composite dispersions. Under conditions of low pH the adsorption of LBG on the silica particle surface is expected to occur through hydrogen bonding between the polysaccharide hydroxyls and the silanol groups on the silica surface. For the other polysaccharide composite dispersions, CHI and XG, the affinity between their chains and silica particles is expected to be high due to charged nature of the polymers which can favour electrostatic interactions as well as the hydrogen bonding already mentioned.

The influence of the higher ionic strength was more evident for LBG and CHI composite dispersions: for XG/SiO_2 dispersions the quantity and size of the silica clusters was increased whilst for CHI/SiO_2 dispersions the microstructure was dependent on the time. For XG/SiO_2 dispersions, the higher ionic strength does not seem to influence the microstructure of system. Moreover, in spite of the different microstructures obtained for these dispersions at different pH values no significant effect was observed in their rheological behaviour

The structural organization of the composite systems had significant effects upon the biopolymers rheology. Several indicators support that the composite systems exhibit weak-gel structure, being the solid-like behaviour more pronounced as the amount of the filler increases or under conditions of low ionic density of the silica particles (lower pH or higher ionic strength), i.e. those conditions that favour particle aggregation and particle-polymer interactions.

The composite systems are characterized by long relaxation times, apparent yield stresses, and elastic moduli that are weakly dependent on strain frequency. However, in the conditions studied, XG/SiO_2 dispersions did not show a clear yield stress in comparison with the other biopolymers.

Jamming of the constituent particles in diverse systems including colloidal suspensions and certain molecular systems can originate fluid-to-solid transitions due solely to their kinetic entrapment and the arrest of the particle's dynamics [323]. However, when the particles are dispersed in a polymer matrix the polymer-particle interactions are expected to play a determinant role, both in the cases of non-adsorbing or adsorbing polymers. In fact, the observed structure for our composites

polysaccharide-silica materials discards the hypothesis of a simple particle jamming mechanism to explain their solid-like behaviour.

Particle-particle interactions building up the particle clusters and particle-polymer interactions responsible for the self-organization of the silica clusters around and/or within the polymer domains give rise to quiescent structural evolution. In general, the LBG/SiO_2 and CHI/SiO_2 composites show a very low linearity limit γ_o behaviour, which can be attributable to the high strain sensitivity of the developed three-dimensional temporary network structures. For XG/SiO_2 dispersions, the strain dependence of viscoelastic moduli is practically inexistent and the linearity limit region extends to higher strain values.

For LBG and CHI composite dispersions the mechanical spectra revealed a transition from liquid-like to solid-like viscoelastic behaviour as a function of silica loading whereas for XG composite dispersions a solid-like behaviour is already seen for neat polysaccharide solution. The storage modulus of LBG and CHI composite materials was significantly enhanced relative to the matrix polymer, especially at pH 3, and decreased its dependence upon frequency as the silica loading increased. The modulus plateau at low frequencies is indicative of solid-like behaviour and the existence of a yield stress in some cases or at least the existence of a specific relaxation mechanism is probably due to the presence of the filler in the biopolymer matrix. Even at high frequencies, particularly at pH 3 or at high ionic strength, although the effect of particle loading was weaker, one can still observe the general increase of both moduli as the silica concentration increases, i.e. the short-range dynamics of the polysaccharides chains are also influenced by the presence of the filler particles. Thus, large-scale polymer relaxations in the composite materials are effectively restrained by the presence of the silica particles.

Strong shear thinning behaviours are exhibited by LBG and CHI composite dispersions yielding hysteresis phenomena, compared to the unfilled biopolymer. The weak-gel structures obtained for these systems were easily ruptured under flow. Different flow behaviour was observed for XG nanocomposites, which have shown a shear thinning behaviour similar to that presented by pristine biopolymer. Hysteresis phenomena were not clear for these XG systems and the gel structures obtained were not easily ruptured at low shear rate.

The empirical Cox-Merz rule failed for the cases of the LBG/SiO_2 and CHI/SiO_2 composite materials and especially for those with higher particle loadings. Typically, the quiescent state linear complex viscosity $\eta^*(\omega)$ exceeds the steady shear viscosity $\eta(\dot{\gamma})$, with the discrepancy being largest at low shear rates and for higher silica loadings. Thus the application of continuous steady shear results in significant changes in the dissipation mechanism as compared to the quiescent or near-quiescent state structure that is dominated by the network of biopolymer chains caged on

silica particle clusters. A likely explanation is that some of the network elements (or junctions) that bear stress and are present under quiescent conditions, namely the particle clusters associated to polymer segments, are disrupted during the application of continuous shear. Although the validity of the Cox-Merz rule for XG/SiO_2 composite dispersions has been assessed the results were inconclusive therefore more rheological measurements must be carried.

We hypothesize that the adsorption of the silica particles along the polymer chains and the particle-particle interactions thereafter lead to weak slowing down of segmental dynamics at the polymer-solid interface and additional and/or more permanent junction zones yielding gels with enhanced elasticity. This is due to trapping of polymer chains at the filler surface which may result in a higher entanglement density. Hence, some of the biopolymer segments originally participating in simple topological entanglements (typically observed in these polysaccharide solutions) can now became elastically effective chains forming transient networks where the polymer matrix chains have much lower mobility and the rigidity of the polymer segments, between physical and/or chemical junction points, is reinforced by the cage of interacting particles. In addition, the presence of rigid inclusions (particle clusters) may also distort the strain field around the particles, leading to a frequency- and loading-dependent enhancement in the modulus. Interactions between particles and particle-biopolymer are labile, and although they result in a partial immobilization of the matrix chains, these labile bonds can be easily ruptured under shear.

4 Polysaccharide/silica films

4.1. Introduction

Over the years packaging materials such as glass, metal, wood and paper have been replaced by plastic materials [105]. The first plastic dating back to 1856 was a 'cellulose-based polymer', since then a wide range of essentially synthetic polymer packaging materials with a variety of properties has been developed and a series of processing methods are now used to fabricate packaging materials [324].

Cellophane transparent films rapidly grew to a multi-million dollar business in the U.S. until the commercialization of high polymers in the early 1950s, which afforded equally transparent films, but had better properties and were cheaper [325].

The basic purpose of packaging is to enable the right goods to get to the right place at the right time in a good condition [324]. Among the various forms of plastic packaging, the film form was focused in this thesis. Films are required to exhibit barrier properties to prevent the entrance of any contaminating substances or the exit of any desirable substances that may try to leave, across the film. This property is resistance to diffusion. Moreover, since a film is very thin, it must have high mechanical properties such as high tensile strength, impact resistance and tear strength. The mechanical properties usually depend on molecular structure, molar mass and molar mass distribution. Visibility through a film is often important, so low haze will be required [326-329].

4.1.1. Films from renewable resource

The constant growing use of non-biodegradable packaging films is causing significant ecological and environmental concern and alternative solutions are needed. Biopolymers have been considered as the most promising materials for this purpose as they exist abundantly and may form cost-effective end products. Table 4.1 summarizes the principal components used in the preparation of natural bio-based films.

Table 4.1: Components of biopolymer-based films adapted from [1, 2].

I. Film-forming materials
-Polysaccharides: starch, cellulose derivates, pectin, alginate, carrageenan, chitosan, and natural gums.
-Proteins: casein, whey protein, collagen, gelatin, keratin, fish myofibrilar protein, soy protein, wheat gluten and corn zein.
-Lipids: neutral lipids, fatty acids, and wax.
-Biopolymers produced by micro-organisms: bacterial cellulose, polyhydroxybutyrate, xanthan, pullulan and curdlan.
II. Additives
-Plasticizers: glycerol, glycol, polyethylene glycol, sorbitol and water.
-Functional ingredients: antimicrobials, antioxidant, flavour, colorants, vitamins, and other nutraceuticals.
-Inorganic fillers: silica, titanium, carbon nanotubes and fibers.

The most common biopolymers are polysaccharides such as cellulose, starch, chitin and its primary derivative chitosan whose swellability in water and viscous solution/gel-forming properties are utilized to manufacture a number of industrial and consumer products. Despite the characteristics of biopolymers, they are still underutilized. However it is predicted they will be widely exploited in the near future in environmentally benign applications, notably in systems working in biological environments, among others in membrane-based processes [330]. Among the commercially available polysaccharides, chitosan has received special attention due to the presence of the amino and hydroxyl functional groups [330, 331]. These functional groups confer chitosan singular chemical and biological characteristics, which include: biocompatibility, antibacterial properties, heavy metal ion chelation ability, hydrophilicity and remarkable affinity to proteins. Furthermore, the filmogenic properties of chitosan are another important future of this polymer.

Several aspects of the chitosan filmogenic properties have been addressed by Santos *et al.* [332] including the influence of the molecular weight (MW) and its degree of acetylation (DA). These authors found that lower DA chitosan led to membranes with lower water vapour permeability and swelling in water, and improved mechanical properties, such as higher Young's modulus, tensile strength and elongation. Moreover, decreasing the MW of the chitosan chains, without any significant change in DA, the water vapour permeability and swelling in water of the membranes were lower. Furthermore, the smaller polymer chains spoil the mechanical properties as a result of decreasing entanglement density and crosslinking degree and formation of a looser network.

The effect of the type of acid and concentration used for chitosan dissolution has also been tested [333, 334]. Park *et al.* [334] investigated chitosan films prepared using different chitosan MW (37000, 79000, and 92000 Da) and organic acid solvents (acetic, citric, lactic and malic acids) without plasticizer. Chitosan dissolved in acetic acid solvent resulted in the toughest films followed by malic, lactic, and citric acid, respectively. In addition, the same authors in a different study [335] found that the MW of chitosan after its dissolution in acetic acid was larger than that of samples dissolved in the other three acid solutions. In acetic acid solution, chitosan forms dimmers indicating that the intermolecular interaction is relatively strong, which suggests that these films have a tighter structure than those prepared using other acid solutions. However, water vapour permeability was not influenced significantly by the MW of chitosan or by the type of acid used.

A complete work about various aspects that influence the formation and characterization of chitosan membranes was published by Clasen *et al.* [336]. They studied the alterations of the network structure achieved by addition of plasticizer, cross-linking with dialdehydes and simple formation of chitosan membranes with the polyanion sulfoethyl cellulose. These authors observed that adding glycerol into chitosan membranes led to an increase of the permeability and that the membranes became more flexible and lost mechanical strength. Additional cross-linking of the chitosan with dialdehydes increased the mechanical strength whilst keeping the Young's modulus. However, the permeability was significantly lowered. In addition, the formation of chitosan membrane with the anionic counterion sulfoethyl cellulose led to thin and highly permeable membranes with mechanical properties too low for a practical application and as a consequence these porous membranes were reinforced using a filler material (cellulose mesh) to reach the required properties.

Besides the examples discussed above, a large number of researchers investigated these effects and other aspects that can influence chitosan film properties such as: the effect of plasticizers [337] and fatty acids [338], different drying conditions [339], solar radiation [340] and storage effects [341], addition of other synthetic [342, 343] and natural polymers [344, 345] or, less frequently, chemical modification [346, 347].

4.1.2. Bionanocomposites films

Despite the numerous advantages of natural biopolymers like chitosan as film forming materials, some drawbacks and limitations exist associated with processing. These include: water sensitivity, poor thermal stability, mechanical and water vapour barrier properties. Such limitations cause major restrictions for their industrial use especially under moist environments [1, 348]. Hence,

great attention has recently emerged around bionanocomposites aiming to improve the physico/chemical properties of biopolymer formulations [2, 25, 349]. Studies on natural biopolymer-based nanocomposite films are still limited if compared to their synthetic counterparts, but with the advent of new polymeric materials and composites with inorganic particles a growing interest in developing biodegradable bio-based nanocomposites has taken place [1, 350-353].

Although several nanoparticles have been recognized as possible additives to enhance polymer performance for packaging applications, several studies have focused their attention mainly on layered inorganic solids like clays and silicates, due to their avaibility, low cost, significant improvements and relative simple processability [25].

The use of clay layers is an excellent example to illustrate their potential to yield improved barrier properties to bionanocomposites. As shown in Figure 4.1 these fillers are able to modify the molecule pathway making the diffusive path more tortuous [354].

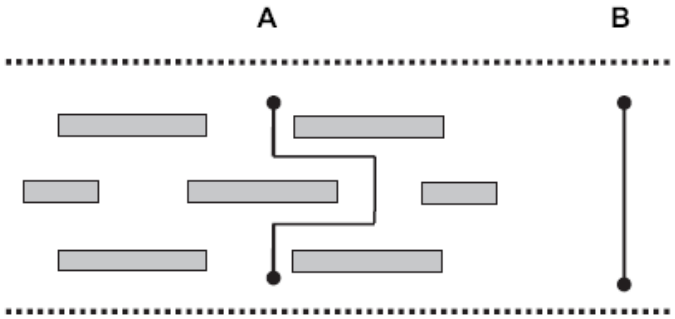

Figure 4.1: Schematic illustration of the tortuosity for a diffusing penetrant introduced in a polymer matrix with or without solid layered, (A) and (B) respectively. Reproduced from [2].

As discussed in Chapter 1, some studies focused on intercalated chitosan/layered silicate nanocomposites films have shown that interesting functional properties, namely enhanced thermal and mechanical properties are achieved [55, 57]. In such nanocomposites, the interfacial interaction between the polymer matrix and the dispersed silicate layers is a crucial factor in attaining their unique properties.

Among nano-scale clays, the montmorillonite is of particular interest and has been studied widely. An interesting bionanocomposite film was prepared by Darder *et al.* [55] using chitosan and montmorillonite. Though they used extraordinarily high amounts of clay (up to 400 wt% of chitosan), they found that the intercalation of the cationic biopolymer chitosan in Sodium montmorillonite provided compact and robust three-dimensional nanocomposites with interesting functional properties, such as improved mechanical properties and high thermal stability. These nanocomposites can be easily processed to construct bulk-modified electrodes for the potentiometric determination of anions.

Wang *et al.* [57] also prepared chitosan/montmorillonite nanocomposites using the solvent intercalation method and found that an intercalated/exfoliated nanostructure was formed with low montmorillonite content and an intercalated/flocculated nanostructure was formed with a high montmorillonite content. They also showed that the nanodispersed clay improved the thermal stability and enhanced the hardness and elastic modulus of the matrix systematically with increasing clay loadings.

Despite the improved properties obtained for the chitosan composites with laminates fillers, in this thesis the use of the silica fillers was investigated. The examples reported in the literature regarding silica-chitosan composite materials have been prepared mainly by *in situ* sol-gel methods [31, 63, 353, 355-357]. Generally it is considered that the *in situ* formation of inorganic particles within the polymer matrix through sol–gel reaction yields nanosized inorganic particles, uniform dispersions and advantageous polymer-filler interactions resulting in favourable mechanical, optical, and electrical properties [106, 358]. However as discussed in Chapter 1 the limitations of the sol-gel process are also real. On the other hand, the large shrinkage of the gel during drying and sintering makes dimensional control of large articles difficult.

Alternatively to *in situ* synthesis, an attractive approach and object of study in this Chapter was to prepare chitosan/silica by simply dispersing morphologically well-defined SiO_2 particles in the polymeric matrix. Besides the intrinsic simplicity of this method, it has not received much attention, which makes our work innovative and attractive especially for further studies involving hybrid functional nanoparticles coated with a silica shell such as Fe_3O_4@SiO_2 [359], SiO_2@ZnO [68], SiO_2@CdS [70], for example.

4.1.2.1. Film preparation

A biopolymer film is essentially a dried and extensively interacting polymer network of a three-dimensional structure with all additives incorporated such as plasticizers, fillers and others [360]. Essentially, two technologies are used for the preparation of biopolymers films, namely dry and wet processes. In the dry process, the thermoplastic biopolymer with low moisture content conditions is heated above its glass transition temperature using extrusion or thermo-compression methods [1]. Mainly starch and protein films have been processed via dry process. Wet processing, also called solvent casting method, is based on the drying of the film-forming solution, which involves solubilisation, casting, and drying steps. In this thesis the wet process was selected for the preparation of chitosan films.

Besides the fact that the casting process is a relatively simple film forming method, the choice of this procedure was based on some of its advantages which include: cost of equipments, tooling and molding are low. Moreover, the films are generally uniform in thickness and optically clear and it is not necessary to use additives for heat stabilization and lubrication as used in other heat-melt processes. On the other hand, there are some disadvantages such as: the output rate is low and cycle time is high, the dimensional accuracy is only fair and the presence of residual moisture and air bubbles may cause problems in the final films features [16].

During film preparation, the first step is to prepare a film-forming solution by dissolving or dispersing the biopolymer and additives in an appropriate solvent, which can be water, alcohol or an aqueous organic aqueous solution such as for chitosan films preparation, where acetic acid is the most widely used. Sometimes the dissolved film-forming solution is heated or the pH adjusted to enhance film formation or improve films properties. Then the solution is dried to make a polymer film by casting onto a flat surface or on a heated drum drier. Figure 4.2 shows the basic principle of simple casting process.

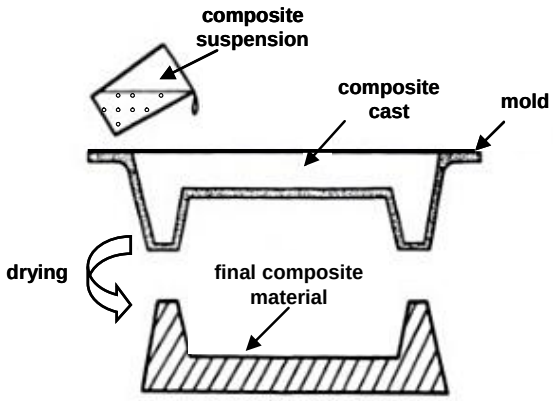

Figure 4.2: Casting process in an open, one-piece mold. Adapted from [16].

Depending on the film forming solution or suspension, the molds may be of different materials, such as: wood, metal, plaster, selected plastics, selected elastomers, or glass [16].

4.1.2.2. Factors affecting film properties

The interaction between biopolymer chains is an important feature in forming a continuous three-dimensional network. Hence, some factors must be taken into account to obtain a cohesive film. The nature, type, and the extent of the interaction depend upon the polymers involved and the film-forming conditions such as the drying process, moisture content, solvent type, plasticizer type,

concentration, pH, and the presence of other additives such as nanoscale fillers [1, 36, 348]. Some of these factors are discussed next.

4.1.2.2.1. Plasticizer

One of the disadvantages of natural polymer films, especially biopolymeric films, is the brittleness of this type of material, for this reason, such films have to be plasticized. Brittleness is an inherent feature attributed to the complex/branched primary structure and weak intermolecular forces of natural polymers. Plasticizers act by reducing the intermolecular forces thus the rigidity of the film structure is reduced and the mobility of the biopolymeric chains is increased, improving their mechanical properties [338, 361].

Plasticizers chemical structure, size, and shape influence its ability to disrupt polymer-chain bonding, including its ability to attract water to the plasticized-polymer system. Plasticizer selection is normally based on compatibility between plasticizer and polymer, permanence in the formed film, and efficiency in terms of the amount necessary to plasticize the films [362, 363]. Good compatibility is achieved when the plasticizer and polymer have a similar chemical structure.

Therefore, different polymers require different plasticizers. For polysaccharide-based edible films, hydrophilic plasticizers containing hydroxyl groups, which form hydrogen bonds with polysaccharides, are the best suited for this use. Examples include glycerol, sorbitol, xylitol, mannitol, polyethylene glycol, ethylene glycol, and propylene glycol [361, 363].

Several studies about the effect of plasticization in chitosan films properties have been carried out [333, 337-339, 341, 361, 363]. The work of Suyatma *et al.* [361] is an important contribution. These authors investigated the effect of hydrophilic plasticizers namely, glycerol (GLY), ethylene glycol (EG), poly(ethylene glycol) (PEG), and propylene glycol (PG) on the mechanical and surface properties of chitosan films. The stability of plasticized films was monitored by storage during 3-20 weeks in a chamber at 50 ± 5% RH and 23 ± ^{o} C. Among the three plasticizers concentrations tested (5, 20 and 40% wt), chitosan films plasticized with 20% wt GLY and PEG showed better stability during storage (around 5 months), higher strain, and lower tensile stress than films plasticized by PG. Films prepared with EG had high strain and low stress comparable to films prepared with GLY and PEG, but they were not stable during storage. In most cases, the elongation of plasticized films decreased with the storage time, which might be due to the recrystalization of chitosan and the loss of moisture and plasticizer from the film matrix. In general, plasticization improved the ductility and hydrophilicty of the chitosan films.

Moreover, Caner e*t al*. [333] observed that chitosan plasticization using PEG was stable until 9 weeks of storage while Butler *et al*. [350] found that the water barrier and mechanical properties of plasticized chitosan films with glycerol changed during storage, but oxygen and ethylene permeability remained constant during the storage period.

As regards the effect of the plasticizer on chitosan/silica films no references were found. One of the few studies reported in the literature describes the alternated addition of silica and PEG during the preparation of chitosan membranes. In that study, Clasen *et al.*[336] altered the structure of the membrane during its formation but removed the fillers from the membrane afterwards. These membranes had macro- and microporous structures with variable pore sizes in a range of 0.5-100 μm and superior gas and fluid capabilities. However, as expected, the membranes presented poor mechanical properties and needed some other reinforcement to reach the mechanical stability comparable to the pure chitosan membranes.

4.1.2.2.2. Addition and modification of nanofillers

Another practical way of tuning the properties of natural biopolymer films is to use functional fillers. Traditionally, mineral fillers such as clay, silica, and talc have been used in film preparation in distinct concentrations in order to reduce cost or to improve performance in some way [1]. In general, the loading of fillers into polymeric matrix is small, since larger concentrations can lead to high attrition from polymer chains sliding into particles [1, 17].

Filler particles change the distribution of the end-to-end vectors of polymer chains due to the fact that the filler excludes the chains from the volumes it occupies and these changes then cause alterations in the mechanical properties of the polymer matrix [17]. Hence, addition of any type of fillers to polymeric matrices requires a careful choice of procedures regarding the preparation method and surface stabilization to ensure homogeneous distribution of the fillers as discussed in Chapter 2.

4.1.2.2.3. Drying Process

Drying is an essentially simple process which constitutes a very important step during film-forming, since water is a strong plasticizer for film materials although not necessarily a good solvent [364].

Water plasticization of biopolymers has been extensively studied particularly in the context of food solids [333, 339, 361, 363, 365-368]. According to Levine *et al.* [250], the mechanism of water

plasticization is governed by the free volume concept similar to other plasticizer types. Water being a low molecular weight compound increases polymer free volume and allows an increase in the segmental mobility of the backbone chain causing a reduction of the glass transition temperature (T_g). Additionally, at temperatures above T_g water plasticization influences the viscoelastic, thermomechanical, electrical, guest and host diffusion, and gas permeability properties of completely amorphous and partially crystalline polymer systems [364].

Different types of drying techniques have been used to remove the water from chitosan film systems, including drying at ambient temperature after spreading the solution over a levelled plate, oven drying, infrared drying, microwave drying, oxygen plasma and UV/ozone irradiation [339, 365]. The choice of the technique to be used must be criterious as it has a direct effect on plasticization of the films and consequently on their properties [365].

In the case of nanocomposite films, the drying process is even more complex as it can affect the process of agglomeration of the filler particles in the biopolymer matrix. The presence of fillers can cause the compression of polymer chains specifically during the formation of networks by cross linking in solution followed by removal of the solvent. In these systems removal of solvent by drying is crucial, which puts the chains into a 'super contracted' state (Figure 4.3) [17] varying the principal properties of the material. When these fillers are in a agglomerate state the rheology of the polymer/filler composites can be significantly affected giving a significant rise to the viscosity as filler loading increases [369].

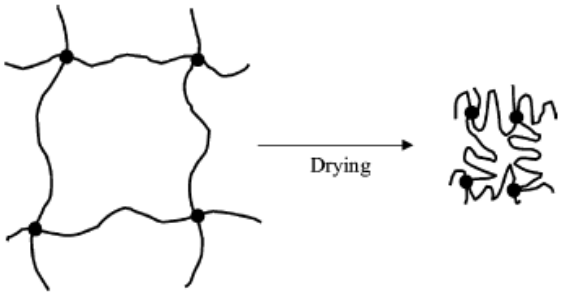

Figure 4.3: Forming a 'super-contracted' network by cross linking in solution, followed by drying. Reproduced from [17].

4.1.3. Functional properties

The development of bionanocomposites films with potential applications as membranes and packaging materials represents an ecological alternative to conventional polymer composites, as the properties of the biodegradable polymers used ensure that the materials produced are environmentally friendly [2, 351, 370]. On the other hand, the use of nanomaterials helps overcome

some of the limitations of biopolymers. Hence, the type of nanomaterial used and preparation method have to be finely turned and the functional properties of the resulting bionanocomposite films evaluated.

The structure of the bio based films prepared in this thesis has been characterized by Fourier transform infrared spectroscopy (FTIR). SiO_2 dispersion degree has been studied by scanning electron microscopy (SEM) and atomic force microscopy (AFM). The barrier properties of the films have been analysed by water vapour permeability (WVP) measurements and the wettability of the films by water was monitored by contact angle measurements. The mechanical properties have been investigated through tensile at break assays and thermal features by thermogravimetric analysis (TGA).

4.1.3.1. Mechanical properties

The mechanical properties of a material describe how it responds under strain/stress solicitation. There are only three types of mechanical forces that can affect materials which are compression, tension, and shear [16]. The mechanical test most often used to study the mechanical properties of films is the uniaxial tensile test. In this type of tests the build-up of force is measured as the specimen is being deformed at a constant rate. A force versus elongation curve is obtained which is then converted into a stress versus strain curve.

A typical stress-strain curve is shown in Figure 4.4. From tensile tests the modulus of elasticity, elongation, tensile strength, yield point, yield strength, and other tensile properties can be determined.

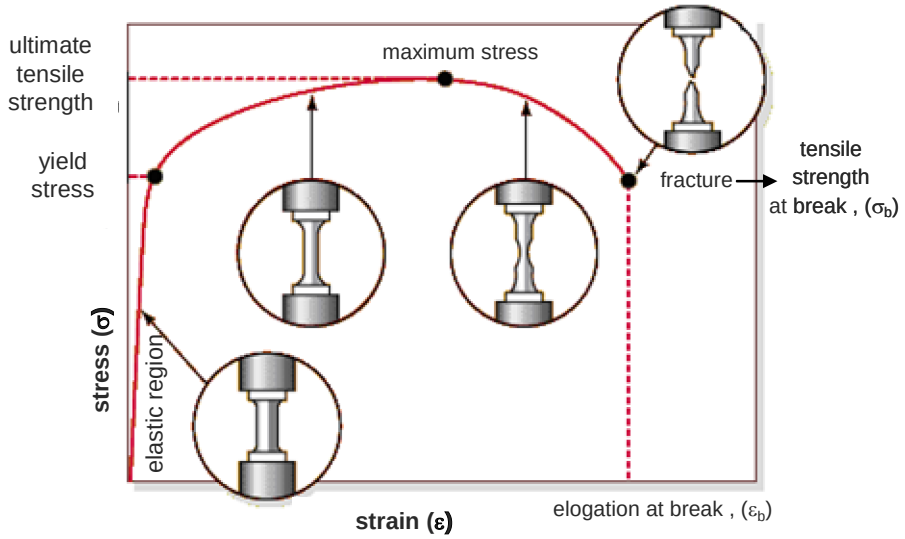

Figure 4.4: Example of a stress-strain curve. Adapted from [18].

As can be seen in the Figure 4.4, the stress and strain initially increase linearly. This is the linear-elastic portion of the curve, i.e. the strain is reversible and no plastic deformation has occurred. The slope of the line in this region is the modulus of elasticity or Young's modulus (E) which is a measure of the stiffness of a given material.

Ultimate tensile strength is indicated by the maximum of a stress-strain curve. It is determined by taking the force required to fracture the material divided by its cross-sectional area. For brittle materials, the ultimate tensile strength will be at the end of the linear-elastic portion of the stress-strain curve or close to the elastic limit. For ductile materials, the ultimate tensile strength will be outside of the elastic region, i.e. in the plastic region of the stress-strain curve. In our case, due to the large variability of samples ranging from very brittle to extremely ductile, we decided to evaluate the tensile strength at break (σ_b), i.e., the stress coordinate on the stress-strain curve at the point of rupture/fracture.

The ductility of a material is a measure of the extent to which it will deform before fracture. The conventional measure of ductility is the strain at fracture (usually called elongation at break, ε_b). Elongation is the change in axial length divided by the original length of the specimen or portion of the specimen and is expressed as a percentage [371]. Figure 4.5 illustrates the elongation behaviours obtained for different polymer samples through stress-strain curves.

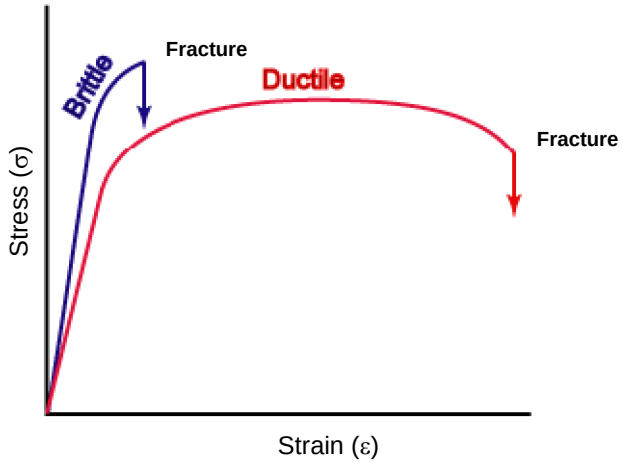

Figure 4.5: Stress-strain curves for different polymer films. Reproduced from [19].

In general brittle materials present smaller elongation than ductile materials, but a true interpretation of the mechanical properties of a material is not as simple as it seems. In mechanical properties evaluation all parameters (Young's modulus, tensile strength and elongation at break) must be jointly analysed. Besides the nature and density of intermolecular interactions between the biopolymer films constituents, the presence of filler and plasticizer, the thickness of the film and

the experimental conditions, such as sample size, temperature, relative humidity and the magnitude of the applied strain will affect the results [371].

Dynamical Mechanical Analysis (DMA) is also a very important tool in the characterization of the mechanical behaviour of different materials. It is a technique where an oscillatory force is applied to a sample allowing the materials response to stress, temperature, frequency and other values to be studied. DMA measures stiffness and damping, which are reported as modulus and tan δ. Because a sinusoidal force is applied, we can express the modulus as an in-phase component, the storage modulus, E', and an out of phase component, the loss modulus, E''. The storage modulus is the measure of the sample elastic behaviour. The ratio of the loss to the storage moduli is the tan δ and is often called damping. Damping is a measure of the energy dissipation of a material and it is defined as:

$$tan\ \delta = E''/E' \qquad \text{Equation 4.1}$$

The choice of the geometry is a very important step in DMA measurements and it is dictated by the sample physical state at the beginning of the experiment.

4.1.3.2. Barrier properties

Barrier materials possess the ability to restrict the passage of gases, vapours, and organic liquids [372]. Although synthetic polymeric materials have been frequently used as barrier materials in the packaging industry, the use of natural biopolymers, particularly in the food packaging industry, has significantly grown since they are completely biodegradable, edible in some cases and provide efficient barriers against oils and lipids [348, 349, 351, 373]. However, their moisture barrier properties are poor due to their hydrophilic nature [351].

The permeability or transmission rate of gases and vapours through any polymeric material is dependent upon two factors: the solubility of a gas or vapour and the rate of diffusion through the barrier material. The solubility depends on the chemical relationships between the permeant molecule and the polymer, whilst the rate of diffusion depends on the size of the permeant molecule and the structural configuration of the barrier polymer [372]. In addition, environmental and processing conditions that affect the composition and structure of polymer films are of particular relevance to the barrier properties of the material [374].

Water vapour and oxygen are two of the main permeants studied in film packaging applications as they may transfer from the internal or external environment through the polymer package wall resulting in a continuous change in product quality and shelf-life [375]. In this thesis, studies focused exclusively on water vapour permeability.

The water vapour transmission rate (WVTR) is defined as the steady flow of water vapour per unit time through unit area of material in the direction normal to the surface of the material under defined conditions of temperature and humidity. The WVTR is given by equation 4.2;

$$WVTR = \frac{m}{\exp osed\ \ film\ area} \qquad \text{Equation 4.2}$$

where *m* is the slope of the weight gain *versus* time curve built until steady state conditions are reached.

The permeance to water vapour (WVP) is the WVTR through the unit area of the material, induced by a unit difference of vapour pressure between two specific surfaces of the material under defined conditions of temperature and relative humidity [376]. The WVP is given by Equation 4.3:

$$WVP = \frac{WVTR}{DP} \times\ film\ thickness \qquad \text{Equation 4.3}$$

Units: $g\ .\ mm/h\ .\ m^2\ .\ kPa$

where $DP = S \times (R1 - R2)$ and *S* is the saturation vapour pressure at assay temperature (kPa), *R1* is the relative humidity at one side and *R2* is the relative humidity at the other side of the filler sample. *S* was calculated as a function of temperature given by Equation 4.4.

$$S = 0.61078 \exp\left(\frac{17.269T}{T} + 237.3\right) \qquad \text{Equation 4.4}$$

4.1.3.3. Surface properties

The knowledge about surface properties of bionanocomposites provides supplementary understanding of film behaviour as well as the chemical structure, orientation and mobility of groups within the topmost atomic layers at the interface [20].

At present no single technique can provide all the relevant information about a surface, especially if it includes factors such as conformation and mobility in addition to chemistry. Thus, as far as possible, more than one technique must be employed in order to gain sufficient information about a particular surface. The most commonly used surface characterization techniques for biopolymers are contact angle measurements, attenuated Fourier transform infrared spectroscopy (FTIR) and surface spectroscopic and spectrometric techniques such as electron spectroscopy for chemical analysis (ESCA) and secondary ion mass spectrometry (SIMS). Other techniques such as scanning electron microscopy (SEM) and atomic force microscopy (AFM) are often employed to study the surface morphology of the films. A comparison of the surface depth that each method can analyze is shown in Figure 4.6.

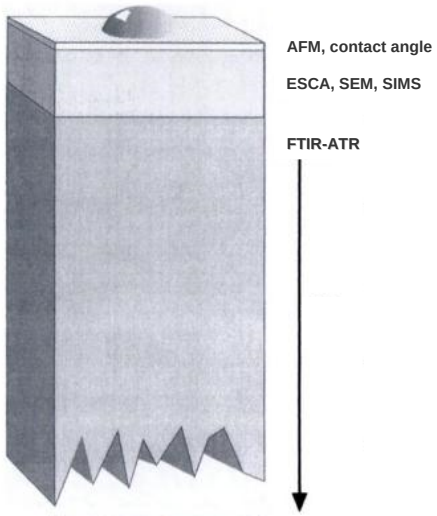

Figure 4.6: Comparison of the depth measurements of major surface characterization techniques. Adapted from [20].

In this Chapter, structural and surface informations about the bionanocomposite films were evaluated by FTIR, AFM, SEM and water contact angle (WCA) measurements.

In the majority of the papers on bionanocomposites, Fourier transform infrared analyses have been carried out in order to understand possible interaction between filler and biopolymer. Depending on the size, surface area, porosity of the filler and especially the method used in film forming, the FTIR spectra can provide distinct results about structural properties and mechanisms of interactions between components [377, 378].

FTIR equipped with attenuated total reflectance (FTIR-ATR) is a very versatile non destructive analyzing technique that requires no pre-treatment and is suitable for depth profiling of membrane surfaces. The lack of surface sensitive of this technique compared to other techniques as shown in Figure 4.7 means that much of the structural information may refer to the bulk composition rather

than to the topmost layers. In fact, some studies using FTIR-ATR to characterize surfaces have reported no observable differences between the bulk and surface structure on the basis of infrared spectra, contrary to what was observed with other surface techniques.

Wetting properties are also essential surface features of packaging materials. Wetting is defined by the contact angle formed between the test liquid and the film. As the contact angle increases the potential for the two to interact decreases [379]. The overall interaction between a film surface and a wetting liquid depends on the degree of contact achieved and the magnitude of the intermolecular forces involved (liquid–vapour, γ_{LV}, solid–liquid, γ_{SL}, and solid–vapour, γ_{SV}). The latter are affected by several factors, including film surface free energy, liquid surface tension, and roughness [380]. The wetting of a solid surface is governed by the Young relation (Equation 4.5), which establishes the equilibrium between the contact angle θ and the three aforementioned interfacial tensions.

$$\gamma_{LV} \times \cos\theta = \gamma_{SV} - \gamma_{SL} \qquad \text{Equation 4.5}$$

For smooth surfaces, the most frequently applied approach for quantifying the wettability of plastic materials is the sessile drop method, whereby the contact angle is measured by observing the liquid drop from the side.

Although the measurement of contact angle is simple and a sensitive tool for evaluating surface energy status [21] this is not the case for rough and heterogeneous surfaces (Figure 4.7). The real contact angle (θ) is the angle between the tangent to the liquid–fluid interface and the real, local surface of the solid. The apparent contact angle (θ_{ap}) is the angle between the tangent to the liquid–vapour interface and the line that represents the nominal solid surface. Obviously, the difference between the two contact angles may be very large. It turns out, that the real contact angle equals the Young contact angle (Equation 4.5), if line tension is negligible. Hence the real contact angle is the one needed for assigning the surface tension of solid surfaces. However, it is yet experimentally inaccessible on rough surfaces. On smooth, but chemically heterogeneous surfaces it may vary from one point to another, again making its measurement very difficult [21].

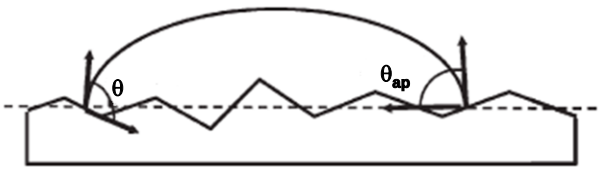

Figure 4.7: Real contact angle (θ) and the apparent contact angle (θ_{ap}) on rough surfaces. Adapted from [21].

Scanning electron microscopy (SEM) is the most powerful technique for surface characterization but must be complemented with other surface characterization analyses [381]. In order to interpret analytically a composite material surface by microscopy, we will need to observe:

- grain size and orientation;
- degree of homogeneity of the multiphase material;
- whether the sample is porous;
- topography of fractured surfaces, and whether the material reveals intergranular or transgranular fracture, besides other features;

The majority of composite studies use SEM analyses to visualise and understand material's surface features. Particularly for bionanocomposites this technique has been fundamental for this purpose. Nevertheless, some difficulties had to be overcome. There are two major problems in the observation of polymer based composite [382]. Firstly, polymers are poor conductors of electricity and charge rapidly builds up on the specimen when it is bombarded with an electron beam. A conductive coating must be applied to remedy this problem. Secondly, polymers are often damaged by the energetic impinging electrons, causing artefacts to appear. This problem requires the use of low accelerating potentials, which may, in turn, limit resolution and reduce contrast.

With the advent of high brightness field emission guns, low voltage SEM has become highly practical and is now widely used with this type of materials [381]. Using this kind of equipment, we have achieved good resolution in our bionanocomposite SEM images.

Among scanning probe microscopy (SPM) techniques, the tapping mode atomic force (AFM) is the most frequently used technique for characterizing nanometer-scale structures. In this technique a probe moves along the specimen surface to determine topography, material properties, or chemical structure. In general the AFM images illustrate a problem common to all SPM: the observed surface is a convolution of the actual surface and of the probe tip [383]. In its original contact mode AFM, the tip is kept in contact with specimen. Though non-contact mode AFM does not suffer from tip or sample degradation effects that are sometimes observed after taking numerous scans with contact AFM. This makes non-contact AFM preferable to contact AFM for measuring soft samples. Due to roughness and softness of our bio-nacomposites the non-contact mode was chosen for AFM analyses.

4.1.3.4. Thermal properties

Thermogravimetric analysis (TGA) monitors the change in mass as a function of temperature, time, and/or atmosphere. This technique is commonly employed to determine degradation temperatures, absorbed moisture content of materials and the level of inorganic and organic components in materials as well as solvent residues. One of the most important parameter which is possible to obtain by TGA analysis is the degradation temperature which helps determining the maximum limits at which the material losses its characteristics [384].

4.2. Experimental Part

4.2.1. Materials

In a first attempt to prepare the composite films, SiO_2 and SiO_2@APS suspensions were prepared by dispersing a convenient amount of silica particles in 5 mL of 0.1 mol/L acetic acid solution, stirred overnight and then treated by ultrasonics for 30 min.

Chitosan from crab shells (with a degree of deacetylation of about 85% and medium weight molecular) was purchased from Sigma-Aldrich. Chitosan solutions (2 wt.%) were prepared in 0.1 mol/L acetic acid by dispersion of the chitosan powder overnight under moderate stirring followed by filtration under vacuum through a porous glass filter (G2).

4.2.2. Film formation

Self-supported silica-chitosan composite films were prepared by a traditional solvent-casting method [332]. Two different ionic conditions were tested, corresponding to a low pH value where the biopolymer is essentially ionized and a neutral pH value where the chitosan amine groups are essentially non-protonated. Previous results on the effect of plasticizer type (glycerol or PEG) and concentration (15 - 30 wt.%) on chitosan (CHI) films were considered to select the experimental conditions used in this work [385]. Mixtures of CHI solution, plasticizer and silica suspension in the appropriate ratios were stirred for about 10 min at room temperature. Two distinct procedures were tested regarding the preparation of the mixtures, named Procedure 1 and Procedure 2. In Procedure 1, the aqueous silica suspension was added to the chitosan solution containing the plasticizer. In Procedure 2, the aqueous silica suspension was added to the plasticizer and the resulting suspension was stirred overnight and then added to the chitosan solution. Silica suspension concentration varied between 1, 5 and 10 wt.%. Then, the pH value was adjusted to 3

and the mixture was heated at 50 °C for 10 min. After cooling to room temperature the mixture was de-gassed under vacuum for 1 hour. Final concentrations relative to the polymer were 1.3 wt.% of chitosan, 0.2 wt.% plasticizer, and 0.07 wt.% silica particles. Films were cast by weighing 30 g of the chitosan/plasticizer/SiO_2 mixture onto poly(methyl methacrylate) PMMA plates with 139 cm^2 of area. The solvent was allowed to evaporate for 16 h in a ventilated oven at 30 °C. At this stage, the dry films still contained residual solvent and the amino groups would be essentially protonated. To prepare neutralised films, the films were peeled from the casting surface and placed in 0.1 mol/L NaOH for 30 min. The films were then washed extensively with distilled water until reaching a neutral pH, dried for 2 hours at 30 °C in a ventilated oven, and then left for a further 16 hours at room temperature. Unless otherwise mentioned, both neutralised and non-neutralised films were conditioned in a small plexiglas chamber at 53% relative humidity (RH) (in the presence of a magnesium nitrate saturated solution) and 23 ± 2 °C for at least 48 hours prior to testing. Drying and storage equipments for films are shown in Figure 4.8. Before testing, the thickness of the film samples was measured using a digital micrometer (model MDC-25S, Mitutoya Corp., Tokyo, Japan). Mean thickness was calculated from 5 measurements taken at different locations on each film sample. A similar procedure was used to prepare and store CHI/plasticizer/SiO_2@APS films.

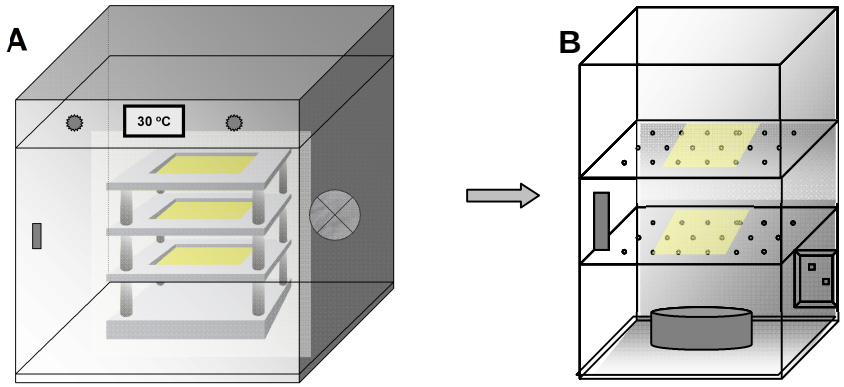

Figure 4.8: (**A**) Ventilated oven at 30 °C used to dry the films on PMMA plates and (**B**) storage of the films in small plexiglas chamber at controlled RH.

4.2.3. Film characterization

4.2.3.1. FTIR-ATR characterization

The Fourier transform infrared (FTIR) spectra of the film samples were acquired using a Golden-gate single reflection attenuated total reflectance (ATR) in a Bruker IFS-55 spectrometer at a resolution of 8 cm^{-1} and 256 co-added scans.

4.2.3.2. Mechanical properties

Tensile properties of the neutralised and non-neutralised films were tested on a texture analyser equipment (model TA.Hdi, Stable Micro Systems, England) equipped with fixed grips lined with thin rubber on the ends. The specimens were cut into 10 mm wide and 90 mm long strips as shown in the Figure 4.9. The initial grip length was 50 mm and the specimens were uniaxially stretched at a constant crosshead speed of 0.5 mm/s. All experiments were conducted at 25 ± 2 ^{o}C and 50 ± 2 % RH. At least, ten samples of each film type were tested. Tensile at break assays were based on the standard method ASTM D 882-83. Young's modulus (E), percentage elongation or strain at break (ε_b) and tensile strength or stress at break (σ_b), were determined from stress–strain curves obtained from tensile tests to films failure.

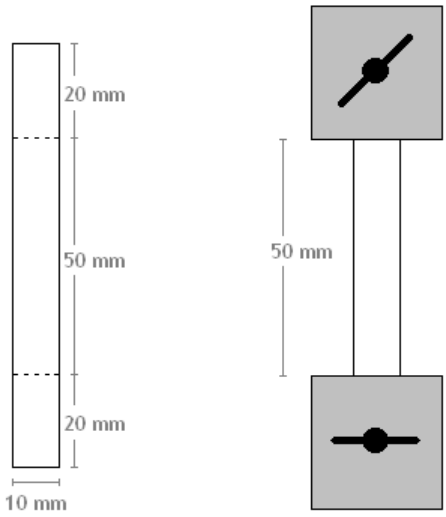

Figure 4.9: Film specimens with 10x90 mm which 40 mm (20 mm at each end) correspond to the exposed film surface for adherence to grips from texture analyser equipment. Reproduced from [22].

DMA measurements were carried out on a Tritec 2000 DMA Triton equipment operating in the tensile mode. Tests were performed in a frequency range of 1 – 100 rad/s in a displacement of 3 mm at ambient temperature (25 ^{o}C). Test specimens with a typical size of 0.5 mm x 1 mm were analysed upon drying under distinct conditions. Firstly, the specimens kept under constant RH were analysed. Next the films were dried in the DMA oven up to 120 ^{o}C and analysed after cooled. The viscoelastic modulus (E' and E'') were obtained as a function of frequency.

4.2.3.3. Contact angle measurements

Static water contact angles of neutralised and non-neutralised films obtained by Procedure 1 were measured at room temperature using a surface energy evaluation system (Brno University, Czech

Republic) in a sessile drop configuration (using ultrapure water) coupled with a video camera and image analysis software. At least ten droplet images were obtained for each film sample. The images were acquired within 0.1 s after the water drop touched the film surface in order to minimize the errors caused by water absorption of the film surface.

As regards the neutralised and non-neutralised films obtained by Procedure 2, contact angle measurements were performed using a OCA 20 Dataphysics instrument, which was acquired in the meantime. Using ultrapure water as test liquid, a drop (3 μL) was automatically dosed by a syringe on the surface of the film. The evolution of the drop shape was recorded with a camera coupled to the system. The determination of contact angles was calculated with the image analysis software, according to the circumference method. The final results take into account the average of 5 drops placed in different positions of the film (upward and downward surfaces).

4.2.3.4. Water vapour apparent permeability

Water vapour transmission rate (WVTR) was measured following a previously described method [332] which is based on the ASTM standard method D96-95 ("*desiccant method*'') [386].

Circular boxes (Figure 4.11) made of PMMA (with diameter = 8 cm, external height = 2 cm, internal diameter = 5 cm and internal height = 1.8 cm) were used in these analyses. The boxes are closed by a lead with 4 built-in screws coupled with threads. The circular film samples (diameter = 6 cm) were cut previously and fixed between the circular box surface and the fixing ring made also of PMMA as illustrated in the Figure 4.10. Silicone was used to improve the fixation of the sample on the box. Beforehand, the boxes already contained around 16 g of anhydrous calcium chloride ($CaCl_2$) previously dried in an oven at 200 ºC during 2 hours in order to get around 0.6 cm in height between the film and the $CaCl_2$ (0% relative humidity). The exposed area of each film was around 19.6 cm^2.

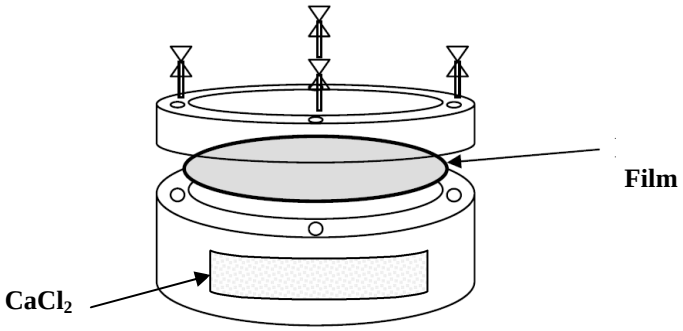

Figure 4.10: Scheme of circular box containing $CaCl_2$ used in the determination of the water vapour apparent permeability. Reproduced from [23].

The boxes with the samples were cautiously weighed and then conditioned in a closed plexiglas chamber with air circulation provided by a fan (152 m/min). Inside the chamber the RH was 46 ± 2% and the temperature around 23 ± 2 ^{o}C. The RH ensured by saturated solution of magnesium nitrate in chamber and temperature were monitored by a hygrometer/thermometer (Term Hygro, Cole Parmer). The boxes containing the samples were weighed each hour. Steady state conditions were assumed to be reached when the rate of change in weight of the cup became constant (approx. 8 h). At least 3 replicates for each type of film were performed. Despite the two different film surfaces the water permeability results of the surfaces were similar. Thus, the permeability tests were carried out only on the top surface exposed to humidity.

The WVTR and WVP were calculated as previously described in § 4.1.3.2 by Equations 4.2 and 4.3, respectively. A typical weight gain *versus* time is shown in Figure 4.11.

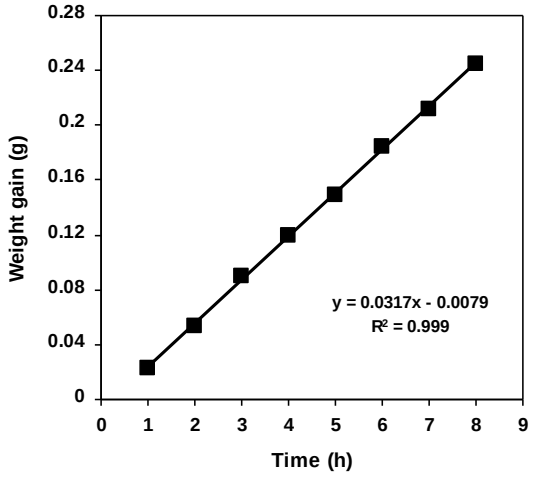

Figure 4.11: Example of a linear regression used to calculate the WVTR.

4.2.3.5. Thermal analysis

The thermal properties of films were carried out by thermogravimetric analysis (TGA). The neutralised and not-neutralised films were cut into small pieces and about 10 mg of such film sample were placed inside an aluminium pan. The thermoanalyzer (Shimadzu TGA-50, Japan) was operated under nitrogen atmosphere between 25 and 900 ^{o}C at a heating rate of 10 ^{o}C/min.

4.2.3.6. Morphology and surface topography

Scanning electron microscopy (SEM) images were taken using a Ultra-high Resolution Analytical Scanning Electron Microscope HR-FESEM Hitachi SU-70 operating at 2 kV. Samples were mounted on carbon tape and coated with carbon for SEM analysis.

Surface characterization by atomic force microscopy (AFM) was carried out using a scanning probe microscope from Scientec (Picoforce multimode SPM with a Nanoscope IV control unit). A silicon nitride tip (Veeco, type DNP) with cantilever spring constant of 25-75 N/m (as stated by the manufacturer) was used in non soft-contact mode fixing the surface load to the electrostatic repulsive barrier.

4.2.3.7. Statistical analysis

All tensile tests, contact angle and water vapour permeability measurements were replicated at least five times for each sample. A one-way ANOVA statistical tool was used to examinate any significant difference between groups classified on each independent variable under study. A Newman–Keuls post-hoc test was performed to test for specific statistical significance among data means. Analysis was performed using Statistica (software v. 6.0, StatSoft Inc.).

4.3. Results and Discussion

For the preparation of bionanocomposite films non-modified and modified silica particles were used. As discussed in Chapter 2, the stability of the fillers is of crucial importance in the development of enhanced new materials. In order to improve silica particles stability in the CHI matrix besides the surface modification of silica particles, two different methods of preparation of CHI composite films were tested. These methods for film formation were named as Procedure 1 and Procedure 2. As described in the experimental section the principal difference between these methods is that in Procedure 1 the plasticizer was mixed directly with the chitosan while in the Procedure 2, the plasticizer was mixed and stirred overnight with silica particles suspension in order to favour a better dispersability of the inorganic fillers. Composite films containing SiO_2 particles without surface modification were prepared by Procedures 1 and 2 whilst composite films containing SiO_2@APS particles were only prepared using the Procedure 2.

Taking into account the applicability of these new materials as packaging material all the films were also analysed upon neutralization. Moreover, although for all film prepared in this thesis both surfaces have been investigated, no significant differences were registered. Thus, only the results obtained for the top part of the films, i.e. the side in contact with air during drying are presented.

In the next sections a detailed study about the characterization and properties of the new composite films (neutralised and non-neutralised) prepared using different strategies is discussed.

Prior to study the effect of silica particles on the properties of CHI films, it was important to study the effect of the type and amount of plasticizer in order to guarantee the best performance of the composite films.

4.3.1. Plasticizer effect on film properties

As mentioned previously in § 4.1.2.2.1, plasticizers reduce the intermolecular interactions between adjacent chains of the biopolymer, resulting in increased mobility of these chains and therefore the materials become more flexible. Thus, at macroscopic level changes in physical or functional properties of the films are identified [338, 361].

According to Jongjareonrak *et al.* [387], who investigated the effects of the type and concentration of plasticizers on the mechanical properties of fish skin gelatin edible films, the choice of the appropriate plasticizer depends on the nature, size and the structure of plasticizer as well as the compatibility between polymer molecules and plasticizer. In view of this two polyols, GLY and PEG at two concentrations (15 and 30 wt.%) were first tested for the preparation of chitosan films. In order to evaluate the influence of type and amount of plasticizer on the mechanical properties of the chitosan films, tensile tests were carried out. The results obtained for Young's modulus (E), tensile strength (σ_b) and percentage elongation (ε_b) at break for the different plasticized chitosan films are illustrated in Figure 4.12. For comparison purposes the data obtained for unplasticized chitosan film are also shown.

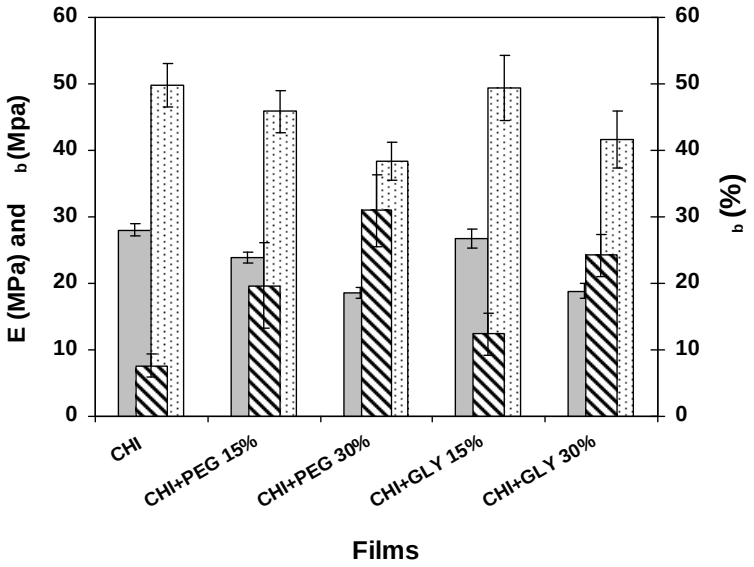

Figure 4.12: Plasticizer effects on the mechanical properties of chitosan films: Young's modulus (E, gray color), tensile strength at break (σ_b, dark points) and percentage elongation at break (ε_b, dark lines). CHI means chitosan.

From Figure 4.12 it is clear that both GLY and PEG influenced the mechanical properties of chitosan films. As expected the percentage of elongation at break, ε_b, increased with increasing concentration of plasticizer both for PEG and GLY whilst the Young's modulus, E, and tensile strength at break, σ_b, did not vary significantly except when the concentration of plasticizer used was 30 wt.%. In this case a slight reduction of E and σ_b was observed.

The fact that CHI/PEG films showed slightly lower values of tensile strength than those prepared using GLY both in the same concentration is attributed to the difference in MW of the plasticizer [388] but may also be associated with their affinity to water which is also a plasticizer. In fact, notice should be made that films prepared with PEG exhibited reversible cloudiness which was not observed for those prepared using GLY indicating the latter were less hygroscopic. Despite of the fact that GLY is more hygroscopic than PEG, due to its reduced dimensions it is capable of being easily inserted between the chitosan chains [52] and thus does not absorb so much water. On the other hand, the interaction between PEG and chitosan macromolecules could also retard the mobility of PEG, i.e. making it difficult for PEG macromolecules to reorganize and probably generating more free volume, which can facilitate absorption of water and the deformation under the same conditions [336, 389].

In view of the results discussed above it was considered that for the potential application of the films in question in the packaging industry, where transparency and a balance between (σ_b, ε_b and E) are an issue, the films prepared with 15 wt.% were selected to further investigate to effect of silica particles. This plasticizer type and concentration was also tested by other researchers in the preparation of biopolymer films [48, 54].

4.3.2. CHI/SiO_2 films prepared by Procedure 1

The preparation of the CHI composite films by Procedure 1 followed the experimental procedure implemented in our group for bio based film preparation [332, 390]. In particular, for our case, the plasticizer was previously mixed with CHI solution and after this an aqueous dispersion of SiO_2 nanoparticles (AD ~ 300 nm) was added. The films were prepared onto PMMA plates and dried as described in § 4.2.2. The effect of silica particles was investigate under the light of the different characterization techniques such as FTIR, SEM, WVP, tensile tests, DMA,TGA and WCA.

4.3.2.1. Effect of silica on films properties

In order to analyse the effect of silica on the mechanical, surface, thermal, structural and morphological properties of the chitosan films, different silica contents (1, 5 and 10 wt.%) have been used to prepare chitosan composite films using GLY (15 wt.%) as plasticizer. Before adding SiO_2 particles into the chitosan matrix, these particles were characterized by different techniques as discussed in the Chapter 2.

4.3.2.1.1. Tensile properties

Tensile parameters (Young's modulus (E), tensile strength (σ_b) and percentage elongation at break (ε_b)) were measured for the pristine chitosan films, plasticized films and for those loaded with 1, 5 and 10 wt.% silica, under acidic conditions and after neutralization in order to evaluate the effect of silica on the mechanical properties of the plasticized chitosan films. The results obtained are summarized in the Table 4.2.

Table 4.2: Effect of silica on the mechanical properties of pristine and plasticized chitosan films: Young's modulus, tensile strength at break and percentage elongation at break (standard deviations given in parentheses).

Films	***Acid conditions***			***Neutralised films***		
	E (MPa)	σ_b (MPa)	ε_b (%)	*E* (MPa)	σ_b (MPa)	ε_b (%)
CHI	28 (1) *x*	50 (3) *x*	8 (2) *x*	39 (1) *x*	68 (4) *x*	8 (2) *x*
CHI+GLY	27 (1) *x*	49 (5) *x*	14 (2) *y*	34 (2) *y*	60 (4) *y*	11 (3) *x*
CHI+GLY+1%Si	21 (1) *y*	54 (5) *x*	35 (3) *w*	-	-	-
CHI+GLY+5%Si	21 (1) *y*	52 (6) *x*	35 (3) *w*	36 (1) *y*	61 (3) *y*	7 (1) *x*
CHI+GLY+10%Si	21 (1) *y*	50 (5) *x*	34 (4) *w*	-	-	-

Different letters within a column indicate significant differences ($p < 0.05$)
CHI and Si mean chitosan and silica particles, respectively.

As discussed above, plasticizers are well-known for reducing film brittleness and increasing film flexibility. They act mainly by disrupting hydrogen bonding between polymer chains, thus reducing intermolecular forces and increasing chain mobility. Therefore, as expected, the presence of the plasticizer increased the elongation at break, an effect more pronounced for the non-neutralised

films, and decreased the Young modulus and tensile strength at break. These last effects were more noticeable in the case of the neutralised films (Table 4.2).

In general, neutralization increased the tensile strength at break and the Young's modulus, but decreased film elongation. These results may be explained by the decrease in charge density of chitosan and subsequent increase of intermolecular interactions between chitosan chains.

As regards the composite films, the presence of SiO_2 caused the reduction of Young's modulus of films and improved their elongation, an effect more pronounced for the non-neutralised films. However, no significant differences were observed regarding the tensile strength at break (Table 4.2). For the neutralised composite films the presence of the filler had no significant effect on the Young's modulus or on the tensile strength or elongation at break. In conclusion, the effect of silica on the mechanical properties of the chitosan films seems to be much more pronounced for the non-neutralised films, indicating that the lower ionization of the amine groups on chitosan chains leads to different effects of the filler.

In order to understand these results one has to bear in mind that higher elongation means a reduction of brittleness. As the non-neutralised composite films are less rigid and less brittle materials they require higher energy for fracture. This may be so because at pH 3, the higher ionization of the biopolymer in the non-neutralised films increases interchain repulsion. Moreover, in the absence of any significant interactions between the filler and the polymer matrix, the filler particles act as internal lubricants by reducing frictional forces between polymer chains. Therefore, the presence of the filler associated with the loosen polymer network decreases short range intermolecular forces and helps to relieve local stresses, thus reducing Young's modulus and enabling higher elongation to be obtained.

Additionally, it was observed that the mechanical properties of the films did not change significantly with increasing amount of silica in spite of the fact that particle aggregation becomes more obvious with the increase of silica loading. In order to have a suitable balance of film transparency and filler loading, it was decided to focus on a moderate silica mass fraction of 5 wt. % (renamed silica) in the following characterizations of the chitosan composite films. Some images displaying the transparency of the different chitosan films are shown in Figure 4.13.

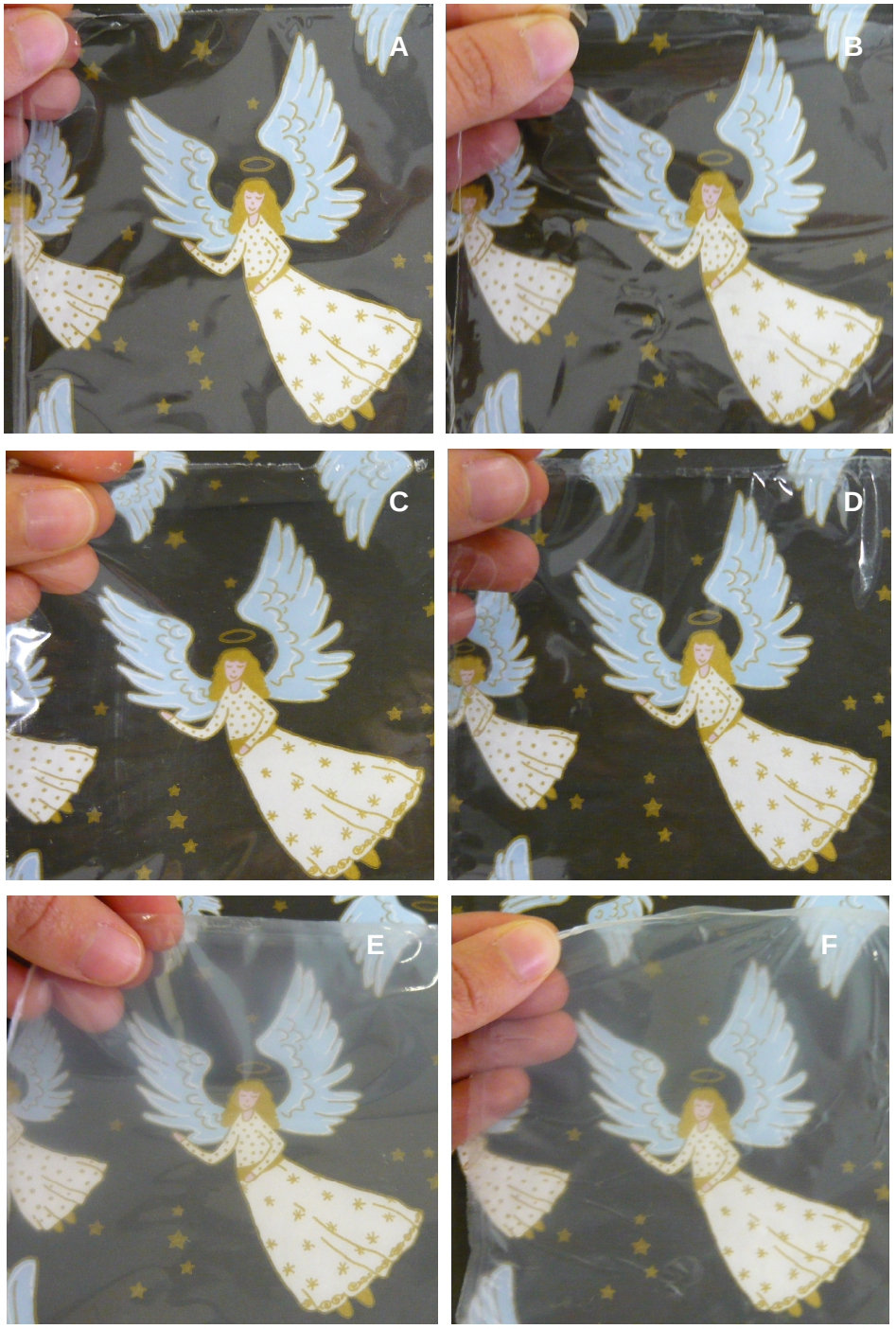

Figure 4.13: Images of chitosan films. (**A**) non-neutralised chitosan film, (**B**) neutralised chitosan film, (**C**) non-neutralised plasticized chitosan film, (**D**) neutralised plasticized chitosan film, (**E**) non-neutralised plasticized chitosan/silica film, (**F**) non-neutralised plasticized chitosan/silica film.

Regarding the visual comparison of images of the neutralised and non-neutralised films illustrated in Figure 4.13, it is easily seen that chitosan and plasticized chitosan films (Figure 4.13A, B, C and D) did not have their transparency altered before and after neutralization. However, neutralised and

non-neutralised plasticized chitosan/silica films (Figure 4.13E and F) are equally less transparent. Lai *et al*. [377] suggested that for a material to remain transparent, silica particles should disperse at very fine scale to allow light to be transmit easily. Hence, these preliminary results indicate that silica particles tended to aggregate resulting in less transparent films.

Although reinforcing effects and properties improvement at low filler loading levels have been identified for several polymer–inorganic composite materials most of the reported in the literature were achieved mainly by using elongated nanostructures, either as carbon nanotubes or cellulose whiskers, or polymer-layered nanocomposites. For example, drastic reinforcing effects are typically observed for elastomers loaded with hard fillers [391], for latex-cellulose fibre composites[392], or for layered silicate composites [353, 393]. However, when isotropic nanoparticles are used, such as the spherical-like silica particles used in the present study, reinforcement effects are strongly dependent on the filler and polymer surface characteristics and subsequent interactions as reported by Oberdisse for latex-silica nanocomposites [394].

The reinforcement effect may also be related to the kind of polymer network that can be formed. It may be assumed that reinforcement effects are more marked when the polymer network shows a higher degree of crosslinking and when the polymer segments between crosslinks show high rigidity. This is the case observed for films prepared from the latex networks, consisting essentially of an entangled melt, or for elastomers, where a rubber network exists stabilized by covalent bonds. Any of these scenarios are quite different from the macromolecular organization that would be present in the chitosan films.

The state of dispersion and aggregation has also a strong influence on the mechanical properties [395]. In fact, another condition for the reinforcement to occur seems to be the existence of significant interactions between the polymer and the filler, as is the case when the polymer-silica composites are prepared by sol-gel *in situ* methods or when the silicate fillers have a high aspect ratio (i.e., length to diameter ratio, like clay platelets, fibres or nanotubes) together with a good dispersion in the polymer matrix. Yeh *et al.* [357] have actually reported enhanced mechanical properties and thermostability for chitosan-silica hybrid materials prepared by *in situ* sol-gel methods, for which good silica dispersion and hydrogen bonds between the biopolymer and the silica have been identified.

The absence of significant reinforcement effects observed for our chitosan-silica composite films is likely associated to different factors, namely the particle low aspect ratio, the poor dispersion of the silica particles in the polymer matrix, the absence of any significant interactions between chitosan and the filler, and the loosen polymer network that characterizes the chitosan matrix especially in

the non-neutralised films. To verify this, further chemical and structural analyses were carried out as discussed next.

4.3.2.2.2. Spectroscopic analysis (FTIR-ATR)

FTIR analysis of the pristine chitosan films and composites was performed to identify possible interactions between the polymer matrix and the filler as well as possible structural changes caused by film neutralization.

Figure 4.14 shows representative infrared spectra of a SiO_2 sample and of plasticized chitosan films with and without silica particles. The region from 1800 to 1200 cm^{-1} is shown in detail in Figure 4.15 as several absorption bands in this region are influenced by intermolecular interactions, namely hydrogen bonding.

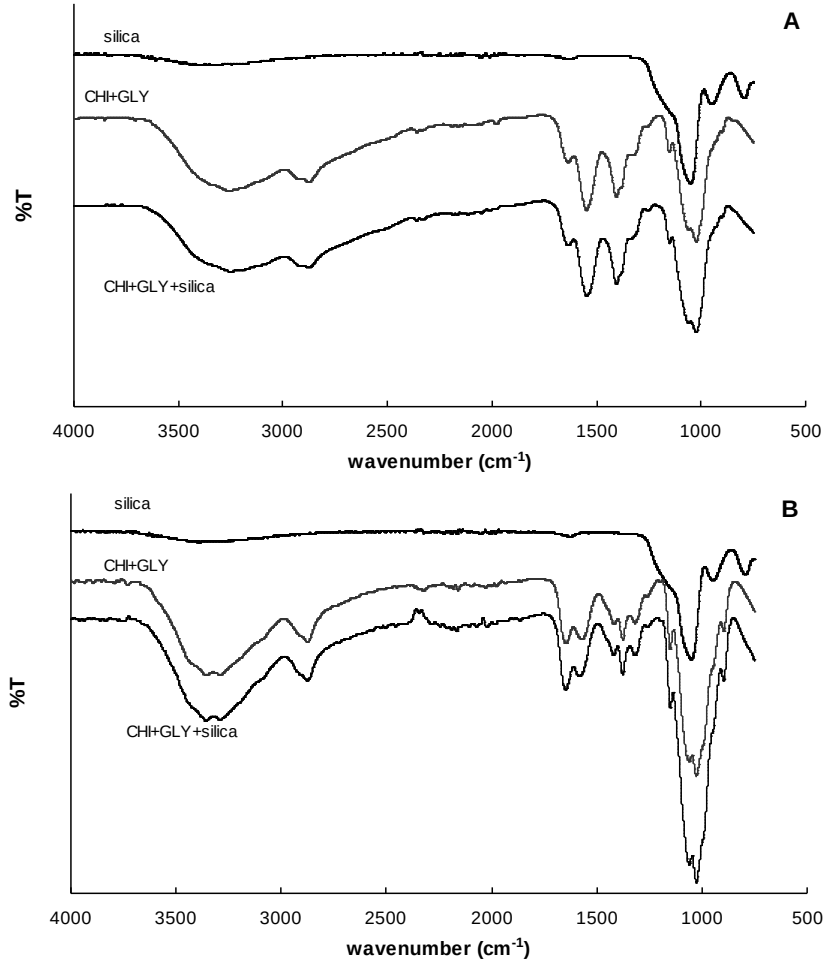

Figure 4.14: FTIR spectra for silica, palsticized chitosan and the plasticized composite chitosan/silica films: (**A**) Non-neutralised films; (**B**) Neutralised films. Spectra have been normalised at 2923 cm^{-1} (C-H band) for better comparison.

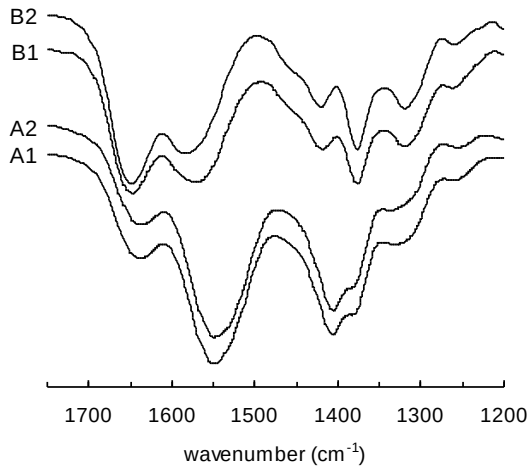

Figure 4.15: Details of the FTIR spectra of (**A**) non-neutralised films, A1 – plasticized chitosan film, A2 – plasticized chitosan/silica film; and (**B**) for neutralised films, B1 – plasticized chitosan film, B2 – plasticized chitosan/silica film.

The typical bands of amorphous silica have been identified as discussed in the Chapter 2. Chitosan spectra also showed typical vibration bands of the chitosan functional groups, related with the amino and acetyl groups, and of polysaccharides in general, i.e. the hydroxyl groups and the piranose ring [61, 62].

For the non-neutralised films, the FTIR spectra showed the typical absorption peaks at aprox. 1640 and 1550 cm^{-1}, assigned to the carbonyl stretching (amide I) and N–H bending (amide II and amine related in this case to the protonated amine group $-NH_3^+$) of the glucosamine unit, respectively.

As the starting chitosan had a degree of acetylation around 15%, both amide and amine moieties are present in the film. Therefore, the band at aprox. 1640 cm^{-1} may contain the amide I and the antisymmetric $-NH_3^+$ deformation, while the band at aprox. 1550 cm^{-1} will likely contain the amide II, N-H bending vibration as well as the symmetric $-NH_3^+$ deformation.

One can also observe the absorption peaks of the C-OH bound at 1060 cm^{-1} and 1025 cm^{-1} and those of the C-O-C at 1150 cm^{-1} (in glycosidic linkage) and of the C-O-C ~ 1075 cm^{-1} characteristic of the piranose ring. C-N stretching vibrations also occur in the 1190-920 cm^{-1} region and overlap the vibrations from the carbohydrate ring. N-H stretching occurs in the 3350-3200 cm^{-1} region overlapping the OH stretch (ν_{OH}) from the carbohydrate ring.

In the presence of silica, no changes were observed for these bands regarding either the peak wavenumber or the relative band areas. Moreover, as the amount of silica in the film is small compared to the biopolymer, and the characteristic bands of silica overlap with the bands of the polysaccharide, the vibrational bands characteristic of the silica could not be observed in the

spectra of the chitosan-silica composites. This is particularly true in the range between 870-1200 cm^{-1} where the high absorbance observed for the chitosan spectra masks the silica characteristic bands at 1050 cm^{-1} (Si-O-Si) and 950 cm^{-1} (Si-OH).

For the neutralised films, the frequency of both amide bands is shifted toward lower frequency values: amide I ($\nu_{C=O}$) ~ 1650 cm^{-1} and amide II (δ_{N-H}) ~ 1570 cm^{-1} (mainly related to the -NH_2 band). Also, decreasing the ionization degree of the amine groups led to a strong decrease in the absorbance ratio $A_{amide\ II}/A_{amide\ I}$. In addition, significant changes are also observed in the range 1350-1450 cm-1 which is considered to be conformation-sensitive for polysaccharides. The band around 1375 cm^{-1} has been assigned to the CH_3 symmetrical deformation and that around 1405-1420 cm^{-1} attributed to the CH_2 bending. Furthermore, the relative absorption assigned to the vibrational range of the –C–O–C– in the piranose ring and glycoside linkage clearly increases with neutralization.

Despite of the presence of silica nanoparticles, most of the typical chitosan absorption bands remained largely unchanged for the neutralised composite film (CHI+plasticizer+SiO_2). However, a small effect was observed in the amide vibrational range (Figure 4.15). The frequency of the vibrational band (δ_{N-H}) at ~ 1570 cm^{-1} is shifted toward a lower value around ~ 1585 cm^{-1}, most likely arising from hydrogen bonds between the surface hydroxyl groups of silica and the amine groups in chitosan molecules, which are now more feasible due to the lower ionization of the amine groups. Moreover the presence of silica caused a further decrease in the absorbance ratio $A_{amide\ II}/A_{amide\ I}$, also supporting this scenario. As expected, the region corresponding to the vibrational range of the –C–O–C– in the glycosidic linkage was not significantly affected by the presence of silica.

In conclusion, spectroscopic analysis did not reveal any significant physical crosslinking (e.g. via hydrogen bonding) between the biopolymer and the filler. The occurrence of hydrogen bonds between amino groups in chitosan and silanol groups of silica has been reported for hybrid materials prepared by a *in situ* sol-gel processes [9, 59] and has been proposed as the main responsible for the compatibility of the two components. For our systems, under low ionization conditions, hydrogen bonds may have been developed between the N-H groups of chitosan and the Si-OH groups on silica surface, but even so at a very low extension.

4.3.2.2.3. Morphological properties

Surface morphology of the plasticized chitosan films and the composite chitosan-silica films was studied by SEM and AFM in order to investigate the dispersion of the silica particles in the

chitosan matrix and/or the possible aggregation of the filler particles under the experimental conditions used. Figures 4.16 and 4.17 show the surface morphology of different composite films.

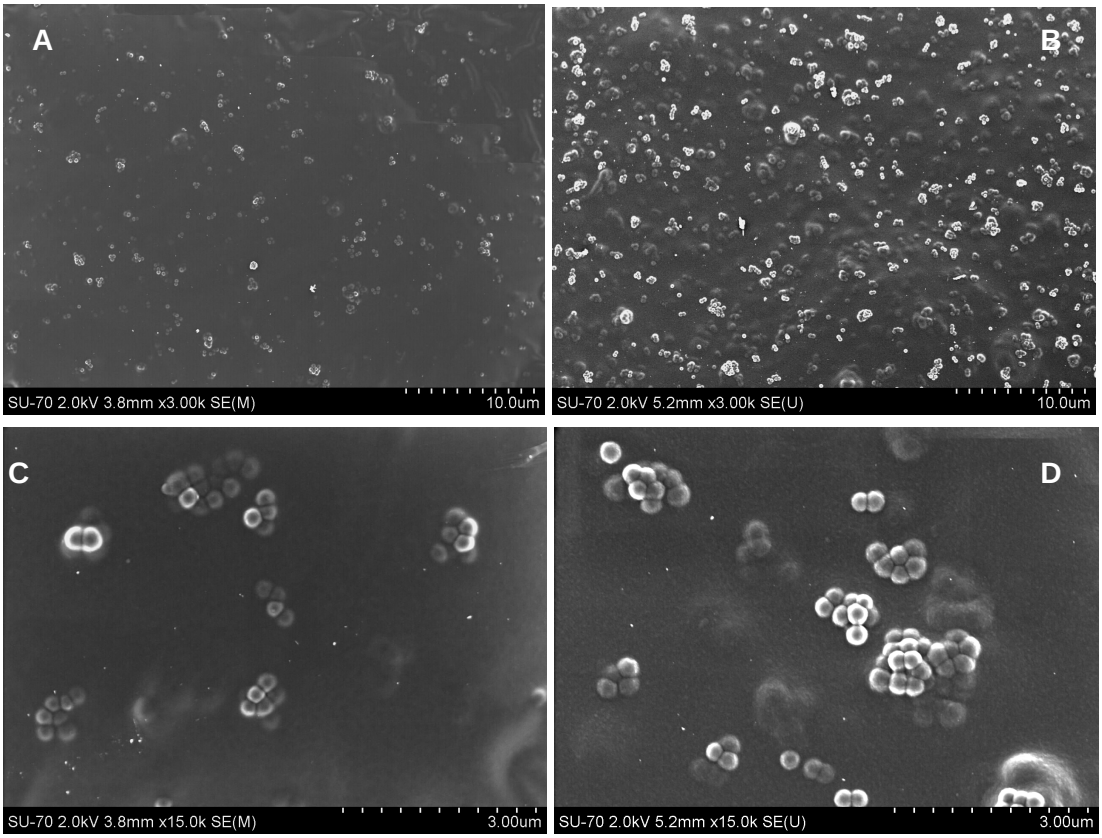

Figure 4.16: SEM micrographs of (**A,C**) non-neutralised plasticized chitosan composite films and (**B,D**) neutralised plasticized chitosan composite films.

Both microscopic approaches have revealed the poor silica dispersion into the chitosan matrix. Even in the absence of electrolytes, the low charge density of the silica particles under the pH conditions used to prepare the films is expected to induce particle flocculation. In addition, strong silanol interactions (Si-OH) between the silica particles are likely to occur, thus preventing the fine dispersion of the particles into the polymer matrix. In fact, as can be observed in Figure 2.13, most of the silica particles are dispersed in the chitosan matrix as aggregates, some of them as large as 1.5 μm.

The SEM images shown in Figure 4.16 reveal films with a grained appearance, where the bright spots represent the size and particle distribution of the silica aggregates. As it can be observed, the silica particles are far from being completely and uniformly dispersed in the continuous polymer matrix and the systems obtained are essentially phase separated microcomposites. One can observe large silica aggregates around 1.5 μm, smaller aggregates and even isolated silica particles.

Neutralization of the composite films did not lead to any significant changes of silica dispersion but clearly makes the aggregates more exposed at the surface of the film.

Due to the hydrophilic surfaces of the silica particles, good compatibility between the biopolymer and the filler could be expected, especially if significant intermolecular interactions were allowed to develop between the polymer and the filler. However, this was not the case for our silica-chitosan composite films, and at acidic pH and in absence of important polymer-filler interactions, aggregation of the low ionized silica particles is clearly favoured. In addition, as previously reported [396], nanosize silica particles can self-assemble into a well-ordered arrangement during solvent evaporation originating clusters of particles stabilized by attractive depletion and van der Waals forces, rather than well-dispersed primary particles, embedded in the polymer matrix.

The thickness of the films was in the 22-29 μm range and generally, for the same mass of polymer per unit area, the film thickness decreased upon neutralization of the film to 18-21 μm indicating that the membrane density increased due to the decrease of polymer ionization. This is due to the fact that after neutralization of the chitosan films the electrostatic repulsion between polymer chains are expected to decrease, causing some shrinkage of the polymer matrix. As a result, the silica particles were more exposed on the film surface as observed in Figure 4.16.

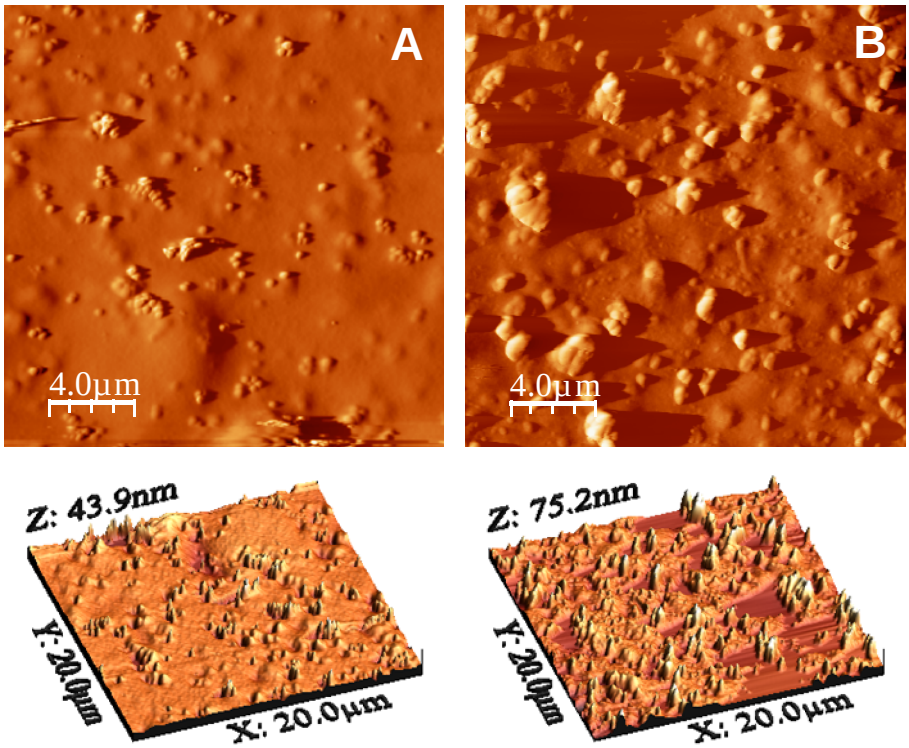

Figure 4.17: AFM micrographs showing surface topology of (**A**) non-neutralised plasticized chitosan composite films and (**B**) neutralised plasticized chitosan composite films.

Figure 4.17 shows the AFM images of the prepared plasticized chitosan-silica composite films. Besides revealing the presence of silica aggregates of different size in the polymeric matrix, the AFM analysis also revealed important differences on the surface topography between the non-neutralised and neutralised composite films as a function of the degree of ionization of the polymer. In the non-neutralised films (Figure 4.17A) the silica particles are essentially imbedded into the polymer matrix but in the neutralised films (Figure 4.17B) the silica particles are more exposed. In fact, the surface roughness increases considerably. These observations are in agreement with the SEM results.

4.3.2.2.4. Thermal stability

To assess the effect of the silica particles in the thermal stability of the composite films thermogravimetric analysis (TGA) of the different films was performed. Figure 4.18 shows the derivative thermogravimetric curves obtained for the chitosan films and chitosan loaded with 5% (relative to polymer weight) silica particles. All thermograms exhibit a similar decomposition pattern with a maximum at 309 ^{o}C. The first weight loss peak in the temperature range 50-100 ^{o}C is due to evaporation of the absorbed water. The residue at 900 ^{o}C confirmed the successful incorporation of the silica particles into the composite materials and allowed us to determine the actual silica content present in the composite films which was around 5 wt.% as theoretically predicted.

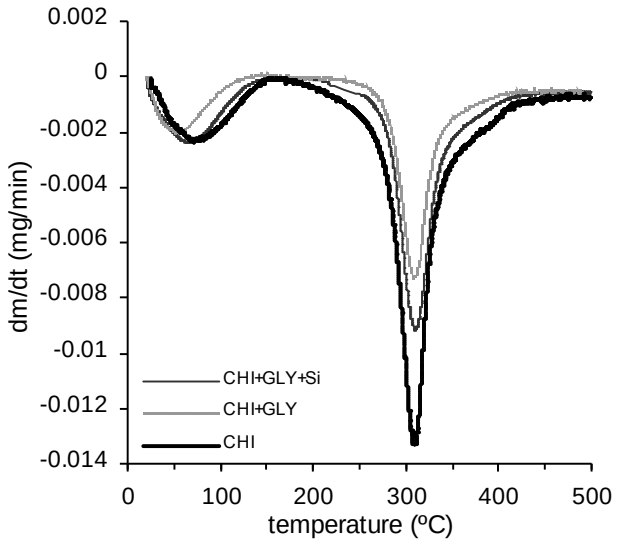

Figure 4.18: Thermal gravimetric analysis curves of chitosan films and chitosan loaded with 5 wt.% silica particles.

One frequently observed characteristic of nanocomposites is the thermal properties improvement often arising at very low filler content. In the area of synthetic polymer nanocomposites there are several examples concerning their increased thermal stability, namely for polymer-layered silicate nanocomposites [36, 397]. However, for the systems studied in this work, the incorporation of the inorganic phase does not seem to promote any significant effect on the thermal degradation of the material. This may also result from the poor interactions between SiO_2 and the matrix.

4.3.2.2.5. Water contact angle

Contact angle measurements of water droplets on the film surfaces were used to characterize the surface properties of plasticized chitosan films and chitosan-silica composites. Table 4.3 shows the results obtained for the water contact angle (WCA) measurements.

Table 4.3: Effect of silica on the water contact angle (WCA) of plasticized chitosan films (standard deviations given in parentheses).

Films	***Acid conditions***	***Neutralised films***
	WCA (º)	*WCA* (º)
CHI	100 (3) *x*	88 (2) *x*
CHI+GLY	106 (1) *y*	87 (3) *x*
CHI+GLY+5%Si	97 (3) *x*	92 (1) *y*

Different letters within a column indicate significant differences ($p < 0.05$)

For the non-neutralised films the presence of silica particles reduces slightly the WCA indicating that the presence of the filler may decrease the surface hydrophobicity of the composite chitosan films. The natural hydrophilicity of the silica particles associated to the more open polymer network in the case of the non-neutralised films allows a more pronounced space-filling effect which might explain this behaviour. Contrarily, for the neutralised films, a slight increase in WCA was observed.

For the non-neutralised films, the presence of glycerol as plasticizer increases the WCA of the films. Despite its hydrophilic nature the glycerol increases the surface hydrophobicity of the non-neutralised chitosan film. Yet, as mentioned in § 4.3.1, due to the low MW of GLY it may be able to penetrate deeper in the polymer matrix and the polysaccharide moieties exposed to the surface are then more hydrophobic. No significant effects were observed for the plasticizer regarding the surface hydrophobicity of the neutralised films.

Other authors however have shown that the addition of plasticizers (GLY, PEG, etc.) reduces the water contact angle of chitosan films [361]. In fact, the plasticizer effect is complex and different results can be obtained depending on the plasticizer amount, size and possible interaction with the polymer matrix. Moreover, the mechanism associated with the observed plasticizer effect on the surface hydrophobicity has been related with the hygroscopicity (the water binding capacity) of the plasticizer [361] and with a preferred orientation of hydrophobic moieties at the film-air interface in the case of protein-based films [398, 399]. However, in the case of chitosan, the origin of this effect is still unclear.

4.3.2.2.6. Water vapour permeability

The water vapour permeability values measured for the chitosan, plasticized CHI and chitosan-silica composite films are also shown in Table 4.4. In general, the neutralised films showed higher WVP values in comparison with the non-neutralised films.

Table 4.4: Effect of silica on the water vapour permeability (WVP) of plasticized chitosan films (standard deviations given in parentheses).

Films	***Acid conditions***	***Neutralised films***
	WVP (mm g/h kPa m^2)	*WVP* (mm g/h kPa m^2)
CHI	0.27 (0.02) *x*	0.47 (0.03) *x*
CHI+GLY	0.27 (0.01) *x*	0.53 (0.06) *y*
CHI+GLY+5%Si	0.34 (0.04) *y*	0.42 (0.02) *x*

Different letters within a column indicate significant differences ($p < 0.05$)

For the non-neutralised films the presence of silica particles slightly increased the WVP of films probably associated with the increase of the surface hydrophilicity of the composite chitosan films. These effects are in fact prevalent to the increased tortuosity of the path.

Contrarily, for the neutralised films, the presence of the silica particles decreases the WVP. Similar behaviour was observed for other chitosan-silica nanocomposites. The decrease in WVP of nanocomposite films has been attributed to the presence of ordered dispersed nanoparticle layers with large aspect ratios in the polymer matrix, which would force the water vapour to travel through the film by more tortuous paths thereby increasing the effective path length for diffusion [36, 353]. It has been shown that the reduction in relative permeability of hybrid chitosan-silica

films is more pronounced in the case of fully exfoliated rather long layered silicates. Once again, the high aspect ratio associated with important polymer-filler interactions seems to be determinant for the observed effects of the filler on the film properties. In our case, despite the worse particle dispersion within the polymer matrix and the lower aspect ratio of the individual spherical silica particles, the silica aggregates may play a similar role.

In addition, one can expect that the silica particle aggregates have a more important effect on the chitosan chain organization within the film. As discussed earlier, after neutralization the polymer charge density is lower, allowing more pronounced intermolecular interactions between the polymer chains, which explain the increase in membrane density and probably the lower free volume in the polymer matrix. Hence, the reduction of WVP may also be related to a rigidified polymer region around the inorganic filler, which would be more important for the neutralised films due to the lower free volume cavity within the film. Similar effects have been described to explain the reduced permeability of polymer-inorganic composites [400].

4.3.3. CHI/SiO_2 films prepared by procedure 2

In view of the results obtained which clearly evidenced the significant aggregation of silica particle, another strategy was followed to prepare CHI/SiO_2 composite films. As it is well known that due to the high surface energy of inorganic nanoparticles, their colloidal stability is reduced and they tend to self-aggregate, in this new procedure silica particles were first dispersed in the plasticizer (GLY) and this suspension was then mixed with the chitosan solution. Using this approach, GLY would have a dual role, i.e., of plasticizer and of stabilizer of the colloidal SiO_2 nanoparticles. In fact, Gulley *et al*. [401] have studied the stability of silica suspension (AD = 8 nm) using a homologous series of polyols, that varied in the number of carbons in the linear chain and the number of hydroxyl groups. They showed that small polyols are surprisingly effective at reducing the rate of aggregation of colloidal silica at high pH and salt concentration. From this study it was shown that the silica stabilization depends on the number of hydroxyl groups of the polyols indicating that hydrophilicity is the dominant characteristic that determines stabilizing effectiveness. These hydroxyl groups apparently interact with silanol groups on the cluster surface and alter the interactions between colloidal silica particles.

As discussed in section § 4.3.2 chitosan composite films were prepared using different SiO_2 contents (1, 5 and 10 wt.%) and GLY (15 wt.%). However, contrarily to the Procedure 1, the SiO_2 particles were previously mixed with GLY before being added to CHI matrix. This new procedure was named as Procedure 2. Mechanical, structural, morphological, barrier and surface properties of

these films were analysed in order to evaluate the effect of less aggregated silica particles on the chitosan matrix.

4.3.3.1. Tensile properties

Tensile parameters (Young's modulus, (E), tensile strength at break (σ_b), and elongation percent at break, (ε_b) were measured for the plasticized chitosan films and for chitosan composite films loaded with 1, 5 and 10 wt.% of silica under acidic conditions and after neutralization in order to evaluate the silica effect on the mechanical properties of the chitosan films. The results obtained are summarized in the Table 4.5.

Table 4.5: Effect of silica on the mechanical properties of pristine and composite chitosan films: Young's modulus (E), tensile strength at break (σ_b) and percentage elongation at break (ε_b) (standard deviations given in parentheses).

Films	***Acid conditions***			***Neutralised films***		
	E (MPa)	σ_b (MPa)	ε_b (%)	*E* (MPa)	σ_b (MPa)	ε_b (%)
CHI	28 (1) *x*	50 (3) *x*	8 (2) *x*	39 (1) *x*	68 (4) *x*	8 (2) *x*
CHI+GLY	27 (1) *x*	49 (5) *x*	14 (2) *x*	34 (2) *x*	60 (4) *x*	11 (3) *x*
CHI+GLY+Si1%	10 (1) *y*	53 (3) *x*	49 (6) *y*	-	-	-
CHI+GLY+Si5%	15(1) *z*	47 (2) *y*	42 (2) *y*	42 (2) *y*	68 (3) *x*	12 (4) *x*
CHI+GLY+Si10%	27(1) *x*	43 (2) *z*	27 (3) *z*	-	-	-

Different letters within a column indicate significant differences ($p < 0.05$)

The results shown in the Table 4.5 for non-neutralised composite films show that the Young's modulus decreased at low silica content (1 and 5 wt. %) and equalled that of chitosan only when 10 wt.% silica was used.

Initially these values when compared with those obtained for films prepared using Procedure 1 suggest that the mixing sequence during film preparation might be the main reason for these differences. However, the drying procedure [365, 368] and level of humidity proved to be critical, since the presence of water is acting as a plasticizer in the films [250, 364]. To get a better understanding of this effect, chitosan films with and without silica have been dried under distinct conditions and finally analysed by DMA. One set of films was dried under standard conditions and the other set was dried in the DMA oven up to 120 ^oC for 1 hour in order to remove H_2O

completely. The storage modulus (E') was plotted as a function of frequency and the results are shown in Figure 4.19.

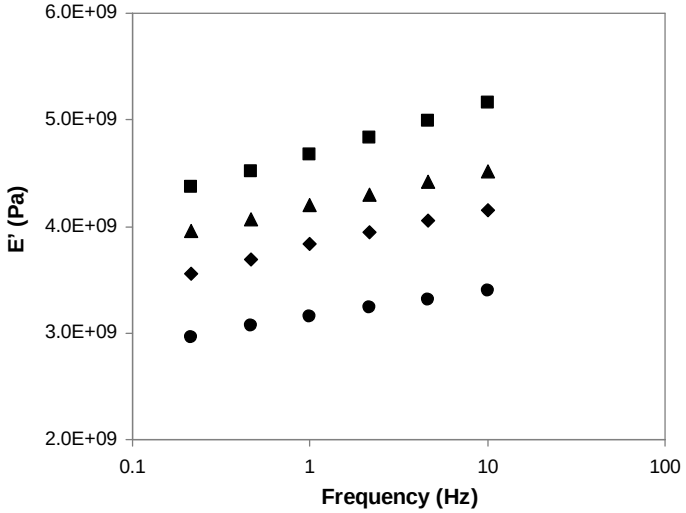

Figure 4.19: Storage modulus of non-neutralised plasticized films as function of frequency: (♦) CHI and (●) CHI/SiO_2 films standard and (▲) CHI and (■) CHI/SiO_2 films fully dry. The amount of silica particles into chitosan matrix was 5 wt.%.

As it can be observed the presence of water leads to completely distinct results. The storage moduli of the fully dry films were higher than those of films dried under standard conditions. Moreover, for fully dry conditions the composite chitosan film presented higher E' than that obtained for chitosan film. Effectively, the presence of water molecules is altering the properties of chitosan films. Despite of this observation, potential application as packaging material of this type of film require the use of standard drying conditions due to the hygroscopic nature of polysaccharides. Therefore the subsequent characterization analyses were carried out under standard conditions. In conclusion, for non-neutralised films the reduction of E is clearly associated with the plasticizing effect of water.

As regards to the percentage of elongation and tensile strength at break of non-neutralised CHI/silica films a decrease of these properties was identified with increasing silica loading. As the Young modulus is a measure of a material's ability to resist deformation upon a force, the higher the modulus, the less the film would deform upon a force [389]. On the other hand, since the non-neutralised composite films with gradual increase of silica load contents become more rigid and more brittle they require lower energy for fracture, which is in accordance with tensile strength results shown in the Table 4.5.

For neutralised films, tensile assays were only carried out for plasticized chitosan/silica film loaded with 5 wt.% of silica particles, as it proved the best loading percentage. Both Young's modulus and

tensile strength increased in comparison to plasticized chitosan film while the elongation remained constant. These results proved that using this new procedure allows silica particles to enhance the mechanical properties of the films. In this case they are acting as a real mechanical reinforcement. As silica particles can be better dispersed in the bulk film, the rigidified chitosan region around the silica probably is augmented and consequently reinforcement is achieved. On the other hand, after neutralization the films present a lower free volume due to more pronounced intermolecular interactions between the polymer chains and possibly less space for free water molecules do adsorb.

4.3.3.2. Spectroscopic analysis (FTIR-ATR)

FTIR analyses of chitosan/silica films prepared by Procedure 2 were carried out to assess the occurrence of any interactions between the polymer matrix and the filler previously mixed with GLY. Moreover, any possible structural changes caused by film neutralization were also analysed.

The most significant regions of the FTIR spectra of chitosan composites films in acidic conditions and after neutralization are depicted in Figure 4.20. For comparison purposes the data obtained for pristine plasticized chitosan films under both conditions are also shown. The region from 1800 to 1200 cm^{-1} is shown in detail as several absorption bands in this region are influenced by intermolecular interactions, namely hydrogen bonding.

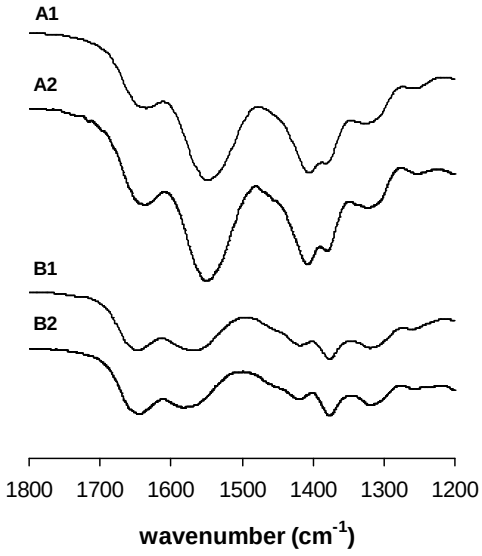

Figure 4.20: Details of the FTIR-ATR spectra of (**A**) non-neutralised films, A1 – plasticized CHI film, A2 – plasticized CHI/silica film; and (**B**) for neutralised films, B1 – plasticized CHI film, B2 – plasticized CHI/silica film. The amount of silica particles into chitosan matrix was 5% wt.

As can be observed the spectra shown in Figure 4.20 are very similar to those obtained for the films prepared by Procedure 1. Neutralised CHI/silica films presented both amide bands shifted toward lower frequency values when compared to non-neutralised composites films. As expected upon neutralization the ionization degree of the amine groups was decreased leading to a decrease in the absorbance ratio $A_{amide\ II}/A_{amide\ I}$. Furthermore, increasing amounts of silica in the composite films still did not show the vibrational bands characteristic of the silica. In summary the principal conclusions achieved for plasticized CHI/silica films prepared by Procedure 1 apply to composites films obtained by Procedure 2.

4.3.3.3. Morphological properties

Although these silica particles suspensions dispersed with GLY in CH_3COOH medium at pH 3 have shown by DLS an evident decrease in the aggregates dimension before being added to the polymer matrix, the same was not observed in the plasticized chitosan composite films. This fact is illustrated by SEM images in Figure 4.21.

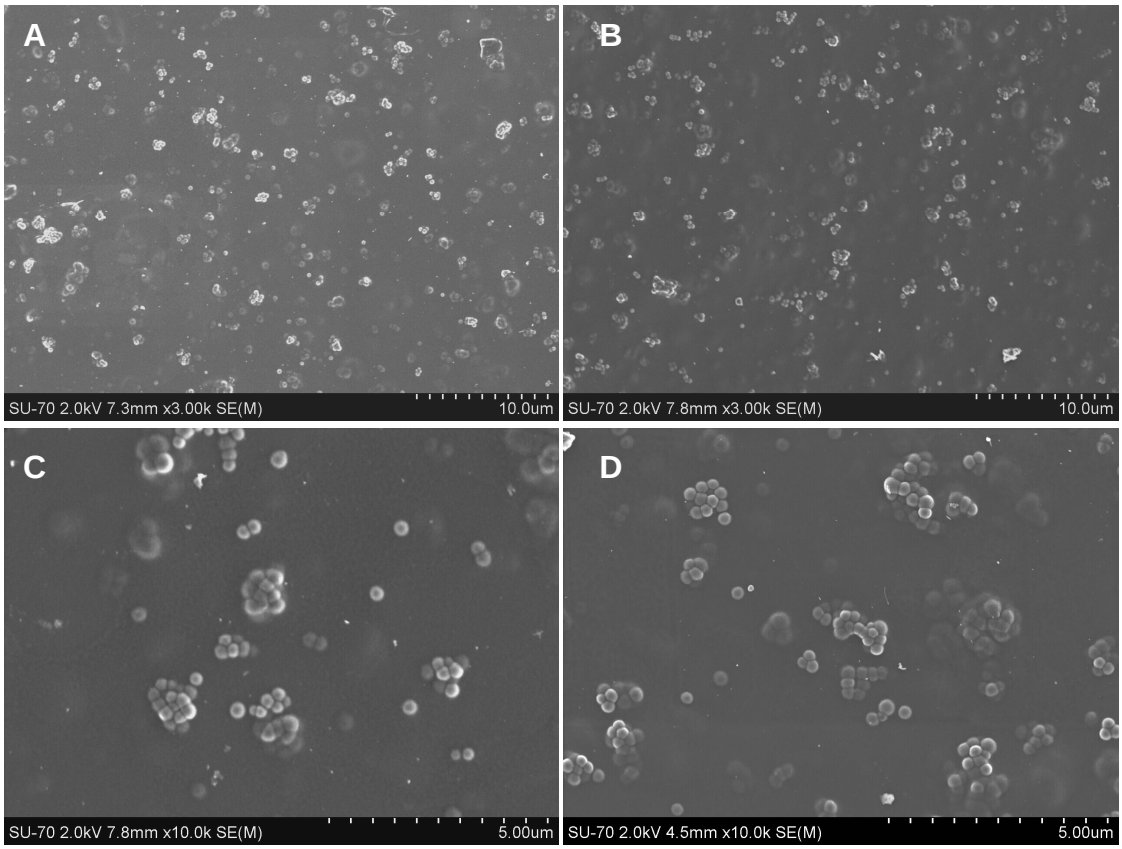

Figure 4.21: SEM micrographs of (**A, C**) non-neutralised plasticized chitosan composite films and (**B, D**) neutralised plasticized chitosan composite films obtained by Procedure 2. The amount of silica particles into chitosan matrix was 5 wt. %

Similarly to the plasticized chitosan composite films prepared by Procedure 1 (Figure 4.16), the films prepared via Procedure 2 also showed a grained appearance with large aggregates imbedded into the polymer matrix or exposed at the films surfaces. From Figure 4.21, the presence of more isolated silica particles is observed than in the films previously obtained; nevertheless, small and large aggregates are still observed. Neutralization of these composite films did not bring important differences to their surface morphology but the thickness of the films was reduced from 20 to 17 μm after neutralization. In general, the thickness of composite films obtained by Procedure 2 was smaller than those prepared by Procedure 1. This fact may be related with the way in which the silica particles were packed in the chitosan matrix and hypothetically with a lower degree of shrinkage of the polymer matrix upon neutralization, meaning that particles should be more imbedded in chitosan matrix and less exposed on the surface as a result of a reduction of electrostatic repulsion. These principal considerations were also observed in the other neutralised composite films prepared with higher amounts of silica particles. In view of these results no further morphological characterization by AFM was carried out.

The transparency of the films was also analysed. Figure 4.22 shows the images of non-neutralised and neutralised plasticized chitosan composite films.

Figure 4.22: Images of (**A**) non-neutralised and (**B**) neutralised plasticized CHI/silica films obtained by procedure 2. The amount of silica particles into chitosan matrix was 5 wt. %.

Based on a visual comparison shown in Figure 4.22, there are no significant differences between plasticized CHI/silica films before and after neutralization. Moreover, the transparency of the composite films prepared following this new procedure is similar to that of the films prepared using Procedure 1 (Figure 4.13).

4.3.3.4. Water contact angle and Water vapour permeability

The surface and barrier properties of the CHI/SiO_2 composite films prepared by Procedure 2 were evaluated through water contact angle measurements and water vapour permeability values. Table 4.6 summarizes the results obtained.

Table 4.6: Effects of the silica particles on the water contact angle (WCA) and water vapour permeability (WVP) of CHI, plasticized CHI and chitosan composite films (standard deviations given in parentheses).

Films	***Acid conditions***		***Neutralised films***	
	WCA (º)	***WVP*** (mm g/h kPa m^2)	***WCA*** (º)	***WVP*** (mm g/h kPa m^2)
CHI	100 (3) *x*	0.27 (0.02) *x*	88 (2) *x*	0.47 (0.03) *x*
CHI+GLY	106 (1) *x*	0.27 (0.01) *x*	87 (3) *x*	0.53 (0.06) *x*
CHI+GLY+Si1%	107(1) *x*	0.24 (0.01) *y*	102 (5) *y*	0.40 (0.01) y
CHI+GLY+Si5%	116 (2) *y*	0.29 (0.01) *x*	101 (1) *y*	0.43 (0.01) *z*
CHI+GLY+Si10%	117 (1) *y*	0.32 (0.02) *z*	104 (1) *y*	0.53 (0.01) *x*

Different letters within a column indicate significant differences ($p < 0.05$)

For the non-neutralised films, the presence of silica slightly increased its WCA indicating an increase of its surface hydrophobicity. In general, this effect tended to be more pronounced for higher amounts of silica particles. These results are distinct to that CHI/5 wt.% SiO_2 film prepared by Procedure 1. As mentioned before the natural hidrophilicity of the silica particles coupled with the addition of plasticizer should result in decreasing hydrophobicity of the chitosan composite films. One possible explanation for this increase of surface hydrophobicity can be related with the procedure followed in the preparation of the films. Probably the complex set of interactions between the functional groups from GLY, SiO_2 particles and CHI via hydrogen bonds may lead to a reduction of hydrophilicity. In fact this is already noted for the non-neutralised CHI/GLY film which presents a slightly higher hydrophobicity than the CHI films derived from the interactions between their functional groups.

For neutralised films, increasing the concentration of SiO_2 also led to an increase of WCA in comparison to plasticized CHI. However, comparatively to the non-neutralised composite films these values were lower. This result may be due to the fact that upon neutralization the silica particles may have migrated to the surface and/or some surface porosity may have developed as a result of removal of fillers during neutralization steps.

Relatively to water vapour permeability values measured for non-neutralised and neutralised plasticized CHI/silica films shown also in the Table 4.6, a similar behaviour is observed to that of films prepared by the original Procedure 1 (Table 4.4)

For non-neutralised plasticized CHI/silica films a positive effect of the silica on their barrier properties is observed for composite films with 1 wt.% SiO_2. For neutralised films this good effect on the their barrier properties was observed up to filler content of 5 wt.%. Once again, as previously mentioned, silica particle distribution plays an important role on the chitosan chain organization within the film. The better size distribution of these particles in both systems allows a better dispersion of nanoparticles at low SiO_2 concentration in the chitosan matrix, which difficults the passage of water vapour through the films. This behaviour is more pronounced for neutralised films since the intermolecular interactions between the polymer chains at lower ionization are augmented. However for higher silica contents, percolation effects seem to facilitate the vapour path thus increasing the WVP of the system.

4.3.4. CHI/SiO_2@APS films prepared by procedure 2

In view of the promising results obtained using Procedure 2, but still limited, silica particles were modified with an amino siloxane coupling ligant, the 3-aminopropyltriethoxysilane (APS). The applied coating alters the charge, functionality and reactivity of the surface and can enhance stability and dispersability of particles. Therefore, interfacial interactions between the inorganic nanoparticles and the organic matrix can be improved. In fact, filler surface silanization is the method commonly used for enhancing filler dispersion in organic phases and is a way to reduce agglomeration and to promote compatibility and bonding with the matrix [402]. In our study, besides the covering of the silica particles with APS, these particles were still mixed with GLY (15 wt.%) and re-dispersed in acetic acid (CH_3COOH) prior to mixing with the chitosan solution. The complete characterization of these particles is shown in the Chapter 2. Even in the presence of CH_3COOH (used as solvent in the preparation of the films), silica@APS kept an excellent size distribution and no aggregates were detected as shown in Figure 2.13.

Composite chitosan films were prepared using different SiO_2@APS contents (1, 5 and 10 wt.%). The films under acidic conditions and after neutralization had their mechanical, surface, thermal, structural and morphological properties studied in order to analyse the effect of well-dispersed SiO_2@APS particles in the chitosan matrix.

4.3.4.1. Tensile properties

In order to evaluate the SiO_2@APS effect on the mechanical properties of the chitosan films and composite films, tensile parameters (Young's modulus, tensile strength at break, and elongation percent at break) were measured. The plasticized composite films were loaded with 1, 5 and 10 wt.% of SiO_2@APS. These measurements were carried out under acidic conditions and after film neutralization and the results are shown in Table 4.7.

Table 4.7: Effect of the SiO_2@APS on the mechanical properties of CHI, plasticized composite chitosan films: Young's modulus (E), stress at break (σ_b) and percentage elongation at break (ε_b) (standard deviations given in parentheses).

Films	***Acid conditions***			***Neutralised films***		
	E (MPa)	σ_b (Mpa)	ε_b (%)	*E* (Mpa)	σ_b (Mpa)	ε_b (%)
CHI	28 (1) *x*	50 (3) *x*	8 (2) *x*	39 (1) *x*	68 (4) *x*	8 (2) *x*
CHI+GLY	27 (1) *x*	49 (5) *x*	14 (2) *x*	34 (2) *x*	60 (4) *x*	11 (3) *x*
CHI+GLY+SiAPS1%	21 (1) *y*	34 (2) *y*	7 (1) *y*	41 (3) *y*	66 (7) *x*	4 (1) *y*
CHI+GLY+SiAPS5%	18 (1) *v*	29 (1) *z*	13 (4) *x*	42 (2) *y*	75 (6) *y*	6 (2) *yz*
CHI+GLY+SiAPS10%	20 (1) *y*	31 (1) *yz*	12 (3) *x*	45 (2) *z*	81 (7) *y*	7 (2) *z*

Different letters within a column indicate significant differences ($p < 0.05$)

In general, for non-neutralised plasticized composite films the presence of SiO_2@APS decreased all tensile parameters. The absence of significant reinforcement effects can be related essentially with the presence of water molecules adsorbed on SiO_2@APS particles. These particles as well as GLY are indeed highly hygroscopic compounds and they tend to capture more easily water molecules. More than the classical plasticizing effect of water and glycerol previously reported, it would be also interesting to know what their real impact is on the diffusion process of another compound incorporated in the polymer network as the case of the presence of SiO_2@APS in chitosan matrix.

Dynamic mechanical analysis (DMA) was once again used to verify the water plasticization effect on the mechanical properties of the non-neutralised composites films. As done for composite films prepared by Procedure 2 (§ 4.3.3), the storage modulus, *E´* of the chitosan films with and without silica was measured by DMA. For this, two distinct conditions of drying were tested. One set of films was dried under standard conditions and the other set was dried in the DMA oven up to

120°C for 1 hour in order to remove H_2O completely. The storage modulus, *E'* was plotted as a function of frequency and the results are shown in Figure 4.23.

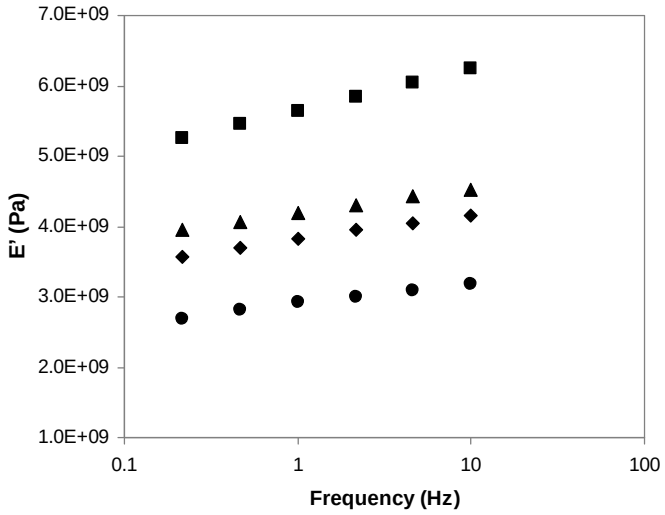

Figure 4.23: Storage modulus of non-neutralised plasticized films as function of frequency: (♦) CHI and (●) CHI/SiO_2@APS films standard and (▲) CHI and (■) CHI/SiO_2@APS films fully dry. The amount of SiO_2@APS particles into chitosan matrix was 5% wt.

The storage modulus observed in the Figure 4.23 for CHI/SiO_2@APS film upon full water removal is significantly higher than that obtained for composite film standard and for CHI/SiO_2 film shown in Figure 4.19. From this result it is possible to affirm that water molecules are masking the mechanical properties of the non-neutralised composite films. In fact, the presence of SiO_2@APS in the dry CHI composite films improved its mechanical properties in comparison with the dry CHI/SiO_2 film shown in Figure 4.19.

Despite of the presence of water, for neutralised plasticized CHI/SiO_2@APS films the presence of progressive SiO_2@APS loading within chitosan matrix increased the Young's modulus and tensile strength parameters and decreased the elongation at break of the composites films (Table 4.7). These results are even more significant than those obtained for neutralised plasticized CHI/SiO_2 films prepared by Procedure 2. Neutralised films are stiffer and show excellent mechanical properties.

4.3.4.2. Spectroscopic analysis (FTIR-ATR)

FTIR spectra of non-neutralised and neutralised plasticized chitosan/SiO_2@APS are shown in the Figure 4.24.

Although the FTIR analysis has provided evidence of successful silica surface modification with APS as discussed in Chapter 2, no changes were observed for SiO_2@APS characteristic bands when added to the chitosan matrix regarding either the peak wavenumber or the relative band areas. Once again, the characteristic filler bands were overlapped with bands of the chitosan as a result of the small content of SiO_2@APS in chitosan films comparatively to polysaccharide amount.

For neutralised films, the behaviour was also similar to previous FTIR analyses made for CHI/SiO_2 films prepared by Procedures 1 and 2. The presence of SiO_2@APS seems to change the frequency of the amide II vibrational band (δ_{N-H}) at 1570 cm^{-1} to a lower value around ~ 1585 cm^{-1}. Moreover, an additional decrease in the absorbance ratio $A_{amide\ II}/A_{amide\ I}$ was also noticed as a result of the presence of filler.

Even increasing silica@APS concentration (up 10 wt.%), most of the typical chitosan absorption bands remained essentially unchanged for neutralised and non neutralised composite films indicating the absence of hydrogen bonding between compounds involved or at least at very low extension as in the case of neutralised composite films.

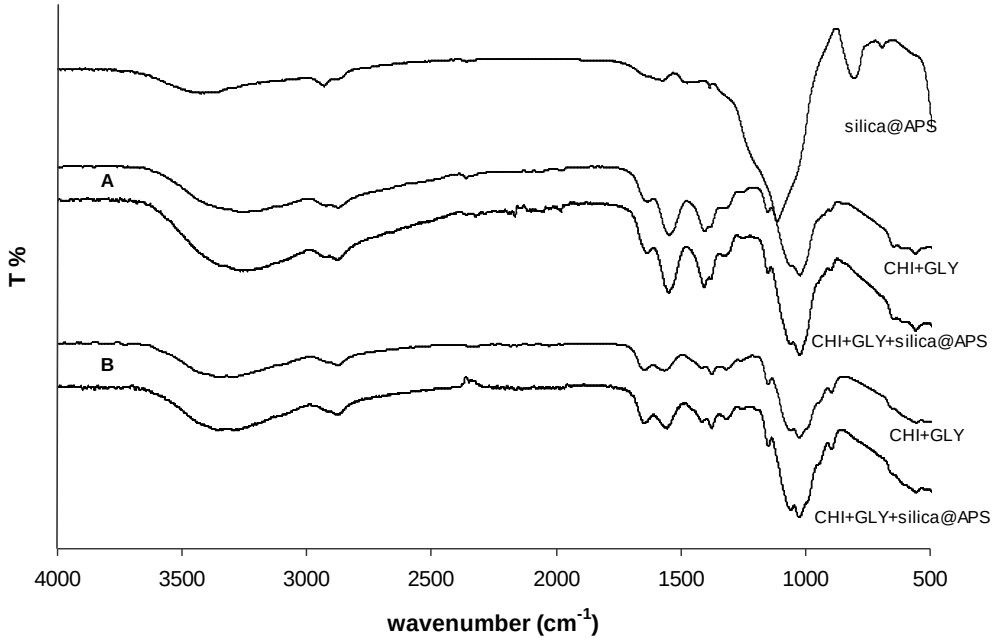

Figure 4.24: FTIR spectra for SiO_2@APS, plasticized chitosan and composite CHI/SiO_2@APS films: (A) Non-neutralised films; (B) Neutralised films. Spectra have been normalised at 2923 cm^{-1} (C-H band) for better comparison. The amount of SiO_2@APS particles into chitosan matrix was 5 wt.%.

4.3.4.3. Morphological properties

As described in the Chapter 2, the surface modification of silica particles with APS as well as the addition of GLY assured a good size distribution of these particles in acetic acid medium in a wide

range of pH. Although the silica@APS particles have been well disperse before and after mixture with chitosan matrix, with AD = 265 and 365 nm, respectively, it is necessary to observe if these particles maintain this good dispersion after drying of the composite films.

To further confirm the aforementioned observations, micrographs were taken by SEM on the surface and of a cross section of the plasticized chitosan/SiO_2@APS films (Figure 4.25).

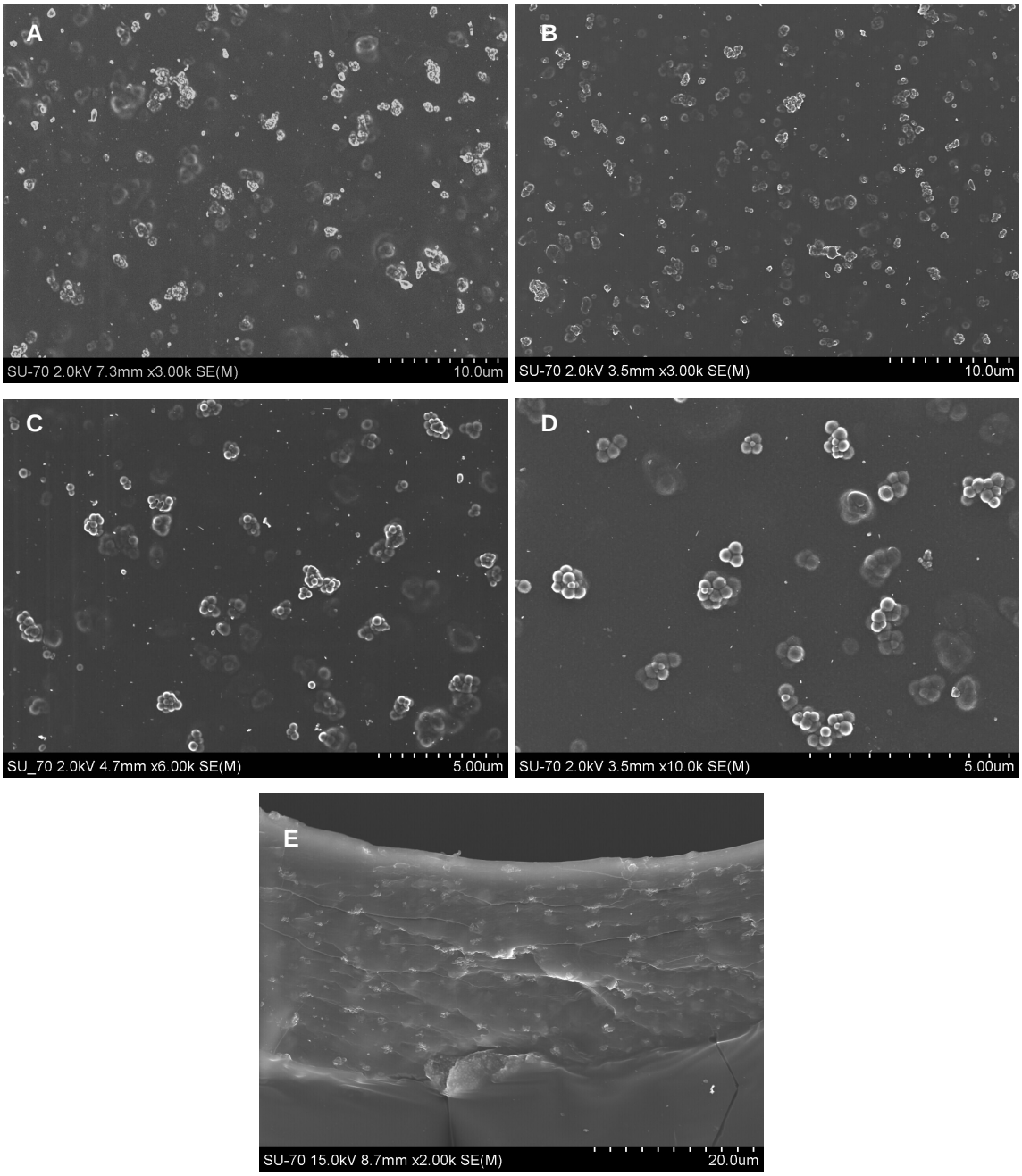

Figure 4.25: SEM micrographs of (**A, C**) non-neutralised plasticized chitosan composite films and (**B, D, E**) neutralised plasticized chitosan composite films obtained by Procedure 2. The amount of SiO_2@APS particles into chitosan matrix was 5% wt.

SEM images have revealed the poor SiO_2@APS dispersability on the surface of chitosan film in spite of the good size distribution of these particles in CH_3COOH medium or even when mixed with chitosan suspension.

Basically, no clear differences were found between the micrographs observed in Figure 4.25 and those presented in Figures 4.16 and 4.21 for plasticized CHI/silica films prepared by Procedures 1 and 2. Large aggregates and films with a grained appearance once again were observed in the SEM images. Increasing the SiO_2@APS concentration in chitosan matrix leads to an increase of the effects (not shown). Neutralization of the composite films did not bring any significant changes of silica@APS dispersion but, as expected, the thickness of the films was visibly decreased. On the other hand, the cross section of the neutralised CHI/SiO_2@APS film illustrated in Figure 4.25E showed that in spite of the poor particle size distribution, the aggregates are reasonably dispersed in the continuous polymer matrix with some organization similar to small islands.

SiO_2@APS in the chitosan solution seem be completely stable and uniformly dispersed. Therefore, the origin of the aggregation process in the composite film is still not entirely clear, but one possible explanation for this effect can be associated with the film drying process and the presence of free water molecules. According to the literature [339, 368] during the drying process, the water molecules are constantly eliminated. The elimination of the water molecules during the process creates a fluid drag which causes the particles to come closer to each other favouring their aggregation to reach greater stability [368].

Even chitosan also has its functional characteristics modified depending on the different drying conditions. Srinivasa *et al*. [339] prepared chitosan-based packaging films employing wet casting followed by different drying processes. The film properties were compared with those prepared under ambient temperature drying (27~ ^oC). They verified that infrared drying (ID) seems to be faster and superior in preserving desirable functional characteristics of chitosan films. In comparison with other drying process, chitosan films dried by ID process presented the lower water vapour permeability and oxygen transmission rate, important properties to the versatile use of these films in modified atmosphere packaging of fruits and vegetables [374].

The transparency of the non-neutralised and neutralised plasticized CHI/SiO_2@APS films is illustrated in the Figure 4.26. Visually the image obtained for plasticized composite film before neutralization (Figure 4.26A) seems to be slightly more transparent than that observed for the film after neutralization (Figure 4.26B). Taking into account the better size distribution of SiO_2@APS within chitosan matrix, it is still unclear the absence of transparency of these composite films.

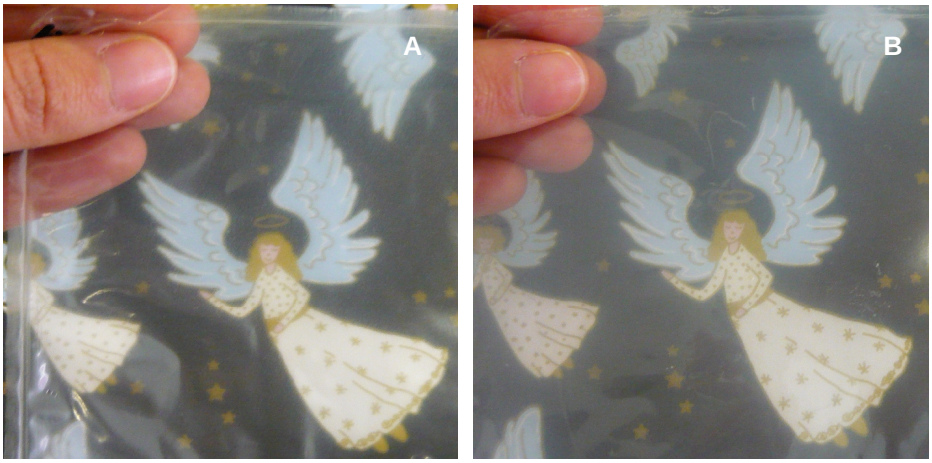

Figure 4.26: Images of (**A**) non-neutralised and (**B**) neutralised plasticized CHI/SiO_2@APS films.

4.3.4.4. Thermal stability

The thermal stability of the non-neutralised and neutralised plasticized CHI/SiO_2@APS films was studied by thermogravimetric analysis (TGA). Figure 4.27 shows the differential thermogravimetric curves obtained for composite films loaded with 5 wt.% of SiO_2@APS.

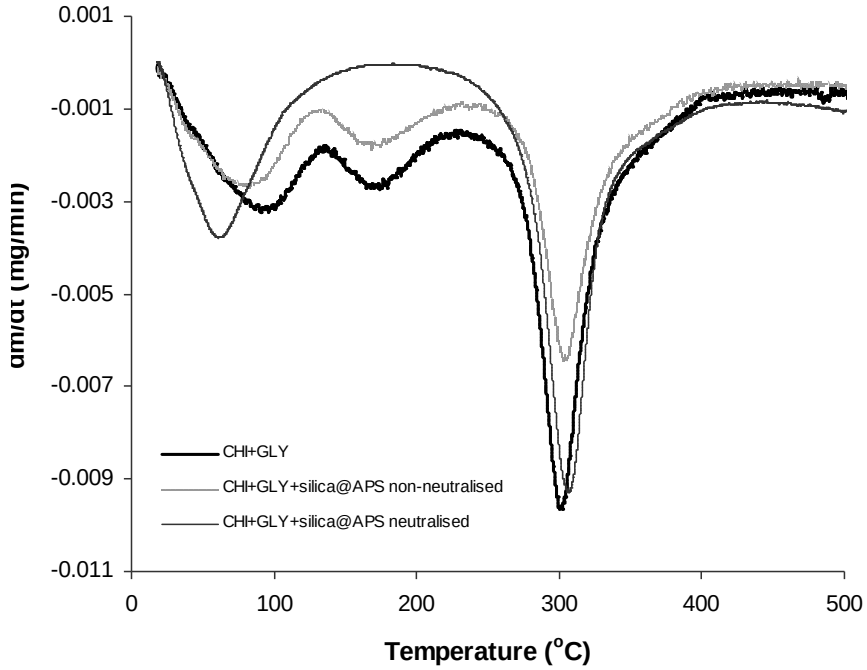

Figure 4.27: Thermal gravimetric analysis curves of plasticized CHI and CHI/ SiO_2@APS composite films.

As can be seen in Figure 4.27, the neutralised and non-neutralised plasticized chitosan and plasticized CHI/SiO_2@APS films show different well-distinguished steps of degradation. For non-

neutralised films three steps of degradation are observed while for neutralised films only two degradation steps are detected.

The first step recorded in the temperature range 60 - 100 ^oC is approximately similar for all films and corresponds to the evaporation of physisorbed water. The second step observed only for non-neutralised films is recorded in the temperature range 130 - 220 ^oC and can be associated to the loss of the remain water inside the films. This step was not detected for the neutralised composite film. The non-neutralised films can adsorb more water due to their higher ionization degree and higher hydrophilicity. The last peak in the temperature range 260–340 ^oC was similar for all films illustrated in Figure 4.27. This peak corresponds to the decomposition temperature of chitosan. For the non-neutralised CHI/SiO_2@APS film with 5 wt.% of SiO_2@APS, the maximum decomposition temperature (306 ^oC) was slightly higher than the neutralised plasticized CHI film (304 ^oC). For neutralised CHI/SiO_2@APS film the decomposition temperature was around 310 ^oC. This is an indication that in both situations, i.e., low and high ionization of the composited films, the addition of SiO_2@APS particles promotes chitosan stabilization against thermal degradation. This is probably because of the shielding effect of the silica@APS particles [378], which allows better interaction between the polymeric matrix and the fillers.

4.3.4.5. Water contact angle and Water vapour permeability

Water contact angle measurements (WCA) on plasticized CHI/SiO_2@APS surface films and their water vapour permeability (WVP) values are summarized in Table 4.8.

Table 4.8: Effect of modified silica particles on water contact angle (WCA) and water vapour permeability (WVP) of CHI, plasticized CHI and CHI composite films (standard deviations given in parentheses).

Films	***Acid conditions***		***Neutralised films***	
	WCA (º)	***WVP*** (mm g/h kPa m^2)	***WCA*** (º)	***WVP*** (mm g/h kPa m^2)
CHI	100 (3) *x*	0.27 (0.02) *x*	88 (2) *x*	0.47 (0.03) *x*
CHI+GLY	106 (1) *x*	0.27 (0.01) *x*	87 (3) *x*	0.53 (0.06) y
CHI+GLY+SiAPS1%	108 (1) *x*	0.16 (0.004) *y*	92 (1) *y*	0.42 (0.001) *x*
CHI+GLY+SiAPS5%	118 (1) *y*	0.17 (0.01) *y*	96 (1) y	0.44 (0.003) *x*
CHI+GLY+SiAPS10%	118 (1) *y*	0.23 (0.01) *z*	87(3) *x*	0.60 (0.04) *y*

Different letters within a column indicate significant differences ($p < 0.05$)

The presence of SiO_2@APS did not lead to significant difference in WCA results for non-neutralised chitosan films in comparison to those results obtained for CHI/SiO_2 films prepared by Procedure 2 shown in § 4.3.3.4. In addition, with increasing SiO_2@APS contents the WCA values were practically equal for all non-neutralised composite films. Due to the hydrophilicity of SiO_2@APS particles combined with the addition of plasticizer it was expected that the WCA of these systems would decrease. Yet, the trend observed for the previous systems was kept. This suggests that the interactions via hydrogen bonding may be responsible for the essentially hydrophobic nature of these films.

For neutralised CHI/SiO_2@APS films, the WCA values of the systems were lower in comparison with those shown for neutralised CHI/silica films (Table 4.6). Moreover, similarly to the observed for non-neutralised films, with increasing SiO_2@APS contents the WCA values were practically equal for all neutralised composite films. These results indicate that after neutralization, the SiO_2@APS are possibly more exposed on the film surface and the presence of $–NH_2$ and –OH groups from APS should contribute to reduction of hydrophobic character of these composite films.

The water vapour permeability (WVP) values observed for non-neutralised CHI/SiO_2@APS films were considerable lower than that for plasticized pristine chitosan film, particularly for composite films loaded with 1 and 5 wt.% of SiO_2@APS. As previously mentioned, modified silica particles present a good size distribution in the chitosan matrix. Although after drying SEM micrographs have revealed that superficially this organization is lost, it is difficult to predict as SiO_2@APS particles are internally distributed. Taking into account the WVP values obtained for non-neutralised CHI/SiO_2@APS films, it is possible to associate this behaviour to the presence of more ordered and well dispersed fillers in the chitosan matrix, which could act as barriers to the diffusion of the water vapour.

For neutralised CHI/SiO_2@APS films the WVP results were also similar to those obtained for plasticized chitosan/silica composite films prepared by Procedure 2.

4.4. Conclusions

Prior to solvent casting, the low pH value needed to solubilize the chitosan led to a very low zeta potential of the silica particles. This low ionization was the main cause responsible for particle aggregation, essentially when bare silica particles were used in the Procedure 1. However, as observed for Procedure 2, when modified silica particles were used, in particular SiO_2@APS, their starting size was nanometric up to the preparation of the composite suspensions, prior the drying of

the films. After drying, due to aggregation phenomena the fillers were essentially silica aggregates of micrometic size, which caused a rougher surface topology to be obtained for all CHI composite films. These observations were visualised by SEM images. this aggregation process derived essentially from the drying process also led to less transparent films.

Both polymer and fillers are expected to be sensitive to pH, due to the amine on the chitosan chains and the functional groups at surface of the silica. After film formation, two different ionic conditions were tested, corresponding to a low pH where the biopolymer is essentially ionized and neutral pH at which the amine groups from the chitosan are essentially non-protonated. Due to the "freezing" of the filler particles inside the polymer matrix after solvent evaporation, this pH change did not significantly influence the particle aggregation, but increased intermolecular interactions between the chitosan chains, which caused the shrinkage of the membrane, associated with a worse imbibing of the silica particle aggregates into the film.

Spectroscopic analysis did not reveal any significant physical crosslinking (i.e. via hydrogen bonding) between the biopolymer and the modified or non-modified fillers. Polymer-filler interactions at the surface of the particles are known to be of relevance for the composite properties. In our systems, especially to those prepared by Procedure 1, possible relevant interfacial interactions are compromised due to the relative low surface area of the fillers (mostly aggregates of spherical particles), the lower ionization of the filler particles as well as poor particle dispersion.

In these systems, the mechanical properties of the non-neutralised films were affected by presence silica particles; the Young's modulus decreased whilst film elongation was increased. A slight positive influence on surface hydrophobicity and water vapour permeability was dependent on the pos-treatment neutralization process.

Under the experimental conditions required to solubilise and prepare films from chitosan, improvement in the silica particle's dispersion was clearly needed to obtain true nanocomposite films with improved functional properties. Thus, modified silica particles were used following Procedure 2. When silica particles were initially mixed with GLY, followed by mixing with CHI matrix, the mechanical properties of the resulting non-neutralised composite films were not effectively improved. Yet, they were different from those obtained by Procedure 1. The Young's modulus and film elongation increased with increasing silica loading. However, it was verified that the presence of water in the films influenced the mechanical properties of the films. DMA of fully dry films showed E' values higher than those dried under standard conditions. A positive influence of these silica fillers on the surface hydrophobicity and water vapour permeability was observed for neutralised and non-neutralised films. For non-neutralised films the presence of GLY adsorbed on the SiO_2 slightly increased the WCA of films and decreased their WVP up to 1 wt.%. silica. For neutralised films this joint positive effect was observed up to 5 wt.% SiO_2.

These results constitute an initial perspective of application of these membrane systems and these advantageous properties were further enhanced as SiO_2 modified with APS was added in the CHI matrix and upon neutralisation. In this case, the stiffness of CHI/SiO_2@APS films was improved with increasing SiO_2@APS content. The Young's modulus and tensile strength increased while the film elongation was decreased. Apart from this, even for CHI/SiO_2@APS non-neutralised films, DMA results showed an increase in E', resultant of water loss of films. As regards to the WCA and WVP results, the non-neutralised CHI/SiO_2@APS films showed improved properties for all filler contents tested whilst for neutralised films this joint positive effect was observed up to 5 wt.% SiO_2@APS, similar to the results previously described also using Procedure 2.

Thermal properties were vaguely influenced by the presence of the different fillers, which suggests that more improvements in the interfacial interaction between the filler and the polymer are necessary.

Despite of the simplicity involved in the preparation method and chemical composition of these composite films, it was noted that the surface modification of silica particles contributed to improve silica particle's dispersion both in solution and in the nanocomposite films. Different ionic conditions and appropriate surface modification of the silica particles can significantly improve mechanical and barrier properties and water stability of the chitosan nanocomposites. The results obtained have clearly pointed out to the need for chemically modifying the silica surface or even of chitosan.

5 General conclusions and future work

In spite of the potential characteristic of bionanocomposites, they have not been intensively studied in comparison with synthetic polymer based nanocomposite. Moreover, the majority of the studies found in the literature report essentially the use of sol-gel processes to obtain this type of materials. In this thesis a relatively unexplored approach to prepare inorganic/polysaccharide composites via mixture of components was studied. Surface modification of the silica particles, preparation of bionanocomposite dispersions and films and their characterization by a variety of complementary techniques have been carried out.

The principal constituents of the bionanocomposite dispersions prepared in this thesis were silica particles and polysaccharides of different nature regarding charge and thickening/gelling ability. Bionanocomposite films were prepared using chitosan as host matrix and both bare and modified silica particles.

From the results obtained in the second Chapter, the effect of pH, and ionic strength on the aggregation of silica particles was established. Modification of the silica surface with organosilanes MPS and APS proved to be an efficient method to tune the characteristics of the surface of silica particles for (i) further encapsulation with the functional synthetic polymer PGMA and (ii) for direct use in cationic polysaccharide dispersions. The surface modification of silica particles with APS (SiO_2@APS) ensured the formation of stable colloidal dispersions in acetic acid up to pH 9 and in aqueous chitosan solution at pH 3. In view of these promising results, in future particular attention should be given to the use of other coupling agents with distinct functional groups to promote their colloidal stability in a wider range of biopolymers.

However, the hybrid fillers obtained by encapsulation of SiO_2@MPS in PGMA yielded unstable dispersions when added to xanthan gum dispersions, despite of the use of a variety of surfactants to tune the charge of the hybrid fillers, and the well known characteristics of XG as a stabilizing agent. Therefore, further efforts must be developed to improve this approach which may include surface initiated living radical polymerizations for example.

As regards the bionanocomposite dispersions, it was shown that polysaccharide/silica composite dispersions exhibit a weak-gel rheological response, with a strong dependence on silica content and ionic conditions, i.e. those conditions that favour particle aggregation and particle-polymer interactions. In fact, this phenomenon is more evident for dispersions prepared with the non-gelable polysaccharides, LBG and CHI, whereas for XG composite dispersions, where more specific interactions between the biopolymer chains are expected to occur, a solid-like behaviour was already seen for neat polysaccharide solutions. The latter composite dispersions are less influenced by particle loading, pH or ionic strength. Instead, the structured behaviour seems to be due to the enhancement of XG chain's rigidity as the pH or the ionic strength increase. Microstructural

analyses and the linear and nonlinear rheological measurements are consistent with the composite structure of a network of particles surrounding and encaging polymer fibrils and lamellar structures that exhibited several rheological properties characteristic of weak or more structured-gel systems depending on the characteristics of the polysaccharide.

Although an interconnected structure of silica particles for CHI and XG composite dispersions was demonstrated by direct microscopic observations, for LBG dispersions the silica particles form clusters that self-organize on the polymer fibrils or lamellar structures. This fact seems to suggest a higher or different interaction between the silica particles and those charged polysaccharides. The more likely underlying mechanism for reinforcement and nonlinear behaviour appears to be the confinement of polymer chains caused by the silica particle organization. Thus polymer mobility is compromised by polymer imprisonment within the particle clusters and/or hindered due to adsorption at the particle surfaces. Relaxation of polymer chains is then expected to be dramatically altered. Changes in polymer dynamics caused by the particles explain the formation of transient networks.

Adequate manipulation of filler concentration and/or ionization yielded solid-like structured systems with complex viscoelastic behaviours, solid-like materials under quiescent conditions but flowing easily under applied stress conditions, when compared with the typical liquid-like and shear-thinning behaviour of the net polysaccharide solution. The pseudo-gelling properties of the pristine XG make the XG/silica dispersions much less sensitive to the presence of the particles (amount and charge).

Although it was shown that some bionanocomposite dispersions are fragile by nature due to the marginal stability of the forces building up the network within the material, they may be tailored and lead to novel mechanical responses that may be relevant in certain application areas. In particular due to the promising rheological results obtained for XG composite dispersions more studies on their rheological/microstructural properties are still needed to get a better understanding of the effect of the silica particles at different conditions and possibly to apply these materials in interesting fields, such as in secondary oil recovery.

Regarding the bionanocomposites films prepared at pH 3 by solvent casting process using the simple mixture of the constituents, due to the low pH value required to dissolve chitosan, the silica particles aggregated even before film formation. This aggregation was responsible for the rough surface morphology obtained. Moreover, no significant enhancement of the physical-chemical, mechanical, thermal and barrier properties was achieved.

Alternatively, dispersion of bare and APS modified silica particles in the plasticizer prior to addition to the CHI solution afforded better dispersions especially for SiO_2@APS. This was

confirmed by DLS measurements. Yet, when unmodified silica particles were used, the fillers were also aggregated in the ensuing composites films and the properties were not effectively better though some improvement was obtained. In the case of SiO_2@APS the presence of aggregates in the composite films must be associated with the complex mechanisms involved during drying. Nevertheless, the mechanical properties have been enhanced namely for the neutralised films. However, information about the mechanical properties is not fully reliable due to the plasticizing effect of water and the hydrophilic nature of the materials involved as proven by DMA tests on films dried under distinct conditions. The WCA and WVP results of both neutralised and non-neutralised CHI/SiO_2@APS films were also enhanced up to specific particles loadings, which varied depending of the film properties and conditions studied. From these results it is evident that the surface of the silica particles plays a significant role but further improvements will require other studies involving the modification of the polysaccharide and of the film drying conditions.

In conclusion, the fundamental studies in terms of the microstructural, rheological, mechanical, morphological and barrier properties investigated in this thesis have contributed to a better understanding of these systems and of the potentials and limitations of the simple mixture approach for preparing silica based bionanocomposites. In addition, the methodology studied is simple, relatively easy to implement and very flexible thus offering a promising alternative route to the sol-method which is associated with significant limitations despite of its widespread use. As a final note, it is stressed that the potential of the approached studied is particularly promising when the use of a variety of silica coated (multi)functional hybrid materials is considered.

6 References

[1] Rhim, J.-W.; Ng, P. K. W.; "Natural biopolymer-based nanocomposite films for packaging applications", *Critical Reviews in Food Science and Nutrition*, **2007**, *47*, 411 - 433.

[2] Sorrentino, A.; Gorrasi, G.; Vittoria, V.; "Potential perspectives of bio-nanocomposites for food packaging applications", *Trends in Food Science & Technology*, **2007**, *18*, 84-95.

[3] http://en.wikipedia.org/wiki/Nacre, cited in 12/07/2009.

[4] Zuo, S.; Wei, Y.; "Microstructure observation and mechanical behavior modeling for limnetic nacre", *Acta Mechanica Sinica*, **2008**, *24*, 83-89.

[5] Bourgeat-Lami, E.; "Organic-inorganic nanostructured colloids", *Journal of Nanoscience and Nanotechnology*, **2002**, *2*,

[6] Alkan, M.; Dogan, M.; "Surface chemistry of silica gels", in Encyclopedia of Surface and Colloid Science, Ed: Hubbard, A. T.; *Marcel Dekker, Inc.*, **2002,** New York

[7] Gonçalves e Silva, M.; "Comportamento reológico de emulsões de água em óleo na indústria petrolifera", *Universidade Federal de Itajubá*,Governo do Brasil, **2000,** Itajubá.

[8] Schramm, G.; "Reologia e Reometria - Fundamentos Teóricos e Práticos", *Artliber editora*, **2006,** São Paulo.

[9] Smidsrod, O.; Moe, S. T.; "Biopolymer Chemistry", *Tapir Academic press*, **2008,** Trondheim.

[10] Jouffrey, B.; Svejcar, J.; "Microstructural Investigation and Analysis", *Wiley-VCH*, **2000,** Weinhein.

[11] Wang, J.; Somasundaran, P.; "Study of galactomannose interaction with solids using AFM, IR and allied techniques", *Journal of Colloid and Interface Science*, **2007**, *309*, 373-383.

[12] Kumar, M. N. V. R.; "A review of chitin and chitosan applications", *Reactive & Functional Polymers*, **2000**, *46*, 1-27.

[13] Marguerite, R.; "Main properties and current applications of some polysaccharides as biomaterials", *Polymer International*, **2008**, *57*, 397-430.

[14] Bergmann, D.; Furth, G.; Mayer, C.; "Binding of bivalent cations by xanthan in aqueous solution", *International Journal of Biological Macromolecules*, **2008**, *43*, 245-251.

[15] Baird, J. K.; Pettitt, D. J.; "Biogums used in food and made by fermenations", in Biotechnology and food ingredients Ed: Goldberg, I.; Williams, R.; *Van Nostrand Reinhold*, **1991,** New York.

[16] Lokensgard, E.; "Casting processes and materials", in Industrial plastics: Theory and Applications, Ed: Lokensgard, E.; *Thompson, Delmar Learning*, **2004,** Clifton Park: New York.

[17] Mark, J. E.; Abou-Hussein, R.; Sen, T. Z.; Kloczkowski, A.; "Some simulations on filler reinforcement in elastomers", *Polymer*, **2005**, *46*, 8894-8904.

[18] http://www.britannica.com/EBchecked/topic-art/587505/113923/The-stress-strain-curve-illustrating-the-stretching-of-a-piece, cited in 28/09/2009.

[19] http://www.ndt-ed.org/EducationResources/CommunityCollege/Materials/Mechanical/Tensile.htm, cited in 29/09/2009.

[20] Lamba, N. M. K.; Woodhouse, K. A.; Cooper, S. L.; Lelah, M. D.; "Polyurethanes in biomedical applications", *CRC Press*, **1998,** New York.

[21] Marmur, A.; "Soft contact: measurement and interpretation of contact angles", *Soft Matter*, **2006**, *2*, 12-17.

[22] Ferreira, P. J. O.; "Matrizes fibrosas de biopolímeros produzidas por electrospinning", Tese de Mestrado, Universidade of Aveiro, **2008,** Aveiro.

[23] Santos, C. A. N. S.; "Propriedades de Filmes de Quitosano – Influência do grau de acetilação e da massa molecular do biopolímero", Tese de Mestrado, Universidade de Aveiro, **2006,** Aveiro.

[24] Sinha Ray, S.; Bousmina, M.; "Biodegradable polymers and their layered silicate nanocomposites: In greening the 21st century materials world", *Progress in Materials Science*, **2005**, *50*, 962-1079.

[25] Azeredo, H. M. C.; "Nanocomposites for food packaging applications", *Food Research International*, **2009**, *42*, 1240-1253.

[26] Darder, M.; Aranda, P.; Ruiz-Hitzky, E.; "Bionanocomposites: A new concept of ecological, bioinspired, and functional hybrid materials", *Advanced Materials*, **2007**, *19*, 1309-1319.

[27] Ruiz-Hitzky, E.; Darder, M.; Aranda, P.; "An introduction to bio-nanohybrid materials", in Bio-inorganic hybrid nanomaterials: strategies, syntheses, characterization and application, Ed: Ruiz-Hitzky, E.; Ariga, K.; Lvov, Y.; *Wiley-VCH*, **2008,** Weinheim.

[28] Kickelbick, G.; "Concepts for the incorporation of inorganic building blocks into organic polymers on a nanoscale", *Progress in Polymer Science*, **2003**, *28*, 83-114.

[29] Esteves, A. C. C.; Barros-Timmons, A. M.; Trindade, T.; "Nanocompósitos de matriz polimérica: estratégias de síntese de materiais híbridos", *Quimica Nova*, **2004**, *27*, 798-806.

[30] Allouche, J.; Boissiere, M.; Helary, C.; Livage, J.; Coradin, T.; "Biomimetic core-shell gelatine/silica nanoparticles : A new example of biopolymer-based nanocomposites", *Journal of material chemistry*, **2006**, *16*, 3120-3125.

[31] Coradin, T.; Allouche, J.; Boissiere, M.; Livage, J.; "Sol-gel biopolymer/silica nanocomposites in biotechnology", *Current Nanoscience*, **2006**, *2*, 219-230.

[32] Boissière, M.; Allouche, J.; Chanéac, C.; Brayner, R.; Devoisselle, J.-M.; Livage, J.; Coradin, T.; "Potentialities of silica/alginate nanoparticles as Hybrid Magnetic Carriers", *International Journal of Pharmaceutics*, **2007**, *344*, 128-134.

[33] Tan, W. B.; Huang, N.; Zhang, Y.; "Ultrafine biocompatible chitosan nanoparticles encapsulating multi-coloured quantum dots for bioapplications", *Journal of Colloid and Interface Science*, **2007**, *310*, 464-470.

[34] Baccile, N.; Babonneau, F.; Thomas, B.; Coradin, T.; "Introducing ecodesign in silica sol-gel materials", *Journal of Materials Chemistry*, **2009**, *19*, 8537-8559.

[35] Finnie, K.; Waller, D.; Perret, F.; Krause-Heuer, A.; Lin, H.; Hanna, J.; Barbé, C.; "Biodegradability of sol–gel silica microparticles for drug delivery", *Journal of Sol-Gel Science and Technology*, **2009**, *49*, 12-18.

[36] Alexandre, M.; Dubois, P.; "Polymer-layered silicate nanocomposites: Preparation, properties and uses of a new class of materials ", *Materials Science and Engineering R: Reports*, **2000**, *28*, 1-63.

[37] Stöber, W.; Fink, A.; Bohn, E.; "Controlled growth of monodisperse silica spheres in the micron size range", *Journal of Colloid and Interface Science*, **1968**, *26*, 62-69.

[38] Pinto, R. J. B.; Marques, P. A. A. P.; Barros-Timmons, A. M.; Trindade, T.; Neto, C. P.; "Novel SiO_2/cellulose nanocomposites obtained by in situ synthesis and via polyelectrolytes assembly", *Composites Science and Technology*, **2008**, *68*, 1088-1093.

[39] Bourgeat-Lami, E.; Lang, J.; "Encapsulation of inorganic particles by dispersion polymerization in polar media: 1. Silica nanoparticles encapsulated by polystyrene", *Journal of Colloid and Interface Science*, **1998**, *197*, 293-308.

[40] Herron, N.; Thorn, D. L.; "Nanoparticles: Uses and relationships to molecular clusters", *Advanced Materials*, **1998**, *10* 1173-1184.

[41] Nakamura, H.; Matsui, Y.; "Silica gel nanotubes obtained by the sol-gel method", *Journal of the American Chemical Society*, **1995**, *117*, 2651-2652.

[42] Maser, W. K.; Benito, A. M.; Martínez, M. T.; "Production of carbon nanotubes: the light approach", *Carbon*, **2002**, *40*, 1685-1695.

[43] Ras, R. H. A.; Kemell, M.; Wit, J. D.; Ritala, M.; Brinke, G. T.; Leskelä, M.; Ikkala, O.; "Hollow inorganic nanospheres and nanotubes with tunable wall thicknesses by atomic layer deposition on self-assembled polymeric templates", *Advanced Materials*, **2007**, *19*, 102-106.

[44] Ghislandi, M.; Prado, L.; Oyerviedes, A. D.; Wittich, H.; Schulte, K.; Barros-Timmons, A.; "Functionalization of carbon nanofibers (CNFs) through atom transfer radical polymerization for the preparation of poly(tert-butyl acrylate)/CNF materials: Spectroscopic, thermal, morphological, and physical characterizations", *Journal of Polymer Science Part A: Polymer Chemistry*, **2008**, *46*, 3326-3335.

[45] Oksman, K.; Mathew, A. P.; Bondeson, D.; Kvien, I.; "Manufacturing process of cellulose whiskers/polylactic acid nanocomposites", *Composites Science and Technology*, **2006**, *66*, 2776-2784.

[46] Chivrac, F.; Pollet, E.; Avérous, L.; "Progress in nano-biocomposites based on polysaccharides and nanoclays", *Materials Science and Engineering: R: Reports*, **2009**, *67*, 1-17.

[47] Geng, Y.; Wang, S. J.; Kim, J.-K.; "Preparation of graphite nanoplatelets and graphene sheets", *Journal of Colloid and Interface Science*, **2009**, *336*, 592-598.

[48] Albuquerque, R.; Neves, M. C.; Mendonca, M. H.; Trindade, T.; Monteiro, O. C.; "Adsorption and catalytic properties of SiO_2/Bi_2S_3 nanocomposites on the methylene blue photodecolorization process", *Colloids and Surfaces A: Physicochemical and Engineering Aspects*, **2008**, *328*, 107-113.

[49] Samir, M. A. S. A.; Alloin, F.; Dufresne, A.; "Review of recent research into cellulosic whiskers, their properties and their application in nanocomposite field", *Biomacromolecules*, **2005**, *6*, 612-626.

[50] Dalmas, F.; Cavaillé, J.-Y.; Gauthier, C.; Chazeau, L.; Dendievel, R.; "Viscoelastic behavior and electrical properties of flexible nanofiber filled polymer nanocomposites. Influence of processing conditions", *Composites Science and Technology*, **2007**, *67*, 829-839.

[51] Jordan, J.; Jacob, K. I.; Tannenbaum, R.; Sharaf, M. A.; Jasiuk, I.; "Experimental trends in polymer nanocomposites - a review", *Materials Science and Engineering A*, **2005**, *393*, 1-11.

[52] Qiao, R.; Brinson, L. C.; "Simulation of interphase percolation and gradients in polymer nanocomposites", *Composites Science and Technology*, **2009**, *69*, 491-499.

[53] Yao, N.; Epstein, A. K.; Liu, W. W.; Sauer, F.; Yang, N.; "Organic-inorganic interfaces and spiral growth in nacre", *Journal of the Royal Society Interface*, **2009** *6*, 367-376.

[54] Bergaya, F.; Theng, B. K. G.; Lagaly, G.; "Handbook of Clay Science", *Elsevier*, **2006,** Amsterdam.

[55] Darder, M.; Colilla, M.; Ruiz-Hitzky, E.; "Biopolymer/clay nanocomposites based on chitosan intercalated in montmorillonite", *Chemistry of Materials*, **2003**, *15*, 3774-3780.

[56] Lin, K. F.; Hsu, C. Y.; Huang, T. S.; Chiu, W.-Y.; Lee, Y.-H.; Young, T. H.; "A novel method to prepare chitosan/montmorillonite nanocomposites", *Journal of Applied Polymer Science*, **2005**, *98*, 2042-2047.

[57] Wang, S. F.; Shen, L.; Tong, Y. J.; Chen, L.; Phang, I. Y.; Lim, P. Q.; Liu, T. X.; "Biopolymer chitosan/montmorillonite nanocomposites: Preparation and characterization", *Polymer Degradation and Stability*, **2005**, *90*, 123-131.

[58] Xu, Y.; Ren, X.; Hanna, M. A.; "Chitosan/clay nanocomposite film preparation and characterization", *Journal of Applied Polymer Science*, **2006**, *99*, 1684-1691.

[59] Tan, W.; Zhang, Y.; Szeto, Y.-S.; Liao, L.; "A novel method to prepare chitosan/montmorillonite nanocomposites in the presence of hydroxy-aluminum oligomeric cations", *Composites Science and Technology*, **2008**, *68*, 2917-2921.

[60] Bharadwaj, R. K.; "Modeling the barrier properties of polymer-layered silicate nanocomposites", *Macromolecules*, **2001**, *34*, 9189-9192.

[61] Adame, D.; Beall, G. W.; "Direct measurement of the constrained polymer region in polyamide/clay nanocomposites and the implications for gas diffusion", *Applied Clay Science*, **2009**, *42*, 545-552.

[62] Liao, S. S.; Cui, F. Z.; Zhang, W.; Feng, Q. L.; "Hierarchically biomimetic bone scaffold materials: Nano-HA/collagen/PLA composite", *Journal of Biomedical Materials Research Part B: Applied Biomaterials*, **2004**, *69B*, 158-165.

[63] Shchipunov, Y. A.; "Entrapment of biopolymers into sol-gel derived silica nanocomposites", in Bio-inorganic hybrid nanomaterials: strategies, syntheses, characterization and application, Ed: Ruiz-Hitzky, E.; Ariga, K.; Lvov, Y.; *Wiley-VCH*, **2008,** Weinheim.

[64] Coradin, T.; Livage, J.; "Aqueous silicates in biological sol-gel applications: new perspectives for old precursors", *Accounts of Chemical Research*, **2007**, *40*, 819-826.

[65] Sakka, S.; "Handbook of sol-gel science and technology processing characterization and applications. Volume III: Applications of sol-gel science and technology", *Kluwer Academic Publishers*, **2005,**

[66] Brinker, C. J.; Scherer, G. W.; "Sol–gel science, the physics and chemistry of sol–gel processing", **1989,** San Diego.

[67] Fateixa, S.; Neves, M. C.; Almeida, A.; Oliveira, J.; Trindade, T.; "Anti-fungal activity of SiO_2/Ag_2S nanocomposites against *Aspergillus niger*", *Colloids and Surfaces B: Biointerfaces*, **2009**, *74*, 304-308.

[68] Neves, M. C.; Trindade, T.; Peres, M.; Wang, J.; Soares, M. J.; Neves, A.; Monteiro, T.; "Photoluminescence of zinc oxide supported on submicron silica particles", *Materials Science & Engineering C-Biomimetic and Supramolecular Systems*, **2005**, *25*, 654-657.

[69] Neves, M. C.; Soares, J.; Hempelmann, R.; Monteiro, T.; Trindade, T.; "Growth of cadmium selenide nanocrystals on submicron silica", *Journal of Crystal Growth*, **2005**, *279*, 433-438.

[70] Monteiro, O. C.; Esteves, A. C. C.; Trindade, T.; "The synthesis of SiO_2@CdS nanocomposites using single-molecule precursors", *Chemistry of Materials*, **2002**, *14*, 2900-2904.

[71] Graham, T.; "On liquid diffusion applied to analysis", *Journal of the Chemical Society*, **1862**, *15*, 216-270.

[72] Pinto, R. J. B.; Marques, P. A. A. P.; Martins, M. A.; Neto, C. P.; Trindade, T.; "Electrostatic assembly and growth of gold nanoparticles in cellulosic fibres", *Journal of Colloid and Interface Science*, **2007**, *312*, 506-512.

[73] Hussing, N.; Schubert, U.; "Porous inorganic-organic hybrid materials", in Functional hybrid materials, Ed: Gómez-Romero, P.; Sánchez, C.; *Wiley-VCH*, **2004,** Weinheim.

[74] Coradin, T.; Bah, S.; Livage, J.; "Gelatine/silicate interactions: from nanoparticles to composite gels", *Colloids and Surfaces B: Biointerfaces*, **2004**, *35*, 53-58.

[75] Coradin, T.; Boissière, M.; Livage, J.; "Sol-gel chemistry in medicinal science", *Current Medicinal Chemistry*, **2006**, *13*, 99-108.

[76] Coradin, T.; Livage, J.; "Mesoporous alginate/silica biocomposites for enzyme immobilization", *Comptes Rendus Chimie*, **2003**, *6*, 147-152.

[77] Coradin, T.; Marchal, A.; Abdoul-Aribi, N.; Livage, J.; "Gelatine thin films as biomimetic surfaces for silica particles formation", *Colloids and Surfaces B: Biointerfaces*, **2005**, *44*, 191-196.

[78] Coradin, T.; Mercey, E.; Lisnard, L.; Livage, J.; "Design of silica-coated microcapsules for bioencapsulation ", *Chem. Commun.*, **2001**, 2496 - 2497.

[79] Gill, I.; Ballesteros, A.; "Bioencapsulation within synthetic polymers (Part 1): sol–gel encapsulated biologicals", *Trends in Biotechnology*, **2000**, *18*, 282-296.

[80] Shchipunov, Y. A.; "Sol-gel-derived biomaterials of silica and carrageenans", *Journal of Colloid and Interface Science*, **2003**, *268*, 68-76.

[81] Shchipunov, Y. A.; Karpenko, T. Y.; Bakunina, I. Y.; Burtseva, Y. V.; Zvyagintseva, T. N.; "A new precursor for the immobilization of enzymes inside sol–gel-derived hybrid silica nanocomposites containing polysaccharides", *Journal of Biochemical and Biophysical Methods*, **2004**, *58*, 25-38.

[82] Shchipunov, Y. A.; Karpenko, T. Y.; "Hybrid Polysaccharide-Silica Nanocomposites Prepared by the Sol-Gel Technique", *Langmuir*, **2004**, *20*, 3882-3887.

[83] Shchipunov, Y. A.; Karpenko, T. Y.; Krekoten, A. V.; "Hybrid organic-inorganic nanocomposites fabricated with a novel biocompatible precursor using sol-gel processing", *Composite Interfaces*, **2005**, *11*, 587-607.

[84] Shchipunov, Y. A.; Kojima, A.; Imae, T.; "Polysaccharides as a template for silicate generated by sol-gel processes", *Journal of Colloid and Interface Science*, **2005**, *285*, 574-580.

[85] Shchipunov, Y. A.; Burtseva, Y. V.; Karpenko, T. Y.; Shevchenko, N. M.; Zvyagintseva, T. N.; "Highly efficient immobilization of endo-1,3-β-D-glucanases (laminarinases) from marine mollusks in novel hybrid polysaccharide-silica nanocomposites with regulated composition", *Journal of Molecular Catalysis B: Enzymatic*, **2006**, *40*, 16-23.

[86] Ayers, M. R.; Hunt, A. J. in *Synthesis and properties of chitosan-silica hybrid aerogels*, Lawrence Berkeley National Laboratory, Berkeley, **2001**.

[87] Molvinger, K.; Quignard, F.; Brunel, D.; Boissiere, M.; Devoisselle, J.-M.; "Porous chitosan-silica hybrid microspheres as a potential catalyst", *Chemistry of Materials*, **2004**, *16*, 3367-3372.

[88] Rashidova, S. S.; Shakarova, D. S.; Ruzimuradov, O. N.; Satubaldieva, D. T.; Zalyalieva, S. V.; Shpigun, O. A.; Varlamov, V. P.; Kabulov, B. D.; "Bionanocompositional chitosan-silica sorbent for liquid chromatography", *Journal of Chromatography B*, **2004**, *800*, 49-53.

[89] Shao, J.; Ge, H.; Yang, Y.; "Immobilization of polyphenol oxidase on chitosan–SiO_2 gel for removal of aqueous phenol", *Biotechnology Letters*, **2007**, *29*, 901-905.

[90] Lee, E.-J.; Shin, D.-S.; Kim, H.-E.; Kim, H.-W.; Koh, Y.-H.; Jang, J.-H.; "Membrane of hybrid chitosan-silica xerogel for guided bone regeneration", *Biomaterials*, **2009**, *30*, 743-750.

[91] Darder, M.; Lopez-Blanco, M.; Aranda, P.; Aznar, A. J.; Bravo, J.; Ruiz-Hitzky, E.; "Microfibrous chitosan/sepiolite nanocomposites", *Chemistry of Materials*, **2006**, *18*, 1602-1610.

[92] Radin, S.; El-Bassyouni, G.; Vresilovic, E. J.; Schepers, E.; Ducheyne, P.; "In vivo tissue response to resorbable silica xerogels as controlled-release materials", *Biomaterials*, **2005**, *26*, 1043–1052.

[93] Sequeira, S.; Evtuguin, D. V.; Portugal, I.; "Preparation and properties of cellulose/silica hybrid composites", *Polymer Composites*, **2009**, *30*, 1275-1282.

[94] Portugal, I.; Dias, V. M.; Duarte, R. F.; Evtuguin, D. V.; "Hydration of cellulose/silica hybrids assessed by sorption isotherms", *Journal of Physical Chemistry B*, **2010**, *114*, 4047-4055.

[95] Marques, P.; Nogueira, H. I. S.; Pinto, R. J. B.; Neto, C. P.; Trindade, T.; "Silver-bacterial cellulosic sponges as active SERS substrates", *Journal of Raman Spectroscopy*, **2008**, *39*, 439-443.

[96] Pinto, R. J. B.; Marques, P. A. A. P.; Neto, C. P.; Trindade, T.; Daina, S.; Sadocco, P.; "Antibacterial activity of nanocomposites of silver and bacterial or vegetable cellulosic fibers", *Acta Biomaterialia*, **2009**, *5*, 2279-2289.

[97] Marques, P. A. A. P.; Trindade, T.; Neto, C. P.; "Titanium dioxide/cellulose nanocomposites prepared by a controlled hydrolysis method", *Composites Science and Technology*, **2006**, *66*, 1038-1044.

[98] Goncalves, G.; Marques, P. A. A. P.; Pinto, R. J. B.; Trindade, T.; Neto, C. P.; "Surface modification of cellulosic fibres for multi-purpose TiO_2 based nanocomposites", *Composites Science and Technology*, **2009**, *69*, 1051-1056.

[99] Goncalves, G.; Marques, P. A. A. P.; Neto, C. P.; Trindade, T.; Peres, M.; Monteiro, T.; "Growth, structural, and optical characterization of ZnO-coated cellulosic fibers", *Crystal Growth & Design*, **2009**, *9*, 386-390.

[100] Vilela, C.; Freire, C. S. R.; Marques, P. A. A. P.; Trindade, T.; Neto, C. P.; Fardim, P.; "Synthesis and characterization of new $CaCO_3$/cellulose nanocomposites prepared by controlled hydrolysis of dimethylcarbonate", *Carbohydrate Polymers*, **2009**, *79*, 1150-1156.

[101] Daniel-da-Silva, A. L.; Lóio, R.; Lopes-da-Silva, J. A.; Trindade, T.; Goodfellow, B. J.; Gil, A. M.; "Effects of magnetite nanoparticles on the thermorheological properties of carrageenan hydrogels", *Journal of Colloid and Interface Science*, **2008**, *324*, 205-211.

[102] Daniel-da-Silva, A. L.; Fateixa, S.; Guiomar, A. J.; Costa, B. F. O.; Silva, N. J. O.; Trindade, T.; Goodfellow, B. J.; Gil, A. M.; "Biofunctionalized magnetic hydrogel nanospheres of magnetite and κ-carrageenan", *Nanotechnology*, **2009**, *20*, 10.

[103] Daniel-da-Silva, A. L.; Pinto, F.; Lopes-da-Silva, J. A.; Trindade, T.; Goodfellow, B. J.; Gil, A. M.; "Rheological behavior of thermoreversible [κ]-carrageenan/nanosilica gels", *Journal of Colloid and Interface Science*, **2008**, *320*, 575-581.

[104] Oh, M.-H.; So, J.-H.; Yang, S.-M.; "Rheological evidence for the silica-mediated gelation of xanthan gum", *Journal of Colloid and Interface Science*, **1999**, *216*, 320-328.

[105] Yu, Y.-Y.; Chen, W.-C.; "Transparent organic-inorganic hybrid thin films prepared from acrylic polymer and aqueous monodispersed colloidal silica", *Materials Chemistry and Physics*, **2003**, *82*, 388-395.

[106] Radhakrishnan, B.; Ranjan, R.; Brittain, W. J.; "Surface initiated polymerizations from silica nanoparticles", *Soft Matter*, **2006**, *2*, 386–396.

[107] Xia, H.-L.; Tang, F.-Q.; "Surface synthesis of zinc oxide nanoparticles on silica spheres: preparation and characterization", *The Journal of Physical Chemistry B*, **2003**, *107*, 9175-9178.

[108] Dhas, N. A.; Zaban, A.; Gedanken, A.; "Surface synthesis of zinc sulfide nanoparticles on silica microspheres: Sonochemical preparation, characterization, and optical properties", *Chemistry of Materials*, **1999**, *11*, 806-813.

[109] Monteiro, O. C.; Neves, M. C.; Trindade, T.; "Submicron silica nanocoating with zinc sulfide using a single-source method", *Journal Nanoscience and Nanotechnology*, **2004**, *4*, 137.

[110] Peixoto, S. M. R.; "Síntese e caracterização de nanocompósitos funcionais", Tese de Mestrado, Universidade de Aveiro, **2008,** Aveiro.

[111] Iler, R. K.; "The chemistry of silica: solubility, polymerization, colloid and surface properties and biochemistry. ", *John Wiley & Sons*, **1979,** Chichester: New York.

[112] van Blaaderen, A.; Vrij, A.; "Synthesis and characterization of monodisperse colloidal organo-silica spheres", *Journal of Colloid and Interface Science*, **1993**, *156*, 1-18.

[113] Leite, C. A. P.; de Souza, E. F.; Galembeck, F.; "Core-and-shell nature of Stöber silica particles", *Journal Brazilian Chemical Society*, **2001**, *12*,

[114] Nassar, E. J.; Messaddeq, Y.; Ribeiro, S. J. L.; "Influência da catálise ácida e básica na preparação da sílica funcionalizada pelo método sol-gel ", *Quimica Nova*, **2002**, *25*, 27-31.

[115] Park, S. K.; Kim, K. D.; Kim, H. T.; "Preparation of silica nanoparticles: determination of the optimal synthesis conditions for small and uniform particles", *Colloids and Surfaces A: Physicochemical and Engineering Aspects*, **2002**, *197*, 7-17.

[116] Green, D. L.; Lin, J. S.; Lam, Y.-F.; Hu, M. Z. C.; Schaefer, D. W.; Harris, M. T.; "Size, volume fraction, and nucleation of Stober silica nanoparticles", *Journal of Colloid and Interface Science*, **2003**, *266*, 346-358.

[117] Nozawa, K.; Gailhanou, H.; Raison, L.; Panizza, P.; Ushiki, H.; Sellier, E.; Delville, J. P.; Delville, M. H.; "Smart control of monodisperse Sotber silica particles: Effect of reactant addition rate on growth process", *Langmuir*, **2004**, *21*, 1516-1523.

[118] Bergna, H. E.; "Colloidal chemistry of silica: an overview", in Colloidal Silica: Fundamentals and Applications, Ed: Bergna, H. E.; Roberts, W. O.; *Taylor & Francis*, **2005,** New York.

[119] Sanchez, C.; Soler-Illia, G. J. D. A. A.; Ribot, F.; Grosso, D.; "Design of functional nano-structured materials through the use of controlled hybrid organic-inorganic interfaces", *Comptes Rendus Chimie*, **2003**, *6*, 1131-1151.

[120] Chen, H.; Zhou, S.; Gu, G.; Wu, L.; "Study on modification and dispersion of nano-silica", *Journal of Dispersion Science and Technology*, **2005** *26*, 27-37.

[121] Zou, H.; Wu, S.; Shen, J.; "Polymer/silica nanocomposites: preparation, characterization, properties, and applications", *Chemical Reviews*, **2008**, *108*, 3893-3957.

[122] Wiese, G. R.; Healy, T. W.; "Effect of particle size on colloid stability", *Transactions of the Faraday Society*, **1970**, *66*, 490 - 499.

[123] Ebelmen, M.; "Sur les combinaisons des acides borique et silicique avec les ethers", *Ann. Chim. Phys.*, **1846**, *16*, 129.

[124] Ebelmen, M.; "Sur l'hyalite artificielle et l'hydrophane", *Comptes Rendus de l'Académie des sciences*, **1847**, *25*, 854.

[125] Mark, J. E.; Allcock, H. R.; West, R.; "Inorganic Polymers ", *Oxford University Press*, **2005,** New York.

[126] Corriu, R.; Mehdi, A.; Reyé, C.; "Nanoporous materials: a good opportunity for nanosciences", *Journal of Organometallic Chemistry*, **2004**, *689*, 4437-4450.

[127] Okudera, H.; Hozumi, A.; "The formation and growth mechanisms of silica thin film and spherical particles through the Stöber process", *Thin Solid Films*, **2003**, *434*, 62-68.

[128] Shi, J. in *Steric Stabilization*, Center for Industrial Sensors and Measurements, Columbus: USA, **2002**.

[129] García-González, C. A.; Andanson, J. M.; Kazarian, S. G.; Domingo, C.; Saurina, J.; "Application of principal component analysis to the thermal characterization of silanized nanoparticles obtained at supercritical carbon dioxide conditions", *Analytica Chimica Acta*, **2009**, *635*, 227-234.

[130] Luo, Y.; RONG, M. Z.; ZHANG, M. Q.; FRIEDRICH, K.; "Surface grafting onto SiC nanoparticles with glycidyl methacrylate in emulsion ", *Journal of Polymer Science Part A: Polymer Chemistry*, **2004**, *42*, 3842-3852.

[131] Ardes-Guisot, N.; Durand, J.-O.; Granier, M.; Perzyna, A.; Coffinier, Y.; Grandidier, B.; Wallart, X.; Stievenard, D.; "Trichlorosilane isocyanate as coupling agent for mild conditions functionalization of silica-coated surfaces", *Langmuir*, **2005**, *21*, 9406-9408.

[132] Bourgeat-Lami, E.; Espiard, P.; Guyot, A.; "Poly(ethyl acrylate) latexes encapsulating nanoparticles of silica: 1. Functionalization and dispersion of silica", *Polymer*, **1995**, *36*, 4385-4389.

[133] Özcan, M.; Matinlinna, J. P.; Vallittu, P. K.; Huysmans, M.-C.; "Effect of drying time of 3-methacryloxypropyltrimethoxysilane on the shear bond strength of a composite resin to silica-coated base/noble alloys", *Dental Materials*, **2004**, *20*, 586-590.

[134] Philipse, A. P.; Vrij, A.; "Preparation and properties of nonaqueous model dispersions of chemically modified, charged silica spheres", *Journal of Colloid and Interface Science*, **1989**, *128*, 121-136.

[135] Vrancken, K. C.; Possemiers, K.; Van Der Voort, P.; Vansant, E. F.; "Surface modification of silica gels with aminoorganosilanes", *Colloids and Surfaces A: Physicochemical and Engineering Aspects*, **1995**, *98*, 235-241.

[136] Kallury, K. M. R.; Macdonald, P. M.; Thompson, M.; "Effect of surface water and base catalysis on the silanization of silica by (aminopropyl)alkoxysilanes studied by X-ray photoelectron spectroscopy and 13C cross-polarization/magic angle spinning nuclear magnetic resonance", *Langmuir*, **1994**, *10*, 492-499.

[137] Hao, X.; Fei, Y.; Eric, E. M.; Raoul, K.; "Room-temperature preparation and characterization of poly(ethylene glycol)-coated silica nanoparticles for biomedical applications", *Journal of Biomedical Materials Research Part A*, **2003**, *66A*, 870-879.

[138] Rao, A. V.; Kulkarni, M. M.; "Effect of glycerol additive on physical properties of hydrophobic silica aerogels", *Materials Chemistry and Physics*, **2003**, *77*, 819-825.

[139] Bijsterbosch, H. D.; Cohen Stuart, M. A.; Fleer, G. J.; "Effect of block and graft copolymers on the stability of colloidal silica", *Journal of Colloid and Interface Science*, **1999**, *210*, 37-42.

[140] Qi, D.-M.; Bao, Y.-Z.; Weng, Z.-X.; Huang, Z.-M.; "Preparation of acrylate polymer/silica nanocomposite particles with high silica encapsulation efficiency via miniemulsion polymerization", *Polymer*, **2006**, *47*, 4622-4629.

[141] Mingna, X.; Limin, W.; Shuxue, Z.; Bo, Y.; "Preparation and characterization of acrylic latex/nano-SiO_2 composites", *Polymer International*, **2002**, *51*, 693-698.

[142] Landfester, K.; Schork, F. J.; Kusuma, V. A.; "Particle size distribution in mini-emulsion polymerization", *Comptes Rendus Chimie*, **2003**, *6*, 1337-1342.

[143] Sondi, I.; Fedynyshyn, T. H.; Sinta, R.; Matijevic, E.; "Encapsulation of nanosized silica by *in situ* polymerization of tert-butyl acrylate monomer ", *Langmuir*, **2000**, *16*, 9031-9034.

[144] Landfester, K.; "Polyreactions in miniemulsions", *Macromolecular Rapid Communications*, **2001**, *22*, 896-936.

[145] Esteves, A. C. C.; "Nanocompósitos de matriz polimérica do tipo SiO_2/polímero e CdS/polímero", Tese de Mestrado, Universidade de Aveiro, **2002,** Aveiro.

[146] Zhong, Z.; Jian, Y.; Zhao-Xia, G.; "Preparation of epoxy-functionalized polystyrene/silica core-shell composite nanoparticles", *Journal of Polymer Science Part A: Polymer Chemistry*, **2004**, *42*, 2253-2262.

[147] Chern, C. S.; "Emulsion polymerization mechanisms and kinetics", *Progress in Polymer Science*, **2006**, *31*, 443-486.

[148] Lehocky, M.; Esteves, A. C.; Barros-Timmons, A. M.; Coutinho, J. A. P.; "Preparation and characterization of hybrid organic/inorganic nanocomposites by in situ miniemulsion polymerization", *Materials Science Forum*, **2006**, *514-516*, 1201-1205.

[149] Feng, Y.; Gordon, L. N.; "PMMA/silica nanocomposite studies: synthesis and properties", *Journal of Applied Polymer Science*, **2004**, *91*, 3844-3850.

[150] Lin, C.-C.; Wang, Y.-F.; "Suspension polymerization of methyl methacrylate. I. Modeling of reaction kinetics", *Journal of Applied Polymer Science*, **1981**, *26*, 3909-3915.

[151] Vivaldo-Lima, E.; Wood, P. E.; Hamielec, A. E.; Penlidis, A.; "An updated review on suspension polymerization", *Industrial & Engineering Chemistry Research*, **1997**, *36*, 939-965.

[152] Horák, D.; "Magnetic polyglycidylmethacrylate microspheres by dispersion polymerization", *Journal of Polymer Science Part A: Polymer Chemistry*, **2001**, *39*, 3707-3715.

[153] Elmas, B.; Tuncel, M.; YalçIn, G.; Senel, S.; Tuncel, A.; "Synthesis of uniform, fluorescent poly(glycidyl methacrylate) based particles and their characterization by confocal laser scanning microscopy", *Colloids and Surfaces A: Physicochemical and Engineering Aspects*, **2005**, *269*, 125-134.

[154] Jyongsik, J.; Joonwon, B.; Sungrok, K.; "Synthesis and curing of poly(glycidyl methacrylate) nanoparticles", *Journal of Polymer Science Part A: Polymer Chemistry*, **2005**, *43*, 2258-2265.

[155] Norakankorn, C.; Pan, Q.; Rempel, G. L.; Kiatkamjonwong, S.; "Synthesis of core/shell structure of glycidyl-functionalized poly(methyl methacrylate) latex nanoparticles via differential microemulsion polymerization", *European Polymer Journal*, **2009**, *45*, 2977-2986.

[156] Shchipunov, Y. A.; Karpenko, T. Y.; Krekoten, A. V.; Postnova, I. V.; "Gelling of otherwise nongelable polysaccharides", *Journal of Colloid and Interface Science*, **2005**, *287*, 373-378.

[157] Marcu, I.; Daniels, E. S.; Dimonie, V. L.; Hagiopol, C.; Roberts, J. E.; El-Aasser, M. S.; "Incorporation of alkoxysilanes into model latex systems: vinyl copolymerization of vinyltriethoxysilane and n-butyl acrylate", *Macromolecules*, **2002**, *36*, 328-332.

[158] Chern, C.-S.; "Principles and Applications of Emulsion Polymerization", *Wiley*, **2008,**

[159] Santos, A. M.; Guillot, J.; McKenna, T. F.; "Partitioning of styrene, butyl acrylate and methacrylic acid in emulsion systems", *Chemical Engineering Science*, **1998**, *53*, 2143-2151.

[160] Espiard, P.; Guyot, A.; "Poly(ethyl acrylate) latexes encapsulating nanoparticles of silica: 2. Grafting process onto silica", *Polymer*, **1995**, *36*, 4391-4395.

[161] Espiard, P.; Guyot, A.; Perez, J.; Vigier, G.; David, L.; "Poly(ethyl acrylate) latexes encapsulating nanoparticles of silica: 3. Morphology and mechanical properties of reinforced films", *Polymer*, **1995**, *36*, 4397-4403.

[162] Li, L.; Kang, E.; Neoh, K.; "Preparation of well-defined polymer-silicon wafer hybrids via surface-initiated RAFT-mediated process", *Applied Surface Science*, **2008**, *254*, 2600-2604.

[163] Wang, Z.; Zhao, Z.; Zhang, J.; Li, Z.; Gao, Y.; Wang, C.; Zhang, H.; Yang, B.; "Multifunctional nanoparticles/silica microsphere assemblies using polyglycidyl methacrylate shells as supports", *Journal of Colloid and Interface Science*, **2009**, *339*, 83-90.

[164] Washburn, E. W.; "The Dynamics of Capillary Flow", *Physical Review*, **1921**, *17*, 273.

[165] Foschiera, J. L.; Pizzolato, T. M.; Benvenutti, E. V.; "FTIR thermal analysis on organofunctionalized silica gel", *Journal of the Brazilian Chemical Society*, **2001,** *12*, 159-164.

[166] Matsoukas, T.; Gulari, E.; "Dynamics of growth of silica particles from ammonia-catalyzed hydrolysis of tetra-ethyl-orthosilicate", *Journal of Colloid and Interface Science*, **1988**, *124*, 252-261.

[167] Silverstein, R. M.; Bassler, G. C.; "Spectrometric identification of organic compounds", *John Wiley and Sons*, **1967,** New York.

[168] Lenza, R. F. S.; Vasconcelos, W. L.; "Preparation of Silica by Sol-Gel Method Using Formamide", *Materials Research*, **2001**, *4*, 189-194.

[169] Esteves, A. C. C.; "Síntese e caracterização de nanocompósitos funcionais de matriz polimérica", Tese de Doutoramento, Universidade de Aveiro, **2007,** Aveiro.

[170] Hunter, R. J.; "Foundations of Colloid Science", *Oxford University Press*, **2001,** Oxford: U.K.

[171] Kobayashi, M.; Juillerat, F.; Galletto, P.; Bowen, P.; Borkovec, M.; "Aggregation and charging of colloidal silica particles: effect of particle size", *Langmuir*, **2005**, *21*, 5761-5769.

[172] Johnson, A.-C. J. H.; Greenwood, P.; HagstroÌˆm, M.; Abbas, Z.; Wall, S.; "Aggregation of nanosized colloidal silica in the presence of various alkali cations investigated by the electrospray technique", *Langmuir*, **2008**, *24*, 12798-12806.

[173] Coates, J.; "Interpretation of infrared spectra, a practical approach", in Encyclopedia of Analytical Chemistry, Ed: Meyers, R. A.; *John Wiley & Sons* **2000,** Chichester.

[174] Moraes, S. L.; Rezende, M. O. O.; "Determinação da concentração micelar crítica de ácidos húmicos por medidas de condutividade e espectroscopia", *Quimica Nova*, **2004**, *27*, 701-705.

[175] Ananthalakshmi, N. R.; Wadgaonkar, P. P.; Sivaram, S.; Varma, I. K.; "Thermal behaviour of glycidyl methacrylate homopolymers and copolymers", *Journal of Thermal Analysis and Calorimetry*, **1999**, *58*, 533-539.

[176] Huang, J.-W.; Kang, C.-C.; "Unusual thermal degradation behavior of PEGMA in air at different heating rates", *Polymer Journal*, **2004**, *36*, 574-576.

[177] Galgali, G.; Ramesh, C.; Lele, A.; "A rheological study on the kinetics of hybrid formation in polypropylene nanocomposites", *Macromolecules*, **2001**, *34*, 852-858.

[178] Krishnamoorti, R.; Yurekli, K.; "Rheology of polymer layered silicate nanocomposites", *Current Opinion in Colloid and Interface Science*, **2001**, *6*, 464-470.

[179] Solomon, M. J.; Almusallam, A. S.; Seefeldt, K. F.; Somwangthanaroj, A.; Varadan, P.; "Rheology of polypropylene/clay hybrid materials", *Macromolecules*, **2001**, *34*, 1864-1872.

[180] Zhang, Q.; Archer, L. A.; "Poly(ethylene oxide)/silica nanocomposites: Structure and rheology", *Langmuir*, **2002**, *18*, 10435-10442.

[181] Du, F.; Scogna, R. C.; Zhou, W.; Brand, S.; Fischer, J. E.; Winey, K. I.; "Nanotube networks in polymer nanocomposites: rheology and electrical conductivity", *Macromolecules*, **2004**, *37*, 9048-9055.

[182] Paquien, J. N.; Galy, J.; Gerard, J. F.; Pouchelon, A.; "Rheological studies of fumed silica-polydimethylsiloxane suspensions", *Colloids and Surfaces A: Physicochemical and Engineering Aspects*, **2005**, *260*, 165-172.

[183] Buscall, R.; Mills, P.; Goodwin, J. W.; Larson, D. W.; "Scaling behaviour of rheology aggregate networks formed from colloidal particles", *Journal of the Chemical Society, Faraday Transactions*, **1988**, *84* 4249-4260.

[184] Shih, W. H.; Shih, W. Y.; Kim, S. J.; Lui, J.; Aksay, I. A.; "Scaling behaviour of elasticity properties of colloidal gels", *Physical Review A*, **1994**, *42*, 4772-4779.

[185] Cassagnau, P.; "Melt rheology of organoclay and fumed silica nanocomposites", *Polymer*, **2008**, *49*, 2183-2196.

[186] Chatterjee, T.; Krishnamoorti, R.; "Steady shear response of carbon nanotube networks dispersed in poly(ethylene oxide)", *Macromolecules*, **2008**, *41*, 5333-5338.

[187] Trappe, V.; Weitz, D. A.; "Scaling of the viscoelasticity of weakly attractive particles", *Physical Review Letters*, **2000**, *85*, 449-452.

[188] Pashkovski, E. E.; Masters, J. G.; Mehreteab, A.; "Viscoelastic scaling of colloidal gels in polymer solutions", *Langmuir*, **2003**, *19*, 3589-3595.

[189] Sternstein, S. S.; Zhu, A. J.; "Reinforcement mechanism of nanofilled polymer melts as elucidated by nonlinear viscoelastic behaviour", *Macromolecules*, **2002**, *35*, 7262-7273.

[190] Salaniwal, S.; Kumar, S. K.; Douglas, J. F.; "Amorphous solidification in polymer-platelet nanocomposites", *Physical Review Letters*, **2002**, *89*, 258301-258304.

[191] Trompette, J. L.; Bordes, C.; "Rheological study of the gelation kinetics of a concentrated latex suspension in the presence of nonadsorbing polymer chains", *Langmuir*, **2000**, *16*, 9627-9633.

[192] Burns, J. L.; Yan, Y.; Jameson, G. J.; Biggs, S.; "The effect of molecular weight of nonadsorbing polymer on the structure of depletion-induced flocs", *Journal of Colloid and Interface Science*, **2002**, *247*, 24-32.

[193] Trompette, J. L.; Charnay, C.; Partyka, S.; "Storage stability and rheological behaviour of talc−polyacrylylglycinamide gelified suspensions", *Langmuir*, **1998**, *14*, 4475-4481.

[194] Otsubo, Y.; "Rheological behaviour of suspensions flocculated by weak bridging of polymer coils", *Journal of Colloid and Interface Science*, **1999**, *215*, 99-105.

[195] Surve, M.; Pryamitsyn, V.; Ganesan, V.; "Polymer-bridged gels of nanoparticles in solutions of adsorbing polymers", *Journal of Chemical Physics*, **2006**, *125*, 064903.

[196] Lapasin, R.; Pricl, S.; "Rheology of industrial polysaccharides: Theory and applications ", *Blackie Academic & Professional*, **1999,** Padstow, Cornwall.

[197] Williams, P. A.; Phillips, G. O.; "Handbook of hydrocolloids", *Woodhead Publishing Limited*, **2000,** Cambridge.

[198] Renaud, M.; Belgacem, M. N.; Rinaudo, M.; "Rheological behaviour of polysaccharide aqueous solutions", *Polymer*, **2005**, *46*, 12348-12358.

[199] Lopes da Silva, J. A.; Cardoso, S. M.; Tavares, C.; Monteiro, S. R.; "Biopolímero e biomateriais", in Química de Polímeros, Ed: Seixas de Melo, J. S.; Moreno, M. J.; Burrows, H. D.; Gil, M. H.; *Imprensa da Universidade de Coimbra*, **2004,** Coimbra.

[200] Lopes da Silva, J. A.; Coutinho, J. A. P.; "Dynamic rheological analysis of the gelation behaviour of waxy crude oils", *Rheologica Acta*, **2004**, *43*, 433-441.

[201] Barnes, H. A.; Hutton, J. F.; Walters, K.; "An introduction to rheology ", *Elsevier*, **1991,** Amsterdã.

[202] Graessley, W. W.; "The entanglement concept in polymer rheology", *Advances in Polymer Science*, **1974**, *16*, 1-179.

[203] Castro, A. G.; Covas, J. A.; Diogo, A. C.; "Reologia e suas Aplicações Industriais", *Instituto Piaget*, **2001,** Lisboa.

[204] Morris, E. R.; Cutler, A. N.; Ross-Murphy, S. B.; Rees, D. A.; Price, J.; "Concentration and shear rate dependence of viscosity in random coil polysaccharide solutions", *Carbohydrate Polymers*, **1981**, *1*, 5-21.

[205] Lopes da Silva, J. A.; Rao, M. A.; "Pectins: structure, funcionalities, and uses", in Food Polysaccharides and their Applications, Ed: Stephen, A. M.; Phillips, G. O.; Williams, P. A.; *Taylor and Francis*, **2006,** New York.

[206] Lopes da Silva, J. A.; Rao, M. A.; "Rheological behavior of food gels", in Rheology of Fluid and Semisolid Foods: Principles and Applications, Ed: Rao, M. A.; *Spring Science and Business Media*, **2007,** New York, USA.

[207] Hermans, P. H.; "Gels", in Colloid Science, Ed: Kruyt, H. R.; *Elsevier publishing Company*, **1949,** Amsterdam, The Netherlands.

[208] Burchard, W.; Ross-Murphy, S. B.; "Physical gels from synthetic and biological macromolecules. ", in Physical Networks: Polymers and Gels, Ed: Burchard, W.; Ross-Murphy, S. B.; *Elsevier*, **1990,** Oxford.

[209] Scborsch, C.; Gamier, C.; Doublier, J.-L.; "Viscoelastic properties of xanthan/galactomannan mixtures: comparison of guar gum with locust bean gum", *Carbohydrate Polymers*, **1997**, *34*, 165-175.

[210] Clark, A. H.; Ross-Murphy, S. B.; "Structural and mechanical properties of biopolymer gels ", *Advanced in Polymer Science*, **1987**, *83*, 57-192.

[211] Flory, P. J.; "Principles of Polymer Chemistry", *Cornelle University*, **1953,** New York: USA.

[212] Tung, C.-Y. M.; Dynes, P. J.; "Relationship between viscoelastic properties and gelation in thermosetting systems", *Journal of Applied Polymer Science*, **1982**, *27*, 569-574.

[213] Winter, H. H.; Chambon, F.; "Analysis of linear viscoelasticity of a crosslinking polymer at the gel point", *Journal of Rheology*, **1986**, *30*, 367-382.

[214] Tanner, R. I.; Walters, K.; "Rheology: an Historical Perspective", *Elsevier Science B.V.*, **1998,** Amsterdam, The Netherlands.

[215] Barnes, H. A.; "A handbook of elementary rheology", *University of Wales Institute of Non-newtonian Fluid Mechanics, Department of Mathematics*, **2000,** Wales.

[216] Shenoy, A. V.; "Rheology of Filled Polymer Systems ", *Springer*, **1999,** Dordrecht, The Netherlands.

[217] Einstein, A.; "Eine neue Bestimmung der Moleküldimensionen, Ann. Physik, 19, 289-306 (1906). A new determination of molecular dimensions, Ann. Physik, 34, 591-592 (1911). Investigation on the theory of the Brownian movement, Dover Publications, USA (1956).",

[218] Ward, S. G.; Whitmore, R. L.; "Studies of the viscosity and sedimentation of suspensions Part 1: The viscosity of suspension of spherical particles", *British Journal of Applied Physics*, **1950**, *1* 286-290.

[219] Defeng, W.; Chixing, Z.; Wei, Y.; Xie, F.; "Effect of flocculated structure on rheology of poly(butylene terephthalate)/clay nanocomposites", *Journal of Polymer Science Part B: Polymer Physics*, **2005**, *43*, 2807-2818.

[220] Napper, D. H.; Netschey, A.; "Studies of the steric stabilization of colloidal particles", *Journal of Colloid and Interface Science*, **1971**, *37*, 528-535.

[221] Fryling, C. F.; "The viscosity of small particle, electrolyte- and soap-deficient synthetic latex gels", *Journal of Colloid Science*, **1963**, *18*, 713-732.

[222] Barnes, H. A.; "A review of the slip (wall depletion) of polymer solutions, emulsions and particle suspensions in viscometers: its cause, character, and cure", *Journal of Non-Newtonian Fluid Mechanics*, **1995**, *56*, 221-251.

[223] Berry, V. K.; "Transmission electron microscopy and related tecniques in the structure and morphological characterization of polymer nanocomposites", in Polymer Nanocomposites Handbook, Ed: Gupta, R. K.; Kennel, E.; Kim, K.-J.; *CRC Press*, **2009,** New York.

[224] McKenna, B. M.; "Texture in Food. Volume 1: Semi-Solid Foods", *Woodhead Publishing*, **2003,** Cambridge.

[225] Neukom, H.; "Galactomannans: properties and Applications", *Lebensm.-Wiss. u.-Technol.*, **1989**, *22*, 41-45.

[226] Seaman, J. K.; "Locust Guar Gum", in Handbook of Water-Soluble Gums & Resins, Ed: in Davidson, R. L.; *McGraw-Hill, Inc.*, **1980,** New York.

[227] Dakia, P. A.; Blecker, C.; Robert, C.; Wathelet, B.; Paquot, M.; "Composition and physicochemical properties of locust bean gum extracted from whole seeds by acid or water dehulling pre-treatment", *Food Hydrocolloids*, **2008**, *22*, 807-818.

[228] Daas, P. J. H.; Schols, H. A.; de Jongh, H. H. J.; "On the galactosyl distribution of commercial galactomannans", *Carbohydrate Research*, **2000**, *329*, 609-619.

[229] Richardson, P. H.; Willmer, J.; Foster, T. J.; "Dilute solution properties of guar and locust bean gum in sucrose solutions", *Food Hydrocolloids*, **1998**, *12*, 339-348.

[230] Dea, I. C. M.; Morrison, A.; "Chemistry and Interactions of seed galactomannans", *Advances in Carbohydrate Chemistry and Biochemistry*, **1975**, *31*, 241-312.

[231] Deuel, H.; Neukom, H.; "Some properties of locust bean gum", *Natural plant hydrocolloids (Advances in Chemistry Series)*, **1954**, *11*, 51-61.

[232] Dea, I. C. M.; Morris, E. R.; Rees, D. A.; Welsh, E. J.; Branes, H. A.; Price, J.; "Associations of like and unlike polysaccharides: mechanism and specificity in galactomannans, interacting bacterial polysaccharides and related systems", *Carbohydrate Research*, **1977**, *57*, 249-272.

[233] Richardson, P. H.; Clark, A. H.; Russell, A. L.; Aymard, P.; Norton, I. T.; "Galactomannan gelation: a thermal and rheological investigation analyzed using the cascade model", *Macromolecules*, **1999**, *32*, 1519-1527.

[234] Lazaridou, A.; Biliaderis, C. G.; Izydorczyk, M. S.; "Structural characteristics and rheological properties of locust bean galactomannans: a comparison of samples from different carob tree populations", *Journal of the Science of Food and Agriculture*, **2001**, *81*, 68-75.

[235] Rizzo, V.; Tomaselli, F.; Gentile, A.; La Malfa, S.; Maccarone, E.; "Rheological properties and sugar composition of locust bean gum from different carob varieties (*Ceratonia siliqua L.*)", *Journal of Agricultural and Food Chemistry*, **2004**, *52*, 7925-7930.

[236] McCleary, B. V.; Dea, I. C. M.; Windust, J.; Cooke, D.; "Interaction properties of -galactose-depleted guar galactomannan samples", *Carbohydrate Polymers*, **1984**, *4*, 253-270.

[237] Kulicke, W.-M.; Reinhardt, U.; Arendt, O.; "Rheo-mechanical and rheo-optical investigations of locust bean gum/kappa-carrageenan mixtures", *Macromolecular Rapid Communications*, **1998**, *19*, 219-222.

[238] Casas, J. A.; Garcia-Ochoa, F.; "Viscosity of solutions of xanthan/locust bean gum mixtures", *Journal of the Science of Food and Agriculture*, **1999**, *79*, 25-31

[239] Arda, E.; Kara, S.; Pekcan, Ö.; "Synergistic effect of the locust bean gum on the thermal phase transitions of [kappa]-carrageenan gels", *Food Hydrocolloids*, **2009**, *23*, 451-459.

[240] http://www.cpkelco.com/products-locust-bean-gum.html, cited in 16/04/2010.

[241] Sittikijyothin, W.; Torres, D.; Gonçalves, M. P.; "Modelling the rheological behaviour of galactomannan aqueous solutions", *Carbohydrate Polymers*, **2005**, *59*, 339-350.

[242] Smyth, C.; Kudryashov, E. D.; Buckin, V.; "High-frequency shear and volume viscoelastic moduli of casein particle gel", *Colloids and Surfaces A: Physicochemical and Engineering Aspects*, **2001**, *183-185*, 517-526.

[243] Lopes-da-Silva, J. A.; Santos, D. M. J.; Freitas, A.; Brites, C.; Gil, A. M.; "Rheological and nuclear magnetic resonance (NMR) study of the hydration and heating of undeveloped wheat doughs", *Journal of Agricultural and Food Chemistry*, **2007**, *55*, 5636-5644.

[244] Bower, C.; Gallegos, C.; Mackley, M. R.; Madiedo, J. M.; "The rheological and microstructural characterisation of the non-linear flow behaviour of concentrated oil-in-water emulsions", *Rheologica Acta*, **1999**, *38*, 145-159.

[245] Yziquel, F.; Carreau, P. J.; Tanguy, P. A.; "Non-linear viscoelastic behaviour of fumed silica suspensions", *Rheologica Acta*, **1999**, *38*, 14-25.

[246] Kinloch, I. A.; Roberts, S. A.; Windle, A. H.; "A rheological study of concentrated aqueous nanotube dispersions", *Polymer*, **2002**, *43*, 7483-7491.

[247] Craciun, L.; Carreau, P. J.; Heuzey, M. C.; Van de Ven, T. G. M.; Moan, M.; "Rheological properties of concentrated latex suspensions of poly(styrene-butadiene)", *Rheologica Acta*, **2003**, *42*, 410-420.

[248] Raghavan, S. R.; Khan, S. A.; "Shear-induced microstructural changing in flocculated suspensions of fumed silica", *Journal of Rheology*, **1995**, *39*, 1311-1325.

[249] Miyazaki, K.; Wyss, H. M.; Weitz, D. A.; Reichman, D. R.; "Nonlinear viscoelasticity of metastable complex fluids", *Europhysics Letters*, **2006**, *75*, 915-921.

[250] Ferry, J. D.; "Viscoelastic Properties of Polymers", *John Wiley & Sons*, **1980,** New York.

[251] Potschke, P.; Fornes, T. D.; Paul, D. R.; "Rheological behaviour of multiwalled carbon nanotube/polycarbonate composites", *Polymer*, **2002**, *43*, 3247-3255.

[252] Ren, J.; Krishnamoorti, R.; "Nonlinear viscoelastic properties of layered-silicate-based intercalated nanocomposites", *Macromolecules*, **2003**, *36* 4443-4451.

[253] Barnes, H. A.; "The yield stress-a review or παντα, ρει-everything flows?", *Journal of Non-Newtonian Fluid Mechanics*, **1999**, *81*, 133-178.

[254] Malkin, A. Y.; "Rheology of filled polymers", *Advances in Polymer Science*, **1990**, *96*, 69-97.

[255] Odier, A.; "Mémoire sur la Composition Chimique des Parties Cornées des Insectes", *Mémoires de la Société d'Histoire Naturelle de Paris*, **1823**, *1*, 29-42.

[256] Cauchie, H. M.; "An attempt to estimate crustacean chitin production in the hydrosphere", in Advances in Chitin Science, Ed: Domard, A.; Roberts, G. A. F.; Vårum, K. M.; *Jacques André Publisher*, **1998,** Lyon.

[257] Peniche, C.; Argüelles-Monal, W.; Goycoolea, F. M.; "Chitin and chitosan: major sources, properties and applications", in Monomers, Polymers and Composites from Renewable Resources, Ed: Belgacem, M. N.; Gandini, A.; *Elsevier*, **2008,** Amsterdam.

[258] Knorr, D.; "Recovery and utilization of chitin and chitosan in food processing waste management", *Food technology*, **1991**, *45* 114-122.

[259] Vårum, K. M.; Ottøy, M. H.; Smidsrød, O.; "Water-solubility of partially N-acetylated chitosans as a function of pH: effect of chemical composition and depolymerisation", *Carbohydrate Polymers*, **1994**, *25*, 65-70.

[260] Aiba, S.-I.; "Studies on chitosan: 3. Evidence for the presence of random and block copolymer structures in partially N-acetylated chitosans", *International Journal of Biological Macromolecules*, **1991**, *13*, 40-44.

[261] Goosen, M. F. A.; "Applications of Chitin and Chitosan", *Technomic Publishing Company, Inc.*, **1997,** Lancaster, Pennsylvania: U.S.A.

[262] Hwang, J. K.; Shin, H. H.; "Rheological properties of chitosan solutions", *Korea-Australia Rheology Journal*, **2001**, *12*, 175-179.

[263] Terbojevich, M., Muzzarelli, R. A. A. ; "Chitosan", in Handbook of hydrocolloids, Ed: Phillips, G. O., Williams, P. A.; *Woodhead Publishing*, **2000,** UK.

[264] Rinaudo, M.; "Chitin and chitosan: Properties and applications", *Progress in Polymer Science*, **2006**, *31*, 603-632.

[265] Philippova, O. E.; Volkov, E. V.; Sitnikova, N. L.; Khokhlov, A. R.; Desbrieres, J.; Rinaudo, M.; "Two types of hydrophobic aggregates in aqueous solutions of chitosan and its hydrophobic derivative", *Biomacromolecules*, **2001**, *2*, 483-490.

[266] Brugnerotto, J.; Desbrières, J.; Heux, L.; Mazeau, K.; Rinaudo, M.; "Overview on structural characterization of chitosan molecules in relation with their behavior in solution", *Macromolecular Symposia*, **2001**, *168*, 1-20.

[267] Mazeau, K.; Pérez, S.; Rinaudo, M.; "Predicted influence of N- acetyl group content on the conformational extension of chitin and chitosan chains", *Journal of Carbohydrate Chemistry*, **2000**, *19*, 1269 - 1284.

[268] Mazeau, K.; Rinaudo, M.; "The prediction of the characteristics of some polysaccharides from molecular modeling. Comparison with effective behavior", *Food Hydrocolloids*, **2004**, *18*, 885-898.

[269] Brugnerotto, J.; Lizardi, J.; Goycoolea, F. M.; Argüelles-Monal, W.; Desbrières, J.; Rinaudo, M.; "An infrared investigation in relation with chitin and chitosan characterization", *Polymer*, **2001**, *42*, 3569-3580.

[270] Brunn, P. O.; Vorwerk, J.; "Determination of the steady-state shear viscosity from measurements of the apparent viscosity for some common types of viscometers", *Rheologica Acta*, **1993**, *32* 380-397.

[271] Maria, M.; "Rheological characteristics of semi-dilute chitosan solutions", *Macromolecular Chemistry and Physics*, **1997**, *198*, 471-484.

[272] Cho, J.; Heuzey, M.-C.; Bégin, A.; Carreau, P. J.; "Viscoelastic properties of chitosan solutions: effect of concentration and ionic strength", *Journal of Food Engineering*, **2006**, *74*, 500-515.

[273] No, H. K.; Kim, S. H.; Lee, S. H.; Park, N. Y.; Prinyawiwatkul, W.; "Stability and antibacterial activity of chitosan solutions affected by storage temperature and time", *Carbohydrate Polymers*, **2006**, *65*, 174-178.

[274] Wang, W.; Xu, D.; "Viscosity and flow properties of concentrated solutions of chitosan with different degrees of deacetylation", *International Journal of Biological Macromolecules*, **1994**, *16*, 149-152.

[275] Chen, Y. C.; Wang, C. H.; Lai, L. S.; Lin, K. W.; "Rheological properties of chitosan and its interaction with porcine myofibrillar proteins as influenced by chitosan's degree of deacetylation and concentration", *Journal of Food Science*, **2003**, *68*, 826-831.

[276] Muzzarelli, R. A. A.; Tomasetti, M.; Ilari, P.; "Deploymerization of chitosan with the aid of papain", *Enzyme and Microbial Technology*, **1994**, *16*, 110-114.

[277] Yao, K. D.; Peng, T.; Goosen, M. F. A.; Min, J. M.; He, Y. Y.; "pH-Sensitivity of hydrogels based on complex forming chitosan: polyether interpenetrating polymer network", *Journal of Applied Polymer Science*, **1993**, *48*, 343-354.

[278] Kim, J. H.; Lee, Y. M.; "Synthesis and properties of diethylaminoethyl chitosan", *Polymer*, **1993**, *34*, 1952-1957.

[279] Nyström, B.; Kjøniksen, A.-L.; Iversen, C.; "Characterization of association phenomena in aqueous systems of chitosan of different hydrophobicity", *Advances in Colloid and Interface Science*, **1999**, *79*, 81-103.

[280] Hirano, S.; "Chitin and chitosan as novel biotechnological materials", *Polymer International*, **1999**, *48*, 732-734.

[281] Aubry, T.; Largenton, B.; Moan, M.; "Rheological Study of Fumed Silica Suspensions in Chitosan Solutions", *Langmuir*, **1999**, *15*, 2380-2383.

[282] Smitha, S.; Shajesh, P.; Mukundan, P.; Warrier, K. G. K.; "Sol-gel synthesis of biocompatible silica-chitosan hybrids and hydrophobic coatings", *Journal of Materials Research*, **2008**, *23* 2053-2060.

[283] Wang, G.-H.; Zhang, L.-M.; "Using novel polysaccharideo-silica hybrid material to construct an amperometric biosensor for hydrogen peroxide", *The Journal of Physical Chemistry B*, **2006**, *110*, 24864-24868.

[284] Desbrieres, J.; "Viscosity of semiflexible chitosan solutions: influence of concentration, temperature, and role of intermolecular interactions", *Biomacromolecules*, **2002**, *3*, 342-349.

[285] Russel, W. B.; Saville, D. A.; Schowalter, W. R.; "Colloidal Dispersions", *Cambridge University Press*, **1989,** Cambridge.

[286] Dragan, E. S.; "New trends in ionic (Co)polymers and hybrids ", *Nova Publisher*, **2007,** New York.

[287] So, J.-H.; Oh, W.-K.; Yang, S.-M.; "Microstructure and phase behavior of concentrated silica particle suspensions", *Korean Journal of Chemical Engineering*, **2004**, *21*, 921-928.

[288] Winter, H.; "Three views of viscoelasticity for Cox–Merz materials", *Rheologica Acta*, **2009**, *48*, 241-243.

[289] Larson, R.; "The structure and rheology of complex fluids", *Oxford University Press*, **1999,** New York.

[290] Liang, S.; Liu, L.; Huang, Q.; Yam, K. L.; "Unique rheological behavior of chitosan-modified nanoclay at highly hydrated state", *Journal of Physical Chemistry B*, **2009**, *113*, 5823-5828.

[291] Casas, J. A.; Santos, V. E.; García-Ochoa, F.; "Xanthan gum production under several operational conditions: molecular structure and rheological properties", *Enzyme and Microbial Technology*, **2000**, *26*, 282-291.

[292] García-Ochoa, F.; Santos, V. E.; Casas, J. A.; Gómez, E.; "Xanthan gum: production, recovery, and properties", *Biotechnology Advances*, **2000**, *18*, 549-579.

[293] Paradossi, G.; Brant, D. A.; "Light scattering study of a series of xanthan fractions in aqueous solution", *Macromolecules*, **1982**, *15*, 874-879.

[294] Paoletti, S.; Cesàro, A.; Delben, F.; "Thermally induced conformational transition of xanthan polyelectrolyte", *Carbohydrate Research,*, **1983**, *123*, 173-178.

[295] Horton, D.; Hols, O.; Walaszak, Z.; Wernau, W. C.; "Structural and biosynthetic studies on xanthan by 13C-N.M.R. spectroscopy", *Carbohydrate Research*, **1985**, *141*, 340-346.

[296] Morris, E. R.; Rees, D. A.; Young, G.; Walkinshaw, M. D.; Darke, A.; "Order-disorder transition for a bacterial polysaccharide in solution. A role for polysaccharide conformation in recognition between Xanthomonas pathogen and its plant host", *Journal of Molecular Biology*, **1977**, *110*, 1-16.

[297] Milas, M.; Rinaudo, M.; "Conformational investigation on the bacterial polysaccharide xanthan", *Carbohydrate Research*, **1979**, *76*, 189-196.

[298] Liu, W.; Norisuye, T.; "Thermally induced conformation change of xanthan: interpretation of viscosity behaviour in 0.01 aqueous sodium chloride", *International Journal of Biological Macromolecules*, **1988**, *10*, 44-50.

[299] Matsuda, Y.; Biyajima, Y.; Sato, T.; "Thermal Denaturation, Renaturation, and Aggregation of a Double-Helical Polysaccharide Xanthan in Aqueous Solution", *Polymer Journal*, **2009**, *41*, 526-532.

[300] Rochefort, W. E.; Middleman, S.; "Rheology of xanthan gum: salt, temperature, and strain effects in oscillatory and steady shear experiments", *Journal of Rheology*, **1987**, *31*, 337-369.

[301] Muller, G.; Anhourrache, M.; Lecourtier, J.; Chauveteau, G.; "Salt dependence of the conformation of a single stranded xanthan", *International Journal of Biological Macromolecules*, **1986**, *8*, 167.

[302] Rinaudo, M.; Milas, M.; "Xanthan properties in aqueous solution", *Carbohydrate Polymers*, **1982**, *2*, 264-269.

[303] Milas, M.; Rinaudo, M.; Duplessix, R.; Borsali, R.; Lindner, P.; "Small angle neutron scattering from polyelectrolyte solutions: from disordered to ordered xanthan chain conformation", *Macromolecules*, **1995**, *28*, 3119-3124.

[304] Rodd, A. B.; Dunstan, D. E.; Boger, D. V.; "Characterisation of xanthan gum solutions using dynamic light scattering and rheology", *Carbohydrate Polymers*, **2000**, *42*, 159-174.

[305] Ross-Murphy, S. B.; Morris, V. J.; Morris, E. R.; "Molecular viscoelastic of xanthan polysaccharide", *Faraday Symposia of the Chemical Society*, **1983**, *18*, 115-129.

[306] Tako, M.; Nakamura, S.; "Rheological properties of deacetylated xanthan in aqeous media", *Agricultural Biology and Chemistry*, **1984**, *48*, 2987-2993.

[307] Peters, H.-U.; Suh, I. S.; Schumpe, A.; Deckwer, W. D.; "The pyruvate content of xanthan polysaccharide produced under oxygen limitation", *Biotechnology Letters*, **1993**, *15*, 565-566.

[308] Whitcomb, P. J.; Macosko, C. W.; "Rheology of xanthan gum", *Journal of Rheology*, **1978**, *22*, 493-505.

[309] Cotrell, I. W.; Kang, K. S.; Kovacs, P.; "Xanthan gum", in Handbook of Water-Soluble Gums and Resins, Ed: Davidson, R. L.; *McGraw-Hill*, **1980,** NY.

[310] Tam, K. C.; Tiu, C.; "Steady and Dynamic Shear Properties of Aqueous Polymer Solutions", *Journal of Rheology*, **1989**, *33*, 257-280.

[311] Podolsak, A. K.; Tiu, C.; Saeki, T.; Usui, H.; "Rheological properties and some applications for rhamsan and xanthan gum solutions", *Polymer International*, **1996**, *40*, 155-167.

[312] Giboreau, A.; Cuvelier, G.; Launay, B.; "Rheological behaviour of three biopolymer/water systems, with emphasis on yield stress and viscoelastic properties", *Journal of Texture Studies*, **1994**, *25*, 119-138.

[313] Richardson, R. K.; Ross-Murphy, S. B.; "Non-linear viscoelasticity of polysaccharide solutions. 2: Xanthan polysaccharide solutions", *International Journal of Biological Macromolecules*, **1987**, *9*, 257-264.

[314] Speers, R. A.; Tung, R. A.; "Concentration and temperature dependence of flow behaviour of xanthan gum dispersions", *Journal of Food Science*, **1986**, *51*, 96-103.

[315] Rosalan, S.; England, R.; "Review of xanthan gum production from unmodified starches by *Xantomonas campestris sp.*", *Enzyme and Microbial Technology*, **2006**, *39*, 197-207.

[316] Sutherland, I.; "A sticky business. Microbial polysaccharides: current products and future trends", *Microbiology Today*, **2002**, *29*, 70-71.

[317] Silva, M. F.; Fornari, R. C. G.; Mazutti, M. A.; Oliveira, D.; Padilha, F. F.; Cichoski, A. J.; Cansian, R. L.; Di Luccio, M.; Treichel, H.; "Production and characterization of xantham gum by *Xanthomonas campestris* using cheese whey as sole carbon source", *Journal of Food Engineering*, **2009**, *90*, 119-123.

[318] Sanderson, G. R.; "Applications of xanthan gum", *British Polymer Journal*, **1981**, *13*, 71-75.

[319] Han, D.-K.; Yang, C.-Z.; Zhang, Z.-Q.; Lou, Z.-H.; Chang, Y.-I.; "Recent development of enhanced oil recovery in China", *Journal of Petroleum Science and Engineering*, **1999**, *22*, 181-188.

[320] Lazar, I.; Petrisor, I. G.; Yen, T. F.; "Microbial Enhanced Oil Recovery (MEOR)", *Petroleum Science and Technology*, **2007**, *25*, 1353 - 1366.

[321] Oviatt, J. H. W.; Brant, D. A.; "Thermal treatment of semi-dilute aqueous xanthan solutions yields weak gels with properties resembling hyaluronic acid", *International Journal of Biological Macromolecules*, **1993**, *15*, 3-10.

[322] Oliveira, F. C.; Lopes-da-Silva, J. A.; Barros-Timmons, A. M. in *Rheological Properties of SiO_2/Polysaccharides Nanocomposites*, World Polymer Congress, Rio de Janeiro-Brazil, **2006**.

[323] Trappe, V.; Prasad, V.; Cipelletti, L.; Segre, P. N.; Weitz, D. A.; "Jamming phase diagram for attractive particles", *Nature*, **2001**, *411*, 772-775.

[324] Selke, S. E. M.; "Understanding plastics packaging technology", *Carl Hanser Verlag*, **1997,** Munich.

[325] Osborn, K. R.; Jenkins, W. A.; "Plastic Films: Technology and Packaging Applications", *CRC Press*, **1992,** Boca Ranton.

[326] Abdel-Bary, E.; "Handbook of plastic films", *Rapra Technology Limited*, **2003,** Shrewsbury.

[327] Shanks, R.; "Technology of polyolefin film production", in Handbook of Plastic Films, Ed: Abdel-Bary, E. M.; *Rapra Technology Limited*, **2003,** Shrewsbury: U.K.

[328] Min, S.; Zhang, Q. H.; "Packaging for non-thermal food processing", in Innovations in Food Packaging Ed: Han, J. H.; *Elsevier Academic Press*, **2005,** London: U.K.

[329] Ozen, B. F.; Floros, J. D.; "Effects of emerging food processing techniques on the packaging materials", *Trends in Food Science & Technology*, **2001**, *12*, 60-67.

[330] Krajewska, B.; "Membrane-based processes performed with use of chitin/chitosan materials", *Separation and Purification Technology*, **2005**, *41*, 305-312.

[331] Kurita, K.; "Controlled functionalization of the polysaccharide chitin", *Progress in Polymer Science*, **2001**, *26*, 1921-1971.

[332] Santos, C.; Seabra, P.; Veleirinho, B.; Delgadillo, I.; Lopes da Silva, J. A.; "Acetylation and molecular mass effects on barrier and mechanical properties of shortfin squid chitosan membranes", *European Polymer Journal*, **2006**, *42*, 3277-3285.

[333] Caner, C.; Vergano, P. J.; Wiles, J. L.; "Chitosan Film Mechanical and Permeation Properties as Affected by Acid, Plasticizer, and Storage", *Journal of Food Science*, **1998**, *63*, 1049-1053.

[334] Park, S. Y.; Lin, X. Q.; Sano, Y.; "Characterization of chitosan film and structure in solution", in Hydrocolloids Part 1, Ed: Nishinari, K.; *Elsevier Science* **2000,** Amsterdam.

[335] Park, S. Y.; Marsh, K. S.; Rhim, J. W.; "Characteristics of different molecular weight chitosan films affected by the type of organic solvents", *Journal of Food Science*, **2002**, *67*, 194-197.

[336] Clasen, C.; Wilhelms, T.; Kulicke, W. M.; "Formation and characterization of chitosan membranes", *Biomacromolecules*, **2006**, *7*, 3210-3222.

[337] Ziani, K.; Oses, J.; Coma, V.; Maté, J. I.; "Effect of the presence of glycerol and Tween 20 on the chemical and physical properties of films based on chitosan with different degree of deacetylation", *Food Science and Technology*, **2008**, *41*, 2159-2165.

[338] Srinivasa, P. C.; Ramesh, M. N.; Tharanathan, R. N.; "Effect of plasticizers and fatty acids on mechanical and permeability characteristics of chitosan films", *Food Hydrocolloids*, **2007**, *21*, 1113-1122.

[339] Srinivasa, P. C.; Ramesh, M. N.; Kumar, K. R.; Tharanathan, R. N.; "Properties of chitosan films prepared under different drying conditions", *Journal of Food Engineering*, **2004**, *63*, 79-85.

[340] Sionkowska, A.; "Effects of solar radiation on collagen and chitosan films", *Journal of Photochemistry and Photobiology B: Biology*, **2006**, *82*, 9-15.

[341] Srinivasa, P. C.; Ravi, R.; Tharanathan, R. N.; "Effect of storage conditions on the tensile properties of eco-friendly chitosan films by response surface methodology", *Journal of Food Engineering*, **2007**, *80*, 184-189.

[342] Thanpitcha, T.; Sirivat, A.; Jamieson, A. M.; Rujiravanit, R.; "Preparation and characterization of polyaniline/chitosan blend film", *Carbohydrate Polymers*, **2006**, *64*, 560-568.

[343] Donoso, J. P.; Lopes, L. V. S.; Pawlicka, A.; Fuentes, S.; Retuert, P. J.; González, G.; "Nuclear magnetic resonance study of PEO-chitosan based polymer electrolytes", *Electrochimica Acta*, **2007**, *53*, 1455-1460.

[344] Liu, F.; Qin, B.; He, L.; Song, R.; "Novel starch/chitosan blending membrane: Antibacterial, permeable and mechanical properties", *Carbohydrate Polymers*, **2009**, *78*, 146-150.

[345] Shih, C.-M.; Shieh, Y.-T.; Twu, Y.-K.; "Preparation and characterization of cellulose/chitosan blend films", *Carbohydrate Polymers*, **2009**, *78*, 169-174.

[346] Tangpasuthadol, V.; Pongchaisirikul, N.; Hoven, V. P.; "Surface modification of chitosan films: effects of hydrophobicity on protein adsorption", *Carbohydrate Research*, **2003**, *338*, 937-942.

[347] Nosal, W. H.; Thompson, D. W.; Yan, L.; Sarkar, S.; Subramanian, A.; Woollam, J. A.; "Infrared optical properties and AFM of spin-cast chitosan films chemically modified with 1,2 epoxy-3-phenoxy-propane", *Colloids and Surfaces B: Biointerfaces*, **2005**, *46*, 26-31.

[348] Debeaufort, F.; Quezada-Gallo, J. A.; Voilley, A.; "Edible films and coatings: tomorrow's packagings: a review", *Critical Reviews in Food Science and Nutrition*, **1998**, *38*, 299-313.

[349] Siracusa, V.; Rocculi, P.; Romani, S.; Rosa, M. D.; "Biodegradable polymers for food packaging: a review", *Trends in Food Science & Technology*, **2008**, *19*, 634-643.

[350] Butler, B. L.; Vergano, P. J.; Testin, R. F.; Bunn, J. M.; Wiles, J. L.; "Mechanical and barrier properties of edible chitosan films as affected by composition and storage", *Journal of Food Science*, **1996**, *61*, 953-956.

[351] Han, J. H., Gennadios, A. ; "Edible films and coatings: a review", in Innovations in Food Packaging, Ed: Han, J. H.; *Elsevier Academic Press*, **2005,** San Diego, CA.

[352] Krochta, J. M.; Mulder-Johnson, C.; "Edible and biodegradable polymer films: challenges and opportunities", *Food technology*, **1997**, *51*, 61-74.

[353] Rhim, J.-W.; Hong, S.-I.; Park, H.-M.; Ng, P. K. W.; "Preparation and characterization of chitosan-based nanocomposite films with antimicrobial activity", *Journal of Agricultural and Food Chemistry*, **2006**, *54*, 5814-5822.

[354] Sorrentino, A.; Tortora, M.; Vittoria, V.; "Diffusion behavior in polymer-clay nanocomposites", *Journal of Polymer Science Part B: Polymer Physics*, **2006**, *44*, 265-274.

[355] Retuert, J.; Nuñez, A.; Martínez, F.; Yazdani-Pedram, M.; "Synthesis of polymeric organic-inorganic hybrid materials. Partially deacetylated chitin-silica hybrid", *Macromolecular Rapid Communications*, **1997**, *18*, 163-167.

[356] Liu, Y.-L.; Su, Y.-H.; Lai, J.-Y.; "In situ crosslinking of chitosan and formation of chitosan-silica hybrid membranes with using [gamma]-glycidoxypropyltrimethoxysilane as a crosslinking agent", *Polymer*, **2004**, *45*, 6831-6837.

[357] Yeh, J.-T.; Chen, C.-L.; Huang, K.-S.; "Synthesis and properties of chitosan/SiO_2 hybrid materials", *Materials Letters*, **2007**, *61*, 1292-1295.

[358] Di Vona, M. L.; Marani, D.; D'Ottavi, C.; Trombetta, M.; Traversa, E.; Beurroies, I.; Knauth, P.; Licoccia, S.; "A simple new route to covalent organic/inorganic hybrid proton exchange polymeric membranes", *Chemistry of Materials*, **2005**, *18*, 69-75.

[359] Lu, Z.; Dai, J.; Song, X.; Wang, G.; Yang, W.; "Facile synthesis of Fe_3O_4/SiO_2 composite nanoparticles from primary silica particles", *Colloids and Surfaces A: Physicochemical and Engineering Aspects*, **2008**, *317*, 450-456.

[360] Han, J. H.; Zhang, Y.; Buffo, R.; "Surface chemistry of food, packaging and biopolymer material ", in Innovations in Food Packaging, Ed: Han, J. H.; *Elsevier Academic Press*, **2005,** San Diego: CA.

[361] Suyatma, N. E.; Tighzert, L.; Copinet, A.; Coma, V.; "Effects of hydrophilic plasticizers on mechanical, thermal, and surface properties of chitosan films", *Journal of Agricultural and Food Chemistry*, **2005**, *53*, 3950-3957.

[362] Sothornvit, R.; Krochta, J. M.; "Plasticizer effect on mechanical properties of [beta]-lactoglobulin films", *Journal of Food Engineering*, **2001**, *50*, 149-155.

[363] Sothornvit, R.; Krochta, J. M.; "Plasticizers in edible films and coatings. ", in Innovations in Food Packaging, Ed: Han, J. H.; Gennadios, A.; *Elsevier Academic Press*, **2005,** San Diego:CA.

[364] Levine, H.; Slade, L.; "Water as a plasticizer: physicochemical aspects of low-moisture polymeric systems", in In Water Science Reviews, Ed: Franks, F.; *Cambridge University*, **1987,** Cambridge: U.K.

[365] Matienzo, L. J.; Winnacker, S. K.; "Dry processes for surface modification of a biopolymer: chitosan", *Macromolecular Materials and Engineering*, **2002**, *287*, 871-880.

[366] Karbowiak, T.; Hervet, H.; Leger, L.; Champion, D.; Debeaufort, F.; Voilley, A.; "Effect of plasticizers (water and glycerol) on the diffusion of a small molecule in Iota-carrageenan biopolymer films for edible coating application", *Biomacromolecules*, **2006**, *7*, 2011-2019.

[367] Navarro-Tarazaga, M. L.; Sothornvit, R.; Pérez-Gago, M. B.; "Effect of plasticizer type and amount on hydroxypropyl methylcellulose−beeswax edible film properties and postharvest quality of coated plums (Cv. Angeleno)", *Journal of Agricultural and Food Chemistry*, **2008**, *56*, 9502-9509.

[368] Rahman, I. A.; Vejayakumaran, P.; Sipaut, C. S.; Ismail, J.; Chee, C. K.; "Effect of the drying techniques on the morphology of silica nanoparticles synthesized via sol-gel process", *Ceramics International*, **2008**, *34*, 2059-2066.

[369] Sun, Y.; Zhang, Z.; Wong, C. P.; "Study on mono-dispersed nano-size silica by surface modification for underfill applications", *Journal of Colloid and Interface Science*, **2005**, *292*, 436-444.

[370] Scott, G.; "Green polymers", *Polymer Degradation and Stability*, **2000**, *68*, 1-7.

[371] Nielsen, L. E.; Landel, R. F.; "Mechanical properties of polymers and composites", *Marcel Dekker*, **1994,** New York.

[372] Massey, L. K.; "Permeability Properties of Plastics and Elastomers: a Guide to Packaging and Barrier Materials", *Plastic Design Library/Willian Andrew Publishing*, **2003,** Norwivh: New York.

[373] Tharanathan, R. N.; "Biodegradable films and composite coatings: past, present and future", *Trends in Food Science & Technology*, **2003**, *14*, 71-78.

[374] Miller, K. S.; Krochta, J. M.; "Oxygen and aroma barrier properties of edible films: A review", *Trends in Food Science and Technology*, **1997**, *8*, 228-237.

[375] Germain, Y.; "Conception de films polymer à permeabilité contrôlée pour l'embalage alimentaire", *Industriée Alimentaire et Agricules*, **1997**, 137-140.

[376] Robertson, G. L.; "Food packaging: principles and practice", *CRC press Taylor & Francis Group*, **2006,** Boca Raton: FL.

[377] Lai, S. M.; Yang, A. J. M.; Chen, W. C.; Hsiao, J. F.; "The properties and preparation of chitosan/silica hybrids using sol-gel process", *Polymer-Plastics Technology and Engineering*, **2006**, *45*, 997 - 1003.

[378] Chrissafis, K.; Paraskevopoulos, K. M.; Papageorgiou, G. Z.; Bikiaris, D. N.; "Thermal and dynamic mechanical behavior of bionanocomposites: fumed silica nanoparticles dispersed in poly(vinyl pyrrolidone), chitosan, and poly(vinyl alcohol)", *Journal of Applied Polymer Science*, **2008**, *110*, 1739-1749.

[379] van der Leeden, M. C.; Frens, G.; "Surface properties of plastic materials in relation to their adhering performance", *Advanced Engineering Materials*, **2002**, *4*, 280-289.

[380] Meiron, T. S.; Saguy, I. S.; "Wetting properties of food packaging", *Food Research International*, **2007**, *40*, 653-659.

[381] Turner, P. S.; Nockolds, C. E.; Bulcock, S.; "Electron Microscope techiniques for surface characterization", in Surface Analysis Methods in materials Science, Ed: O'Connor, D. J.; Sexton, B. A.; Smart, R. S. C.; *Spring-Verlag*, **2003,** Heidelberg.

[382] Campbell, D.; Pethrick, R. A.; White, J. R.; "Polymer characterization: physical techniques", *Stanley Thornes*, **2000,** Cheltenham: U.K.

[383] Song, J.; Li, Y.; Hinestroza, J. P.; Rojas, O. J.; "Tools to probe nanoscale surface phenomena in cellulose thin films: applications in the area of adsorption and friction", in The Nanoscience and Technology of Renewable Biomaterials, Ed: Lucia, A. L.; Rojas, O. J.; *John Wiley & Sons* **2009,** Chichester: UK.

[384] Menard, K. P.; "Thermomechanical and dynamic mechanical analysis", in Handbook of Plastics Analysis, Ed: Lobo, H.; Bonilla, J. V.; *Marcel Dekker, Inc.*, **2003,** New York.

[385] Oliveira, F. C.; Lopes da Silva, J. A.; Barros-Timmons, A., *ECIS - 21st Conference of the European Colloid and interface Society* (Geneve- Switzerland) **2007**, p. poster 264.

[386] "ASTM", in Annual Book of ASTM Standards, Ed: *American Society for Testing and Materials*, **1995,** Philadelphia.

[387] Jongjareonrak, A.; Benjakul, S.; Visessanguan, W.; Tanaka, M.; "Effects of plasticizers on the properties of edible films from skin gelatin of bigeye snapper and brownstripe red snapper", *European Food Research and Technology*, **2006**, *222*, 229-235.

[388] Lim, K. Y.; Kim, D. H.; Paik, U.; Kim, S. H.; "Effect of the molecular weight of poly(ethylene glycol) on the plasticization of green sheets composed of ultrafine $BaTiO_3$ particles and poly(vinyl butyral)", *Materials Research Bulletin*, **2003**, *38*, 1021-1032.

[389] Sun, G.; Zhang, X.-Z.; Chu, C.-C.; "Formulation and characterization of chitosan-based hydrogel films having both temperature and pH sensitivity", *Journal of Materials Science: Materials in Medicine*, **2007**, *18*, 1563-1577.

[390] Ferreira, C. O.; Nunes, C. A.; Delgadillo, I.; Lopes-da-Silva, J. A.; "Characterization of chitosan-whey protein films at acid pH", *Food Research International*, **2009**, *42*, 807-813.

[391] Boonstra, B. B.; "Role of particulate fillers in elastomer reinforcement: a review", *Polymer*, **1979**, *20*, 691-704.

[392] Favier, V.; Dendievel, R.; Canova, G.; Cavaille, J. Y.; Gilormini, P.; "Simulation and modeling of three-dimensional percolating structures: case of a latex matrix reinforced by a network of cellulose fibers", **1997**, *45*, 1557-1565.

[393] Sinha Ray, S.; Okamoto, M.; "Polymer/layered silicate nanocomposites: a review from preparation to processing", *Progress in Polymer Science*, **2003**, *28*, 1539-1641.

[394] Oberdisse, J.; "Structure and rheological properties of latex-silica nanocomposite films: stress-strain isotherms", *Macromolecules*, **2002**, *35*, 9441-9450.

[395] Oberdisse, J.; "Aggregation of colloidal nanoparticles in polymer matrices", *Soft Matter*, **2006**, *2*, 29-36.

[396] Persello, J.; Boisvert, J. P.; Guyard, A.; Cabane, B.; "Structure of nanometric silica clusters in polymeric composite materials", *Journal of Physical Chemistry B*, **2004**, *108*, 9678-9684.

[397] Doh, J. G.; Cho, I.; "Synthesis and properties of polystyrene-organoammonium montmorillonite hybrid", *Polymer Bulletin*, **1998**, *41*, 511-518.

[398] Bialopiotrowicz, T.; Janczuk, B.; "Surface properties of gelatin films", *Langmuir*, **2002**, *18*, 9462-9468.

[399] Yin, S.-W.; Tang, C.-H.; Wen, Q.-B.; Yang, X.-Q.; "Properties of cast films from hemp (*Cannabis sativa L.*) and soy protein isolates. A comparative study", *Journal of Agricultural and Food Chemistry*, **2007**, *55*, 7399-7404.

[400] Li, Y.; Chung, T.-S.; Cao, C.; Kulprathipanja, S.; "The effects of polymer chain rigidification, zeolite pore size and pore blockage on polyethersulfone (PES)-zeolite. A mixed matrix membranes", *Journal of Membrane Science*, **2005**, *260*, 45-55.

[401] Gulley, G. L.; Martin, J. E.; "Stabilization of colloidal silica using polyols", *Journal of Colloid and Interface Science*, **2001**, *241*, 340-345.

[402] Plueddemann, E. P.; "Silane coupling agents", *Plenum Press*, **1991,** New York.